Transition metal complexes of some N^4-phenylsemicarbazones: crystal structures and spectral studies

Thesis submitted to the

COCHIN UNIVERSITY OF SCIENCE AND TECHNOLOGY

In partial fulfillment of the requirements for the degree of

DOCTOR OF PHILOSOPHY

Under the Faculty of Science

By

MAHESWARAN SITHAMBARESAN

DEPARTMENT OF APPLIED CHEMISTRY

COCHIN UNIVERSITY OF SCIENCE AND TECHNOLOGY

KOCHI-682 022

April 2012

Transition metal complexes of some N⁴-phenylsemicarbazones: crystal structures and spectral studies

Ph. D. Thesis under the faculty of Science

Author:

Maheswaran Sithambaresan
Research fellow, Department of Applied Chemistry
Cochin University of Science and Technology,
Kochi, India
E mail: eesans@yahoo.com

Research advisor:

Dr. M. R. Prathapachandra Kurup
Professor
Department of Applied Chemistry
Cochin University of Science and Technology,
Kochi, India
E mail: mrp@cusat.ac.in

Department of Applied Chemistry
Cochin University of Science and Technology,
Kochi, India

April 2012

Front cover: *Crystal structure of zinc(II) complex of 2-benzoylpyridine-N⁴-phenylsemicarbazone*
Back cover: *Crystal structure of copper(II) complex of 2-benzoylpyridine-N⁴-phenylsemicarbazone*

...to my beloved Parents and dearest wife

Phone Off : 0484-2862423
0484-2575804
Phone Res : 0484-2576904
Fax : 0484-2577595
Email : mrp@cusat.ac.in
mrp_k@yahoo.com

DEPARTMENT OF APPLIED CHEMISTRY
COCHIN UNIVERSITY OF SCIENCE AND TECHNOLOGY
KOCHI - 682 022, INDIA

Prof. M.R. Prathapachandra Kurup   18th April 2012
Professor

Certificate

This is to certify that the thesis entitled *"Transition metal complexes of some N⁴-phenylsemicarbazones: crystal structures and spectral studies"* submitted by Mr. Maheswaran Sithambaresan, in partial fulfillment of the requirements for the degree of Doctor of Philosophy, to the Cochin University of Science and Technology, Kochi-22, is an authentic record of the original research work carried out by him under my guidance and supervision. The results embodied in this thesis, in full or in part, have not been submitted for the award of any other degree.

M. R. Prathapachandra Kurup
(Supervisor)

Declaration

I hereby declare that the work presented in this thesis entitled "**Transition metal complexes of some N⁴-phenylsemicarbazones: crystal structures and spectral studies**" is entirely original and was carried out independently under the supervision of Dr. M. R. Prathapachandra Kurup, Department of Applied Chemistry, Cochin University of Science and Technology and has not been included in any other thesis submitted previously for the award of any other degree.

18-04-12   **Maheswaran Sithambaresan**
Kochi-22

ACKNOWLEDGEMENT

The research described in this thesis was done at the Department of Applied Chemistry, CUSAT. I am grateful to all those who inspired me during this research work and I wish to express my deep feeling of gratitude towards them, without whose valuable suggestions and encouragement, the accomplishment of this thesis would have been impossible.

*First and foremost, I wish to place on record my heartfelt gratefulness to my revered guide **Prof. (Dr.) M.R. Prathapachandra Kurup**, Department of Applied Chemistry for his intensive guidance and whole hearted support and inspiration throughout my research work. Moreover, he has motivated me to learn EPR simulations, DFT studies on metal complexes and solving of single crystal structure using SHELXL. These all lent me hands to complete with publications.*

I am greatly obliged to Prof (Dr.) K. Sreekumar (Head of the Department) and Prof. (Dr.) K. Girish Kumar (Doctoral Committee member and former HOD) for their kind consideration and continuous encouragement. I cannot forget Prof. (Dr.) K.K. Mohammed Yusuff, Prof. (Dr.) S. Sugunan and Dr. S. Prathapan for their valuable suggestions during the presentation of my presynopsis. I acknowledge all faculty members of the Department of Applied Chemistry for their support and advice. I also acknowledge all the non-teaching staff of the Department in taking care of all issues regarding the administration of my academic program.

I am indebted to all the staff of SAIF, Kochi and IIT Bombay. I place my special thanks to Dr. Shibu, SAIF, Kochi and Prof. M.V. Rajasekharan, School of Chemistry, Hyderabad for Single crystal XRD studies.

I am grateful to my senior researchers Dr. E.B. Seena, Dr. S.R. Sheeja, Dr. E.. Manoj, Dr. Reena, Dr. Nancy Mathew, Dr. Neema, Dr. Laly and Renjusha for their boundless support.

PREFACE

The work embodied in this thesis was carried out by the author in the Department of Applied Chemistry, CUSAT, Kochi, during the period 2009-2012. The thesis is an introduction to our attempts to evaluate the coordination behavior of some compounds of our interest. The biological activities of semicarbazones and their metal complexes have been an active area of research during the past years because of their significant role in naturally occurring biological systems. Tridentate NNO and ONO semicarbazone systems formed from heterocyclic and aromatic carbonyl compounds and their transition metal complexes are well-authenticated compounds in this field and their synthesis, crystal structures and spectral studies are well desirable. Hence, we decided to develop a research program aimed at the syntheses, crystal structures and spectral studies of new N^4-phenylsemicarbazones derived from 2-formylpyridine and 3-ethoxysalicylaldehyde and their transition metal complexes and new transition metal complexes of 2-benzoylpyridine-N^4-phenylsemicarbazone. In addition to various physico-chemical methods of analysis, single crystal X-ray diffraction studies were also used for the characterization of the complexes.

The thesis has been divided in to six chapters carrying a detailed account of the semicarbazones and their complexes with some transition metal ions. Chapter 1 describes the survey of applications and recent developments in the field of semicarbazones and their metal complexes. Chapter 2 deals with the syntheses and characterization of 2-formylpyridine-N^4-phenylsemicarbazone and 3-ethoxysalicylaldehyde-N^4-phenylsemicarbazone and 2-benzoylpyridine-N^4-phenylsemicarbazone. The crystal structure of 3-ethoxysalicylaldehyde-N^4-phenylsemicarbazone is also given in this chapter. Chapter 3 explains the syntheses and spectral studies of Ni(II) complexes of 2-formylpyridine-N^4-phenylsemicarbazone and 2-benzoylpyridine-N^4-phenylsemicarbazone along with

the crystal structure of a complex. Chapter 4 comprises the syntheses and spectral studies of copper(II) complexes of 2-formylpyridine-N^4-phenylsemicarbazone and 3-ethoxysalicylaldehyde-N^4-phenylsemicarbazone along with the crystal structures of two complexes. Syntheses and spectral studies of zinc(II) complexes of 2-formylpyridine-N^4-phenylsemicarbazone and 2-benzoylpyridine-N^4-phenylsemicarbazone are discussed in Chapter 5 with the crystal structures of two complexes. Chapter 6 deals with the syntheses and spectral studies of cadmium(II) complexes supported by the crystal structures of two complexes. Summary of the thesis is also given at the end.

Contents

1.1 Semicarbazones: An introduction

Semicarbazones are usually obtained by the condensation of semicarbazide with suitable aldehydes and ketones (Scheme 1.1).
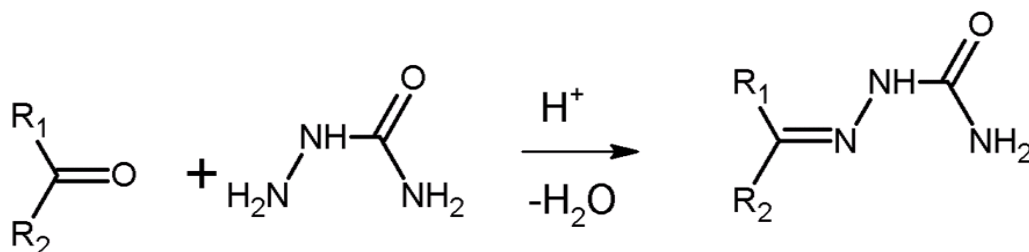
Scheme 1.1 Synthesis of the semicarbazone.

According to IUPAC recommendations, semicarbazones may be named by adding the class name 'semicarbazone' after the name of the condensed aldehyde or ketone. It also includes derivatives with substituents on the amide nitrogen in this class. The IUPAC numbering scheme is shown in the Fig. 1.1.
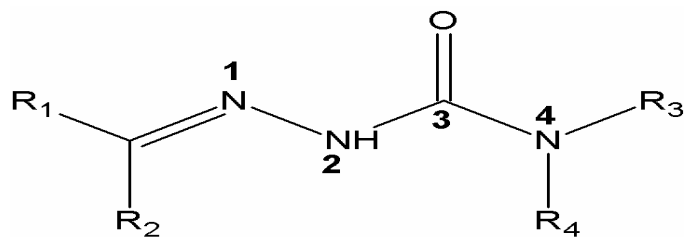
Fig. 1.1 Numbering scheme of the semicarbazone.

An interesting fact is that the semicarbazones exist predominantly in the amido form in the solid state, whereas due to the interaction of the solvent molecules they can exhibit a amido-iminol tautomerism (Fig. 1.2) in solution state. Amido form acts as a neutral ligand and the iminol form can deprotonate and serve as anionic ligand in metal complexes. Thus semicarbazones are versatile ligands in both neutral and anionic forms.
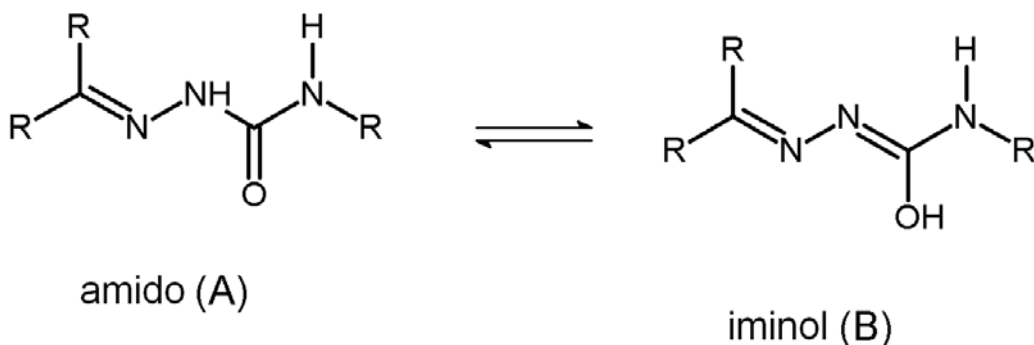
Fig. 1.2 Amido-iminol tautomerism of semicarbazone.

Both tautomeric forms have an efficient electron delocalization along the semicarbazone moiety. Aromatic substituents on the semicarbazone skeleton can further enhance the delocalization of electron charge density. These classes of compounds usually react with metallic cations giving complexes in which the semicarbazones behave as chelating ligands. Upon coordination to a metal center, the delocalization is further increased through the metal chelate rings. The coordination possibilities are further increased if the substituent has additional donor atoms.

1.2. Binding modes of semicarbazones

A review of semicarbazones shows that the C=N–NH–CO–NH$_2$ backbone of unsubstituted semicarbazones in the solid state is usually planar, with O atom trans to the azomethine N atom. However, few semicarbazones are exceptions to this rule [1]. Although there are several electronic and steric factors that may contribute to the adoption of this rearrangement, the most important is probably that the trans arrangement places the amine and azomethine nitrogen atoms in relative positions (Fig. 1.3) suitable for intramolecular hydrogen bonding [2].
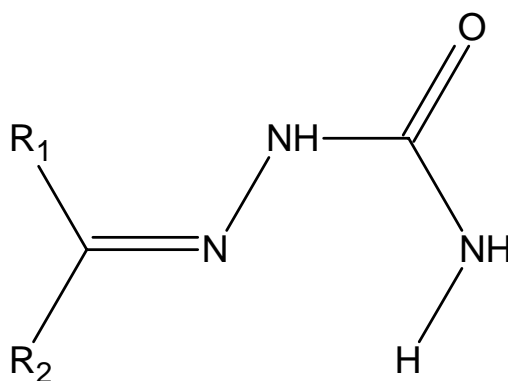
Fig. 1.3 O atom is trans to the azomethine N atom

An interesting aspect is that the semicarbazones show a variety of coordination modes with transition metals. The coordination mode is influenced by the number and type of substituents. This is because the active donor sites of the ligand vary depending upon the substituents. According to the reports, the coordination mode of the semicarbazone is very sensitive towards minor variations in the experimental conditions, the nature of the substituents on the carbonyl compound and the metal salt [3]. The presence of di-2-pyridyl ketone at the carbonyl part attributes many interesting coordinating possibilities for the ligand systems under study. In most of the metal complexes we synthesized

semicarbazones act as tridentate ligand and in some other cases, semicarbazones exhibit as potential quadridentate ones when the second pyridyl nitrogen of di-2-pyridyl ketone involves in coordination process. The ONO tridentate coordination mode of the semicarbazones is given below [4].
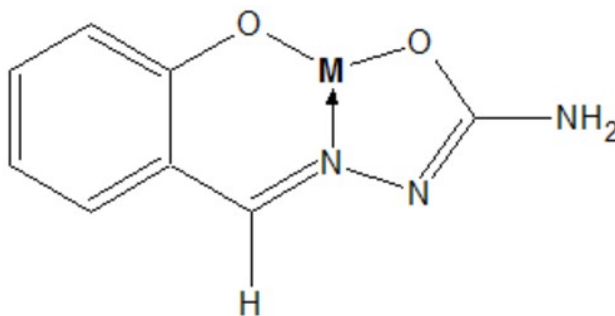
O, N, O-tricoordination.

The different coordination modes of benzaldehyde semicarbazone are given below [5].
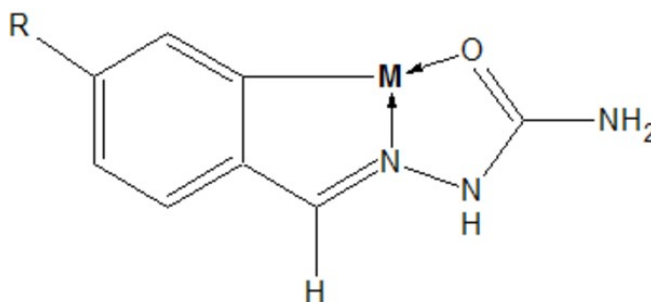
C,N,O-tricoordination.
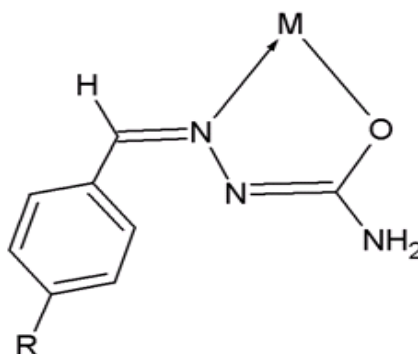
N,O-coordination forming a stable five membered chelate ring.
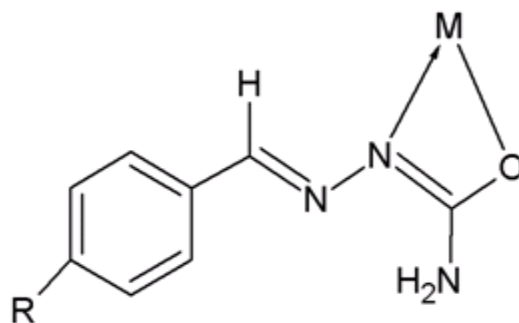
An unusual four-membered chelate ring formation as an N,O donor.

1.3. Applications of semicarbazones and their complexes

The metal complexes of semicarbazones play an essential role in agriculture, pharmaceutical and industrial chemistry and they are used as catalysts, in various biological systems, polymers and dyes, besides some uses antifertility and enzymatic agents. The biological properties of semicarbazones are often related to metal ion coordination. Firstly, lipophilicity, which controls the rate of entry in to the cell, is modified by coordination [6]. Also, the metal complex can be more active than the free ligand. The mechanism of action can involve binding to a metal *in vivo* or the metal complex may be a vehicle for activation of the ligand as the cytotoxic agent. Recently it has been shown that semicarbazones of aromatic and unsaturated carbonyl compounds have anticonvulsant properties [7]. Moreover, coordination may lead to significant reduction of drug-resistance [8]. They are also used as spectrophotometric agents as well for the analysis of metal ions [9] and are frequently used in the qualitative organic analysis of carbonyl compounds [10].

Recently, thiosemicarbazones have been synthesized and screened against the three parasitic cysteine proteases cruzain, falcipain-2, and rhodesain and against their respective parasite sources, *Trypanosoma cruzi*, *Plasmodium falciparium*, and *Trypanosoma brucei* [11]. The results obtained suggested that

thiosemicarbazones represent validated leads that kill several species of protozoan parasites through the inhibition of cysteine proteases as well as through action against other targets. Furthermore, semicarbazones, which can also be regarded as urea derivatives, have gained considerable importance [12] in recent years in the design of enzyme inhibitors [13], as replacement for the amide (–CO–NH–) bond in peptidomimetics [14] and as sources of self-complementary bidirectional hydrogen bonding motif in supramolecular chemistry [15]. Since peptides have poor metabolic stability and limited oral absorption, they are rarely useful drug candidates.

Epilepsies are common and frequently devastating and affect around 1–2% of the world population. The convulsions of approximately 25% of epileptics are inadequately controlled by the standard drug therapy [16,17]. The number of drugs useful for the treatment of epilepsy is remarkably small. Fewer than 20 drugs are currently marketed in the United States, and of these, only five or six are widely used [17]. Semicarbazones are a class of compounds which shows anticonvulsant activity [18]. Arylsemicarbazones can be orally administered and are more active as anticonvulsants than mephenytoin or phenobarbital, besides the fact that they generally exhibit low or absent neurotoxicity [19].

In the development of new metal-based therapeutics, detailed studies on the interactions between biomolecular targets such as DNA and structurally defined transition metal complexes can provide invaluable information [20]. Among the non-platinum compounds exhibiting anticancer properties, those of ruthenium are very promising, showing activity on even such tumors which developed resistance to cisplatin or in which cisplatin is totally inactive. Furthermore, it possesses mutagenic properties [21], exhibits good

antineoplastic activity against several murine metastasizing tumors [22] and interacts *in vitro* with DNA to form covalent bonds with the nucleobases [23].

A variety of 5-nitrofuryl semicarbazone derivatives have been developed for the therapy of Chagas disease, a major problem in the Central and the South America [24]. 4-Bromobenzaldehyde semicarbazone has been used as anticonvulsant. Recently, a review reported on the anticonvulsant activity of thiosemicarbazones, semicarbazones and hydrazones derived from aromatic and unsaturated carbonyl compounds as well as from other precursors [25]. In contrast to thiosemicarbazones, literature records fewer examples of semicarbazones presenting significant anticancer and cytotoxic activity but some nitroso, naphtopyran, and fluorine derivatives showed anti-leukemia effect in mice [26]. Several N^4-substituted semicarbazone derivatives of o- and p- chlorobenzaldehyde and 2,6-dichlorobenzaldehyde exhibit potent anti-hypertensive effects [27]. The orally administered drug naftazone (1,2-naphtoquinone semicarbazone) protects the vascular system through an inhibitory effect on nitric oxide synthesis [28].

1.4. Objectives of the work

The unusual coordination modes of semicarbazones when bound to metals, the wide applications and structural diversity of metal complexes of semicarbazones provoked us to synthesize and characterize the tridentate ONO and NNO-donor semicarbazones and their transition metal complexes. This work is focused on the studies on complexes of three N^4-phenylsemicarbazones synthesized by changing the carbonyl compounds.

This work is concerned with the studies of two new semicarbazones, 2-formylpyridine-N^4-phenylsemicarbazone (HL^1) and 3-ethoxysalicylaldehyde-N^4-phenylsemicarbazone (H$_2$L^2) and a reported semicarbazone,

2-benzoylpyridine-N^4-phenylsemicarbazone (HL^3) [29]. The compositions of these semicarbazones were determined by the CHN analyses and IR, UV and NMR spectral studies were used for the characterization of these compounds. The molecular structure of 3-ethoxysalicylaldehyde-N^4-phenylsemicarbazone (H$_2$L^2) was obtained by single crystal X-ray diffraction studies. Also, we have synthesized Cu(II), Cd(II), Zn(II) and Ni(II) complexes of these three semicarbazones. The complexes were characterized by various spectroscopic techniques, magnetic and conductivity studies. We could isolate single crystals of some complexes of all metals suitable for X-ray diffraction studies. This thesis is divided into six chapters.

Chapter 1 gives an introduction of semicarbazones and their metal complexes with an extensive literature survey relating the applications and recent developments. This includes a detailed idea about coordination modes and stereochemistry of the semicarbazones.

Chapter 2 explains syntheses and characterization of two NNO donor semicarbazones and an ONO donor semicarbazone.

Chapters 3, 4, 5 and 6 describe the syntheses and characterization of Cu(II), Cd(II), Zn(II) and Ni(II) complexes of these semicarbazones.

References

[1]   J.S. Casas, M.S. Garcia-Tasende, J. Sordo, Coord. Chem. Rev. 209 (2000) 197.

[2]   J.N. Brown, K.C. Agarwal, Acta Crystallogr., Sect. B 34 (1978) 2038.

[3]   F. Basuli, S.M. Peng, S. Bhattacharya, Inorg. Chem. 40 (2001) 1126.

[4]   A. Sreekanth, U.L. Kala, C.R. Nayar, M.R.P. Kurup, Polyhedron 23 (2004) 41.

[5]   F. Basuli, S.M. Peng, S. Bhattacharya, Inorg. Chem. 36 (1997) 5645.

[6]   N. Farrell, Coord. Chem. Rev. 1 (2002) 232.

[7]   A. Zahra, S. Ekk, L. Weisheng, M. Yinfa, C. Charles, P. Subhash, J. Inorg. Biochem. 99 (2005) 1526.

[8]   D.X. West, S.B. Padhye, P.B. Sonawane, Structure and Bonding, Springer-Verlag: New York 76 (1991) 1.

[9]   T. Atalay, E.G. Akgemci, Tr. J. Chem. 22 (1998) 123.

[10]   V.M. Kolb, J.W. Stupar, T.E. Janota, W.L. Duax, J. Org. Chem. 54 (1989) 2341.

[11]   D.C. Greenbaum, Z. Mackey, E. Hansell, P. Doyle, J. Gut, C.R. Caffrey, J. Lehman, P.J. Rosenthal, J.H. McKerrow, K.J. Chibale, Med. Chem. 47 (2004) 3212.

[12]   S.M. Hutchins, K.T. Chapman, Tetrahedron Lett. 35 (1994) 4055.

[13]   P.Y.S. Lam, P.K. Jadhav, C.J. Eyermann, C.N. Hodge, Y. Ru, L.T. Bacheler, J.L. Meek, M.J. Otto, M.M. Rayner, Y.N. Wong, C.H. Chang, P.C. Weber, D.A. Jackson, T.R. Sharpe, E.S. Viitanen, Science 263 (1994) 380.

[14]   M. Chorev, M. Goodman, Acc. Chem. Res. 26 (1993) 266.

[15]   X. Zhao, Y.L. Chang, F.W. Fowler, J.W. Lauher, J. Am. Chem. Soc. 112 (1990) 6627.

[16]   J.O. Mc Namara, Drugs effective in the therapy of the epilepsies, in: J.G. Hardman, L.E. Limbird (Eds.), Goodman and Gilman's The Pharmacological Basis of Therapeutics, 10th ed., Mc Graw- Hill, New York, 2001, pp. 521.

[17] P.K. Kadaba, K. Pankaja, G. Lin, L. Zhaiwei, Biochemical and Biophysical Research Communications 296 (2002) 241.

[18] G. Ibrahim, G.M. Bouet, I.H. Hall, M.A. Khan, J. Inorg. Biochem. 81 (2000) 29.

[19] J.R. Dimmock, G. B. Baker, Epilepsy 35 (1994) 648.

[20] D-L. Ma, C.-M. Che, F.-M. Siu, M. Yang, K.-Y. Wong, Inorg. Chem. 46 (2007) 740.

[21] C. Monti-Bragadin, M. Giacca, L. Dolzani, M. Tamaro, Inorg. Chim. Acta 137 (1987) 31.

[22] G. Sava, S. Zorzet, T. Giraldi, G. Mestroni, G. Zassinovich, Eur. J. Cancer Clin. Oncol. 20 (1984) 841.

[23] S. Cauci, E. Alessio, G. Mestroni, F. Quadrifoglio, Inorg. Chim. Acta 137 (1987) 19.

[24] H. Cerecetto, M. Gonzalez, M. Curr. Topics Med. Chem. 2 (2002) 1185.

[25] H. Beraldo, D. Gambino, Mini reviews in Med. Chem. 4 (2004) 159.

[26] S.N. Pandeya, J.R. Dimmock, Pharmazie 48 (1993) 659.

[27] J.D. Warren, D.L. Woodward, J. Med. Chem. 29 (1977) 1520.

[28] P. Sogni, S. Yang, C. Pilette, R. Moreau, A. Gadano, G. Avenard, C. Bloy, D. Lebrec, Eur. J. Pharmacol. 344 (1998) 37.

[29] M.R.P. Kurup, B. Varghese, M. Sithambaresan, S. Krishnan, S.R. Sheeja, E. Suresh, Polyhedron 30 (2011) 70.

........................≪≪≪........................

Syntheses and characterization of N⁴-phenylsemicarbazones

2.1. Introduction

There has been less attention devoted to the synthesis and biological properties of the structurally analogous semicarbazones and their metal complexes, despite the fact that, for some of these compounds, considerable anticonvulsant [1,2], antimicrobial [3] and antitumor [4] activities have been found, and a great advantage of semicarbazone derivatives over their thiosemicarbazone analogues seem to be their lower toxicity. Semicarbazones are compounds having the formula $R_2C=N–NH–(CO)–NH_2$ formally derived by condenzation of aldehyde or ketone with semicarbazide.

Semicarbazones are proved to have monoprotic nature and the additional proton donors present in the substituents will enhance the pH in solution. N^4-phenylsemicarbazones are capable of deprotonation at amide function to give monoprotic chelating ligands (HL) and the presence of a phenolic group in the substituant gives diprotic chelating ligands (H_2L).

This chapter describes the syntheses and spectral characterization of three different N^4-phenylsemicarbazones. The semicarbazones synthesized were

2-formylpyridine-N^4-phenylsemicarbazone (HL^1), 3-ethoxysalicylaldehyde-N^4-phenylsemicarbazone (H$_2$L^2) and 2-benzoylpyridine-N^4-phenylsemicarbazone (HL^3). The structure of H$_2$L^2 has been determined by single crystal X-ray diffraction.

2.2. Experimental

2.2.1. Materials

2-Formylpyridine (Aldrich), 3-ethoxysalicylaldehyde (Aldrich), N(4)-phenylsemicarbazide (Alfa Aesar), 2-benzoylpyridine (Alfa Aesar), were used as received. Methanol was dried over fused CaCl$_2$ and distilled. Other solvents were purified and dried by using standard procedure.

2.2.2. Preparation of semicarbazones

The three semicarbazones are prepared by the condenzation of semicarbazide with appropriate substituted carbonyl compounds.

$$R_2C=O + H_2N-NHCONH_2 \rightarrow R_2C=N-NHCONH_2 + H_2O$$
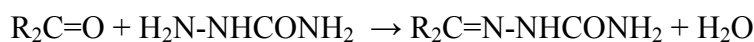
2.2.2.1. Synthesis of 2-formylpyridine-N^4-phenylsemicarbazone (HL^1)

2-Formylpyridine-N^4-phenylsemicarbazone was prepared by the condenzation of 2-formylpyridine and *N*(4)-phenylsemicarbazide. *N*(4)-phenylsemicarbazide (1.511 g, 10 mmol) was dissolved in 20 ml of hot methanol and 2-formylpyridine (10 mmol) was added to it. On cooling colorless needle like crystals (Yield: 72%, m.p.: 168-171 ºC) of the semicarbazone were separated out. It was recrystallized from 1:1 methanol water. The crystals were filtered, washed with methanol, water and ether and dried *in vacuo* over P$_4$O$_{10}$. The scheme for the reaction is shown below (Scheme 2.1).
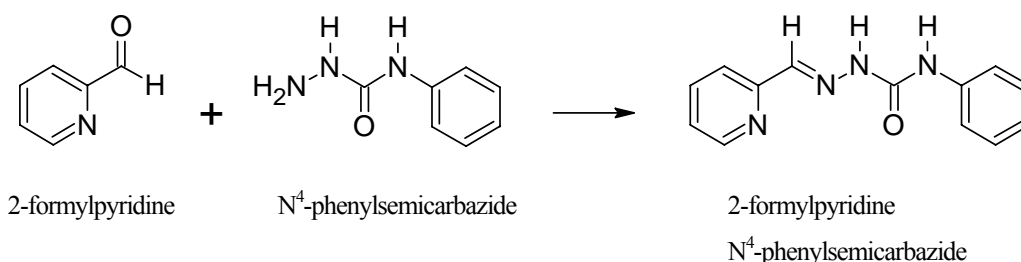
Scheme 2.1 Synthesis of 2-formylpyridine-N⁴-phenylsemicarbazone.

2.2.2.2. Synthesis of 3-ethoxysalicylaldehyde-N⁴-phenylsemicarbazone (H₂L²)

The compound (H_2L^2) was prepared in methanol solution by condenzing 3-ethoxysalicylaldehyde with N^4-phenylsemicarbazide. A methanolic solution (30 ml) of N^4-phenylsemicarbazide (1.511 g, 10 mmol) was added to a solution of 3-ethoxysalicylaldehyde (1.662 g, 10 mmol) in methanol and the reaction mixture was refluxed for 2 h. Few drops of dil. acetic acid were also added to change the pH. On cooling very pale yellow block-shaped crystals (Yield: 81%, m.p.: 180-183 ºC) suitable for single crystal X-ray diffraction were obtained and they were carefully separated. The scheme for the reaction is shown below (Scheme 2.2).
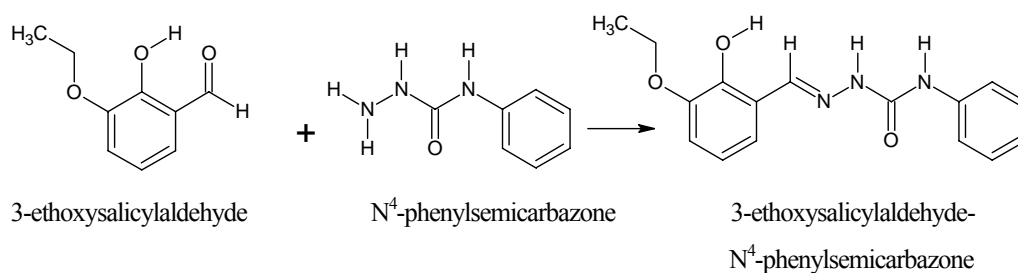
Scheme 2.2 Synthesis of 3-ethoxysalicylaldehyde-N⁴-phenylsemicarbazone.

2.2.2.3. Synthesis of 2-benzoylpyridine-N⁴-phenylsemicarbazone (HL³)

The compound HL^3 was prepared in methanol solution by the condenzation of 2-benzoylpyridine and N^4-phenylsemicarbazide. N^4-

phenylsemicarbazide (1.510 g, 10 mmol) is dissolved in 20 ml of methanol and it is taken in an R.B. flask. A methanolic solution of 2-benzoylpyridine (1.83 g, 10 mmol) was added to the above solution and the reaction mixture was refluxed for one and two hours. On cooling pale yellow crystals of the semicarbazone were separated out and it was recrystallized from methanol (Yield: 76%, m.p.: 188-190 ºC). These crystals were filtered, washed with methanol and ether and dried *in vacuo* over P_4O_{10}. The scheme for the reaction is shown below (Scheme 2.3).

2-benzoylpyridine N^4-phenylsemicarbazone   2-benzoylpyridine-N^4-phenylsemicarbazone
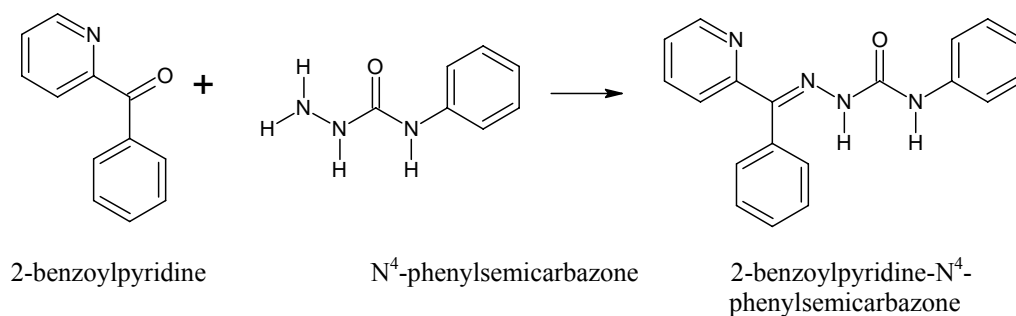
Scheme 2.3 Synthesis of 2-benzoylpyridine-N^4-phenylsemicarbazone

2.2.3. Characterization of semicarbazones

The semicarbazones were characterized by using elemental analyses and ^{1}H NMR, IR and electronic spectra. In addition to that the structure of one of these semicarbazones, H_2L^2 was determined by single crystal X-ray diffraction studies as well. Elemental analyses were carried out using a Vario EL III CHNS analyzer at the SAIF, Kochi, India. Infrared spectra were recorded on a JASCO FT-IR-5300 Spectrometer in the range 4000-400 cm^{-1} using KBr pellets. Electronic spectra were recorded on a Cary 5000 version 1.09 UV-VIS-NIR Spectrophotometer using methanol solutions. The ^{1}H NMR spectra were

recorded using Bruker DRX 500 Spectrometer, with $CDCl_3$ and DMSO as solvents and TMS as standard at the SAIF, Kochi, India.

2.2.4. X-ray crystallography

Single crystals of H_2L^2 suitable for X-ray diffraction studies were obtained from its methanol solution by slow evaporation at room temperature. A crystal with approximate dimensions 0.50 x 0.30 x 0.10 mm^3 was mounted on a Bruker SMART APEX diffractometer, equipped with a graphite crystal, incident-beam monochromator, and a fine focus sealed tube with Mo Kα (λ = 0.71073 Å) as the X-ray source. The crystallographic data along with details of structure solution refinements are given in Table 2.1. The unit cell dimensions were measured and the data collections were performed at 296(2) K. Bruker SMART software was used for data acquisition and Bruker SAINT software for data integration [5]. Absorption corrections were carried out using SADABS based on Laue symmetry using equivalent reflections [6]. The structure was solved by direct methods and refined by full-matrix least-squares calculations with the SHELXL–97 software package [7]. The graphics tool used was DIAMOND version 3.2g [8]. All non-hydrogen atoms were refined anisotropically. All the H atoms on C of this compound were placed in calculated positions, guided by difference maps and refined isotropically. The N3–H3' and O2–H2 hydrogen atoms were located from difference maps and restrained using DFIX instructions while the N2–H2' hydrogen atom was located from difference maps and freely refined.

Table 2.1 Crystal data and structure refinement parameters for H_2L^2

Parameters	Description
Empirical formula	$C_{16} H_{17} N_3 O_3$
Formula weight (M)	299.33
Color, Shape	Colorless, block
Temperature (T) K	296(2)
Wavelength (Mo K) (Å)	0.71073
Crystal system	Monoclinic
Space group	$C2/c$
Unit cell dimensions	
a (Å)	30.1352(13)
b (Å)	5.5552(3)
c (Å)	18.2232(8)
α (°)	90
β (°)	92.753(2)
γ (°)	90
Volume V ($Å^3$)	3047.2(2)
Z	8
D_{calc} (ρ) (Mg m^{-3})	1.296
Absorption coefficient μ(mm^{-1})	0.092
F(000)	1264.0
Crystal size (mm^3)	0.50 x 0.30 x 0.10
θ range for data collection	1.35 to 27.46
Limiting indices	$-37 \leq h \leq 38, -4 \leq k \leq 7, -23 \leq l \leq 23$
Reflections collected	12267
Independent reflections (R_{int})	3454 (0.0352)
Completeness to theta	27.46 99.0 %
Max. and min. transmission	0.9909 and 0.9555
Refinement method	Full-matrix least-squares on F^2
Data / restraints / parameters	3454 / 0 / 212
Goodness-of-fit on F^2	1.059
Final R indices [I > 2σ (I)]	$R_1 = 0.0450$, $wR_2 = 0.1252$
R indices (all data)	$R_1 = 0.0702$, $wR_2 = 0.1562$
Largest diff. peak and hole (e Å $^{-3}$)	0.200 and -0.214

$R_1 = \Sigma ||F_o| - |F_c|| / \Sigma |F_o|$

$wR_2 = [\Sigma w(F_o^2 - F_c^2)^2 / \Sigma w(F_o^2)^2]^{1/2}$

2.3. Results and discussion

2.3.1. Analytical measurements

The stoichiometries, colors and elemental analytical data of synthesized semicarbazones are presented in Table 2.2. The elemental analysis data obtained and calculated values are found to be in good agreement for all the three compounds.

Table 2.2 Preliminary analytical data of the N⁴-phenylsemicarbazones

Compound	Stoichiometry	Color	Found (Calc.)%		
			C	H	N
HL¹	$C_{13}H_{12}N_4O$	colorless	72.47(72.13)	5.20 (5.10)	18.14(17.71)
H₂L²	$C_{16}H_{17}N_3O_3$	pale yellow	63.79(64.20)	6.02(5.72)	13.98(14.04)
HL³	$C_{19}H_{16}N_4O$	Pale yellow	72.46(72.13)	5.16(5.10)	18.08(17.71)

2.3.2. Crystal structure of H₂L²

The molecular structure of H₂L² along with the atom numbering scheme is given in Fig. 2.1. Selected bond lengths and angles are given in Table 2.3. The compound crystallizes into a monoclinic space group *C2/c*. The molecule is almost planar and exists in the *E* configuration with respect to C7=N1 bond. A torsion angle value of 176.4(1)° corresponding to O(3)–C(8)–N(2)–N(1) moiety confirms the trans configuration of the O(3) atom with respect to hydrazine nitrogen atom N(1). As a result, atom N(1) lies cis to N(3), with an N(1)–N(2)–C(8)–N(3) torsion angle of 3.6(2). This arrangement favors the intramolecular hydrogen bond interaction between N(1) and H N(3). Similarly O1 and O2 lies cis to each other with a torsion angle of -0.4(2) and it favors the intramolecular hydrogen bond interaction between O(1) and the H–O(2). These two intramolecular hydrogen bonding interactions (Sym. code: -x+1, -y+1, -z+1) play an important role by stabilizing this conformation. The C(8)–N(2) bond distance [1.3656(19) Å] is appreciably close to that of C–N single bond [1.351(2) Å], confirming the amido form of the ligand. The existence of semicarbazone in the amido form in the solid state is evidenced by the C(8)–O(2) bond distance of 1.2233(19) Å, which is very close to a formal C=O bond length [1.21 Å].

Table 2.3 Selected bond lengths (Å) and bond angles (º) of 3-ethoxysalicylaldehyde-N[4]-phenylsemicarbazone

Bond lengths		Bond angles	
O(3)—C(8)	1.2233(19)	C(2)—O(1)—C(15)	118.74(14)
N(1)—C(7)	1.2759(18)	C(7)—N(1)—N(2)	115.50(12)
N(1)—N(2)	1.3682(19)	C(8)—N(2)—N(1)	122.60(13)
N(2)—C(8)	1.3656(19)	C(8)—N(3)—C(9)	128.26(14)
N(3)—C(8)	1.351(2)	O(3)—C(8)—N(3)	125.96(14)
N(3)—C(9)	1.4102(18)	O(3)—C(8)—N(2)	119.77(14)
O(1)—C(2)	1.3689(18)	N(3)—C(8)—N(2)	114.28(15)
O(2)—C(1)	1.3596(17)	N(1)—C(7)—C(6)	122.20(13)
O(1)—C(15)	1.426(2)	O(2)—C(1)—C(2)	120.06(13)
C(15)—C(16)	1.489(3)	O(1)—C(2)—C(3)	126.71(15)
		O(1)—C(2)—C(1)	113.31(14)
		C(14)—C(9)—N(3)	116.93(13)
		C(10)—C(9)—N(3)	123.84(13)
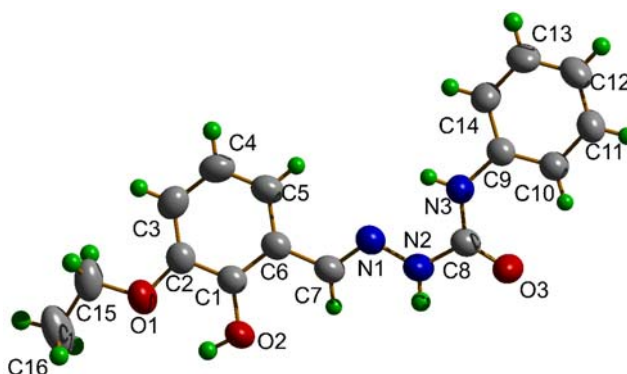
Fig. 2.1 Molecular structure of 3-ethoxysalicylaldehyde-N[4]-phenylsemicarbazone.

The two neighboring molecules are coupled together to form centrosymmetric dimers by intermolecular hydrogen bonding as shown in Fig. 2.2 and such dimers are interconnected through π⋯π interactions (Fig. 2.3). The detailed description of the hydrogen bonding is shown in Table 2.4. The O(2) atom functions as donor and accepter by forming two types of hydrogen bondings.
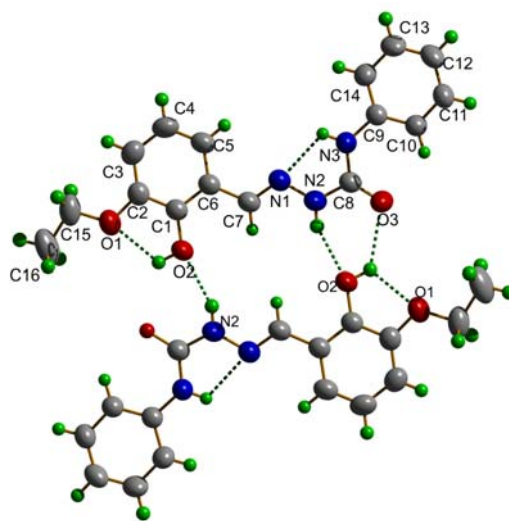
Fig. 2.2 Intermolecular and intramolecular hydrogen bonding in 3-ethoxysalicylaldehyde-N⁴-phenylsemicarbazone.
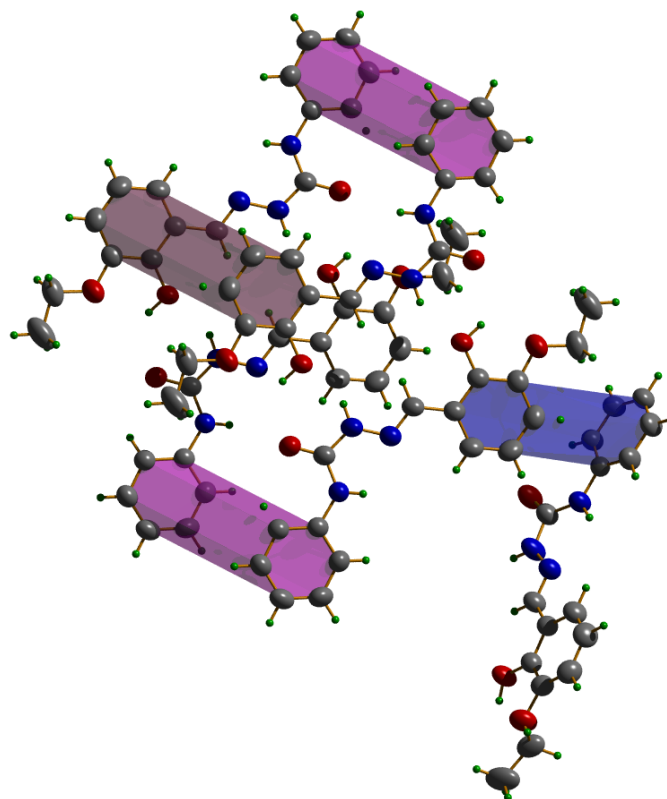
Fig. 2.3 $\pi\cdots\pi$ interactions in 3-ethoxysalicylaldehyde-N⁴-phenylsemicarbazone.

In the crystal lattice (Fig. 2.4), intermolecular hydrogen bonding interactions form centrosymmetric dimers while the very weak $\pi\cdots\pi$ interactions connect such dimers together. The repeating units of two adjacent molecules are aligned in offset manner. The distance between two consecutive parallel rings is more than 5 Å and therefore there are very weak $\pi\cdots\pi$ interactions which connect the two layers making a 2-D supramolecular network in the lattice. There is no C–H$\cdots\pi$ interaction between the adjacent molecules.
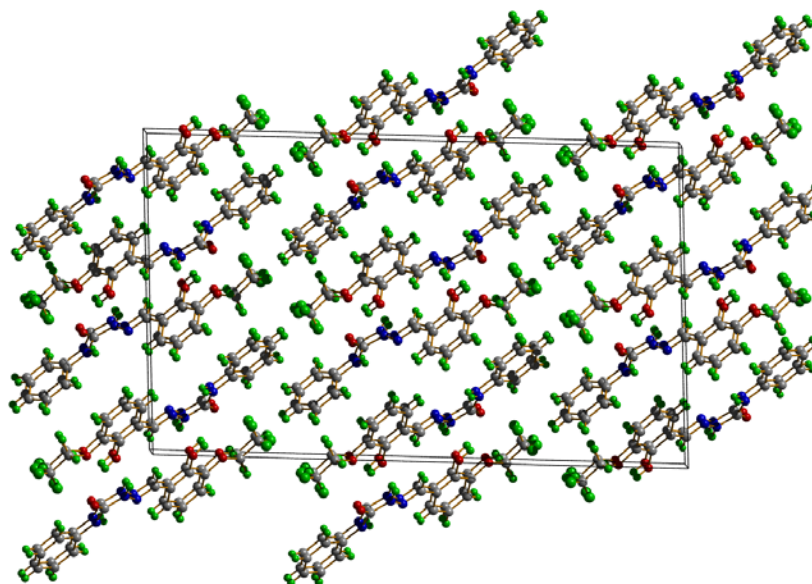
Fig. 2.4 Packing diagram of 3-ethoxysalicylaldehyde-N[4]-phenylsemicarbazone along b axis.

Table 2.4 Hydrogen-bond geometry

D—H$\cdots$A	D$\cdots$H (Å)	H$\cdots$A (Å)	D$\cdots$A (Å)	D—H$\cdots$A (°)
O(2)—H(2)$\cdots$O(1)	0.882	2.130	2.621	114.45
O(2)—H(2)$\cdots$O(3)[a]	0.882	2.276	2.886	126.21
N(3)—H(3')$\cdots$N(1)	0.836	2.247	2.661	110.76
N(2)—H(2')$\cdots$O(2)[a]	0.854	2.128	2.878	146.41

A=acceptor, D=donor, Equivalent position code: [a]= -x+1, -y+1, -z+1

2.3.3. Infrared spectral studies

The significant bands observed in the IR spectra of the ligands along with their relative assignments are presented in the Table 2.5.

Table 2.5 Infrared spectral assignments (cm^{-1}) of the semicarbazone ligands

Compound	ν(C=N)	ν(N–N)	ν(^{4}N–H)	ν(^{2}N–H)	ν(C=O)	ν(O–H)
HL^1	1597	1143	3107	3372	1693	-
H$_2$L^2	1602	1152	3125	3200	1689	3431
HL^3	1600	1132	3118	3375	1698	-

The characteristic IR bands (400-4000 cm^{-1}) of the ligands HL^1, H$_2$L^2 and HL^3 provide significant information regarding the various functional groups present in the ligands. In the IR spectra of these ligands, ν(C=O) bands are present at 1693, 1689 and 1698 cm^{-1} respectively for HL^1, H$_2$L^2 and HL^3. Medium bands in the 3200-3375 cm^{-1} range in the free ligands due to ν(^{2}N–H) vibrations also indicate that the ligands remain in the imido form in the solid state [9,10]. The bands corresponding to ν(^{4}N–H) appear in the range 3107-3125 cm^{-1} [3].

The broad absorption band at 3431 cm^{-1} is due to the O–H stretching mode of phenolic oxygen. The azomethine bands, ν(C=N) appear at 1592-1602 cm^{-1} is in agreement with earlier reports of N(4)-substituted semicarbazones [11]. The IR spectral bands of HL^1, H$_2$L^2 and HL^3 observed at 1143, 1152 and 1132 cm^{-1} corresponds to ν(N–N) [11,12]. The 1600-1400 cm^{-1} region of the spectra is complicated by the presence of amide bands and ring breathing vibrations of the phenyl rings.
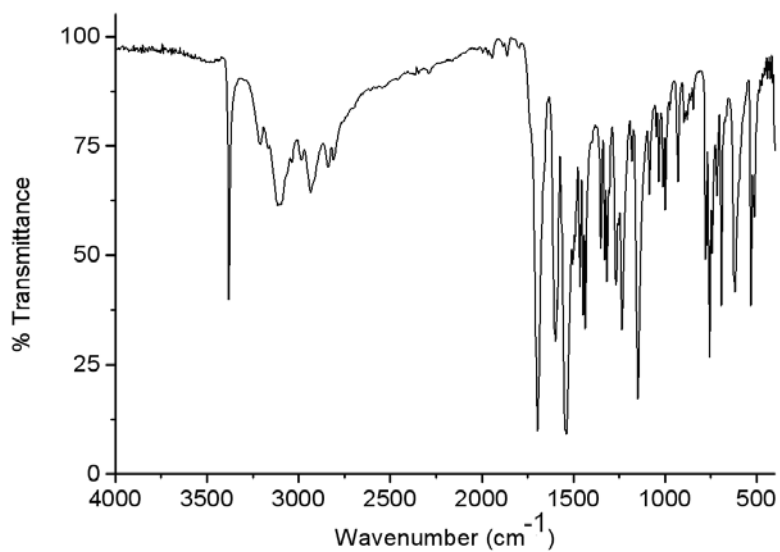
Fig. 2.5 IR spectrum of 2-formylpyridine-N⁴-phenylsemicarbazone.
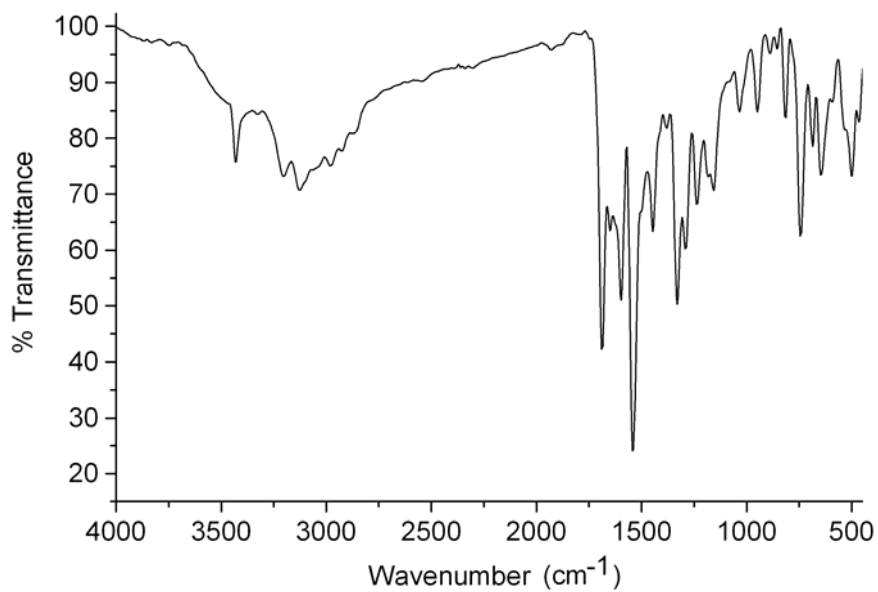
Fig. 2.6 IR spectrum of 3-ethoxysalicylaldehyde-N⁴-phenylsemicarbazone.
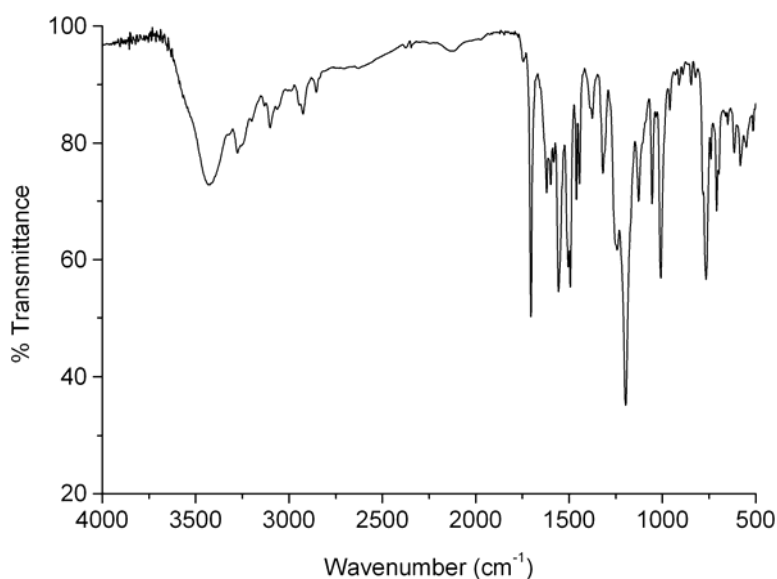
Fig. 2.7 IR spectrum of 2-benzoylpyridine-N⁴-phenylsemicarbazone.

2.3.4. Electronic spectral studies

Table 2.6 Electronic spectral assignments of the semicarbazone ligands

Compound	$\pi \rightarrow \pi^*$ and $n \rightarrow \pi^*$
HL^1	32000, 38100, 42500
H$_2$L^2	30887, 33960, 43227
HL^3	32660, 37797, 42793

The tentative assignments of the significant electronic spectral bands of ligands are presented in Table 2.6. The electronic spectra of HL^1, H$_2$L^2 and HL^3 in methanol solution show the following absorption maxima. Bands in the range 30887-43227 cm^{-1} corresponding to $\pi \rightarrow \pi^*$ and $n \rightarrow \pi^*$ transitions of the benzene ring, imine and carbonyl groups present in the semicarbazone moiety [13].
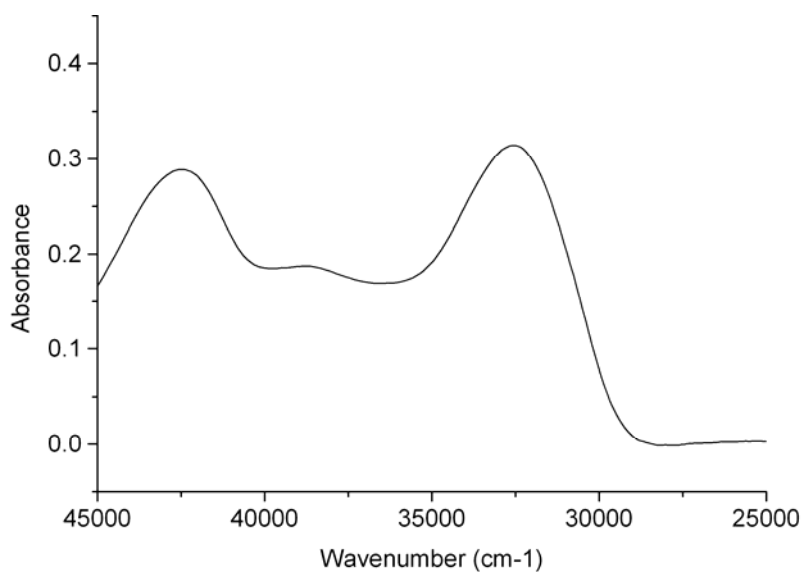
Fig.2.8 Electronic spectrum of 2-formylpyridine-N^4-phenylsemicarbazone.
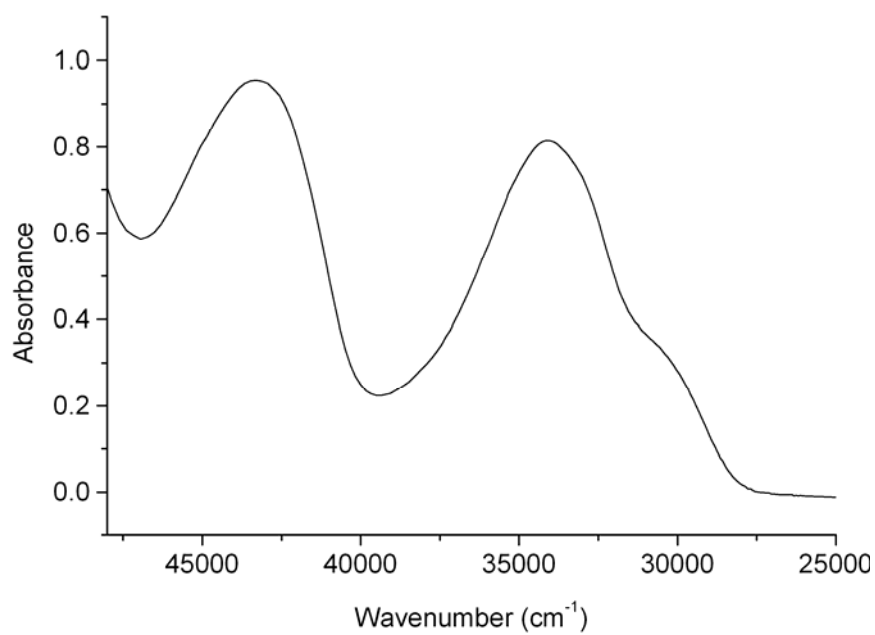
Fig. 2.9 Electronic spectrum of 3-ethoxysalicylaldehyde-N^4-phenylsemicarbazone.
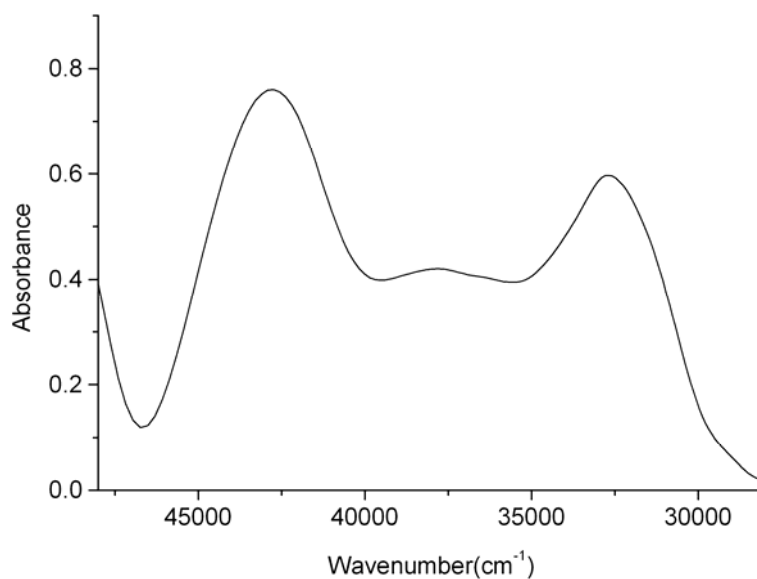
Fig. 2.10 Electronic spectrum of 2-benzoylpyridine-N^4-phenylsemicarbazone.

2.3.5. ^{1}H NMR spectral studies

^{1}H NMR spectrum of HL^1

In the ^{1}H NMR spectrum of HL^1, the signal for ^{2}N–H is observed at $\delta =$ 9.75 ppm. The ^{4}N–H is observed as a singlet at $\delta =$ 8.39 ppm whereas the ^{2}N–H is found at 9.75 which were found with very low intensity after D$_2$O exchange. A singlet at $\delta =$ 7.95 ppm was attributed to the protons of the aldehyde group which is now condenzed with ^{1}N atom of the semicarbazide moiety.
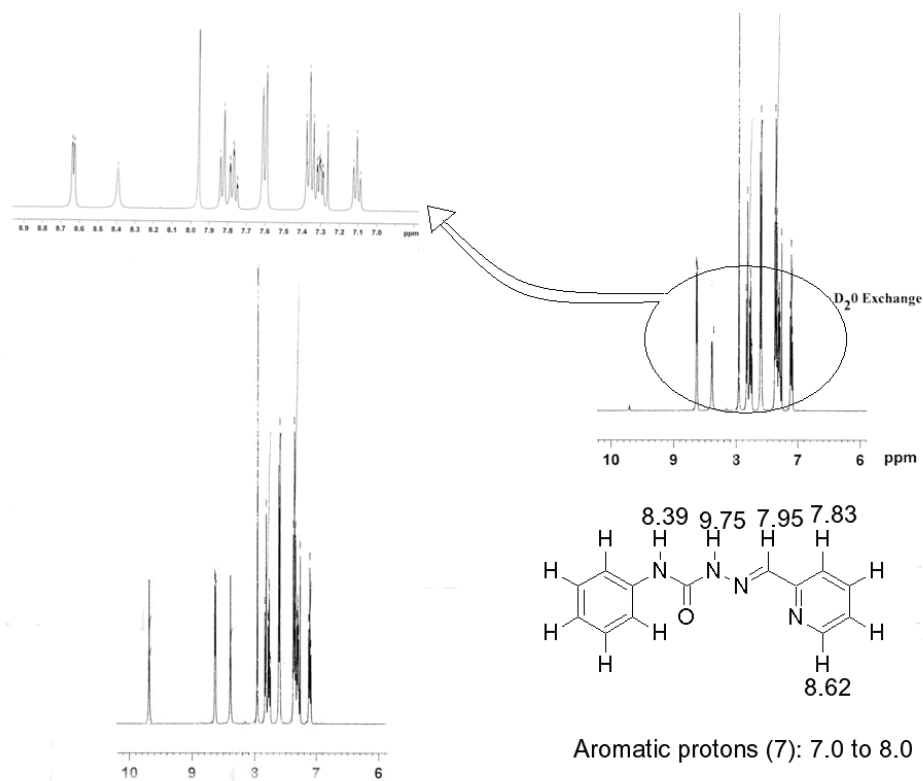
Fig. 2.11 ¹H NMR spectral assignments of 2-formylpyridine-N⁴-phenylsemicarbazone.

The proton near to the ring nitrogen is observed as doublet at 8.62 ppm due to coupling with neighbor ring H. Other signals having triplets and doublets in the range from 7.0 to 8.0 are due to the five protons from phenyl ring and the rest of the two protons left without assignment in the pyridine ring as shown in Fig. 2.11.

¹H NMR spectrum of H₂L²

¹H NMR spectrum of the ligand H₂L² is recorded in CDCl₃. The ¹H resonances were assigned on the basis of chemical shift values and multiplicities. These give insight into the average effective magnetic fields present, interaction of the nuclear spin with the adjacent atoms and the number of equivalent protons. The assignments of the ─NH and ─OH

protons were made by comparison with the spectra recorded in D_2O. ^1H NMR spectral assignment is based on the positions of the atoms given in Fig. 2.12. ^1H NMR spectrum reveals five signals for the salicylaldehyde moiety and three signals for the N-substituted phenyl group. The signal for ^2NH is observed as a singlet at δ = 9.01 ppm [14]. The ^4NH proton is observed as a singlet at δ = 7.74. The signal for OH proton is observed at δ = 10.75. These values are in agreement with 2-hydroxyacetophenone N(4)-substituted semicarbazones [15]. These protons are shifted downfield because they are attached to heteroatom and so are easily subjected to hydrogen bonding and are decoupled by the electrical quadrupole effects.
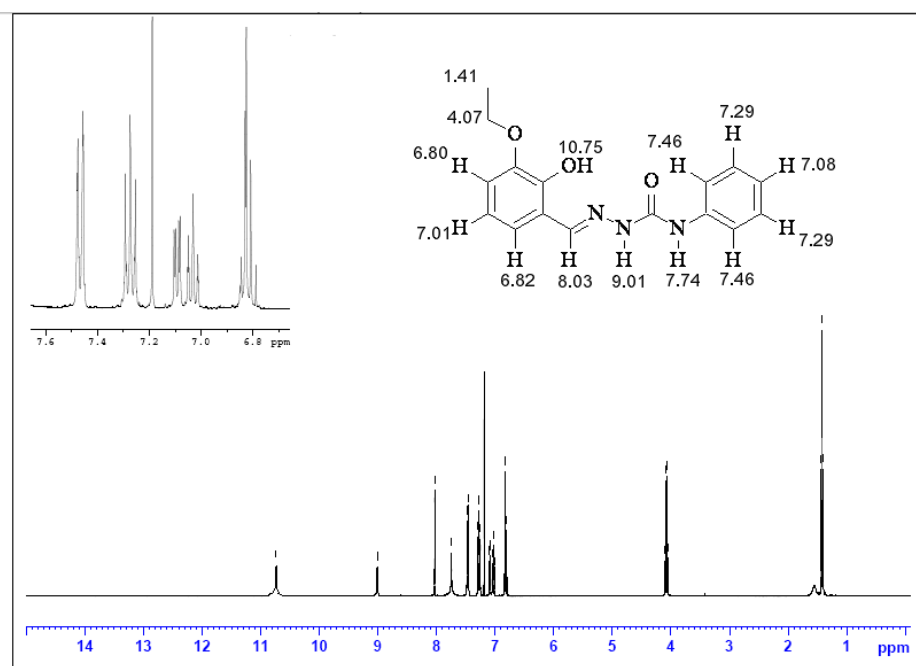
Fig. 2.12 ^1H NMR spectrum and the assignment of 3-ethoxysalicylaldehyde-N⁴-phenylsemicarbazone

Aromatic protons of the 3-ethoxysalicylaldehyde ring protons appear at δ = 6.80(*d*); 7.01 (t); 6.82(*d*) and the ethoxy protons are found at δ =4.08 (q) and δ

=1.42 (t) due to CH_2 and CH_3 protons respectively. Aromatic protons of the N^4-phenyl ring were observed as three signals *viz.*, δ = 7.46(*d*); 7.29(*t*); 7.08 (*t*).

^{1}H NMR spectrum of HL^3

The ^{1}H NMR spectrum of HL^3 in DMSO shows two singlets at δ = 11.70 ppm and δ = 9.20 ppm which correspond to ^{2}N–H and ^{4}N–H respectively. The downfield value of ^{4}N–H proton is due to the deshielding effect of the phenyl group. The signal for ^{2}N–H is more downfield because of hydrogen bonding to the oxygen of DMSO [15,16]. The downfield shifts of these protons are also assigned to their hydrogen bonding interactions with adjacent nitrogen atom of the pyridine ring. Hydrogen bonding decreases the electron density around the proton and thus moves the proton absorption to a lower field [17]. The aromatic protons of the two phenyl groups are assigned to the multiplet which appears at δ values in the range 7-8.5 ppm [18]. ^{1}H NMR spectrum of HL^3 is presented in Fig. 2.13.
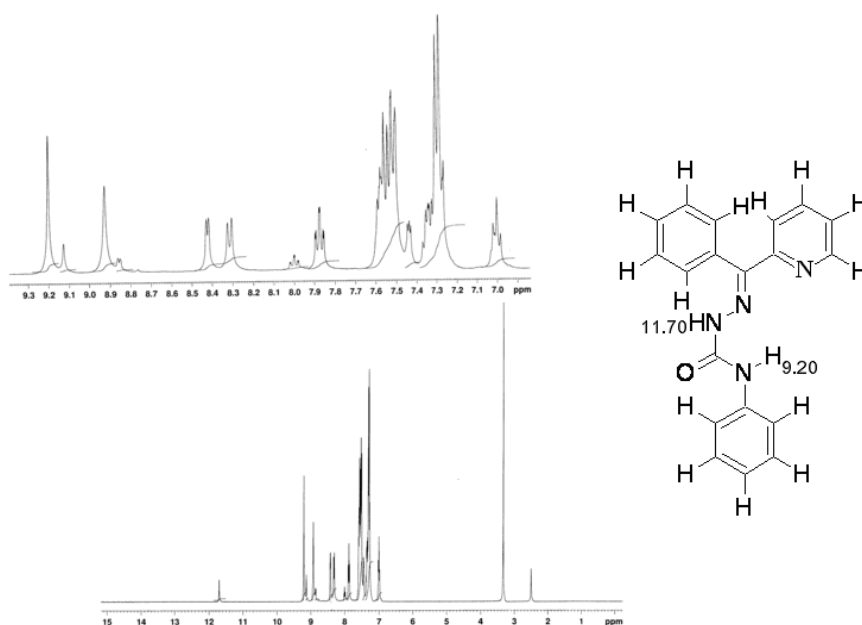
Fig. 2.13 ^{1}H NMR spectrum of 2-benzoylpyridine-N^4-phenylsemicarbazone.

Conclusions

This chapter presents the details regarding the syntheses of three (HL^1, H$_2$L^2, HL^3) NNO and ONO donor ligands. Elemental analysis data are consistent with the empirical formulae of ligands. The compounds are further characterized by IR, and electronic spectral studies. IR spectra of the ligands indicate that they exist in the amido form and the single crystal XRD of the ligand H$_2$L^2 confirms the existence. The connectivities between some of the carbon and hydrogen atoms were established by ^{1}H NMR spectral studies. Single crystal XRD of the ligand H$_2$L^2 suggest that it is a planar molecule having intramolecular and intermolecular hydrogen bonding between them and π···π interactions play major role in packing of those molecules in the unit cell.

References

[1]   J.R. Dimmock, G.B. Baker, Epilepsia 35 (1994) 648.

[2]   S.N. Pandeya, A.K. Agarwal, A. Singh, J.P. Stables, Acta Pharmaceutica, 53 (2003)15.

[3]   U.L. Kala, S. Suma, M.R.P. Kurup, S. Krishnan, R.P. John, Polyhedron 26 (2007) 1427.

[4]   S.N. Pandeya, P. Yogeeswari, E.A. Sausville, A.B. Mauger, V.L. Narayanan, Arzneimittelforschung, 52 (2002) 103.

[5]   SMART and SAINT, Area Detector Software Package and SAX Area Detector Integration Program, Bruker Analytical X-ray; Madison, WI, USA, 1997.

[6]   SADABS, Area Detector Absorption Correction Program; Bruker Analytical X-ray; Madison, WI, 1997.

[7]   G.M. Sheldrick, SHELXTL-PLUS, Crystal Structure Analysis Package; Bruker Analytical X-Ray, Madison, WI, USA, 1997.

[8]   K. Brandenburg, Diamond Version 3.2g, Crystal Impact GbR, Bonn, Germany, 2010.

[9]   Y.-P. Tian, W.-T. Yu, C.-Y.Zhao, M.-H. Jiang, Z.-G. Cai, H.-K. Fun, Polyhedron 21 (2002) 1217.

[10]   R.P. John, A. Sreekanth, M.R.P. Kurup, H.-K. Fun, Polyhedron 24 (2005) 601.

[11]   A.K. El-Sawaf, D.X. West, F.A. El-Saied, R.M. El-Bahnasawy, Trans. Met. Chem. 23 (1998) 649.

[12]   H. Beraldo, A.M. Barreto, R.P. Vieira, A.P. Rebolledo, N.L. Speziali, C.B. Pinheiro, G. Chapuis, J. Mol. Struct. 645 (2003) 213.

[13]   A. Castineiras, E. Bermejo, D.X. West, L.J. Ackerman, J.V. Martinez, S.H-Ortega, Polyhedron 18 (1999) 1463.

[14]   U.L. Kala, Ph.D. Thesis, University of Kerala, 2007.

[15]   I.C. Mendes, L.R. Teixeira, R. Lima, T.G. Carneiro, H. Beraldo, Trans. Met. Chem. 24 (1999) 655.

[16]   W.F. Nacif, H. Beraldo, D.X. West, Spectrochim. Acta 57A (2001) 1847.

[17]   R.M. Silverstein, G.C. Bassler, T.C. Morrill, Spectrometric Identification of Organic Compounds, 4th ed. Wiley, New York, 1981.

[18]   P. Bindu, M.R.P. Kurup, Indian J. Chem. 36A (1997) 1094.

.........................ৰৰৰ.........................

Syntheses, spectral studies and structures of nickel(II) complexes of N^4-phenylsemicarbazones

3.1. Introduction

Nickel is one of the five ferromagnetic elements. The most common oxidation state of nickel is +2, though 0, +1, +3 and +4 Ni complexes are also observed. Nickel is a very abundant natural element. The principal ore mineral is pentlandite: $(Ni,Fe)_9S_8$. The ionic radius of divalent nickel is close to that of divalent iron and magnesium, allowing the three elements to substitute for one another in the crystal lattices of some silicates and oxides. It is also widely used for many other alloys, such as nickel brasses and bronzes, and alloys with copper, chromium, aluminum, lead, cobalt, silver and gold.

The substituted derivatives of N^4-phenylsemicarbazone and their complexes with different metal ions have drawn special attention due to their interaction with enzymes. Nickel forms four, five and six coordinate complexes *viz*, square planar, tetrahedral, trigonal bipyramidal, square pyramidal and octahedral geometries. The coordination compounds of nickel are also studied for their magnetic behavior. Labile four-coordinated nickel(II)

complexes with tridentate semicarbazone ligands exhibit antibacterial activities, where as six coordinated nickel(II) complexes with semicarbazone ligands show no activities against the test microorganisms [1]. Hence the nickel species in various coordination environments are of interest to inorganic biochemists.

This chapter includes a brief discussion of general reagents and the physicochemical methods employed for the preparation and characterization of nickel complexes derived from two semicarbazones viz. 2-formylpyridine-N^4-phenylsemicarbazone [HL^1] and 2-benzoylpyridine-N^4-phenylsemicarbazone [HL^3].

3.2. Experimental

3.2.1. Materials

Nickel(II) acetate tetrahydrate, nickel(II) perchlorate hexahydrate, potassium thiocyanate, sodium azide and nickel(II) bromide were commercial products of higher grade (Aldrich) and used without further purification.

3.2.2. Synthesis of complexes

3.3.2.1. *Synthesis of [Ni(HL^1)(OAc)(SCN)]·3H$_2$O (1)*

Ni(OAc)$_2$·4H$_2$O (0.248 g, 1 mmol) in 15 ml of methanol was added to the methanolic solutions of HL^1 (0.240 g, 1 mmol) and KSCN (0.097 g, 1 mmol) followed by refluxing for 3 h. The compound formed was filtered, washed with ether and dried over P$_4$O$_{10}$ *in vacuo*.

3.3.2.2. *Synthesis of [NiL^{1}N$_3$] (2)*

A methanolic solution of the semicarbazone, HL^1 (0.240 g, 1 mmol) in 20 ml was refluxed with a mixture of methanolic solutions of Ni(OAc)$_2$·4H$_2$O

(0.248 g, 1 mmol) and NaN_3 (0.065 g, 1 mmol) for 4 h. The compound formed was filtered, washed with ether and dried over P_4O_{10} *in vacuo.*

3.3.2.3. *Synthesis of [Ni(HL^1)$_2$] (ClO$_4$)$_2$ · $3\frac{1}{2}$ H$_2$O (3)*

A mixture of methanolic solutions of HL^1 (0.240 g, 1 mmol) and $Ni(ClO_4)_2$·$6H_2O$ (0.166 g, 1 mmol) was refluxed for 4 h. Green colour single crystals suitable for single crystal XRD were separated on slow evaporation.

3.3.2.4. *Synthesis of [Ni(L^3)$_2$] (4)*

$Ni(OAc)_2$·$4H_2O$ (0.248 g, 1 mmol) in 20 ml of methanol was added to a methanolic solution of HL^3 (0.316 g, 1 mmol) and refluxed for 3 h. The compound formed was filtered, washed with ether and dried over P_4O_{10} *in vacuo.*

3.3.2.5. *Synthesis of [NiL^{3}Br] (5)*

HL^3 (0.316 g, 1 mmol) was dissolved in 20 ml of methanol and refluxed with a methanolic solution of $NiBr_2$ (0.218 g, 1 mmol) for 3 h. The compound formed was filtered, washed with ether and dried over P_4O_{10} *in vacuo.*

3.2.3. Physical measurements

Elemental analyses were carried out using a Vario EL III CHNS analyzer at the SAIF, Kochi, India. Infrared spectra were recorded on a JASCO FT-IR-5300 Spectrometer in the range 4000-400 cm^{-1} using KBr pellets and Electronic spectra were recorded on a UV-vis Double Beam UVD-3500 Spectrophotometer using solution in methanol at the Department of Applied Chemistry, Cochin University of Science and Technology, Kochi 22, India. The molar conductivities were measured in DMF (10^{-3} M) solutions at 298 K with a Systronic model 303 direct-reading conductivity bridge. TG-DTG analyses of

the complexes were carried out under nitrogen at a heating rate of 10 $^{\circ}$C min^{-1} in the range 50-1000 $^{\circ}$C using a Perkin Elmer Pyris Diamond TG/DTA analyzer at the Department of Applied Chemistry, CUSAT, Kochi, India.

3.2.4. X-ray crystallography

Single crystals of compound $[Ni(HL^1)_2](ClO_4)_2 \cdot 3\frac{1}{2} H_2O$ (**3**) suitable for X-ray diffraction studies were grown from its solution by slow evaporation at room temperature. A single crystal of dimensions 0.30x0.25x0.2 mm^3 of this complex was selected and mounted on a Bruker SMART APEX diffractometer, equipped with a graphite crystal incident-beam monochromator, and a fine focus sealed tube with Mo Kα ($\lambda = 0.71073$ Å) as the X-ray source. The crystallographic data along with details of structure solution refinements are given in Table 3.1. The unit cell dimensions were measured and the data collection was performed at 293(2) K. Bruker SMART software was used for data acquisition and Bruker SAINT software for data integration [2]. Absorption corrections were carried out using SADABS based on Laue symmetry using equivalent reflections [3]. The structure was solved by direct methods and refined by full-matrix least-squares calculations with the SHELXL–97 software package [4]. The graphics tool used was DIAMOND version 3.2g [5]. All non-hydrogen atoms were refined anisotropically, and all H atoms on C and N were placed in calculated positions, guided by difference maps and refined isotropically, with C–H and N–H bond distances of 0.93 Å and 0.86 Å.

Table 3.1 Crystal refinement parameters of complex **3**

Parameters	Description
Empirical formula	2($C_{26} H_{24} N_8 Ni O_2$), 4(Cl O_4), 7(O)
Formula weight	1588.24
Color	green
Temperature (T) K	293(2)
Wavelength (Mo Kα) (Å)	0.71073
Crystal system	triclinic
Space group	P-1
Cell parameters	
a	11.395(2) Å
b	15.476(3) Å
c	21.074(4) Å
α	72.33(3)°
β	81.55(3)°
γ	82.94(3)°
Volume V (Å^3)	3490.6(12)
Z	2
Calculated density (ρ) (Mg m^{-3})	1.511
Absorption coefficient, μ(mm^{-1})	0.783
F(000)	1624.0
Crystal size (mm^3)	0.30 x 0.25 x 0.2
θ range for data collection	2.520 to 28.115°
Limiting indices	-13≤h≤13, -18≤k≤18, -25≤l≤25
Reflections collected	50011
Unique Reflections (R$_{int}$)	12224 [R(int) = 0.0713]
Completeness to θ	25.00 (99.3 %)
Absorption correction	Semi-empirical from equivalents
Maximum and minimum transmission	0.855 and 0.791
Refinement method	Full-matrix least-squares on F^2
Data / restraints / parameters	12224 / 0 / 911
Goodness-of-fit on F^2	1.049
Final R indices [I > 2σ (I)]	R$_1$ = 0.0814, wR$_2$ = 0.2198
R indices (all data)	R$_1$ = 0.1372, wR$_2$ = 0.2798
Largest difference peak and hole (e Å^{-3})	0.766 and -0.618

$R_1 = \Sigma||F_o| - |F_c|| / \Sigma|F_o|$
$wR_2 = [\Sigma w(F_o^2 - F_c^2)^2 / \Sigma w(F_o^2)^2]^{1/2}$

3.3. Results and discussion

3.3.1. Analytical measurements

Semicarbazones, HL^1/HL^3 react with corresponding Ni(II) salts in the molar ratio 2:1 in the compounds **3** and **4**, whereas in all other compounds the molar ratio is 1:1 (Table 3.2). These two ligands coordinated the metal in the amido form in complexes [Ni(HL^1)(OAc)(SCN)]·3H$_2$O (**1**) and **3** but in iminol form in the other complexes. This phenomenon is confirmed by the single XRD studies and other spectral studies. The molar conductivities of the complexes show that all Ni(II) complexes are non-conductors except the complex **3** which shows 1:1 electrolytic nature because of the ClO$_4^-$ anions present are outside the coordination sphere of the complex. The magnetic moments of the complexes were calculated from the magnetic susceptibility measurements at room temperature. The complexes **1**, **3** and [Ni(L^3)$_2$] (**4**) are paramagnetic while the complexes [NiL^{1}N$_3$] (**2**) and [NiL^{3}Br] (**5**) show diamagnetic behavior and their effective magnetic moments are found to be in the range 2.897-3.177 B.M. The diamagnetic moments for the complexes **2** and **5** suggest square planar coordination environment around the metal centre of these complexes. Five-coordinate high spin Ni(II) complexes have magnetic moment values in the range of 3.0-3.4 B.M. but the lower values for the compound **1** suggests the anomalous magnetic moment of the Ni(II) complex. This behavior is due to the quenching of the orbital contribution to the magnetic moment due to distortion of D$_{3h}$ symmetry [6]. The magnetic moment values of the complexes **3** and **4** are found to be consistent with the octahedral geometry (2.94-3.24) of Ni(II) complexes.

Table 3.2 Preliminary analytical data of Ni(II) complexes of HL[1] and HL[3]

Compound	color	Found (Calculated) %				μ (B.M.)	$\Lambda_M{}^a$
		C	H	N	S		
[Ni(HL[1])(OAc)(SCN)]·3H₂O (**1**)	green	40.91 (40.88)	4.51 (4.50)	14.95 (14.90)	6.41 (6. 82)	2.897	1
[NiL[1]N₃] (**2**)	green	45.87 (45.93)	3.20 (3.26)	28.78 (28.84)	-	0.269	30
[Ni(HL[1])₂] (ClO₄)₂ · $3\frac{1}{2}$ H₂O (**3**)	green	38.86 (38.98)	3.42 (3.90)	13.96 (13.99)	-	3.177	97
[Ni(L[3])₂] (**4**)	green	65.60 (66.20)	4.40 (4.39)	16.29 (16.25)	-	3.021	22
[NiL[3]Br] (**5**)	green	50.32 (50.27)	3.72 (3.33)	12.03(12.34)	-	0.342	20

[a]Molar conductivity (ohm^{-1}cm^{2}mol^{-1}), 10^{-3} M DMF at 298 K

3.3.2. Crystal structure of the complex 3

Figure 3.1 shows the molecular structure of the Ni(II) complex **3** which has two molecules in its asymmetric unit with the atom numbering scheme. There are four ClO_4^- counter ions outside the coordination spheres and seven lattice water molecules also found in the complex. Both the Ni atoms are hexacoordinated and the coordination around the Ni(II) ion can be best described as a distorted octahedron with a NiO_2N_4 chromophore. Each Ni atom is coordinated by two azomethine nitrogen atoms, two oxygen atoms and two pyridyl nitrogen atoms. The coordination of oxygen from the semicarbazone ligand occurs in the neutral form. This is confirmed by the double bond nature of C7A–O1A (1.218 Å) and N2A–C7A (1.363 Å) bond lengths [7]. The C8A–N1A and N1A–N2A bond distances are 1.251(9) Å and 1.338(8) Å respectively, which reveal extensive delocalization over the entire coordination framework is restricted. The angle between the phenyl ring of the semicarbazide part and the pyridyl ring of the ligand varies greatly for the two molecules with angles from 83.2(5)° to 3.4(5)°. Table 3.3 shows the selected bond lengths and bond angles of the compound **3**.
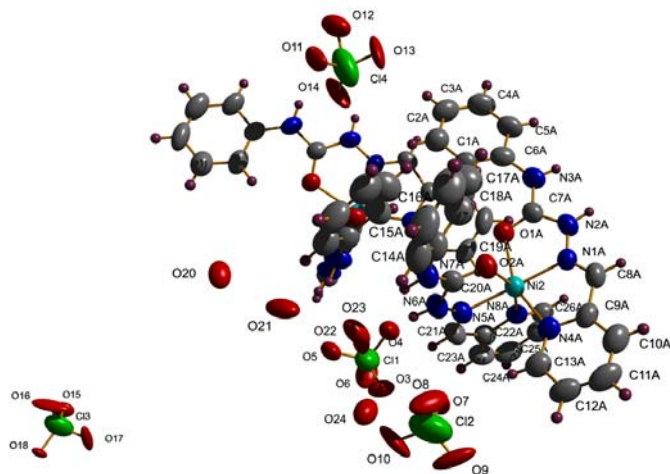
Fig.3.1. Structure and labeling diagram for compound $[Ni(HL^1)_2] (ClO_4)_2 \cdot 3\frac{1}{2} H_2O$ (**3**).

**Table 3.3** Selected bond lengths (Å) and bond angles (°) of compound **3**.

Bond lengths		Bond angles	
Ni(1)—N(1B)	1.998(6)	N(1B)—Ni(1)—N(5B)	174.8(2)
Ni(1)—N(5B)	2.002(6)	N(1B)—Ni(1)—N(4B)	78.4(2)
Ni(1)—N(4B)	2.073(6)	N(5B)—Ni(1)—N(4B)	106.7(2)
Ni(1)—O(2B)	2.084(5)	N(1B)—Ni(1)—O(2B)	77.3(2)
Ni(1)—N(8B)	2.085(6)	N(5B)—Ni(1)—O(2B)	97.8(2)
Ni(1)—O(1B)	2.116(5)	N(4B)—Ni(1)—O(2B)	154.9(2)
Ni(2)—N(1A)	1.997(6)	N(1B)—Ni(1)—N(8B)	100.4(2)
Ni(2)—N(5A)	2.001(6)	N(5B)—Ni(1)—N(8B)	78.0(3)
Ni(2)—N(8A)	2.077(6)	N(4B)—Ni(1)—N(8B)	96.4(2)
Ni(2)—N(4A)	2.086(6)	O(2B)—Ni(1)—N(8B)	94.1(2)
Ni(2)—O(2A)	2.109(5)	N(1B)—Ni(1)—O(1B)	104.8(2)
Ni(2)—O(1A)	2.110(5)	N(5B)—Ni(1)—O(1B)	76.7(2)
O(1A)—C(7A)	1.218(8)	N(4B)—Ni(1)—O(1B)	90.8(2)
O(2A)—C(20A)	1.230(9)	O(2B)—Ni(1)—O(1B)	89.4(2)
O(1B)—C(7B)	1.231(8)	N(8B)—Ni(1)—O(1B)	154.7(2)
O(2B)—C(20B)	1.239(8)	N(1A)—Ni(2)—N(5A)	176.9(3)
N(1A)—C(8A)	1.251(9)	N(1A)—Ni(2)—N(8A)	104.1(2)
N(1A)—N(2A)	1.338(8)	N(5A)—Ni(2)—N(8A)	79.0(3)
N(2A)—C(7A)	1.363(9)	N(1A)—Ni(2)—N(4A)	78.3(2)

|			
N(3A)—C(7A)	1.354(9)	N(5A)—Ni(2)—N(4A)	101.4(2)
N(3A)—C(6A)	1.404(10)	N(8A)—Ni(2)—N(4A)	97.2(2)
N(4A)—C(13A)	1.318(10)	N(1A)—Ni(2)—O(2A)	100.6(2)
N(4A)—C(9A)	1.348(10)	N(5A)—Ni(2)—O(2A)	76.3(2)
N(5A)—C(21A)	1.265(10)	N(8A)—Ni(2)—O(2A)	155.2(2)
N(5A)—N(6A)	1.350(9)	N(4A)—Ni(2)—O(2A)	90.5(2)
N(6A)—C(20A)	1.357(10)	N(1A)—Ni(2)—O(1A)	76.7(2)
N(7A)—C(20A)	1.330(10)	N(5A)—Ni(2)—O(1A)	103.3(2)
N(7A)—C(19A)	1.422(11)	N(8A)—Ni(2)—O(1A)	93.5(2)
N(8A)—C(26A)	1.314(10)	N(4A)—Ni(2)—O(1A)	154.5(2)
N(8A)—C(22A)	1.373(9)	O(2A)—Ni(2)—O(1A)	89.4(2)
N(1B)—C(21B)	1.257(9)	C(7A)—O(1A)—Ni(2)	112.5(5)
N(1B)—N(2B)	1.341(8)	C(20A)—O(2A)—Ni(2)	113.0(5)
N(2B)—C(20B)	1.372(9)	C(7B)—O(1B)—Ni(1)	112.6(5)
N(3B)—C(20B)	1.327(9)	C(20B)—O(2B)—Ni(1)	113.5(4)
N(3B)—C(19B)	1.411(10)	C(8A)—N(1A)—N(2A)	126.2(6)
N(4B)—C(26B)	1.332(9)	C(8A)—N(1A)—Ni(2)	118.6(5)
N(4B)—C(22B)	1.344(9)	N(2A)—N(1A)—Ni(2)	115.1(4)
N(5B)—C(8B)	1.255(10)	N(1A)—N(2A)—C(7A)	114.4(6)
N(5B)—N(6B)	1.334(8)	C(13A)—N(4A)—Ni(2)	129.3(5)
N(6B)—C(7B)	1.359(10)	C(9A)—N(4A)—Ni(2)	112.8(5)
N(7B)—C(7B)	1.337(9)	C(21A)—N(5A)—N(6A)	126.0(7)
N(7B)—C(6B)	1.383(11)	C(21A)—N(5A)—Ni(2)	118.1(5)
N(8B)—C(9B)	1.334(9)	N(6A)—N(5A)—Ni(2)	115.9(5)
N(8B)—C(13B)	1.352(9)		

Ni–N$_{azo}$ bond distances coordinated *via* azomethine N atom are shorter than the other Ni–O and Ni–N$_{py}$ bond distances. The Ni–O bond distances are consistent with the reported values (1.97–2.11 Å) of similar semicarbazone Ni(II) complexes [8]. Even though the bond lengths around the coordination sphere are found to be almost same for the molecules A and B, the bond angles of these two molecules are slightly different, especially the angles of N1–Ni–O2 and N5–Ni–O2 are found to show a discrepancy to a great extent from

100.6(2) to 77.3(2)° and from 76.3(2) to 97.8(2)° respectively for A and B molecules.

The unit cell packing diagram of the complex **3** viewed along *a* axis is given in Figure 3.2. It can be seen that the molecules are packed with the help of strong hydrogen bonding with the perchlorate and water molecules so that they are sandwiched along b axis as shown in Fig. 3.3. Ring puckering analysis shows that the rings containing metal atom have no significant puckering. Meanwhile, many very weak π···π interactions with the minimum centroid-centroid distance of 3.906 Å (Fig. 3.4) and two types of C–H···π interactions which has higher packing motif than π···π interactions are also observed in the molecular packing (Fig. 3.5).
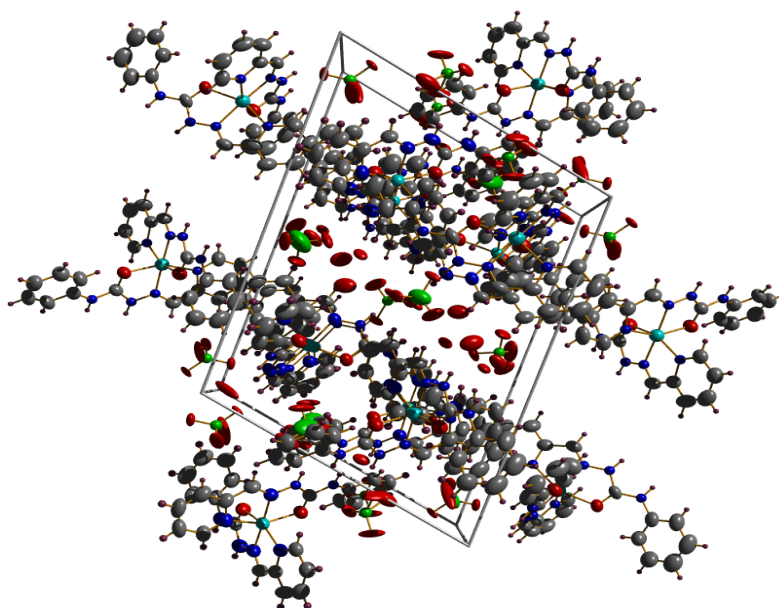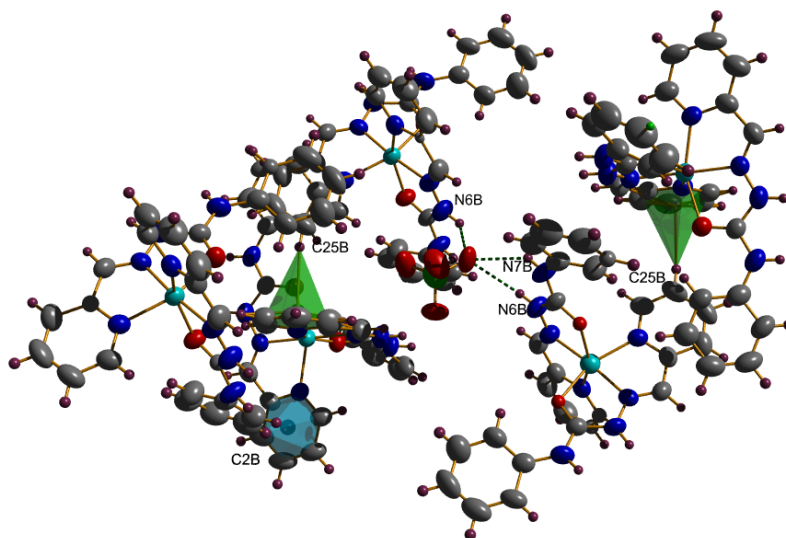

Fig. 3.2 Unit cell packing diagram of compound **3** along a axis.
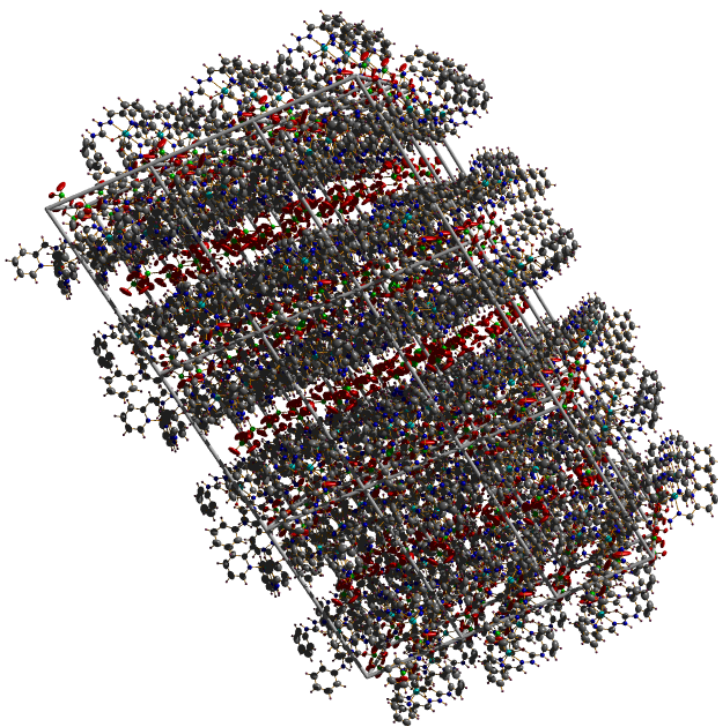
Fig.3.3 Packing arrangement of the molecules of the compound **3** along b axis.
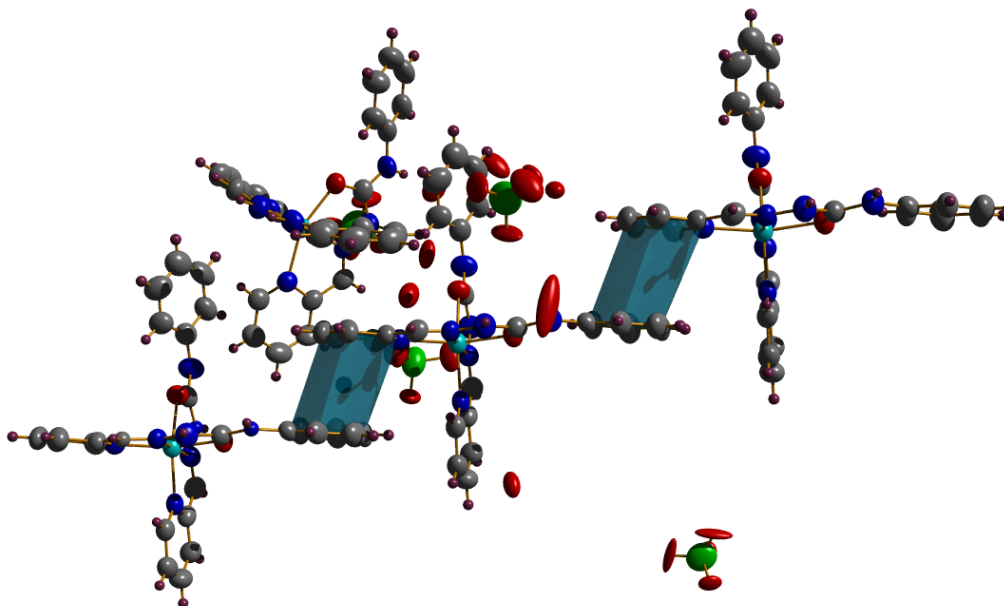
Fig.3.4 $\pi\cdots\pi$ Interactions between Cg13 and Cg16 rings in the compound **3**.

Fig. 3.5 C—H···π interactions in the complex **3**.

A number of hydrogen bonding interactions with perchlorate anions and lattice water molecules play an important role in the molecular packing by linking adjacent molecules together. A detailed description of hydrogen bonding interactions is shown in Fig. 3.6 and the values are tabulated in Table 3.4.
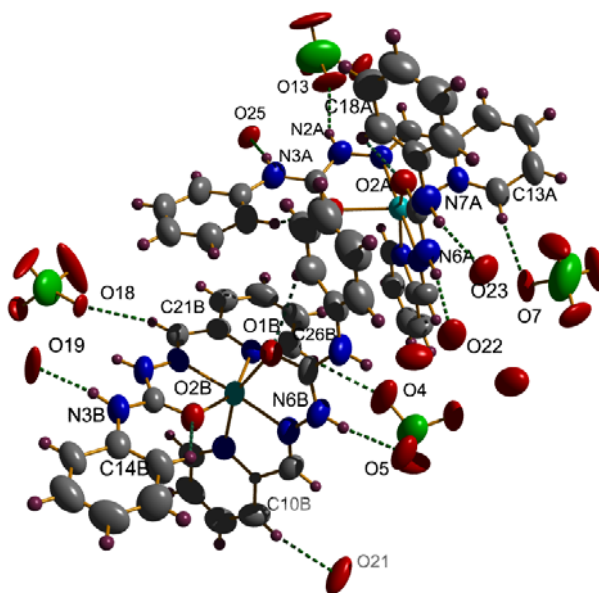
Fig. 3.6 Intermolecular hydrogen bonding network of the compound **3**.

Table 3.4 Interaction parameters of the compound **3**

Hydrogen bonding interactions

D−H···A	D−H (Å)	H···A (Å)	D···A (Å)	∠D−H···A(°)
N2A−H2A···O13 [a]	0.86	2.02	2.82(2)	155
N2B−H2B···O18 [b]	0.86	2.11	2.863(10)	146
N3A−H3A···O25 [b]	0.86	2.00	2.823(14)	161
N3B−H3B···O19	0.86	1.99	2.831(15)	168
N6A−H6A···O22	0.86	2.01	2.849(13)	165
N6B−H6B···O5	0.86	2.28	2.953(11)	135
N6B−H6B···O5 [c]	0.86	2.49	3.184(11)	139
N7A−H7A···O23	0.86	2.05	2.901(12)	168
N7B−H7B···O5 [c]	0.86	2.35	3.072(10)	141
C1A−H1A···O1A	0.93	2.29	2.868(10)	120
C5B−H5B···O1B	0.93	2.41	2.859(11)	110
C10B−H10B···O21 [c]	0.93	2.58	3.42(2)	151
C13A−H13A···O7	0.93	2.60	3.51(2)	168
C14B−H14B···O2B	0.93	2.26	2.828(10)	119
C18A−H18A···O2A	0.93	2.36	2.855(11)	113
C21B−H21B···O18 [b]	0.93	2.52	3.196(13)	130
C26B−H26B···O4	0.93	2.55	3.481(13)	173

C−H···π interactions

X−H(I)···Cg(J)	H···Cg (Å)	X···Cg (Å)	∠X−H···Cg (°)
C(2B)−H(2B1)···Cg(5) [d]	2.82	3.570(12)	138
C(25B)−H(25B)···Cg(6) [e]	2.86	3.762(11)	165

π ···π interactions

Cg(I)···Cg(J)	Cg···Cg (Å)	α (°)	β (°)	γ(°)
Cg(16) ···Cg(13) [d]	3.907(6)	3.4(5)	27.17	28.78
Cg(13) ···Cg(16) [f]	3.906(6)	3.4(5)	28.78	27.17

Cg (5) = N4A, C9A, C10A, C11A, C12A, C13A
Cg (6) = N8A, C22A, C23A, C24A, C25A, C26A
Cg (13) = N4B, C22B, C23B, C24B, C25B, C26B
Cg (16) = C14B, C15B, C16B, C17B, C18B, C19B
Equivalent position codes: a =1-x,1-y,-z; b = x,y,-1+z ; c = 1-x,1-y,1-z;
d = 1+x,y,z ; e = x,y,z ; f= -1+x,y,z ; D, donor; A, acceptor; Cg, centroid

3.3.3. Infrared spectral studies

The significant bands observed in IR spectra of complexes of HL[1] and HL[3] with the tentative assignments are presented in Table 3.5. IR spectra of complexes are presented in Figures 3.7-3.10. The comparison of the IR spectra

of the semicarbazones and the complexes revealed significant variations in the characteristic bands due to coordination with the central metal ion. It is found that the azomethine ν(C=N) band suffered a negative shift in the region 1555-1578 cm^{-1} in all the complexes from **1-5**. The shifting of the azomethine band to lower frequency is attributed to the conjugation of the *p* orbitals on the double bond with the *d* orbital on the metal ion with reduction of the force constant. The bands observed in the region 1596-1598 cm^{-1} in the IR spectra of complexes [NiL^{1}N$_3$] (**2**), [Ni(L^3)$_2$] (**4**) and [NiL^{3}Br] (**5**) are assigned to the newly formed C=N as a result of enolization of the semicarbazones on coordination. These bands are absent in the compounds **1** and **3**, which suggest that the coordination of the semicarbazones in these complexes are in the amido form. This is again supported by the presence of bands at 1648 cm^{-1} for these complexes, attributed to ν(C=O) which are absent in all other complexes. This is further evidenced by the C=O bond length (1.218 Å) of the complex **3** in its crystal structure. The coordination through the azomethine nitrogen is further evidenced by the ν(Ni–N$_{azo}$) bands in the region 502-512 cm^{-1} for the complexes **1-5**. The ν(N–N) frequency shifts to 1127-1170 cm^{-1} which also support coordination through azomethine nitrogen in all the complexes.

The complex [Ni(HL^1)(OAc)SCN]·3H$_2$O (**1**) exhibits a sharp band at 2107 cm^{-1} and a medium band at 692 cm^{-1} correspond to monodentate S bonded thiocyanate group. We can distinguish the nature of the linkage of the acetate anion in the complex depending upon the mode of coordination of the anion [9]. The presence of asymmetric stretching bands at 1577, 1548 cm^{-1} and two symmetric stretching bands at around 1331 cm^{-1} indicates monodentate nature of the acetato group in the complex. A single broad band at 1089 cm^{-1} and a strong band at 624 cm^{-1} for the complex **3** is the evidence for the existence of uncoordinated perchlorate anions in the complex [10]. The presence of a strong

sharp stretching band at 2052 cm^{-1}, a strong band at 1331 cm^{-1} and a broad band at 692 cm^{-1} assignable to δ(N–N–N) for the compound **2** indicates the presence of coordinated azido group in the complex.

Table 3.5 IR spectral assignments for Ni(II), Co(II) and Mn(II) complexes

| Compound	ν(OH)	ν(NH)	ν(C=N$_{azo}$)	ν(CO)	ν(C=N)^a	ν(N–N)	ν(M–N$_{azo}$)
HL^1	-	3372	1597	1693	-	1143	-
[Ni(HL^1)(OAc)(SCN)]·3H$_2$O (**1**)	3405	-	1578	1648	-	1170	506
[NiL^{1}N$_3$] (**2**)	-	-	1561	-	1598	1139	512
[Ni(HL^1)$_2$](ClO$_4$)$_2$ · 3 $\frac{1}{2}$ H$_2$O (**3**)	3440	-	1555	1648	-	1158	506
HL^3	-	3375	1600	1698	-	1132	-
[Ni(L^3)$_2$] (**4**)	-	-	1561	-	1596	1133	512
[NiL^{3}Br] (**5**)	-	-	1561	-	1598	1127	506

^{a} Newly formed C=N stretching frequency during complexation
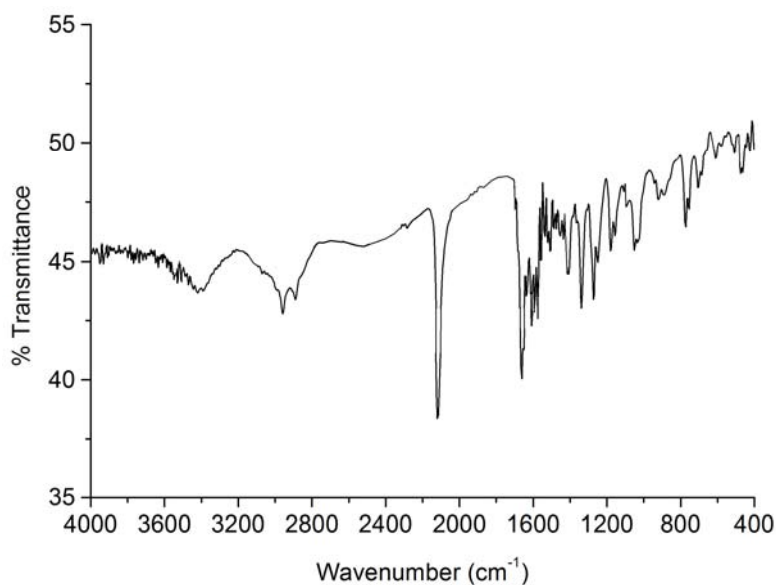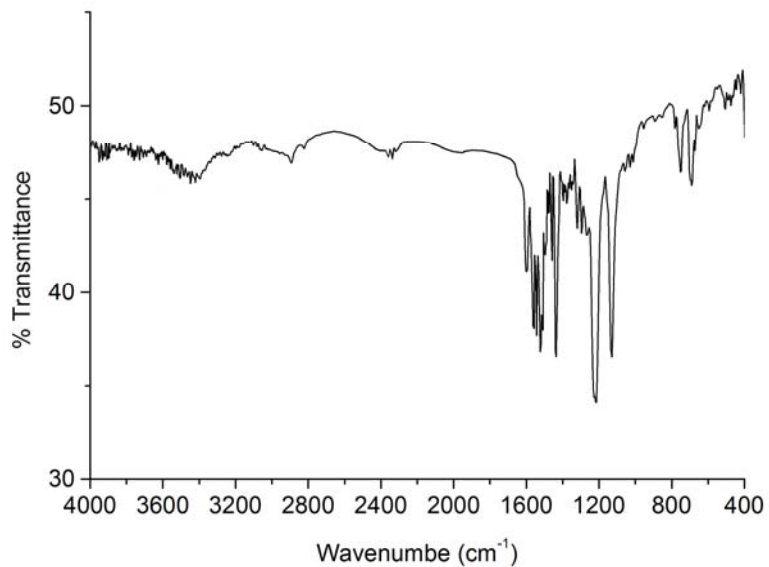

Fig.3.7 IR spectrum of the compound [Ni(HL^1)(OAc)(SCN)]·3H$_2$O (**1**).
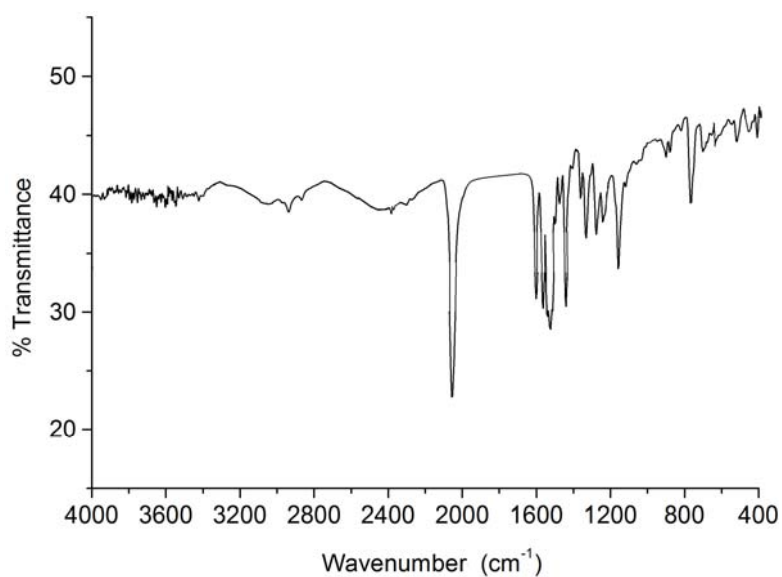
Fig.3.8 IR spectrum of the compound [NiL^{1}N$_3$] (**2**).
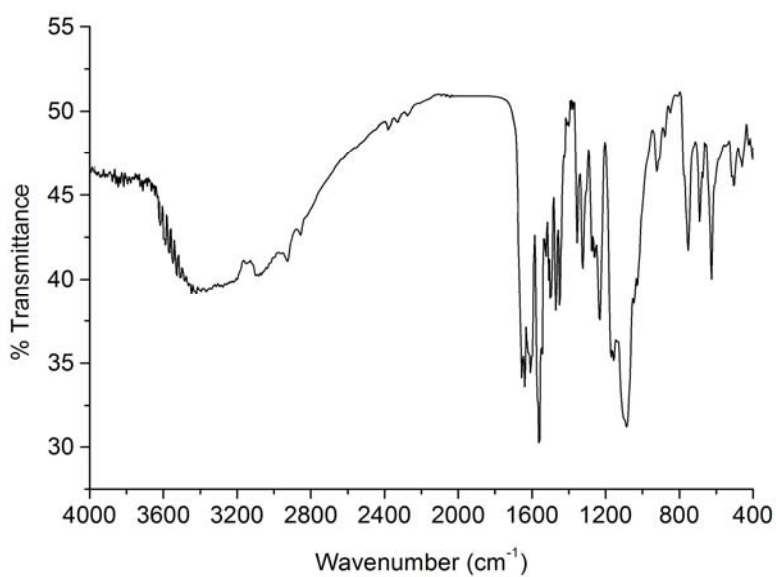
Fig. 3.9 IR spectrum of the compound [Ni(HL^1)$_2$](ClO$_4$)$_2 \cdot 3\frac{1}{2}$H$_2$O (**3**).

**Fig.3.10** IR spectrum of the compound $[NiL^3_2]$ (**4**).
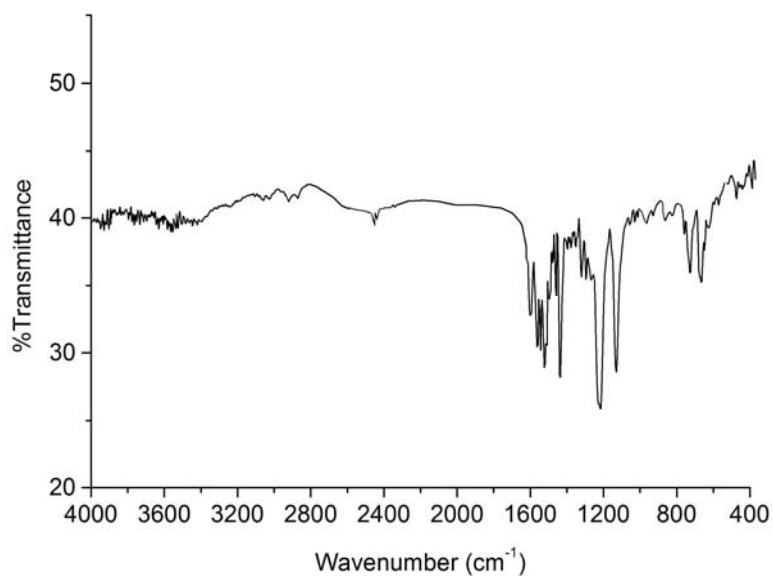
Fig. 3.11 IR spectrum of the compound $[NiL^3Br]$ (**5**).
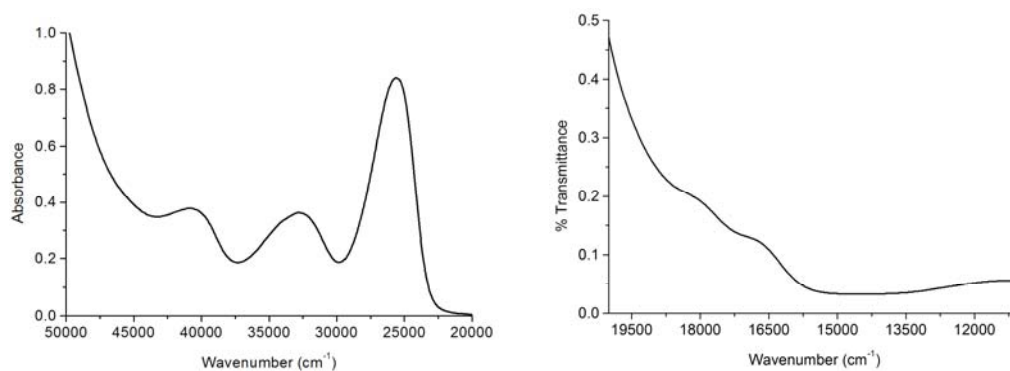
3.3.4. Electronic spectral studies

The electronic spectral data of the complexes in methanol and DMF are summarized in Table 3.6 and the electronic spectra are shown in Fig. 3.12-3.16. The electronic transitions of semicarbazones, HL^1 and HL^3 suffered considerable shift on coordination. The shift of the intraligand bands to longer wavelength region in the complexes is the result of weakening of C–O bond and the conjugation system being enhanced upon complexation [11]. In the electronic spectra of compounds **1-5,** bands in the region 31900-42300 cm^{-1} are assigned as intraligand transitions. The intense bands observed in the range 23700-25600 cm^{-1} are assigned as O→Ni LMCT transitions. The ground state of Ni(II) in an octahedral coordination is $^3A_{2g}$ and expects three spin allowed transitions $^3T_{2g}(F)\leftarrow^3A_{2g}(F)(v_1)$, $^3T_{1g}(F)\leftarrow^3A_{2g}(F)(v_2)$ and $^3T_{1g}(P)\leftarrow^3A_{2g}(F)(v_3)$, the ground state of a square planar Ni(II) complex is $^1A_{1g}$ and it is expected to have three possible transitions as $^1E_g\leftarrow^1A_{1g}$, $^1A_{2g}\leftarrow^1A_{1g}$ and $^1B_{1g}\leftarrow^1A_{1g}$ and the ground state of a pentacoordinated Ni(II) complex is $^3B_1(F)$ and it is expected transitions as $^3E(F)\leftarrow^3B_1(F)$ and $^3A_2,$ $^3E(P)\leftarrow^3B_1(F)$ in an increasing order of energy. However, two bands observed for the complexes **3** and **4** can be assigned to the transitions corresponding to an octahedral geometry $^3T_{2g}(F)\leftarrow^3A_{2g}(F)(v_1)$, $^3T_{1g}(F)\leftarrow^3A_{2g}(F)(v_2)$ and the bands found in the complexes $[NiL^1N_3]$ (**2**) and $[NiL^3Br]$ (**5**) can be assigned to the transition correspond to a square planar geometry $^1Eg\leftarrow^1A_{1g}$, $^1A_{2g}\leftarrow^1A_{1g}$ respectively in the increasing order of energies. The band observed for the complex $[Ni(HL^1)(OAc)(SCN)]\cdot3H_2O$ (**1**) can be assumed as the transition from $^3B_1(F)$ to $^3E(F)$ corresponds to a pentacoordinated Ni(II) complex.

Table 3.6 Electronic spectral assignments of Ni(II) complexes

Compound	*d-d*	LMCT	Intraligand transitions
HL^1	-	-	32000, 38100, 42500
$[Ni(HL^1)(OAc)(SCN)]\cdot 3H_2O$ (**1**)	16500	25600	32680, 42300
$[NiL^1N_3]$ (**2**)	16750, 18000	25600	32850, 40680
$[Ni(HL^1)_2](ClO_4)_2 \cdot 3\frac{1}{2}H_2O$ (**3**)	16450, 17900	25400	32550, 40200
HL^3	-	-	32660, 37797, 42793
$[Ni(L^3)_2]$ (**4**)	16100, 17450	23700	32400, 39200
$[NiL^3Br]$ (**5**)	16250, 17300	24250	32900, 40800
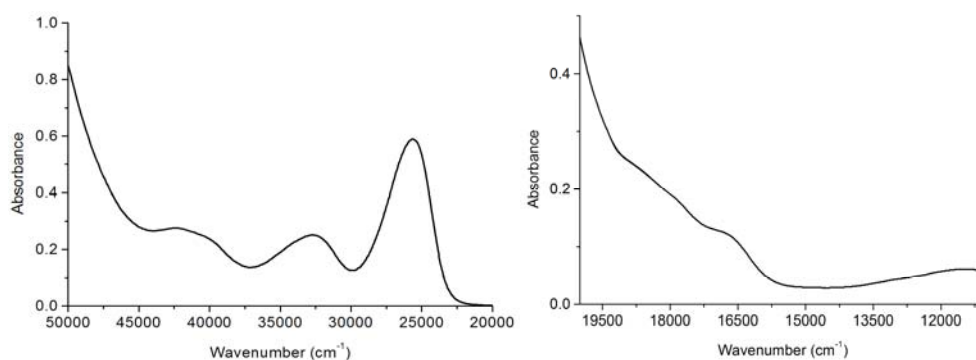
Fig.3.12 Electronic spectra of complex $[Ni(HL^1)(OAc)(SCN)]\cdot 3H_2O$ (**1**).

.

Fig.3.13 Electronic spectra of complex $[NiL^1N_3]$ (**2**).
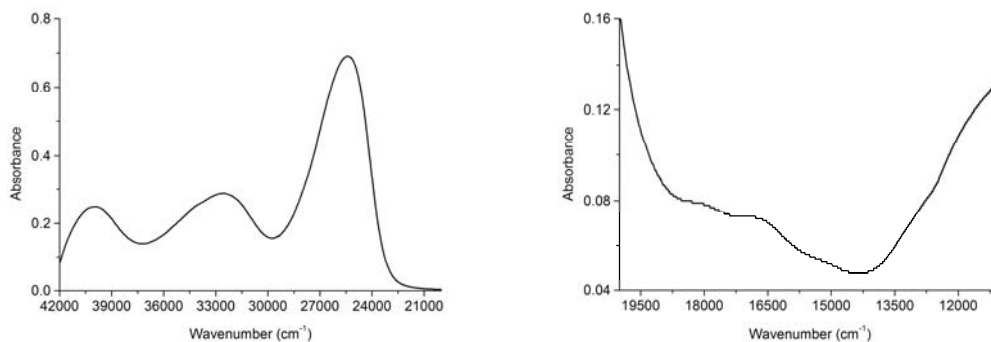
Fig.3.14. Electronic spectra of complex $[Ni(HL^1)_2](ClO_4)_2 \cdot 3\frac{1}{2} H_2O$ (**3**).

Fig. 3.15 Electronic spectra of complex $[Ni(L^3)_2]$ (**4**).

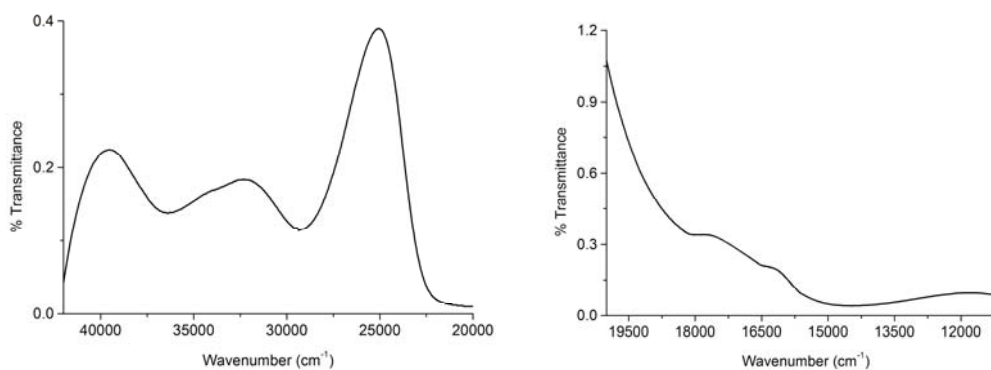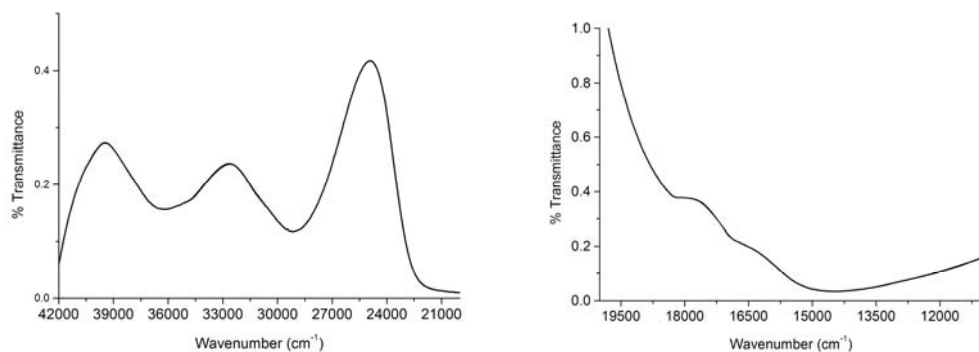**Fig.3.16** Electronic spectra of complex $[NiL^3Br]$ (**5**).

3.3.5. Thermogravimetric studies

Analyses show that the weight losses for lattice water are below 200 ºC [12] and weight losses due to coordinated water molecules are in the range of 200-350 ºC [13]. There are two weight losses in the complex [Ni(HL^1)(OAc)(SCN)]·3H$_2$O (**1**) below 200 ^{o}C with a first weight loss of 3.8% and the second loss of 7.8% showing the presence of totally three moles of lattice water molecules in the complex. The other weight losses (75.6%) may be assignable to the weight loss during the removal of ligand, acetato group and thiocyanato group together in the temperature range from 200 to 950 ^{o}C (Fig.3.17).
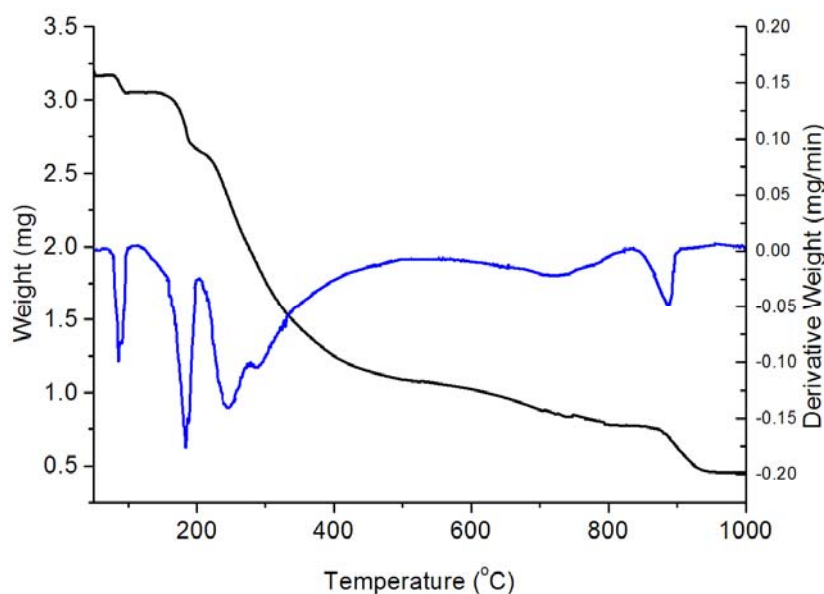
Fig. 3.17 Thermogram of the compound [Ni(HL^1)(OAc)(SCN)]·3H$_2$O (**1**).

The compound **4** has no weight loss below 200 ^{o}C which confirms supporting with the IR data that it contains no lattice water molecules. The total weight loss (91.8%) of the two weight losses in the range from 300-750 ^{o}C is due to the removal of the two ligands from the complex (Fig. 3.18).
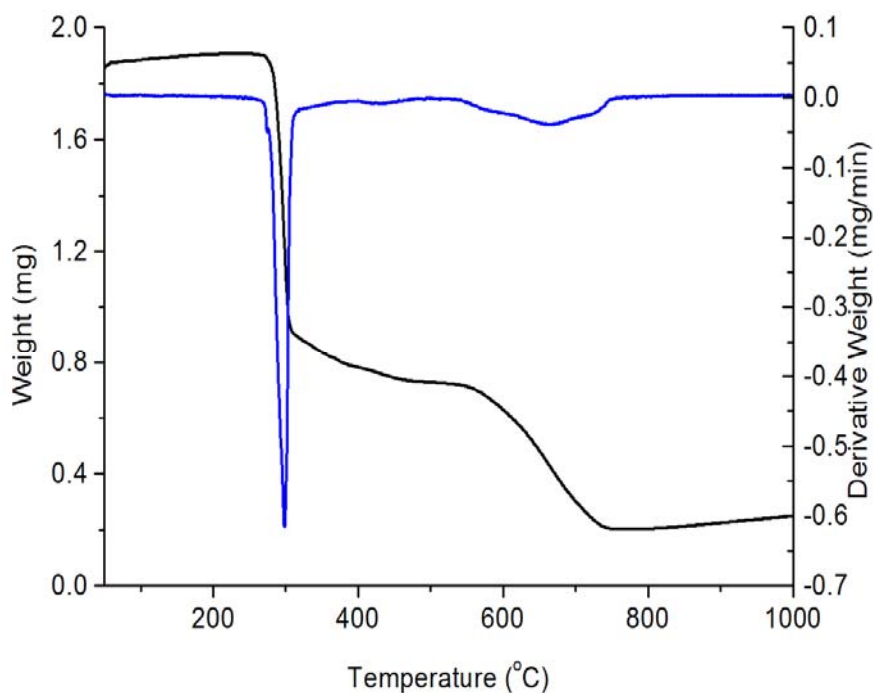
Fig. 3.18 Thermogram of the compound [Ni(L^3)$_2$] (**4**).

The complex **5** contains no lattice water molecule since its thermogram does not show any weight loss below 200 ^{o}C (Fig. 3.19). The bromine atom of the complex **5** is removed first with a weight loss of 17.7% at around 300 ℃. The other weight loss (69.6%) can be assigned to the dissociation of the ligand in the complex. It is understood that the decomposition of this ligand occurs at around 600 ^{o}C from the TG/DTA studies of Cd complexes of the ligand (HL^3) in Chapter 6. This phenomenon further confirms the stoichiometric ratio of the ligand and metal in the complex.
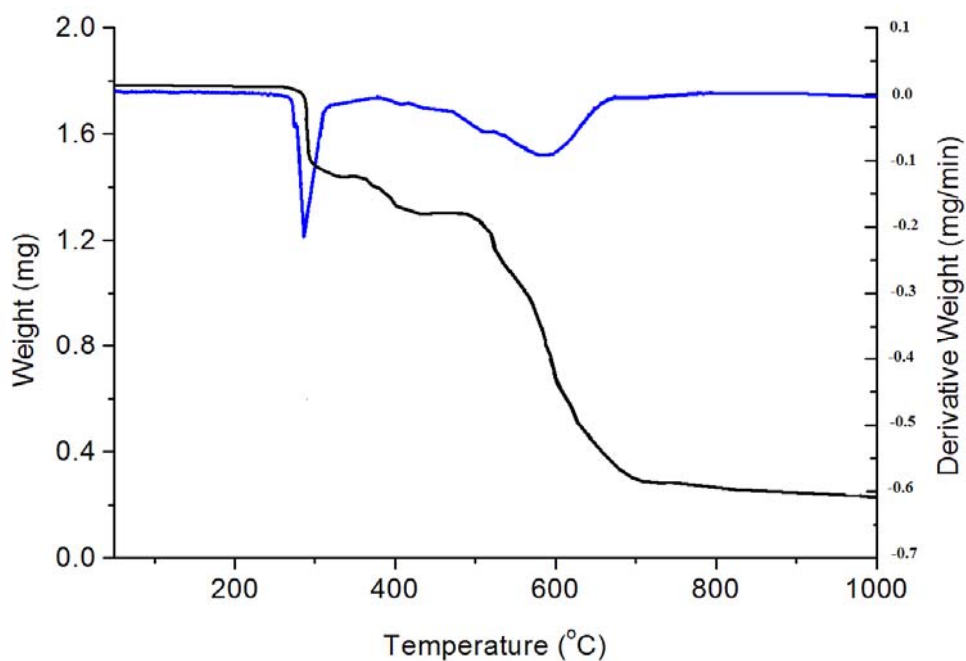
Fig. 3.19 Thermogram of the compound [NiL^{3}Br] (**5**).

References

[1]   N.C. Kasuga, K. Sekino, M. Ishikawa, A. Honda, M. Yokoyama, S. Nakano, N. Shimada, C. Koumo, K. Nomiya, J. Inorg. Biochem. 96 (2003) 298.

[2]   SMART and SAINT, Area Detector Software Package and SAX Area Detector Integration Program, Bruker Analytical X-ray; Madison, WI, USA, 1997.

[3]   SADABS, Area Detector Absorption Correction Program; Bruker Analytical X-ray; Madison, WI, 1997.

[4]   G.M. Sheldrick, *SHELXTL-PLUS,* Crystal Structure Analysis Package; Bruker Analytical X-Ray, Madison, WI, USA, 1997.

[5]   K. Brandenburg, Diamond Version 3.1d, Crystal Impact GbR, Bonn, Germany, 2006.

[6]   R.D. Bereman, G.D. Shields, Inorg. Chem. 18 (1979) 946.

[7]   M. Maneiro, M.R. Bermejo, M. Fondo, A.M. Gonzalez, J. Sanmartin, J.C. Garcia-Monteagudo, R.G. Pritchard, A.M. Tyryshkin, Polyhedron 20 (2001) 711.

[8]   V. M. Leovac, L. S. Jovanovic, V. S. Jevtovic, G. Pelosi, F. Bisceglie, Polyhedron 26 (2007) 2971.

[9]   K. Nakamoto *in* Infrared and Raman Spectra of Inorganic and Coordination Compounds, 4th ed., John Wiley & Sons, New York, 1986.

[10]   B.S. Garg, M.R.P. Kurup, S.K. Jain, Y.K. Bhoon, Trans. Met. Chem. 13 (1988) 309.

[11]   L. Latheef, M.R.P. Kurup, Polyhedron 27 (2008) 35.

[12]   S. Kavlak, H. Kaplan Can, Z.M.O. Rzaev, A. Guner, J. Appl. Polym. Sci. 100 (2006) 3926.

[13]   G.A. Nazri, C. Julien, Solid State Ionics 80 (1995) 271.

........................ண&ண&ண&........................

Syntheses, spectral studies and structures of copper(II) complexes of N⁴-phenylsemicarbazones

4.1. Introduction

Thiosemicarbazones and their metal complexes have been the subject of extensive investigations because of their potential pharmacological properties and a wide variation in their modes of bonding and stereochemistry whereas the semicarbazone analogs received much less attention. However, semicarbazones are also reported to possess versatile structural features [1] and very good antifungal and antibacterial properties [2,3]. Their metal complexes, especially those containing copper(II) are more active than uncoordinated semicarbazones and this enhanced biological activity of metal semicarbazones has been under investigation for some time [4]. A variety of semicarbazones and their metal complexes possess anti-protozoa and anti-convulsant activity also [5].

4.2. Experimental

4.2.1. Materials

Copper acetate monohydrate, copper chloride, copper sulfate pentahydrate, sodium azide, potassium thiocyanate, copper bromide, copper

nitrate (all are BDH, AR grade) were used without further purification. All solvents were purified by standard methods.

4.2.2. Syntheses of the complexes

Copper complexes were synthesized with salts containing different anions and with the two ligands (HL^1, H_2L^2) synthesized using the procedure reported in Chapter 2. These copper complexes are synthesized as described below.

4.2.2.1. Synthesis of [Cu(HL^1)Cl$_2$] (6)

A hot solution of the ligand HL^1 (0.240 g, 1 mmol) in methanol (20 ml) was mixed with 1 mmol of $CuCl_2 \cdot 2H_2O$ (0.170 g, 1 mmol) in methanol solution with constant stirring. The mixture was then stirred for 4 h. The complex was filtered and washed thoroughly with water, methanol and ether and finally dried over P_4O_{10} *in vacuo*.

4.2.2.2. Synthesis of [Cu$_2$L$_2^1$(NO$_3$)$_2$]·H$_2$O (7)

To a hot methanolic solution (15 ml) of the ligand HL^1 (0.240 g, 1 mmol) was added to the methanol solution of $CuNO_3 \cdot 3H_2O$ (0.241 g, 1 mmol). The mixture was stirred for 3 h. The formed product was filtered, washed with water, ethanol and ether and dried *in vacuo* over P_4O_{10}.

4.2.2.3. Synthesis of [Cu(HL^1)(SO$_4$) ·½ H$_2$O (8)

The compound $[CuHL^1(SO_4)] \cdot \frac{1}{2}H_2O$ (**8**) was obtained when a hot solution of HL^1 (0.240 g, 1 mmol) in methanol (15 ml) was mixed with a hot filtered solution of $CuSO_4 \cdot 5H_2O$ (0.249 g, 1 mmol) in methanol with constant stirring. The mixture was then stirred for 5 h. and the resulting solution was kept for two days at room temperature. The crystals formed were separated,

filtered, washed with ethanol, water and ether and then dried over P_4O_{10} *in vacuo*.

4.2.2.4. Synthesis of [Cu$_2$L$^1_2$(OAc)$_2$] (9)

A hot solution of the ligand HL^1 (0.240 g, 1 mmol) in methanol (20 ml) was mixed with hot filtered solution of $Cu(OAc)_2 \cdot H_2O$ (0.199 g, 1 mmol) in methanol with constant stirring. The mixture was then stirred for 3 h. Then the mixture was kept at room temperature for two days. On cooling single crystals suitable for single crystal XRD were collected.

4.2.2.5. Synthesis of [Cu$_2$L$^1_2$Br$_2$]·H$_2$O (10)

A hot solution of HL^1 (0.240 g, 1 mmol) in methanol (10 ml) was mixed with a hot filtered solution of $CuBr_2$ (0.223 g, 1 mmol) in methanol with constant stirring. The mixture was stirred for 4 h. The mixture was kept overnight at room temperature. The formed microcrystals were filtered and thoroughly washed with water, methanol and ether and finally dried over P_4O_{10} *in vacuo*.

4.2.2.6. Synthesis of [CuL^{1}NCS]·2H$_2$O (11)

A hot solution of HL^1 (0.240 g, 1 mmol) in methanol (10 ml) was mixed with a hot filtered methanolic solution of potassium thiocyanate (0.097 g, 1 mmol). A hot filtered solution of $Cu(OAc)_2 \cdot H_2O$ (0.199 g, 1 mmol) was added to this with constant stirring. The mixture was then refluxed for 3 h. The complex separated as microcrystals was filtered and thoroughly washed with water, methanol and ether and finally dried over P_4O_{10} *in vacuo*.

4.2.2.7. Synthesis of [Cu$_2$L$_2^1$N$_3$] (12)

A hot methanolic solution of HL^1 (0.240 g, 1 mmol) (10 ml) was mixed with a hot filtered methanolic solution of sodium azide (0.065 g, 1 mmol). A

hot filtered solution of Cu(OAc)$_2$·H$_2$O (0.199 g, 1 mmol) was added to this with constant stirring. The mixture was then refluxed for 3 h. On cooling, single crystals suitable for single crystal XRD were separated from the mixture.

4.2.2.8. Synthesis of [CuL^2(H$_2$O)] (13)

A hot solution of H$_2$L^2 (0.299 g, 1 mmol) in methanol (15 ml) was mixed with a hot filtered methanolic solution of Cu(OAc)$_2$·H$_2$O (0.199 g, 1 mmol) with constant stirring. The mixture was then refluxed for 3 h. The complex was filtered and thoroughly washed with water, methanol and ether and finally dried over P$_4$O$_{10}$ *in vacuo*.

4.2.2.9. Synthesis of [Cu$_2$(HL^2)$_2$Br$_2$(H$_2$O)$_2$] (14)

A hot solution of H$_2$L^2 (0.299 g, 1 mmol) in methanol (15 ml) was mixed with a hot filtered methanolic solution of CuBr$_2$ (0.223 g, 1 mmol) with constant stirring. The mixture was then refluxed for 4 h. The complex was filtered and thoroughly washed with water, methanol and ether and finally dried over P$_4$O$_{10}$ *in vacuo*.

4.2.3. Physical measurements

Carbon, hydrogen and nitrogen analyses were carried out using a Vario EL III CHNS analyzer at the SAIF, Kochi, India. Infrared spectra were recorded on a JASCO FT-IR-5300 Spectrometer in the range 4000-400 cm^{-1} using KBr pellets. Electronic spectra were recorded on a Cary 5000 version 1.09 UV-VIS-NIR Spectrophotometer using solutions in methanol and DMF. TG-DTG analyses of the complexes were carried out under nitrogen at a heating rate of 10 ^{o}C min^{-1} in the range 50-1000 ^{o}C using a Perkin Elmer Pyris Diamond TG/DTA analyzer at the Department of Applied Chemistry, CUSAT, Kochi, India.

3.2.4. X-ray crystallography

Single crystals of compounds [Cu$_2$L$^1_2$(OAc)$_2$] (**9**) and [Cu$_2$L$_2$(N$_3$)$_2$] (**12**) suitable for X-ray diffraction studies were grown from their solution by slow evaporation at room temperature. A single crystal of dimension 0.30x0.20x0.12 mm^3 of the complex **9** and 0.24x0.20x0.05 mm^3 of the complex **12** were selected and mounted on a Bruker SMART APEX diffractometer, equipped with a graphite crystal, incident-beam monochromator, and a fine focus sealed tube with Mo Kα (λ = 0.71073 Å) as the X-ray source. The crystallographic data along with details of structure solution refinements are given in Table 4.1. The unit cell dimensions were measured and the data collection was performed at 293(2) K. Bruker SMART software was used for data acquisition and Bruker SAINT software for data integration [6]. Absorption corrections were carried out using SADABS based on Laue symmetry using equivalent reflections [7]. The structure was solved by direct methods and refined by full-matrix least-squares calculations with the SHELXL–97 software package [8]. The molecular and crystal structures were plotted using DIAMOND version 3.2g [9]. All non-hydrogen atoms were refined anisotropically, and all H atoms on C and N were placed in calculated positions, guided by difference maps and refined isotropically, with C–H and N–H bond distances of 0.93 Å and 0.86 Å respectively except the N7–H7 hydrogen of the complex [Cu$_2$L$_2^1$N$_3$] (**12**) which was located from the difference Fourier maps and restrained using DFIX instruction with a distance of 0.83(2) Å.

Table 4.1 Crystal refinement parameters of complexes **9** and **12**

Parameters	Compound [Cu$_2$ L$^1_2$(OAc)$_2$] (**9**)	Compound [Cu$_2$L$^1_2$(N$_3$)$_2$] (**12**)
Empirical formula	C$_{30}$H$_{28}$Cu$_2$N$_8$O$_6$	C$_{26}$H$_{22}$Cu$_2$N$_{14}$O$_2$
Formula weight	723.70	689.68
Color	Black	Green
Temperature (T) K	293(2)	298(2)
Wavelength (Mo Kα) (Å)	0.71073	0.71073
Crystal system	Monoclinic	Monoclinic
Space group	$P2_1/c$	C_2/c
Cell parameters		
a	8.469(2) Å	21.809(3) Å
b	10.759(4) Å	7.1427(10) Å
c	18.044(11) Å	19.910(3) Å
α	90°	90°
β	102.68(4)°	93.034(2)
γ	90°	90°
Volume V (Å^3)	1604.0(12)	3097.1(7)
Z	2	4
Calculated density (ρ) (Mg m^{-3})	1.498	1.479
Absorption coefficient, μ(mm^{-1})	1.381	1.422
F(000)	740.0	1400.0
Crystal size (mm^3)	0.30 x 0.20 x 0.12	0.24 x 0.20 x 0.05
θ range for data collection	3.12 to 24.70°	1.87 to 25.92°
Limiting indices	-9≤h≤11, -12≤k≤14, -13≤l≤23	-26≤h≤26, -8≤k≤8, -24≤l≤24
Reflections collected	4230	14446
Unique Reflections (R$_{int}$)	3750 [R(int) = 0.0680]	3013 [R(int) = 0.0539]
Completeness to θ	27.70 (99.7 %)	25.92 (99.7 %)
Absorption correction	Semi-empirical from equivalents	Semi-empirical from equivalents
Maximum and minimum transmission	0.847 and 0.725	0.931 and 0.717
Refinement method	Full-matrix least-squares on F^2	Full-matrix least-squares on F^2
Data / restraints / parameters	3750 / 0 / 209	3013 / 1 / 203
Goodness-of-fit on F^2	1.008	1.002
Final R indices [I > 2σ (I)]	R$_1$=0.0613, wR$_2$=0.1448	R$_1$=0.0521, wR$_2$=0.1287
R indices (all data)	R$_1$=0.0843, wR$_2$=0.1767	R$_1$=0.8347, wR$_2$=0.1303
Largest difference peak and hole (e Å^{-3})	1.347 and -0.704	2.900 and -0.526

$R_1 = \Sigma||F_o| - |F_c|| / \Sigma|F_o|$ $wR_2 = [\Sigma w(F_o^2 - F_c^2)^2 / \Sigma w(F_o^2)^2]^{1/2}$

4. 3. Results and discussion

4.3.1. Analytical measurements

The analytical data of all the complexes are listed in Table 4.2. The CHN obtained showed that all the complexes are analytically pure. HL^1 and H_2L^2 react with copper(II) halides in the molar ratio 1:1 in complexes **6**, **8**, **11** and **13**. The ligand HL^1/H_2L^2 coordinates the metal in amido form in complexes **6**, **8** and **14** whereas HL^1 and H_2L^2 exist in monoanionic iminolate form in complexes **11** and **13** respectively. The complexes **7**, **9**, **10** and **12** are consistent with the general composition $Cu_2L_2Y_2$ where $Y=NO_3$, OAc, Br and N_3 respectively and the two copper atoms are bridged through Y in the case of complexes **7** and **12**. The magnetic measurement values of the complexes **7**, $[Cu_2 L^1_2(OAc)_2]$ (**9**), $[Cu_2L^1_2Br_2]\cdot H_2O$ (**10**) and $[Cu_2L_2^1N_3]$ (**12**) are found to be consistent with the similar reported Cu(II) complexes suggests that the above complexes are dimers. The complex $[CuL_2(H_2O)]$ (**13**) is coordinated only with the ligand H_2L^2 in anionic form. The complex $[Cu_2(HL^2)_2Br_2(H_2O)_2]$ (**14**) has a dimeric structure with two coordinated water molecules and their presence was further supported by TG data and magnetic susceptibility data.

Table 4.2 Preliminary analytical data of Cu(II) complexes of HL^1 and H_2L^2

Compound	Observed (Calculated)%				$\lambda_m{}^a$	$\mu_m{}^b$(BM)
	C	H	N	S		
$[Cu(HL^1)Cl_2]$ (**6**)	41.51 (41.67)	3.66 (3.23)	15.27 (14.95)	-	24	1.826
$[Cu_2L_2^1(NO_3)_2]\cdot H_2O$ (**7**)	41.33 (40.79)	3.25 (3.42)	18.82 (18.29)	-	52	1.037
$[Cu(HL^1)(SO_4)]\cdot \frac{1}{2} H_2O$ (**8**)	38.10 (38.19)	3.29 (3.20)	13.82 (13.70)	7.45 (7.84)	06	1.905
$[Cu_2 L^1_2(OAc)_2]$ (**9**)	48.29 (49.79)	3.78 (3.90)	14.93 (15.48)	-	7.6	1.04
$[Cu_2L^1_2Br_2]\cdot H_2O$ (**10**)	40.04 (39.86)	3.22 (3.09)	14.34 (14.30)	-	20	1.186
$[CuL^1(NCS)]\cdot 2H_2O$ (**11**)	42.61 (42.36)	3.28 (3.81)	18.02 (17.64)	8.60 (8.08)	11	1.743
$[Cu_2L^1_2(N_3)_2]$ (**12**)	45.10 (45.28)	2.49 (3.22)	28.20 (28.43)	-	01	1.20
$[CuL^2(H_2O)]$ (**13**)	48.99 (49.38)	4.52 (4.14)	11.61 (11.52)	-	04	1.713
$[Cu_2(HL^2)_2Br_2(H_2O)_2]$ (**14**)	40.31 (40.42)	4.05 (3.62)	9.30 (9.43)	-	23	1.109

^{a}molar conductivity (ohm^{-1}cm^{2}mol^{-1}), 10^{-3} M DMF at 298 K ^{b}magnetic susceptibility per metal atom.

The complexes are insoluble in most of the polar and non-polar solvents. Though some of the complexes are sparingly soluble in methanol many are soluble in DMF and DMSO. The conductivity measurements were made in DMF solutions and all complexes are found to be non-electrolytes [10].

The magnetic susceptibilities of the polynuclear complexes **7**, **9**, **10**, **12** and **14** suggest considerable interaction between metal centers and the magnetic moments fall in the range 1.037-1.20 B.M. and it can be assumed to be dinuclear complexes [11].

But the room temperature magnetic susceptibilities of the complexes formulated with one metal centre almost have the values very close to the expected spin only value of 1.73 B.M. for a d^9 copper system of its corresponding complexes in the polycrystalline state are in the range 1.713-1.905 B.M.

4.3.2. Crystal structure of complex [Cu$_2$ L1$_2$(OAc)$_2$] (9)

The single crystal X-ray diffraction study of the compound [Cu$_2$L$^1_2$(OAc)$_2$] (**9**) revealed that this compound is a dimer bridged through oxygen of the acetate moiety. The molecular structure of the compound along with atom numbering scheme is given in Fig. 4.1. The asymmetric unit is formed by one half of the molecule and the other half is related by a centre of inversion in the Cu(1)–O(2)–Cu(1A)–O(2A) ring.

The lattice nature is monoclinic space group $P2_1/c$. This structure contains two copper centers where each centre is pentacoordinated with azomethine nitrogen (N1), pyridyl nitrogen (N2), enolate oxygen (O1) of semicarbazone moiety and oxygens (O2, O2A) from two acetate groups. The compound exhibits a distorted square pyramidal geometry with the basal plane

occupied by semicarbazone ligand and the acetate oxygen (O2). Selected bond lengths (Å) and bond angles (°) of $[Cu_2L^1_2(OAc)_2]$ are shown in Table 4.3.

The oxygen (O2A) from acetate group of the adjacent monomer plugs into the axial position resulting in a dimer with a Cu⋯Cu separation of 3.398 Å. The bond lengths of Cu–N (~ 1.930 Å) and Cu–O (2.022 Å) are similar and shorter than that of Cu–O2 indicating the domination of semicarbazone moiety in the bonding. It is found that copper atom is closer to semicarbazone moiety than the acetato group. The Cu–$N_{pyridyl}$ bonds are larger by 0.117 Å than Cu–N_{imine} bonds which show the strength of azomethine nitrogen coordination.

The four coplanar basal atoms show a significant distortion from a square geometry as indicated by the N2–Cu1–O1 bond angle of 159.4(4)°. The deviation of the central copper atom from the basal plane in the direction of the axial oxygen is evident from the bond angles of N1–Cu1–O2, 111.7(4) and N2–Cu1–O2, 94.2(3). Most of the angles involving the central copper atoms are widely different from 90° and 180°, indicating significant distortion from the square pyramidal geometry.

Table 4.3 Selected bond lengths and bond angles of $[Cu_2L^1_2(OAc)_2]$ (**9**)

| Bond length (Å)		Bond angle (°)	
Cu(1)–N(2)	2.047(12)	N(1)–Cu(1)–N(2)	80.9(4)
Cu(1)–N(1)	1.930(9)	N(1)–Cu(1)–O(1)	78.6(4)
Cu(1)–O(1)	2.022(9)	N(2)–Cu(1)–O(1)	159.4(4)
Cu(1)–O(2)	2.401(7)	N(2)–Cu(1)–O(2)	94.2(3)
Cu(1)–O(2A)	1.942(8)	N(2)–Cu(1)–O(2^a)	100.4(4)
C(1)–O(1)	1.266(13)	N(1)–Cu(1)–O(2)	111.7(4)
C(8)–N(1)	1.271(17)	O(1)-Cu(1)-O(2)	91.7(3)
C(1)–N(3)	1.355(15)	N(1)-Cu(1)-O(2^a)	170.6(4)
Cu(1)⋯Cu(1^a)	3.398		
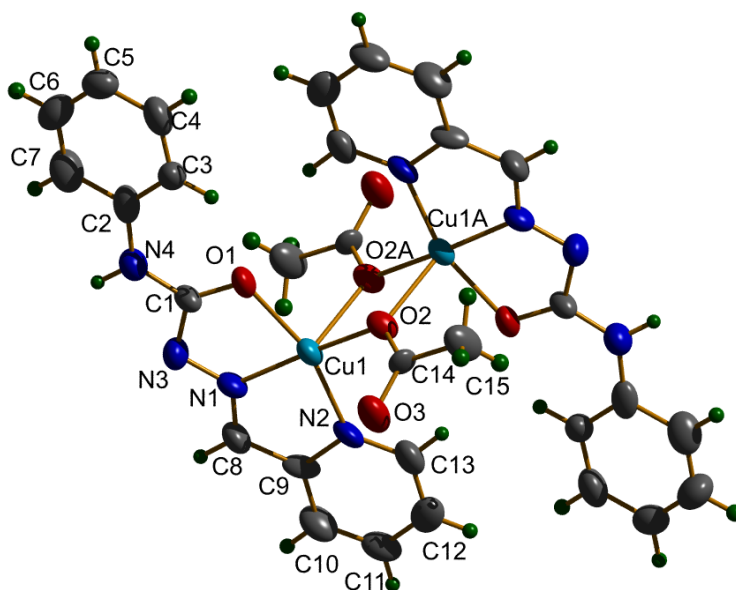
Fig.4.1 The molecular structure of $[Cu_2L^1_2(OAc)_2]$ (**9**) along with the atom numbering scheme.

The unit cell-packing diagram of the compound **9** viewed along a-axis is given in Fig. 4.2.
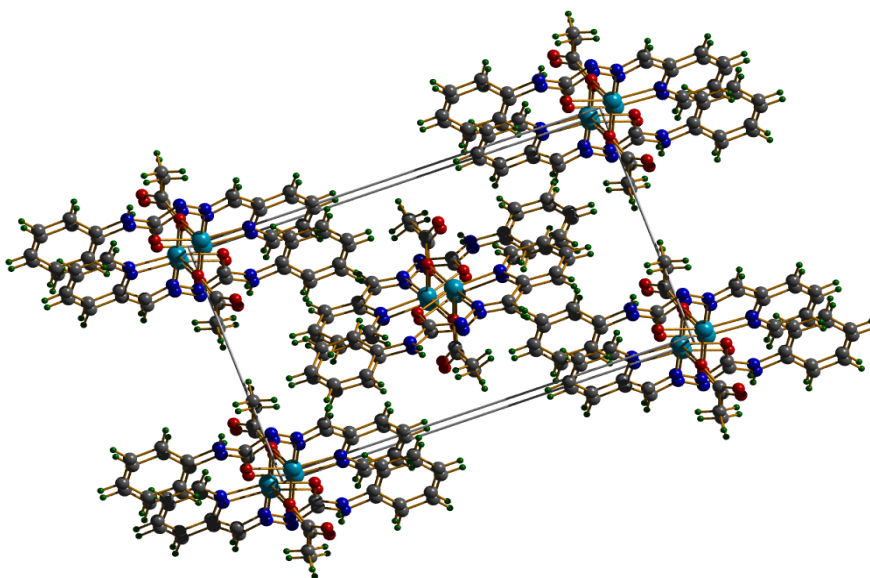

Fig.4.2 Packing diagram of compound $[Cu_2L^1_2(OAc)_2]$ (**9**) along a axis.

It can be observed that the molecules are packed in a 2-dimensional manner with the parallel arrangement of the rings. The adjacent units are interconnected through hydrogen bonding interactions involving the oxygen atom of the acetato group and *N*(4) hydrogen. The molecular structure pointing up the hydrogen bonding in compound **9** is shown in Fig. 4.3.
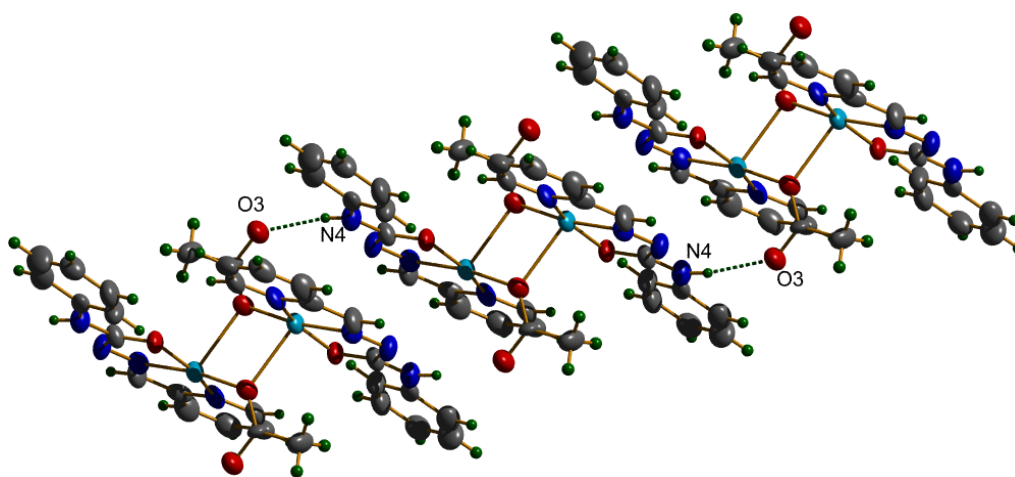
Fig.4.3 Packing diagram of compound [Cu$_2$L$^1_2$(OAc)$_2$] **(9)** showing intermolecular hydrogen bonding.

The intermolecular hydrogen bonding interactions are shown in Table 4.4. The hydrogen bonding interaction is observed with a donor-acceptor distance of 2.995 Å. The $\pi\cdots\pi$ stacking interactions between metal chelate rings and the aromatic π-π interactions between phenyl and pyridyl ring of the neighboring molecules with Cg$\cdots$Cg distances of 3.396(6)Å and 3.727(8) respectively (sym. code: 1-y,1-y,1-z) reinforces crystal structure cohesion in molecular packing in the crystal lattice as shown in Fig. 4.4. The $\pi\cdots\pi$, ring metal and intermolecular hydrogen bonding interactions play an important role in the stabilization of the unit cell [12].
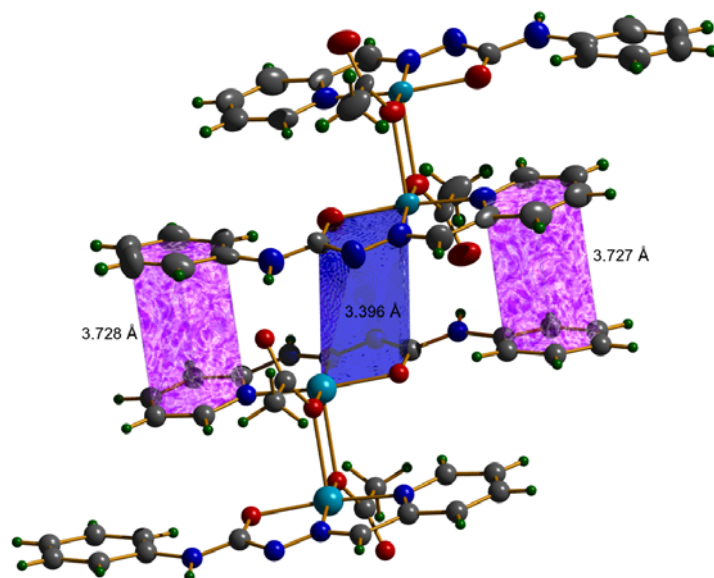
Fig.4.4 molecular structure showing $\pi\cdots\pi$ interactions in compound $[Cu_2L^1_2(OAc)_2]$ (**9**).

Table4.4 Interaction parameters of compound $[Cu_2L^1_2(OAc)_2]$ (**9**)

Hydrogen bonding interactions

D—H···A	D—H (Å)	H···A (Å)	D···A (Å)	∠D—H···A(°)
N(4)—H···O(3)[a]	0.860	2.149	2.995	167.60

$\pi\cdots\pi$ interactions

Cg(I)···Cg(J)	Cg···Cg(Å)	α (°)	β (°)	γ(°)
Cg(2)···Cg(2)[b]	3.396(6)	0.00	16.72	16.72
Cg(4)···Cg(5)[b]	3.727(8)	11.2(7)	22.74	16.78

Cg (2) = Cu(1), O(1), C(1), N(3), N(1)
Cg (4) = N(2), C(9), C(10), C(11), C(12), C(13)
Cg (5) = C(2), C(3), C(4), C(5), C(6), C(7)
Equivalent position codes: a=x+1,y,z; b=1-y,1-y,1-z
D, donor; A, acceptor; Cg, centroid; α, dihedral angles between planes I and J; β, angle between Cg···Cg and Cg(J)_perp; γ, angle between Cg–Cg and Cg(I)_perp

The trigonality index τ is calculated using the equation $\tau = (\beta-\alpha)/60$ [12]

(for perfect square pyramidal and trigonal bipyramidal geometries the values of τ

are zero and unity respectively). The value of τ for this molecule is 0.187, which again confirms the distorted square pyramidal geometry around copper atom.

4.3.3. Crystal structure of the complex $[Cu_2L^1_2(N_3)_2]$ (12)

The single crystal X-ray diffraction study of the compound $[Cu_2L^1_2(N_3)_2]$ (12) showed that the compound exists as an end-on azido bridged dimer. The molecular structure of the compound along with atom numbering scheme is given in Fig. 4.5.
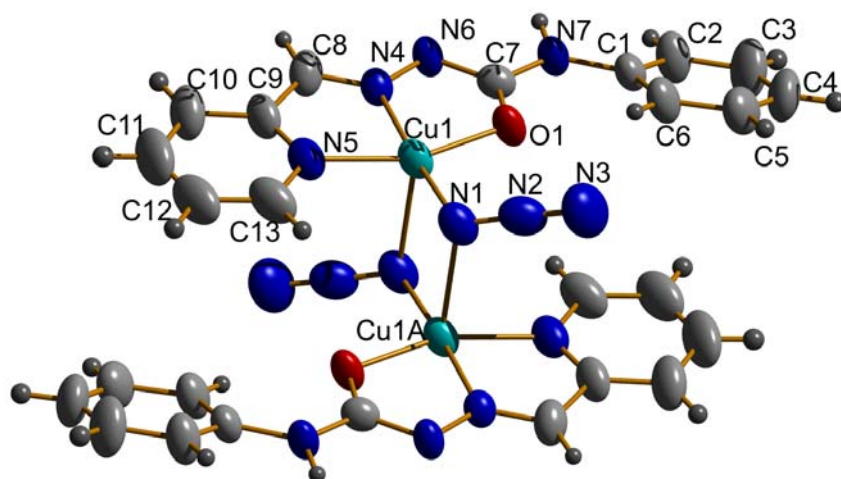
Fig.4.5 The molecular structure of $[Cu_2L^1_2(N_3)_2]$ (12) along with the atom numbering scheme.

This compound crystallizes in monoclinic space group $C2/c$. Each semicarbazone unit acts as a tridentate chelate, coordinating through pyridyl nitrogen, azomethine nitrogen and the enolate oxygen to a single Cu(II) center which is involved in a $\mu_{1,1}$-azido bridging to an identical coordination network, thus each copper atom is in a penta-coordinate environment.

The trigonality index τ is calculated using the equation $\tau = (\beta-\alpha)/60$ [13] (for perfect square pyramidal and trigonal bipyramidal geometries the values of τ are zero and unity respectively). The value of τ for the molecule is 0.26, which shows the coordination polyhedron around each copper atom is a distorted square

pyramid. The base of each distorted square pyramidal unit is occupied by N(1), N(4), N(5) and O(1) atoms, with the apical position occupied by the N(1A) atom of the second azido group. Each azido ligand functions as an electron donor to the coordination network through an end-on azido bridging mode.

The intramolecular Cu⋯Cu distance is found to be 3.1948(17) Å and the axial Cu(1)–N(1A) distance found to be 2.468(8) Å. The nitrogen atoms N(4) and N(1) are closer to the Cu(II) center with the equal bond distance of 1.943 Å compared to Cu(1)–N(5) (2.018 Å) and Cu(1)–O(1) (1.948 Å). The copper atom is slightly deviated from the base of the square pyramid by 0.0981(12) Å. The distortion from the regular square planar structure is evident from the divergence of the bond angles around Cu(II) from 90º. Bond angles of N4–Cu1–N5 and N4–Cu1–O1 are less than 90º while the bond angles of O1–Cu1–N1 and N1–Cu1–N5 are greater than 90º. The found distortion may be due to the rigidity of the chelate rings formed.

Selected bond lengths and bond angles of $[Cu_2L^1_2(N_3)_2]$ are shown in Table 4.5.

Table 4.5 Selected bond lengths and bond angles of $[Cu_2L^1_2(N_3)_2]$ (**12**)

| Bond length (Å)		Bond angle (°)	
Cu(1)–N(5)	2.018(8)	N(5)–Cu(1)–N(4)	80.7(3)
Cu(1)–N(4)	1.943(7)	N(4)–Cu(1)–N(1)	175.3(3)
Cu(1)–O(1)	1.948(6)	N(4)–Cu(1)–O(1)	80.0(3)
Cu(1)–N(1)	1.943(8)	N(1)–Cu(1)–O(1)	97.9(3)
Cu(1)–N(1A)	2.468(8)	N(1)–Cu(1)–N(5)	100.8(3)
O(1)–C(7)	1.269(10)	N(5)–Cu(1)–N(1A)	91.8(3)
N(4)–N(6)	1.365(9)	N(1)–Cu(1)–N(1A)	88.0(3)
N(6)–C(7)	1.350(11)	N1–N2–N3	178.0(12)
N(4)–C(8)	1.285(11)		
N(7)–C(7)	1.347(11)		
Cu⋯Cu	3.1948(17)		

The unit cell packing diagram of the compound $[Cu_2L^1_2(N_3)_2]$ (**12**) viewed along b-axis is given in Fig. 4.6.
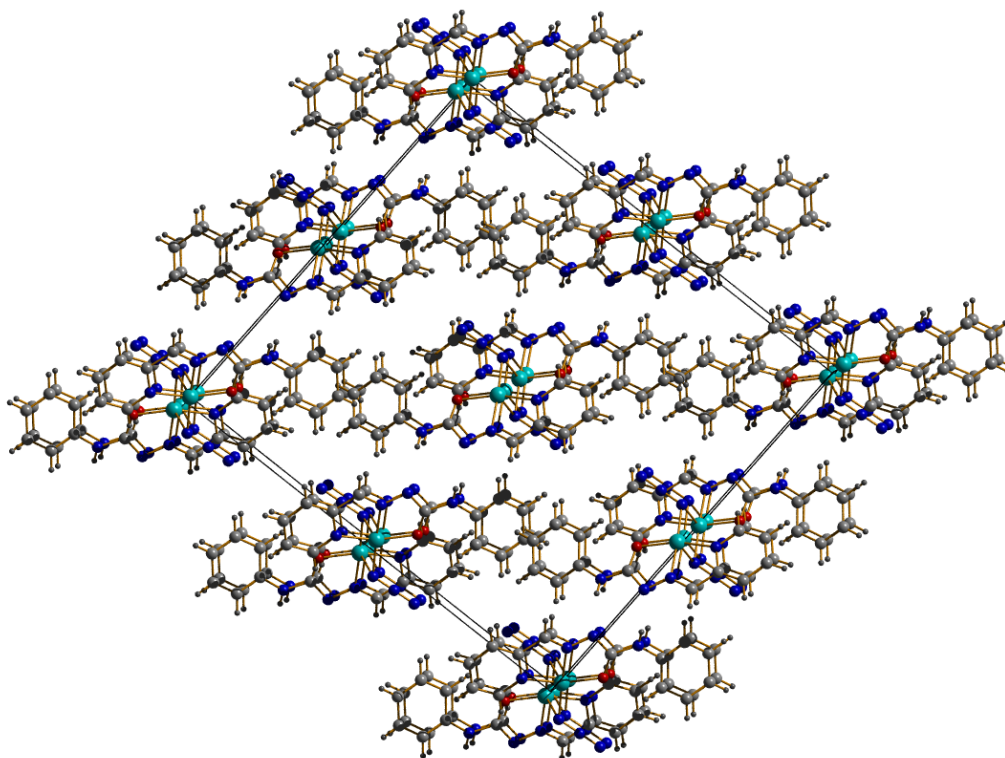
Fig. 4.6 Packing diagram of compound $[Cu_2L^1_2(N_3)_2]$ (**12**) along b-axis.

It can be observed that the molecules are packed in a two-dimensional manner with the parallel arrangement of rings. The adjacent units are interconnected through hydrogen bonding interactions involving N(7) hydrogen and N(6) with donor- acceptor distance of 3.001(9) Å.

Molecular structure of compound **12** showing intermolecular hydrogen bonding is shown in Fig. 4.7.
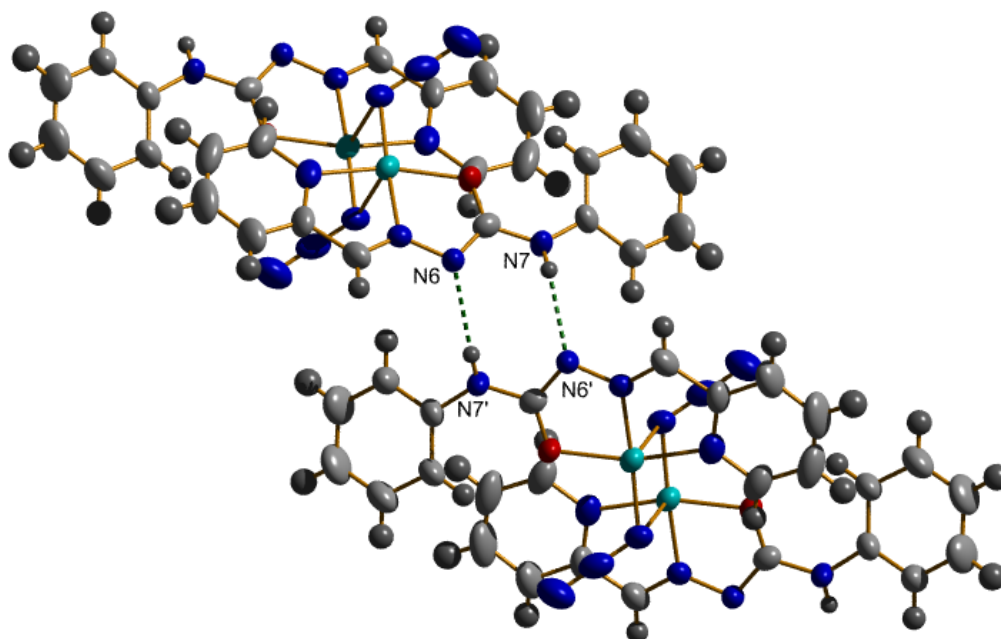
Fig. 4.7 Interconnection of hydrogen bonding in packing of compound [Cu$_2$L^1$_2$(μ-N$_3$)$_2$] (**12**).

Despite the fact that the ring-systems with fewer than three rings contributes little to stacking forces, and that the strength of these forces, which stabilize the stacked conformation, does not differ significantly from the van der Waals forces also experienced by similarly-sized saturated molecules when stacked, we report the all possible interactions which comes in the distance range of van der Waals forces. Thus, the crystal structure may be influenced by $\pi\cdots\pi$ (Fig. 4.8), C–H$\cdots\pi$, ring-metal and hydrogen bonding interactions which are tabulated in Table 4.6. Additional noncovalent Y–X$\cdots\pi$ ring interactions are also found between N(2)–N(3) and Cg(3) and similarly between N(2)–N(3) and Cg(4) with $d_{N(3)\text{-}Cg}$ =3.491 Å and $d_{N(3)\text{-}Cg}$ =3.566 Å respectively [sym. code: 1-x,2-y,-z] as shown in Fig. 4.9. Ring-metal interactions Cg(3)$\cdots$Cu(1) and Cg(4)$\cdots$Cu(1) [sym. code: 1-x,-y,1-z] are observed at a distance of 3.641 and 3.797 Å respectively. The $\pi\cdots\pi$ interactions are rather weak, with a distance ranging from 3.558 to 3.702 Å between the centroids.
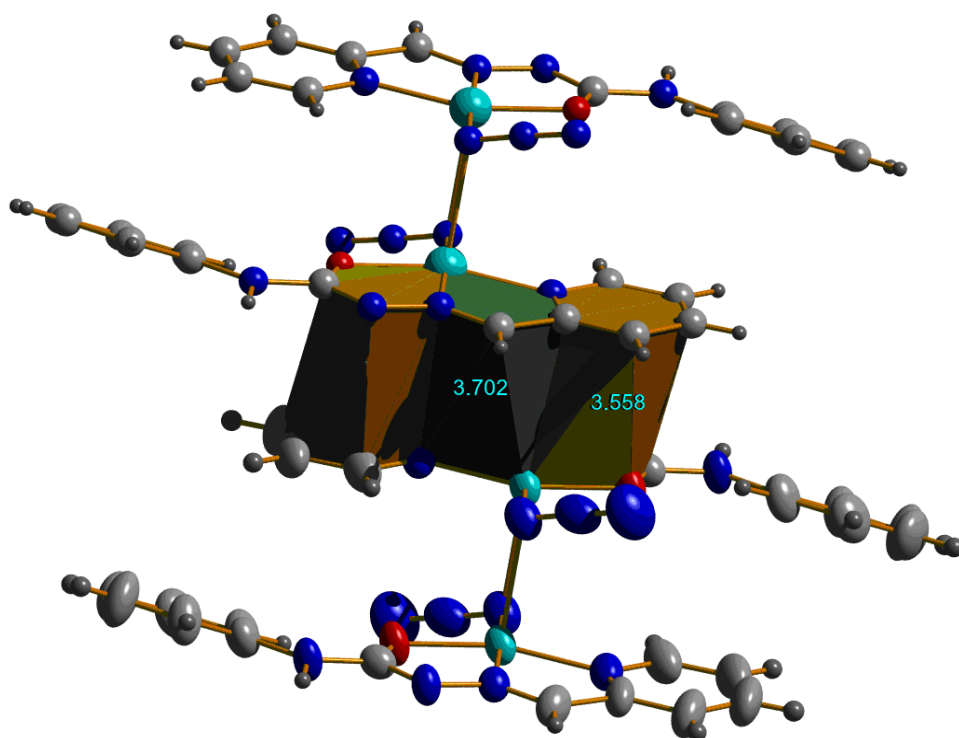
Fig. 4.8 Compound [Cu$_2$L$^1_2$(N$_3$)$_2$] (**12**) showing $\pi\cdots\pi$ interactions between neighboring molecules with Cg$\cdots$Cg distances.
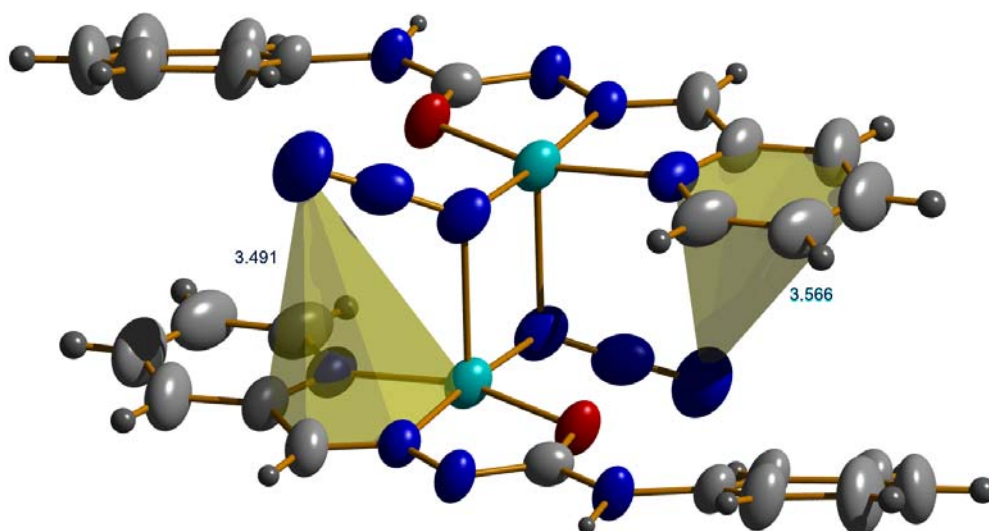
Fig.4.9 Compound [Cu$_2$L$^1_2$(N$_3$)$_2$] (**12**) showing N$\cdots\pi$ interactions within the molecule with N$\cdots$Cg distances.

Table 4.6 Interaction parameters of compound [$Cu_2L_2{}^1N_3$] (**12**)

Hydrogen bonding interactions

D—H···A	D—H (Å)	H···A (Å)	D···A (Å)	∠D—H···A(°)
N(7)—H···N(6)[a]	0.83(7)	2.23(7)	3.001(9)	155(6)
C(6)—H···O(1)	0.9312	2.2693	2.831(11)	118.17

π···π interactions

Cg(I)···Cg(J)	Cg···Cg (Å)	α (°)	β (°)	γ(°)
Cg(4)···Cg(2)[b]	3.558(6)	0.1(5)	13.78	13.83
Cg(3)···Cg(3)[b]	3.702(5)	0	20.06	20.06

C–H···π interactions

X—H(I)···Cg(J)	H···Cg (Å)	X···Cg (Å)	∠X—H···Cg (°)
C(4)-H···Cg(5)[c]	2.72	3.443(14)	135

Ring–metal interactions

Cg(I)···Me(J)	Cg(I)-Me(J) (Å)	β(°)
Cg(3)···Cu(1)[b]	3.641	16.18
Cg(4)···Cu(1)[b]	3.797	23.13

N–N···π interactions

Y—X(I) ···Cg(J)	X···Cg (Å)	∠Y—X···Cg (°)	Y···Cg (Å)
N(2)—N(3) ···Cg(3)[e]	3.491(13)	61.4(7)	3.110(10)
N(2)—N(3) ···Cg(4)[e]	3.566(14)	88.3(8)	3.714(10)

Equivalent position codes: a = 1-x,y,1/2-z; b = 1-x,1-y,-z; c = 1/2-x,1/2+y,1/2-z; d = 1-x,2-y,-z

Cg (2) = Cu(1), O(1), C(7), N(6), N(4); Cg (3) = Cu(1), N(4), C(8), C(9), N(5); Cg (4) = N(5), C(9), C(10), C(11), C(12), C(13); Cg (5)= C(1), C(2), C(3), C(4), C(5), C(6)

D, donor; A, acceptor; Cg, centroid; α, dihedral angles between planes I and J; β, angle between Cg-Cg and Cg(J)_perp; γ, angle between Cg-Cg and Cg(I)_perp.

4.3.4. Infrared spectral studies

The tentative assignments for the IR spectral bands, most useful for determining the ligand's mode of coordination are listed in Table 4.7. A sharp band

at 1597 and 1602 cm^{-1} in the two semicarbazone ligands can be attributed to the characteristic >C=N group in HL^1 and H$_2$L^2 respectively. This band shifts slightly (4-12 cm^{-1}) towards lower frequencies in the copper(II) complexes [13,14] indicating the coordination of azomethine nitrogen to copper. It is further supported by the appearance of new bands at 410-423 cm^{-1} assignable to ν(Cu–N) for these complexes [15]. The increase in ν(N–N) values in the spectra of these complexes is due to the increase in double bond character, off-setting the loss of electron density via donation to the metal and is a confirmation of the coordination of the ligand through the azomethine nitrogen. The appearance of bands in the 1543-1579 cm^{-1} range in complexes is due to asymmetric stretching vibration of the newly formed C=N bond as a result of enolization of the ligand. The ν(N–H) bands of semicarbazones are not distinguishable because of the presence of the broad O–H stretching vibrations in most of the complexes except in [Cu(HL^1)Cl$_2$] (**6**), [Cu$_2$L^1$_2$(OAc)$_2$] (**9**) and [Cu$_2$L^1$_2$(N$_3$)$_2$] (**12**). Disappearance of intense bands of C=O stretching vibrations of semicarbazone complexes except **6** and **8** indicate the enolization of the semicarbazone during complexation (Fig. 4.10 and 4.16). The appearance of new peak in the 455-498 cm^{-1} range again confirms Cu–O coordination [16].
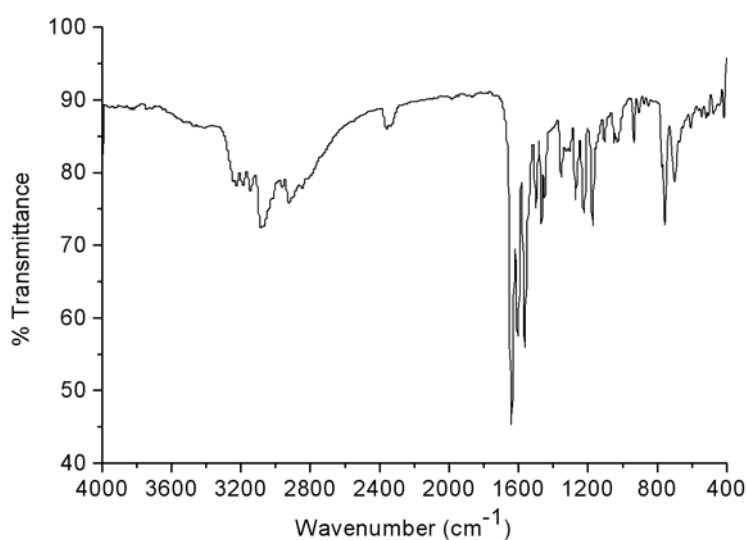

Fig. 4.10 Infrared spectrum of complex [Cu(HL^1)Cl$_2$] (**6**).

Table 4.7 Infrared spectroscopic assignments (cm^{-1}) for the HL^1, H$_2$L^2 and their copper(II) complexes

Compound	ν(C=N)	ν(N–N)	ν(C=O)	ν(Cu–N)	ν(C=N)[a]	ν(Cu–O)
HL^1	1597	1143	1693	-	-	-
[Cu(HL^1)Cl$_2$] (6)	1587	1168	1647	416	-	468
[Cu$_2$L$^1_2$(NO$_3$)$_2$]·H$_2$O (7)	1593	1148	-	420	1543	498
[Cu(HL^1)'SO$_4$]·½H$_2$O (8)	1593	1164	1645	423	-	474
[Cu$_2$ L$^1_2$(OAc)$_2$] (9)	1587	1147	-	417	1579	497
[Cu$_2$L$^1_2$Br$_2$]·H$_2$O (10)	1589	1160	-	408	1568	468
[CuL^1(NCS)]·2H$_2$O (11)	1593	1148	-	410	1561	474
H$_2$L^2	1602	1152	1689	-	-	-
[Cu$_2$L$^1_2$(N$_3$)$_2$] (12)	1590	1148	-	410	1561	481
[CuL^2(H$_2$O)] (13)	1596	1187	-	418	1578	494
[Cu$_2$L$^2_2$Br$_2$(H$_2$O)$_2$] (14)	1597	1159	-	417	1574	455

[a]. newly formed C=N
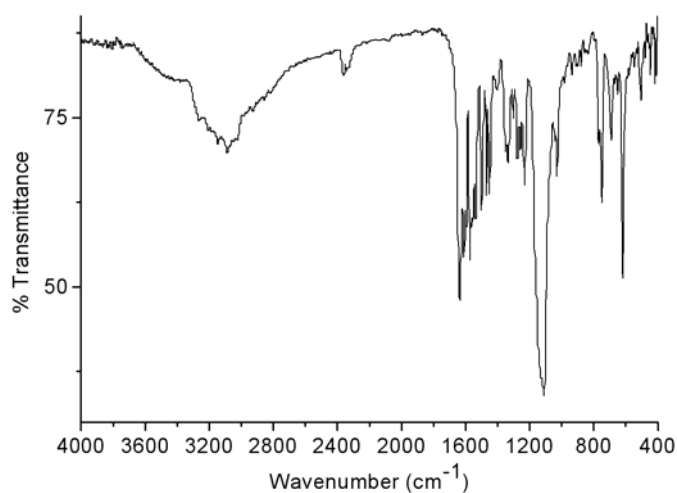
Fig. 4.11 IR spectrum of complex [CuHL^1(SO$_4$)]·½ H$_2$O (**8**).

Appearance of new sharp intense bands at 2115 and 2040 cm^{-1} are due to the presence of NCS and N$_3$ groups in the complexes **11** and **12** respectively as shown in Fig. 4.12 and 4.13. The crystal structure of the complex [Cu$_2$L$_2$^{1}N$_3$] (**12**) confirms the presence of azide and explains its mode of coordination as a monodentate bridging two copper atoms.

Broad bands at 3420-3460 cm^{-1} are due to the presence of lattice water in the complexes except the complexes **6**, **9** and **12**.
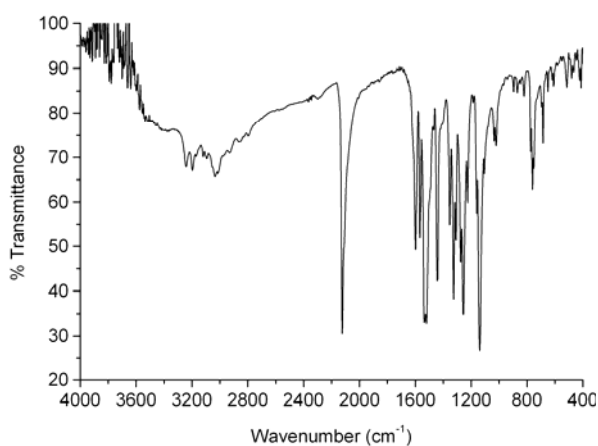
Fig. 4.12 IR spectrum of complex [CuL^{1}NCS]•2H$_2$O (**11**).
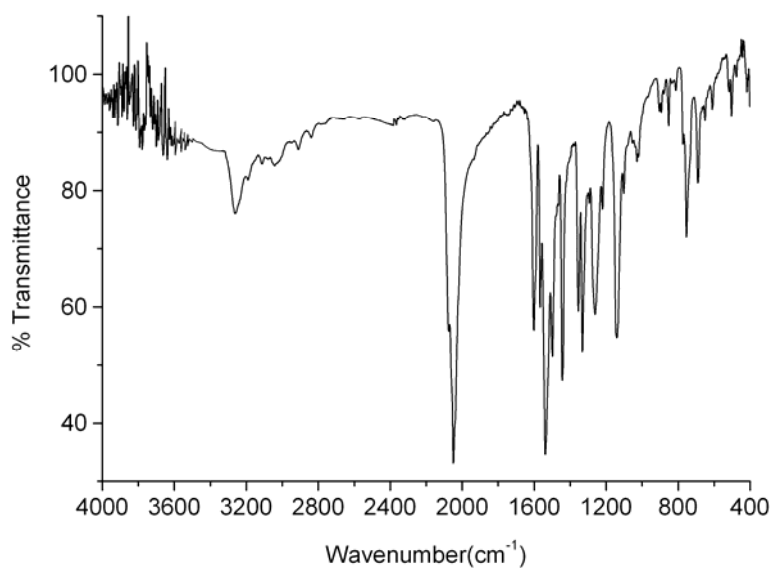
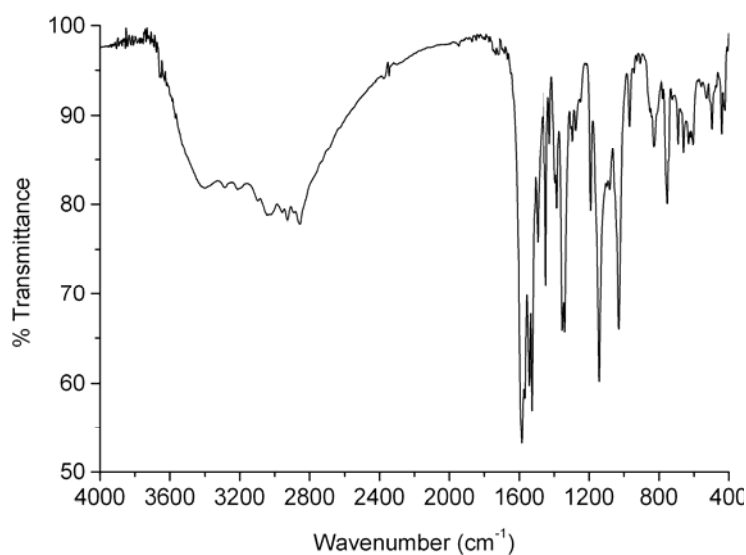**Fig. 4.13** IR spectrum of complex [Cu$_2$L$_2$^{1}N$_3$] **(12)**.

Thus it is seen that the ligands HL^1 and H$_2$L^2 act as a monoanionic tridentate ligand in the complexes **7**, **9**, **10**, **11**, **12**, **13** and **14** whereas in the complexes [Cu(HL^1)Cl$_2$] **(6)** and [CuHL^1(SO$_4$)]·½ H$_2$O **(8)** they act as neutral tridentate ligands. The sulfato complex [Cu(HL^1)SO$_4$]·½ H$_2$O (Fig. 4.11) has bands at 997, 1039 and 1119 cm^{-1} indicating the presence of bidentate bridging sulfato group [17].

Asymmetric stretching frequencies of unidentate acetato moiety at 1571 and 1565 cm^{-1} and its symmetric stretching frequencies at 1571 and 1265 cm^{-1} are clear evidences for the existence of the acetate moiety in the complex **9**. The peaks are magnified and clearly shown in Fig. 4.14.
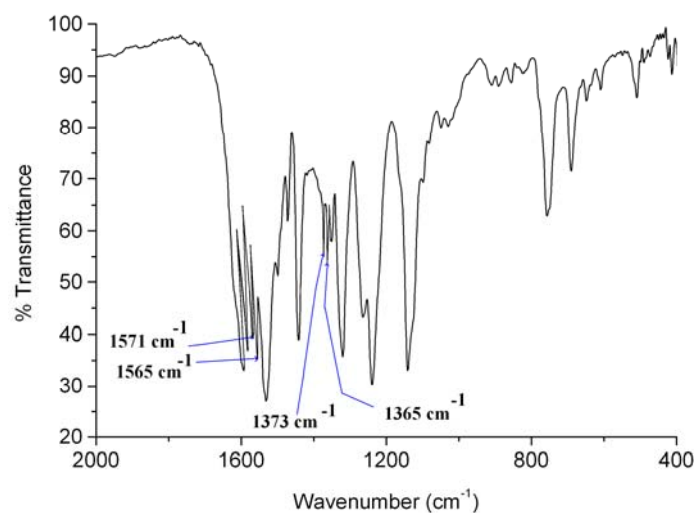
Fig. 4.14 magnified IR spectrum of complex [Cu$_2$ L$^1_2$(OAc)$_2$] (**9**).

The complexes [CuL$_2$(H$_2$O)] (**13**) and [Cu$_2$(HL^2)$_2$Br$_2$(H$_2$O)$_2$] (**14**) (Fig. 4.15 and 4.16) have two sets of bands at 1027, 964 cm^{-1} and 1046, 964 cm^{-1} respectively [18] and therefore it is expected that these bands are due to the coordinated water molecules in these complexes.

Fig. 4.15 IR spectrum of complex [CuL$_2$(H$_2$O)] (**13**).
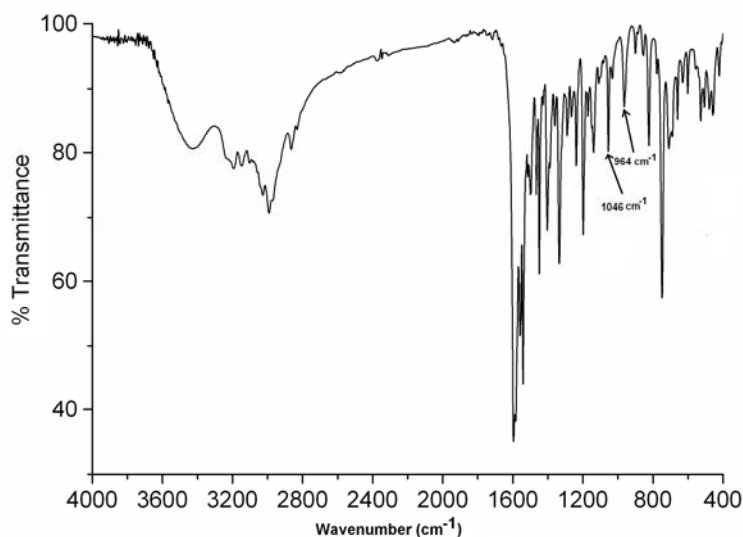
Fig. 4.16 IR spectrum of complex [Cu$_2$(HL^2)$_2$Br$_2$(H$_2$O)$_2$] (**14**).

The SCN group may coordinate to a metal through the nitrogen or sulfur or both sulfur and nitrogen. The CN stretching frequencies are generally lower in N-bonded complexes (near and below 2050 cm^{-1}) than in S-bonded complexes (near 2100 cm^{-1}) and the bridging [M–NCS–M'] complexes exhibits v(CN) well above 2100 cm^1. The v(CS) band for S-bonded complexes are found in the 720-690 cm^{-1} region. The N-bonded complexes exhibit a single sharp δ(NCS) near 480 cm^1, where as the S-bonded complexes show several weak bands near 421 cm^{-1}. However these frequencies are very sensitive to the overall structure of the complex, the nature of the central metal, nature of other ligands in the complex and steric consideration [19].

Here the complex [CuL^{1}NCS]•2H$_2$O (**11**) (Fig. 4.12) exhibited strong and sharp bands at 2115, 748 cm^{-1} and several bands of low intensity near 421 cm^{-1} which can be attributed to the values of a typical S-bonded thiocyanato complexes.

The azido complex **12** (Fig. 4.13) showed a sharp band at 2040 cm^{-1} and another one at 1243 cm^{-1}. These are assigned to ν_a and ν_s of the coordinated azido group. The broad band observed at 647 cm^{-1} for the complex is assigned to δ(N–N–N).

In the spectra of complexes [CuL$_2$(H$_2$O)] (**13**) and [Cu$_2$(HL^2)$_2$Br$_2$(H$_2$O)$_2$] (**14**) bands at 3413 and 3431 cm^{-1} correspond to coordinated water present in them (Fig. 4.15 and 4.16). The N–H stretching frequency is overlapped with the broad coordinated water peak. The appearance of three sets of bands at 824, 604 and 500 cm^{-1} and 824, 595 and 500 cm^{-1} confirms the presence coordinated water in complexes **13** and **14**.

4.3.5. Electronic spectral studies

The significant electronic absorption bands in the spectra of the semicarbazones and all the complexes recorded in methanol and DMF solutions are presented in Table 4.8.

The semicarbazones and copper(II) complexes have two bands; one centered in the 37295-45360 cm^{-1} region and the other in the 30150-33170 cm^{-1} region. These bands are due to $\pi \rightarrow \pi^*$ and $n \rightarrow \pi^*$ transitions (Fig. 4.17-4.25) of phenyl rings and semicarbazide moiety [20]. The charge transfer bands were observed in the 24660-26150 cm^{-1} region and its broadness can be explained as due to the combination of O$\rightarrow$Cu and N$\rightarrow$Cu LMCT transitions [21].

The intraligand absorption maxima found at 32000 cm^{-1} for HL^1 and 30887, 33960 cm^{-1} for H$_2$L^2 due to imine function of the uncomplexed semicarbazones were slightly shifted on complexation. This is an indication of the coordination of imine nitrogen and keto oxygen to the copper atom.

**Table 4.8** Electronic spectral assignments (cm^{-1}) for HL^1, H_2L^2 and their copper(II) complexes

Compound	*d-d*	LMCT	$n \rightarrow \pi^* / \pi \rightarrow \pi^*$
HL^1	-	-	32000, 38100, 42500
$[Cu(HL^1)Cl_2]$ (**6**)	12000	25233	32720, 40295
$[Cu_2L_2^1(NO_3)_2] \cdot H_2O$ (**7**)	12600, 14800	25225	32790, 40075
$[Cu(HL^1)(SO_4)] \cdot \frac{1}{2} H_2O$ (**8**)	12750, 14700, 17300	25225	32790, 40125
$[Cu_2 L_2^1(OAc)_2]$ (**9**)	13150, 14200	24660	32420, 39960
$[Cu_2L_2^1Br_2] \cdot H_2O$ (**10**)	13250	25110	33030, 39960
$[CuL^1(NCS)] \cdot 2H_2O$ (**11**)	14200	25245	33030, 39950
$[Cu_2L_2^1(N_3)_2]$ (**12**)	15500	25175	33170, 39950
H_2L^2	-	-	30887, 33960, 43227
$[CuL^2(H_2O)]$ (**13**)	15400	26150	30150, 37295
$[Cu_2(HL^2)_2Br_2 (H_2O)_2]$ (**14**)	14490	26010	33020, 40770

The spectra of all the complexes exhibit *d-d* bands ~12000 to 17 500 cm^{-1} (Figs. 4.17 to 4.25. For a square planar complex with $d_{x^2-y^2}$ ground state, three transitions are possible *viz*, $d_{x^2-y^2} \rightarrow d_{xy}$, $d_{x^2-y^2} \rightarrow d_{z^2}$ and $d_{x^2-y^2} \rightarrow d_{xz}$, d_{yz} ($^2B_{2g} \leftarrow {}^2B_{1g}$, $^2A_{1g} \leftarrow {}^2B_{1g}$, and $^2E_g \leftarrow {}^2B_{1g}$) and square pyramidal complexes have the transitions of $d_{x^2-y^2} \rightarrow d_{z^2}$, $d_{x^2-y^2} \rightarrow d_{xy}$ and $d_{x^2-y^2} \rightarrow d_{xz}$, d_{yz} [22,23]. The complexes $[CuL^1NCS] \cdot 2H_2O$ (**11**) and $[CuL_2(H_2O)]$ (**13**) are expected to be square planar while the other complexes except the complex $[Cu_2(HL^2)_2Br_2(H_2O)_2]$ (**14**) are expected to be in square pyramidal arrangement. The complexes $[Cu_2 L_2^1(OAc)_2]$ (**9**) and **12** have been proved to having the distorted square pyramidal geometry by the single crystal study. The complex **14** is expected to be an octahedral geometry around copper atom. However, since the four *d* orbitals lie very close together, each transition cannot be expected to be distinguished by their energy in all complexes and hence it is very difficult to resolve the bands into separate components. The broad band observed at 12000, 13250, 14200, 15500, 15400 and 14490 cm^{-1} in the electronic spectra of the complexes **6, 10, 11, 12, 13** and **14** (Fig. 4.17-4.25) are assigned to $^2E_g \leftarrow {}^2T_{2g}$ transition [24]. However, the complex $[Cu(HL^1)(SO_4)] \cdot \frac{1}{2}$

H$_2$O (**8**) showed three distinct bands at 12750, 14700 and 17300 cm^{-1} may be assigned to $^2A_{1g} \leftarrow {}^2B_{1g}$, $^2B_{2g} \leftarrow {}^2B_{1g}$ and $^2E_g \leftarrow {}^2B_{1g}$ respectively. The complexes [Cu$_2$L$_2^1$(NO$_3$)$_2$]·H$_2$O (**7**) and [Cu$_2$ L$^1_2$(OAc)$_2$] (**9**) gave two distinct bands for each may be assigned to the $^2A_{1g} \leftarrow {}^2B_{1g}$ and $^2B_{2g} \leftarrow {}^2B_{1g}$ transitions.
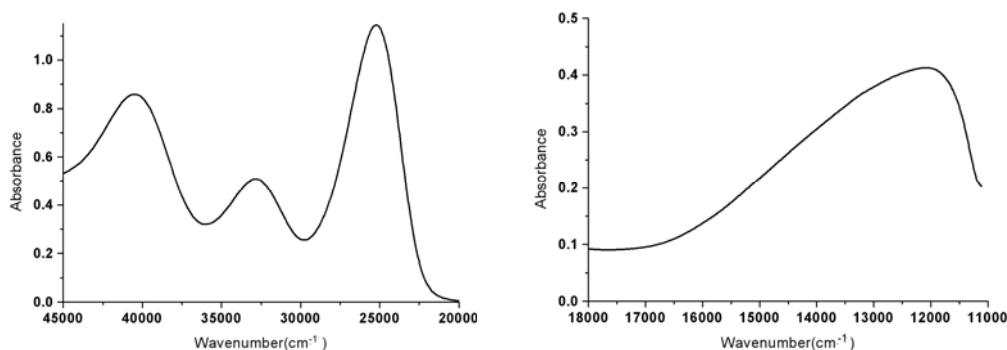
Fig. 4.17 Electronic spectra of complex [Cu(HL^1)Cl$_2$] (**6**).
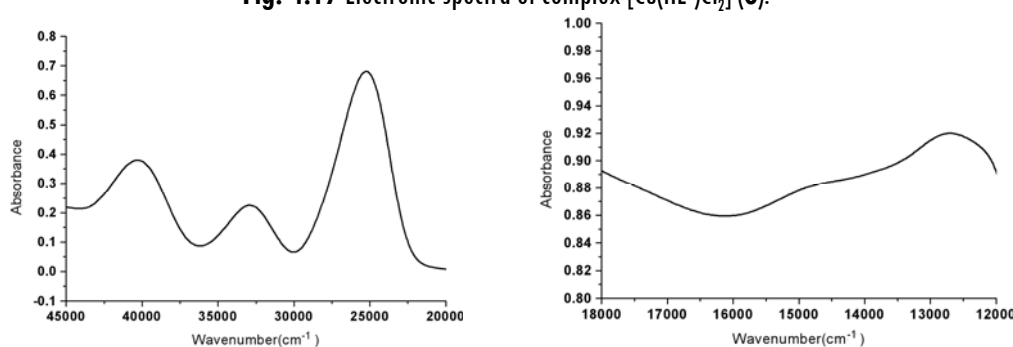
Fig. 4.18 Electronic spectra of complex [Cu$_2$L$_2^1$(NO$_3$)$_2$]·H$_2$O (**7**).
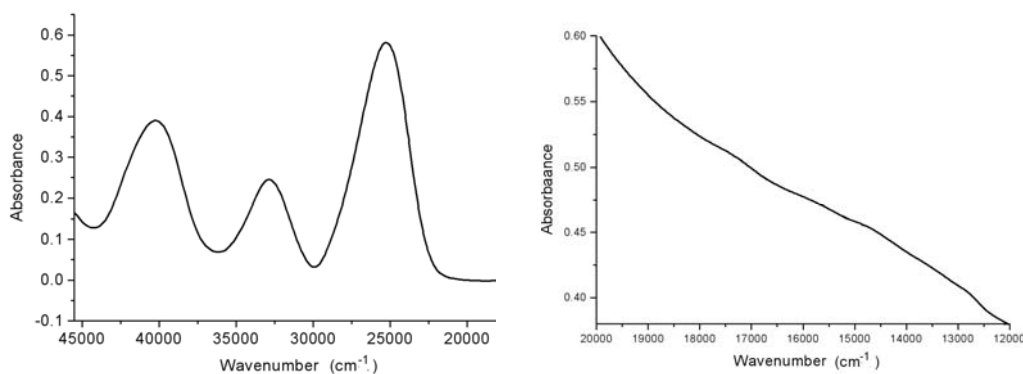
Fig. 4.19 Electronic spectra of complex [CuHL^1(SO$_4$)]·½ H$_2$O (**8**).
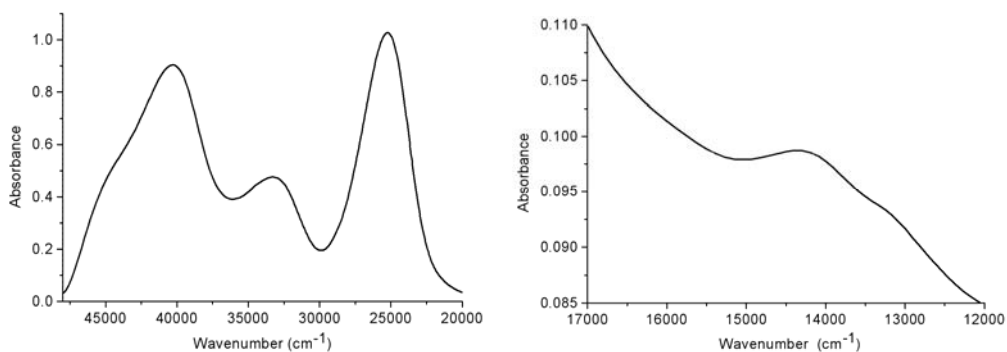
Fig. 4.20 Electronic spectra of complex $[Cu_2 L^1_2(OAc)_2]$ (**9**).
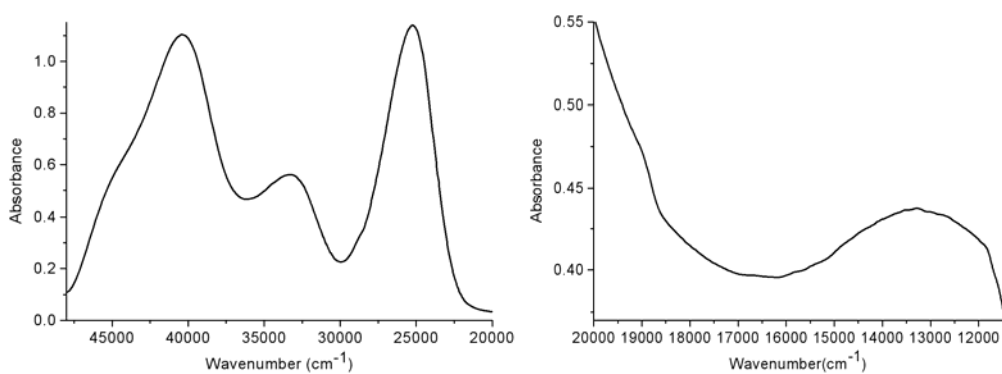
Fig. 4.21 Electronic spectra of complex $[Cu_2L^1_2Br_2] \cdot H_2O$ (**10**).
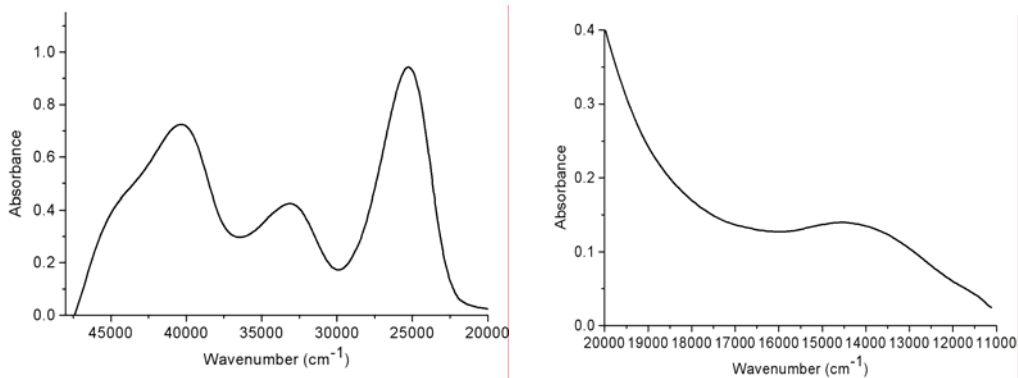
Fig. 4.22 Electronic spectra of complex $[CuL^1NCS] \cdot 2H_2O$ (**11**).
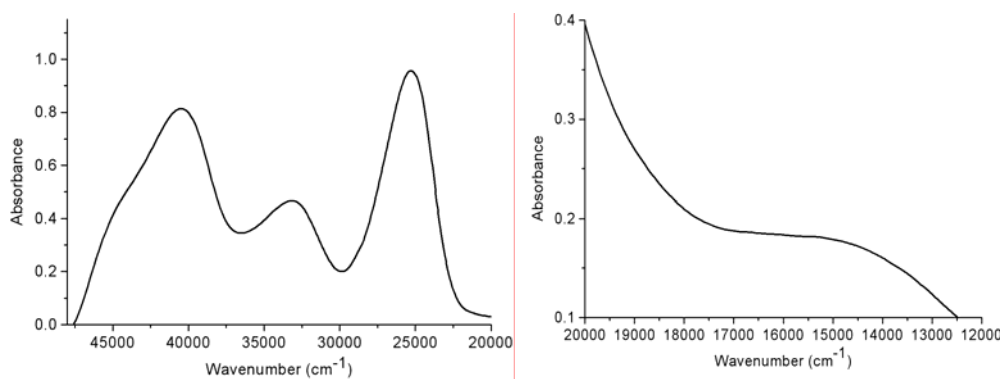
Fig. 4.23 Electronic spectra of complex [Cu$_2$L$_2^1$N$_3$] (**12**).
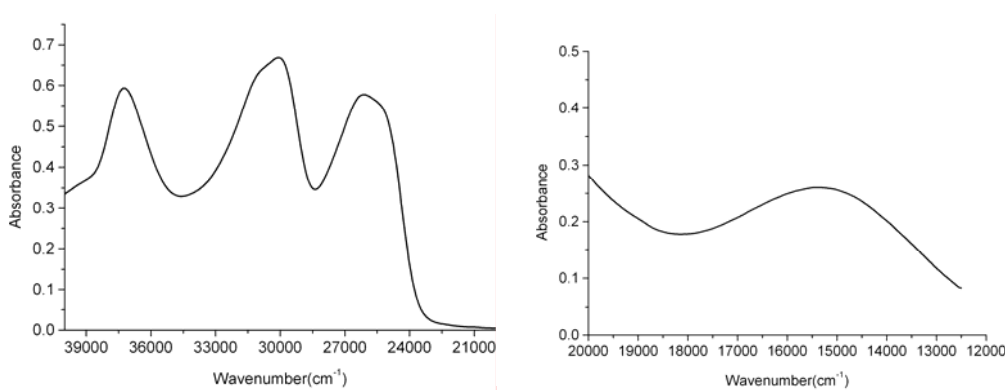
Fig. 4.24 Electronic spectra of complex [CuL$_2$(H$_2$O)] (**13**).
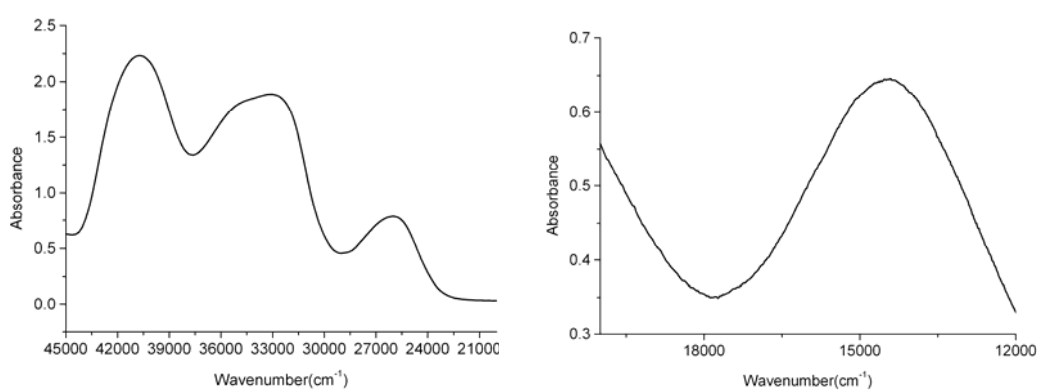
Fig.4.25 Electronic spectra of complex [Cu$_2$(HL^2)$_2$Br$_2$(H$_2$O)$_2$] (**14**).

4.3.6. Thermogravimetric studies

Thermal analyses provide valuable information regarding the thermal stability and nature of water molecules in complexes were obtained. It helps us to distinguish the lattice water molecules and coordinated water molecules present in the compound. Reports show that the weight losses for lattice water are in the range of 90-190 ºC and weight losses due to coordinated water molecules are in the range of 200-350 ºC [25,26]. In complexes **7**, **8**, **10** and **11** there are weight losses in the region 100–180 ºC indicating the presence of lattice water molecules and weight loss is observed in between 320 ºC and 325 ºC in compounds $[CuL_2(H_2O)]$ (**13**) and $[Cu_2(HL^2)_2Br_2(H_2O)_2]$ (**14**) indicating the presence of coordinated water molecule in structure. Moreover, its percentage weight losses of these complexes (5% and 8% respectively) confirm that it has one and two coordinated water molecules respectively. The percentage weight losses of all the ligands and water (75% and 83% respectively) of these two complexes **13** and **14** again confirm the composition (Fig. 4.26 and 4.34).
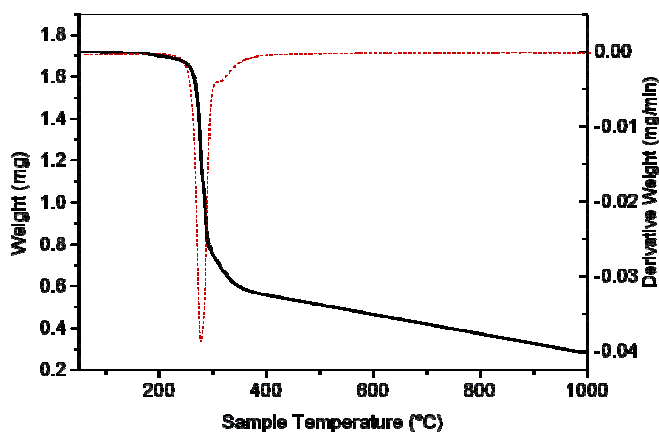
Fig.4.26 Thermogram of complex $[CuL_2(H_2O)]$ (**13**).
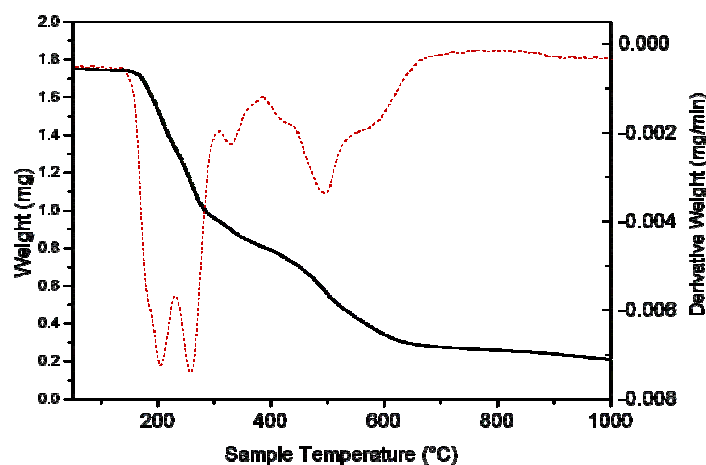
Fig.4.27 Thermogram of complex $[Cu_2(HL^2)_2Br_2(H_2O)_2]$ (**14**).

In the complexes **7**, **8**, **10** and **11** the percentage weight losses of 2.4%, 2.2%, 2.3% and 8.3% agree well with the calculated values indicating the presence of one mole of water in the complex **7**, half mole in complex **8**, one mole in complex $[Cu_2L^1_2Br_2] \cdot H_2O$ (**10**) and two moles in complex $[CuL^1NCS] \cdot 2H_2O$ (**11**) (Fig. 4.28-4.31).
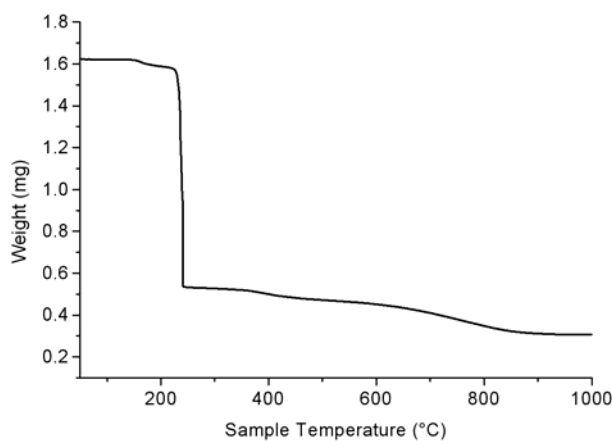
Fig. 4.28 Thermogram of complex $[Cu_2L^1_2(NO_3)_2] \cdot H_2O$ (**7**).
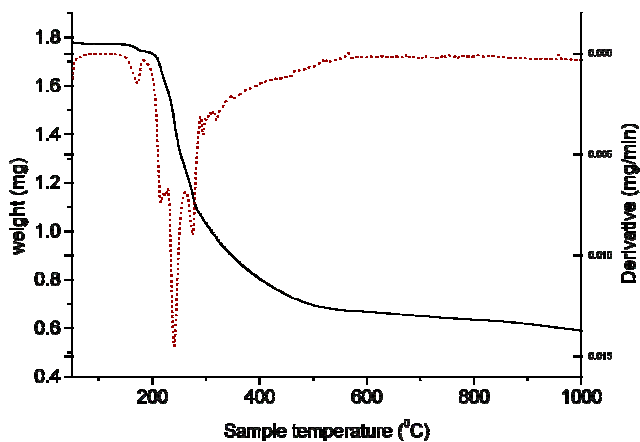
Fig.4.29 Thermogram of complex [CuHL^1(SO$_4$)]·½ H$_2$O (**8**).
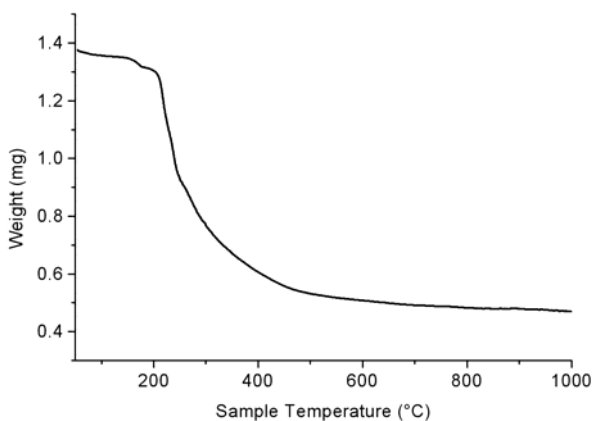
Fig.4.30 Thermogram of complex [Cu$_2$L$^1_2$Br$_2$]•H$_2$O (**10**).
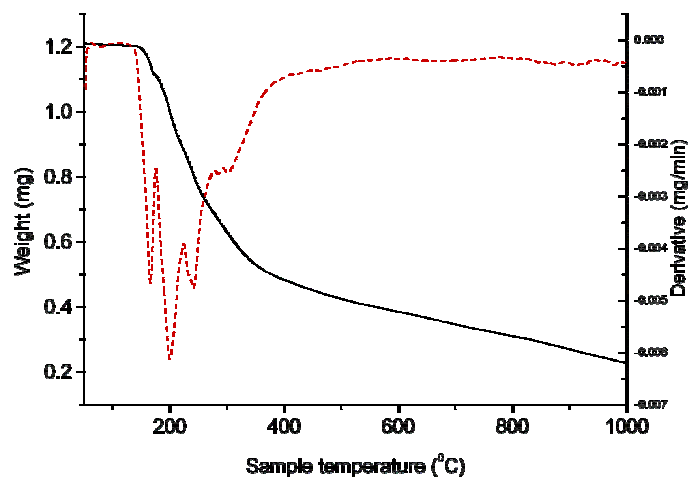
Fig.4.31 Thermogram of complex [CuL^{1}NCS]•2H$_2$O (**11**).

In compounds [Cu(HL^1)Cl$_2$] (**6**), **9** and **12** there are no weight loss in these regions indicating the absence of water molecules (Fig. 4.32-4.34). The complex **6** and **14** decompose in the temperature range of 220-600 ºC and the complex **7** in the rage of 200-800 ºC while the other complexes decompose in the range 200-450.
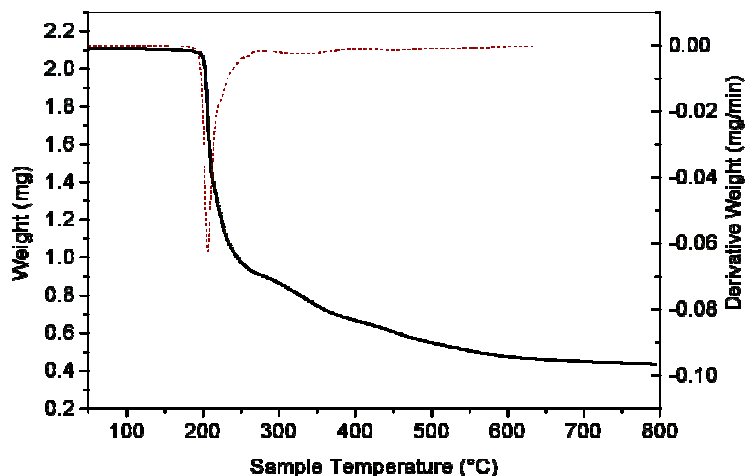
Fig.4.32 Thermogram of complex [Cu(HL^1)Cl$_2$] (**6**).
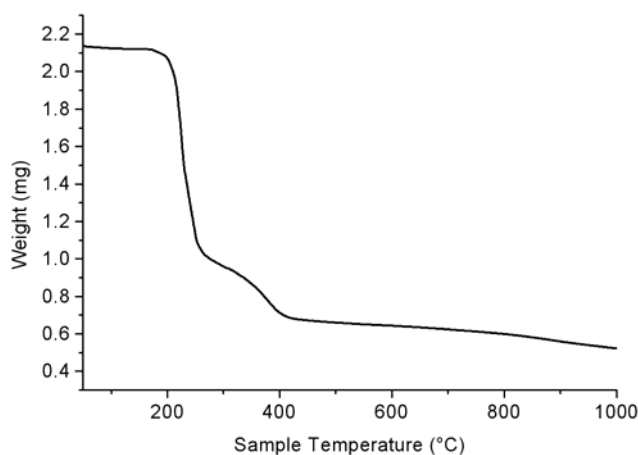
Fig.4.33 Thermogram of complex [Cu$_2$ L$^1_2$(OAc)$_2$] **(9)**.
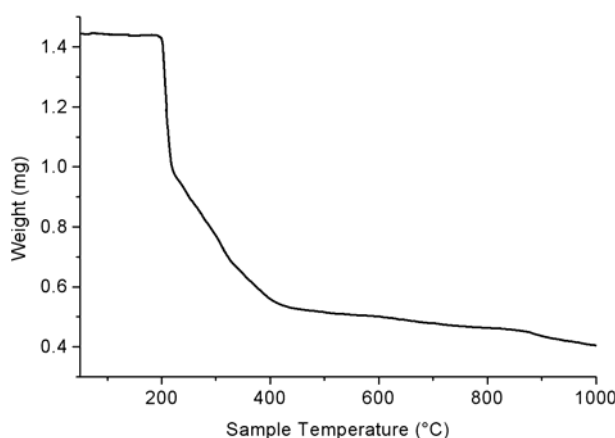
Fig. 4.34 Thermogram of complex [Cu$_2$L$_2$^{1}N$_3$] **(12)**.

4.3.7. EPR spectral studies

The magnetic parameters measured in EPR study are related to the structure of the paramagnetic complex, the number of ligands, nature of bonding and spatial arrangements of the ligands around the central metal ion. The copper(II) ion, with a d^9 configuration, has an effective spin of S = 1/2 and is associated with a spin angular momentum, m$_s$ = ±1/2, leading to a doubly degenerate spin state in the absence of a magnetic field. In a magnetic field the degeneracy is lifted between these states and the energy difference between

them is given by $\Delta E = h\nu = g\beta B$, where h is Planck's constant, ν is the microwave frequency for transition from $m_s = +\frac{1}{2}$ to $m_s = -\frac{1}{2}$, g is the Lande splitting factor (equal to 2.0023 for a free electron), β is the Bohr magneton and B is the magnetic field. For the case of a $3d^9$ copper(II) ion, the appropriate spin Hamiltonian assuming a B_{1g} ground state is given by:

$$\hat{H} = \beta[g_{\parallel}B_aS + g_{\perp}(B_xS_x+B_yS_y)] + A_{\parallel}I_zS_z + A_{\perp}(I_xS_x+I_yS_y)$$

The EPR spectra of the polycrystalline samples at 298 K, DMF solution at 298 and 77 K were recorded in the X-band, using 100-kHz modulaton; g factors were quoted relative to the standard marker TCNE ($g = 2.00277$). The EPR spectra of the complexes recorded in polycrystalline state at room temperature provide information about the coordination environment around copper(II) in these complexes.

The EPR parameters $g_{\parallel}$, $g_{\perp}$, $A_{\parallel}$(Cu) and the energies of d-d transitions were used to evaluate the bonding parameters α^2, β^2 and γ^2 which may be regarded as measures of the covalency in the in-plane σ-bonds, in-plane π-bonds and out-of-plane π-bonds. The value of in-plane σ-bonding parameter α^2 estimated from the expression,

$$\alpha^2 = -A_{\parallel} / 0.036 + (g_{\parallel}-2.00277) + 3/7(g_{\perp}- 2.00277) + 0.04 \text{ [27]}.$$

The following simplified parameters were used to evaluate the bonding parameters [28],

$$K_{\parallel}^2 = (g_{\parallel}-2.00277) \, E_{\text{d-d}} /8\lambda_o$$

$$K_{\perp}^2 = (g_{\perp}-2.00277) \, E_{\text{d-d}} /2\lambda_o$$

Where $K_\parallel^2 = \alpha^2 \beta^2$ and $K_\perp^2 = \alpha^2 \gamma^2$, $K_\parallel$ and $K_\perp$ are orbital reduction factors and λ_o represents the one electron spin orbit coupling constant which equals -828 cm^{-1}.

The EPR spectra of the compounds **6-14** were recorded. The EPR parameters of the copper(II) complexes are presented in the Table 4.9.

The EPR spectra of the compounds **12** and [CuL$_2$(H$_2$O)] (**13**) in the polycrystalline state at 298 K showed only one broad signal at g_{iso} = 2.128 and 2.096 respectively. Such isotropic spectra, consisting of only one broad signal and hence only one g value (g_{iso}), arises from extensive exchange coupling through misalignment of the local molecular axes between different molecules in the unit cell (dipolar broadening) and enhanced spin lattice relaxation. This type of spectra unfortunately give no information on the electronic ground state of copper(II) ions present in the complex.

Table 4.9 Spin Hamiltonian and bonding parameters of copper(II) complexes

	6	7	8	9	10	11	12	13	14
Polycrystalline state at 298 K									
$g_{\parallel}$	2.296	-	2.3	2.25	2.09	2.24	-	-	-
$g_{\perp}$	2.054	-	2.075	2.089	2.22	2.06	-	-	-
g_{isc}/g_{rv}	2.134	-	2.15	2.142	2.176	2.12	2.128	2.096	-
G	5.680	-	4.094	2.856	0.402	4.119	-	-	-
Solution state at 77 K									
$g_{\parallel}$	2.288	2.259	2.409	2.36	2.415	2.257	2.235	-	2.32
$g_{\perp}$	2.094	2.062	2.139	2.05	2.138	2.1	2.113		2.021
$A_{\parallel}$	15.7	18.52	13.1	24.8	12.7	16.7	17.3	-	21.2
α^2	0.830	0.864	0.913	1.176	0.907	0.824	0.820	-	1.002
β^2	0.866	0.876	1.127	0.744	1.000	0.895	0.898	-	0.831
γ^2	0.981	0.845	1.307	0.543	1.147	1.109	1.24	-	0.403
$K_{\parallel}$	0.719	0.757	1.030	0.875	0.908	0.738	0.737	-	0.833
$K_{\perp}$	0.815	0.730	1.195	0.639	1.042	0.915	1.017	-	0.404

The spectra of the compounds, $[Cu(HL^1)Cl_2]$ **(6)**, $[CuHL^1(SO_4)] \cdot \frac{1}{2} H_2O$ **(8)** and $[CuL^1NCS] \cdot 2H_2O$ **(11)** (Fig. 4.35-4.37) in polycrystalline state at 298 K showed axial spectra with well defined $g_\parallel$ and $g_\perp$ features. The variation in the $g_\parallel$ and $g_\perp$ values indicate that the geometry of the compounds in the solid state is affected by the nature of coordinating gegenions. For these complexes, the $g_\parallel > g_\perp > 2.0023$ and a G value falling within the range 4.0–5.6 and therefore they are monomeric complexes with $d_{x^2-y^2}$ ground state [29]. The geometric parameter G which is a measure of the exchange interaction between copper centers in the polycrystalline compound is calculated using the equation, $G = (g_\parallel - 2.0023)/g_\perp - 2.0023)$. If the G value is greater than 4, exchange interaction is negligible [30,31].
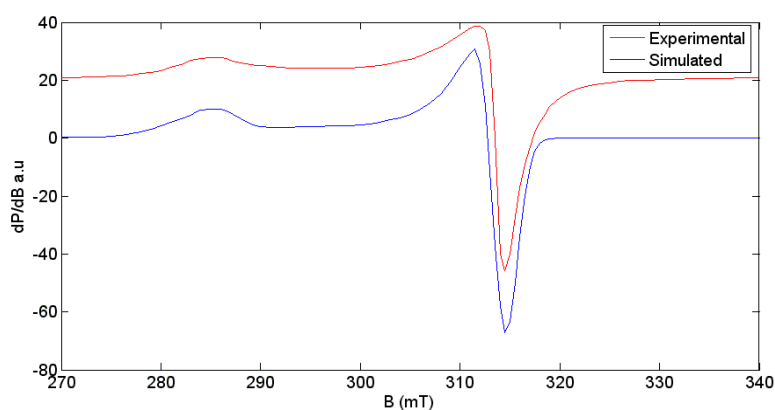
Fig. 4.35 EPR spectrum of complex $[Cu(HL^1)Cl_2]$ **(6)** in polycrystalline state at 298 K.
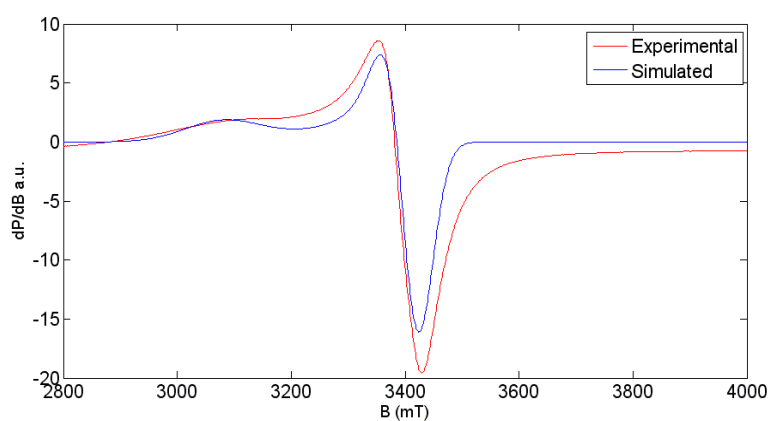
Fig. 4.36 EPR spectrum of complex **8** in polycrystalline state at 298 K.
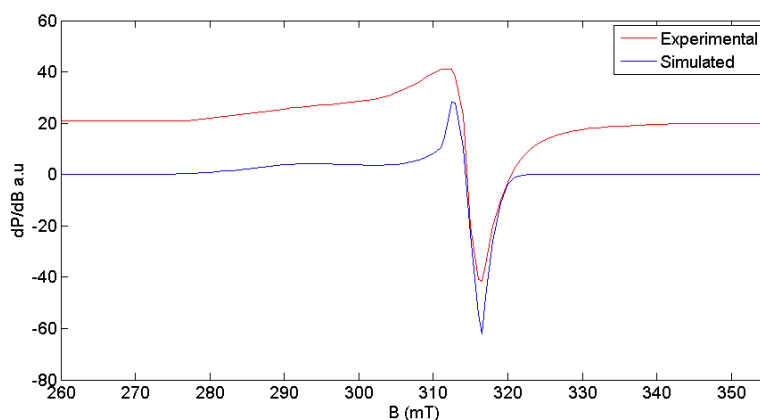
Fig. 4.37 EPR spectrum of complex **11** in polycrystalline state at 298 K.

The complex [Cu(HL^1)Cl$_2$] (**6**) shows negligible exchange interaction and confirms the monomeric nature of the complex while the complex [Cu$_2$ L$^1_2$(OAc)$_2$] (**9**) gives a G value of 2.856 again as a evidence of dimeric nature of the complex which has been clearly described by the single crystal XRD above. The EPR spectrum of the complex **9** (Fig. 4.38) in polycrystalline state shows a rhombic symmetry with three *g* values suggests that it has a distorted square pyramidal structure.
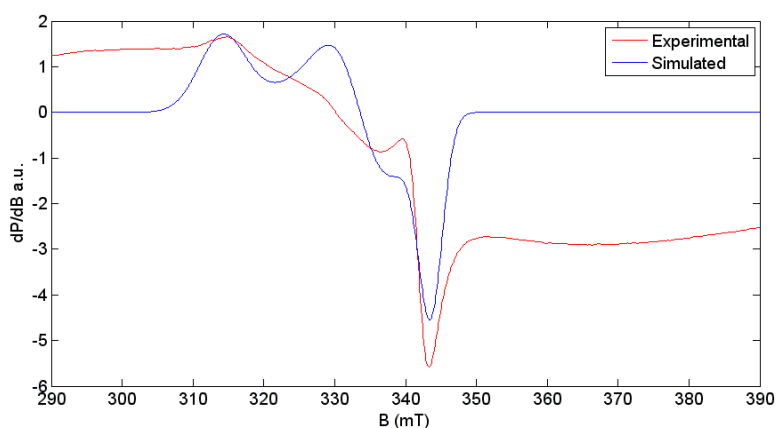
Fig. 4.38 EPR spectrum of complex [Cu$_2$ L$^1_2$(OAc)$_2$] (**9**) in polycrystalline state at 298 K.

The spectra of complex $[Cu_2L^1_2Br_2]\bullet H_2O$ (**10**) is reverse axial (Fig. 4.39) in polycrystalline state at 298 K with well defined $g_{\parallel}$ and $g_{\perp}$ features and the $g_{\perp} > g_{\parallel}$. The $g_{\parallel}$ is found to be 2.09 and $g_{\perp}$ is 2.22. The low G value (0.402) of this complex is an indication for a dimeric behavior which is supported by the magnetic susceptibility (1.186 BM) of the complex.

The absence of signal of the complexes **7** and **14** in polycrystalline state may be due to the strong exchange interaction between the copper atoms in the molecule suggesting a dimer for these two complexes. The magnetic susceptibility values of these two complexes (1.037, 1.023) also add more confidence to our assumption in this regard.
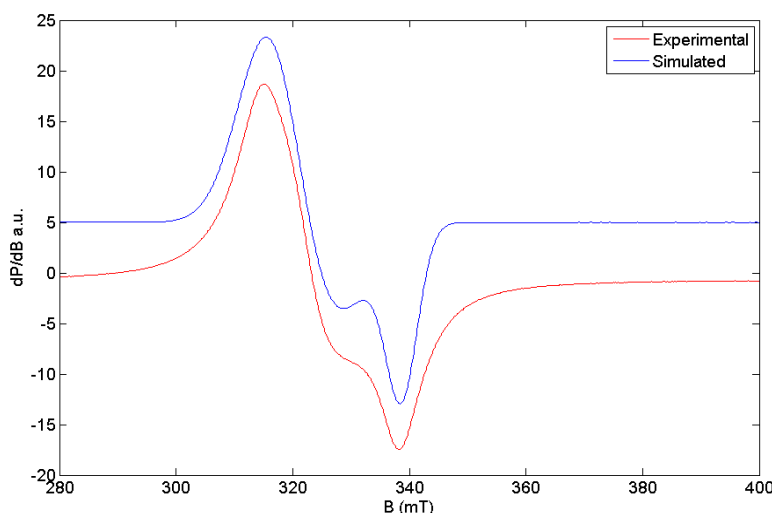
Fig. 4.39 EPR spectrum of complex $[Cu_2L^1_2Br_2]\bullet H_2O$ (**10**) in polycrystalline state at 298 K.

In the EPR spectrum of five coordinate copper(II) complex $[Cu_2L_2^1(NO_3)_2]\cdot H_2O$ (**7**) in frozen DMF, the four fairly resolved hyperfine lines $[^{63,65}Cu, I = 3/2]$ corresponding to -3/2, -1/2, +1/2 and +3/2 transitions. In addition to this the expected five superhyperfine lines of the two coordinated N atoms (one azomethine nitrogen and the other from pyridyl ring) are observed (Fig. 4.40).

As $g_\parallel > g_\perp$, a square pyramidal geometry can be assigned and rules out the possibility of a trigonal bipyramidal structure which would be expected to have $g_\perp > g_\parallel$. The α^2, β^2 and γ^2 values of this complex are less than one indicates that complexes have strong in-plane π-bonding. The orbital reduction factor $K_\parallel < K_\perp$ also support that the complex is involved in in-plane π-bonding [27].
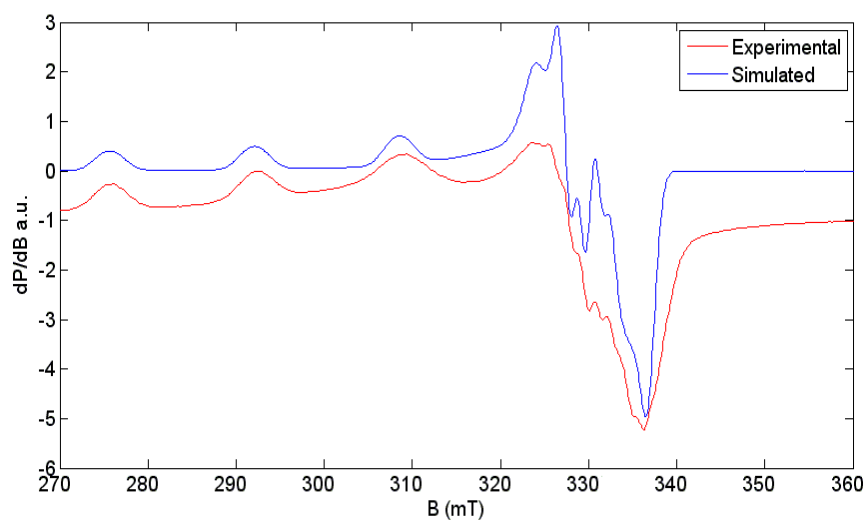
Fig.4.40 EPR spectrum of complex $[Cu_2L_2^1(NO_3)_2]\cdot H_2O$ (**7**) in DMF at 77 K.

The EPR spectra of the five coordinate copper(II) complexes $[Cu_2 L_2^1(OAc)_2]$ (**9**) and **12** in DMF at 77 K (Figs. 4.41 and 4.42) showed well resolved four copper hyperfine lines. The expected superhyperfine splittings of nitrogen atoms are not observed. The $g_\parallel > g_\perp$ suggests a distorted square pyramidal geometry for these complexes which was already proved by the single crystal XRD results. The fraction of lone pair electron density on the copper ion is relatively higher ($\alpha^2=1.176$ and 0.824 respectively) for the complex **9** illustrates that the copper ion engaged with more ionic type bonding with the ligand while the other involve in covalent type bonding. The $g_\parallel > 2.3$ further confirms the nature of ionic bonding in the complex **9**.
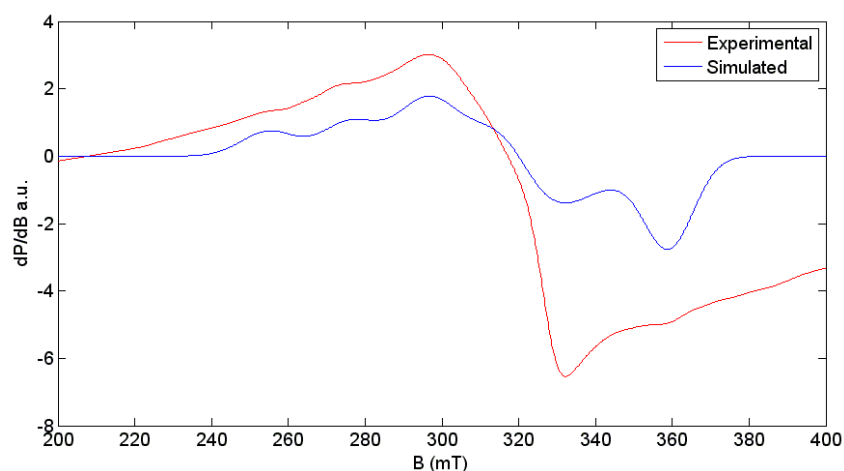
Fig. 4.41 EPR spectrum of complex $[Cu_2 L^1_2(OAc)_2]$ **(9)** in DMF at 77 K.
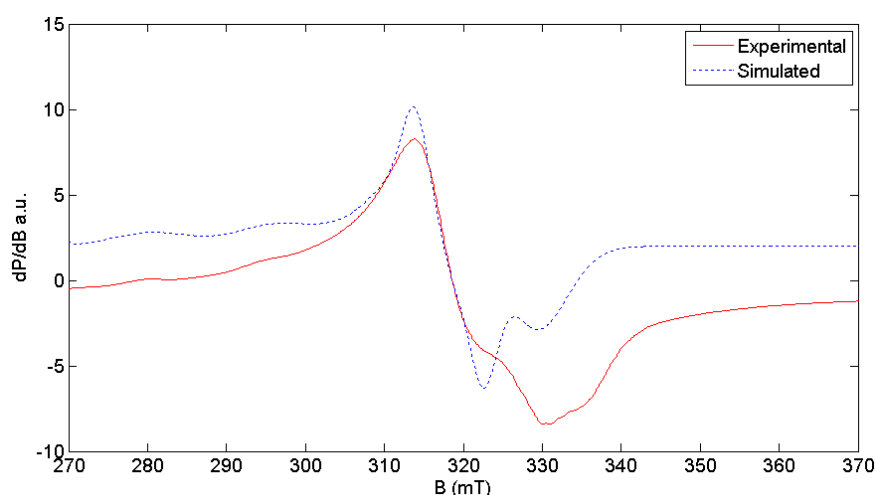
Fig. 4.42 EPR spectrum of complex $[Cu_2L_2^1N_3]$ **(12)** in DMF at 77 K.

The complex $[Cu_2L^1_2Br_2] \cdot H_2O$ **(10)** (Fig. 4.43) showed reverse axial spectra in solid state indicates that it has a d_{z^2} ground state with trigonal bipyramidal geometry but in solution state it gave axial spectrum this may be because of the dissociation of dimeric structure into monomeric in DMF solvent by the involvement of DMF solvent molecule. The $g_{\parallel}/A_{\parallel}$ ratio of the complex in DMF (168.6) is not in the range (90-140 cm) of a square planar structure [32]

confirms the presence of DMF molecule in the complex. The α^2, β^2 and γ^2 parameters of this complex indicating the involvement of more ionic behavior reveals that it has weak in-plane σ- bonding and in-plane π-bonding with the metal ion.
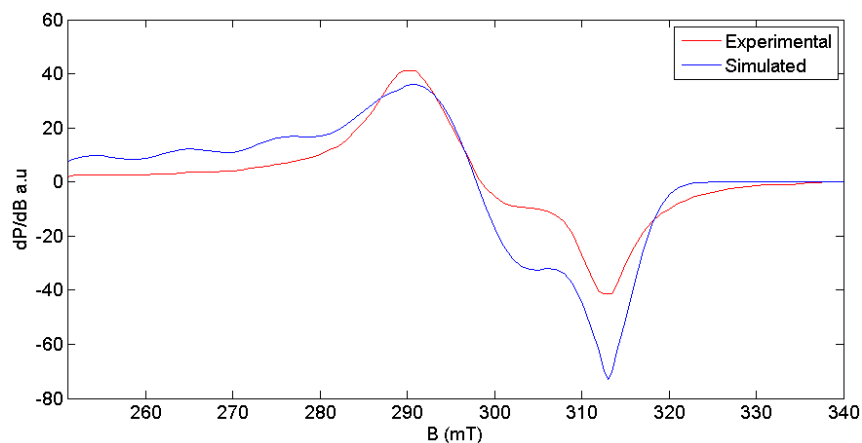
Fig.4.43 EPR spectrum of complex [Cu₂L¹₂Br₂]•H₂O (**10**) in DMF at 77 K.

The isotropic/average *g* values of the complexes [Cu(HL^1)Cl$_2$] (**6**) , **8** and **11** in polycrystalline state are consistent with the average *g* values in solution state (Fig. 4.44, 4.45 and 4.46) suggesting that they are not undergoing any kind of dissociation in the solution state. These spectra in DMF/DMSO at 77 K did not give the expected superhyperfine lines. However, they show well defined four line hyperfine splitting of copper. The $g_{\parallel}/A_{\parallel}$ ratio of the complexes **6** and **11** are 136.4 and 128.3 respectively suggest a square planar geometry while the other lies out of the range of the square planar geometry (90-140 cm^{-1}) indicating a square pyramidal coordination around the metal atom since its ground state orbital is still $d_{x^2-y^2}$. The α^2, β^2 and γ^2 parameters of these complexes provide the information that the metal ligand bonds are more covalent in nature than the other complexes and the $K_{\parallel} < K_{\perp}$ also point out that these complexes have strong in-plane σ-boning and in-plane π-bonding.
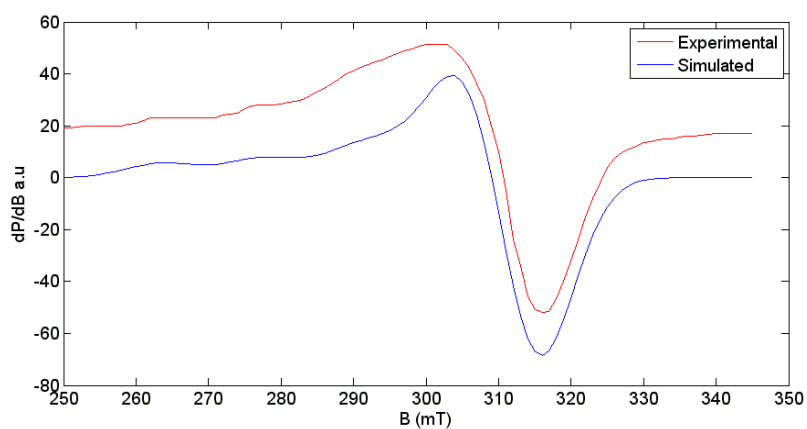
Fig.4.44 EPR spectrum of complex [Cu(HL^1)Cl$_2$] (**6**) in DMF at 77 K.
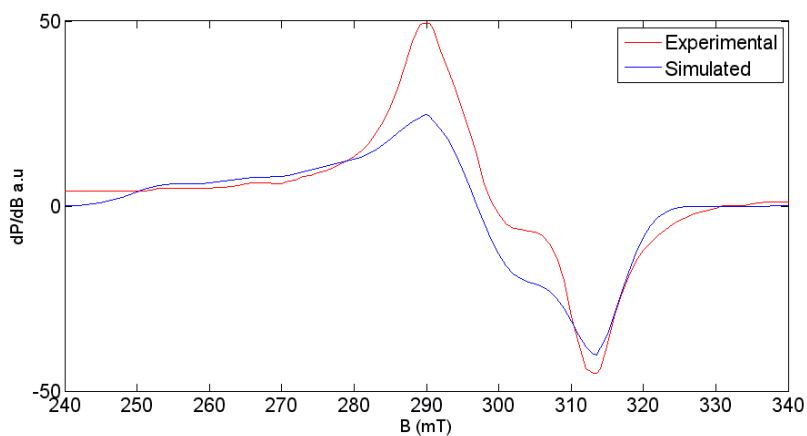
Fig.4.45 EPR spectrum of complex [Cu(HL^1)(SO$_4$)]·½ H$_2$O (**8**) in DMSO at 77 K.
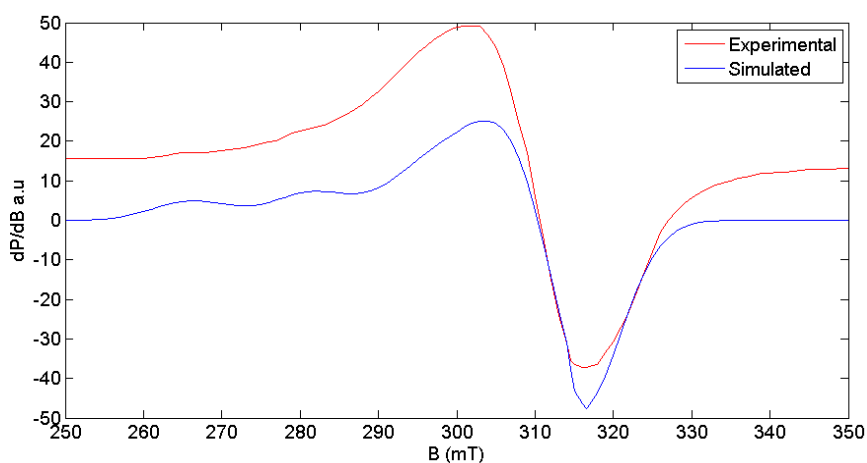
Fig.4.46 EPR spectrum of complex [CuL^{1}NCS]•2H$_2$O (**11**) in DMF at 77 K.

Unfortunately the complex [CuL$_2$(H$_2$O)] (**13**) shows isotropic symmetry in both solid and solution state (Fig. 4.47) because of the poor glass formation in DMF so that we could not furnish any kind of bonding nature of the complex. Though the complex [Cu$_2$(HL^2)$_2$Br$_2$(H$_2$O)$_2$] (**14**) has no signal at solid state spectrum, it gave a well resolved four fold hyperfine splitting in the parallel region in its solution state spectrum at 77 K (Fig. 4.57). The α^2, β^2 and γ^2 parameters show that this complex has very weak in-plane σ-bonding and in-plane π-bonding between the ligand and the metal ion and K$_\perp$< K$_\parallel$ also reveals that it has out-of-plane π-bonding.
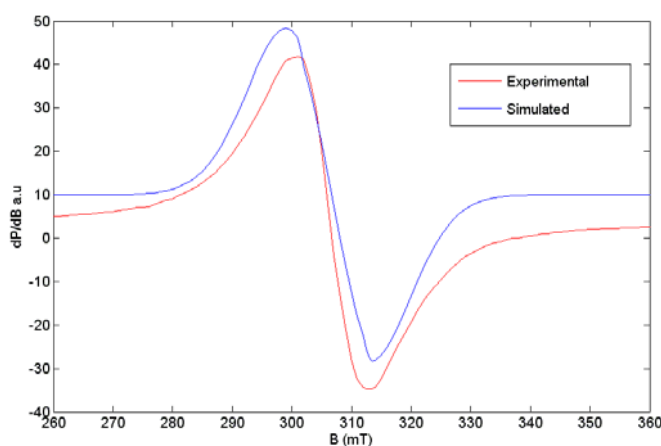
Fig.4.47 EPR spectrum of complex [CuL$_2$(H$_2$O)] (**13**) in DMF at 77 K.
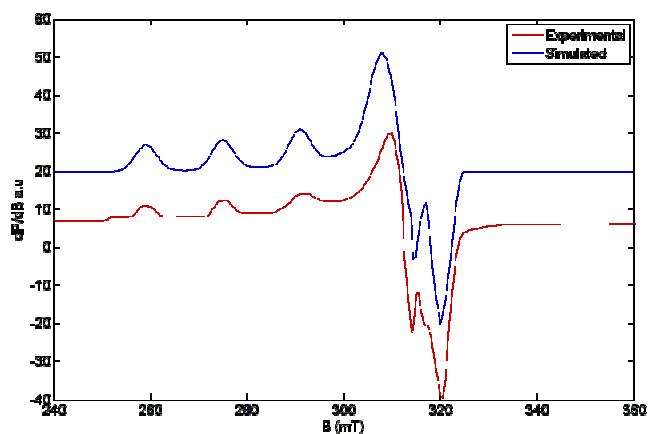
Fig. 4.48 EPR spectrum of complex [Cu$_2$(HL^2)$_2$Br$_2$(H$_2$O)$_2$] (**14**) in DMF at 77 K.

References

[1]   M. Akkurt, S. Ozfuric, S.Ide, Anal. Sci. 16 (2000) 667.

[2]   J.R. Dimmock, R.N. Puthucode, J.M. Smith, M. Hetherington, J.W. Quil, U. Pugazhenthi, T. Lechler, J.P. Stables, J. Med. Chem. 39 (1996) 3984.

[3]   J.R. Dimmock, K.K. Sidhu, S.D. Thumber, S.K. Basran, M. Chen, J. W. Quil, Eur. J. Med. Chem. 30 (1995) 287.

[4]   L.A. Saryan, E. Ankel, C. Krishnamurthi, D.H. Petering, H. Elford, J. Med. Chem. 22 (1979) 1218.

[5]   H. Beraldo, D. Gambino, Mini Reviews in Medicinal Chemistry 4 (2004) 31.

[6]   SMART and SAINT, Area Detector Software Package and SAX Area Detector Integration Program, Bruker Analytical X-ray; Madison, WI, USA, 1997.

[7]   SADABS, Area Detector Absorption Correction Program; Bruker Analytical X-ray; Madison, WI, 1997.

[8]   G.M. Sheldrick, *SHELXTL-PLUS, Crystal Structure Analysis Package*; Bruker Analytical X-Ray, Madison, WI, USA, 1997.

[9]   K. Brandenburg, Diamond Version 3.2g, Crystal Impact GbR, Bonn, Germany, 2010.

[10]   W.J. Geary, Coord. Chem. Rev. 7 (1971) 81.

[11]   D.X. West, J.K. Swearingen, Trans. Met. Chem. 26 (2001) 260.

[12]   A.W. Addison, J.N. Rao, J. Reedijk, G.C. Vershoor, J. Chem. Soc., Dalton Trans. (1984) 1349.H. Sacconi, G. Speroni, J. Am Chem. Soc. 87 (1965) 3102.

[13] G. Murphy, C.O. Sullivan, B. Murphy, B. Hathaway, Inorg. Chem. 37 (1998) 240.

[14] U.L. Kala, S. Suma, M.R.P. Kurup, S. Krishnan, R.P. John, Polyhedron 26 (2007) 1427.

[15] K. Nakamoto, Infrared and Raman Spectra of Inorganic and Coordination Compounds, Part B, fifth edition, Wiley, New York, 1997.

[16] V. Ramesh, P. Umasundari, K.K. Das, Spectrochim. Acta Part A, 54 (1998) 225.

[17] V. Philip, V. Suni, M.R.P. Kurup, M. Nethaji, Polyhedron 25 (2006) 1931.

[18] F. Junnosuke, N. Kazuo, K. Masahisa, J. Am. Chem. Soc 78 (1956) 3295.

[19] P.F. Rapheal, E. Manoj, M.R.P. Kurup, Polyhedron 26 (2006) 818.

[20] M.R.P Kurup, B. Varghese, M. Sithambaresan, S. Krishnan, S.R. Sheeja, E. Suresh, Polyhedron 30 (2010) 70.

[21] R.P. John, A. Sreekanth, V. Rajakannan, T.A. Ajith, M.R.P. Kurup, Polyhedron 23 (2004) 2549.

[22] A.B.P. Lever, Inorganic Electronic Spectroscopy, 2nd ed., Elsevier, Amsterdam, 1984.

[23] B.J. Hathaway, A.A.G. Tomlinson, Coord. Chem. Rev. 5 (1970) 24.

[24] M.J.M. Campbell, Coord. Chem. Rev. 15 (1975) 279.

[25] W. Jingping, H. Qiuxia, N. Jingyang, J. Coord. Chem., 57 (2004) 33.

[26] G.A. Nazri, C. Julien, Solid State Ionics 80 (1995) 271.

[27] B.J. Hathaway, In Comprehensive Coordination Chemistry; Wilkinson, G., Gillard, R. D., McCleverty, J. A., Eds. Permagon: Oxford, 1987; Vol. 5, p 533.

[28] A.W. Addison, T.N. Rao, J. Reedijk, J. van Rijn, G.C. Vershoor, J. Chem. Soc., Dalton Trans. (1984) 1349.

[29] J.R. Wasson, C. Trapp, J. Phys. Chem. 73 (1969) 3763.

[30] J.A. De Bolfo, T.D. Smith, J.F. Boas, J.R. Pilbrow, J.Chem. Soc. Faraday II 72 (1976) 481.

[31] M.J. Bew, B.J. Hathaway, R.J. Faraday, J. Chem. Soc. Dalton Trans. (1972) 1229.

[32] V. Sakaguchi, A.W. Addison, J. Chem. Soc., Dalton Trans. 600 (1979).

........................❧❧❧........................

Syntheses, spectral studies and structures of zinc(II) complexes of N⁴-phenylsemicarbazones

5.1. Introduction

Natural zinc is a mixture of five stable isotopes: ^{64}Zn (48.6 percent), ^{66}Zn (27.9 percent), ^{67}Zn (4.1 percent), ^{68}Zn (18.8 percent), and ^{70}Zn (0.6 percent). Zinc is an essential element, necessary for sustaining all life. In the human body, generally, 2-3 g of zinc is present and about 15 mg per day is necessary for the maintenance of healthy condition. It is estimated that about 3000 proteins in the human body contain zinc. It stimulates the activity of approximately 100 enzymes, which are substances that promote biochemical reactions in the body [1]. In addition, there are over a dozen types of cells in the human body that secrete zinc ions. Brain cells in the mammalian forebrain, cells in the salivary gland, prostate, immune system and intestine are the main types that secrete zinc. Zinc supports a healthy human immune system [2], is needed for wound healing [3], helps maintain the sense of taste and smell [4] and is needed for DNA synthesis. Zinc also supports normal growth and development during pregnancy, childhood and adolescence [5].

Zinc is a component of some enzymes that digest protein in the gastrointestinal tract. The major uses of zinc metal are in galvanizing iron and

steel. When iron and zinc together are exposed to a corrosive medium, they constitute an electrolytic cell, and the zinc is oxidized to Zn^{2+} ion preferentially because of its higher electrode potential. This so-called sacrificial protection, coupled with the much greater corrosion resistance of zinc under atmospheric conditions, is the basis for galvanizing.

Zinc ion has a small radius and acts as a Lewis acid and hence it can play an advantageous role as a catalyst in hydrolysis reactions. The stability of zinc complexes with some ligands present in living system is satisfactorily high but not too high, so that zinc is reactive in complexation. This means high probability of ligand-exchange reactions in zinc complexes in living systems. Irving-Williams stability order applicable to various divalent metal complexes with common ligands shows that the stability of zinc complexes is generally lower than that of copper and is comparable to that of nickel and much higher than that of calcium or magnesium. The bivalent state is stable because of the fully occupied $3d$ orbital, and it is maintained even in highly oxidizing and reducing environments. Fairly high affinity is shown towards the main coordinating atoms such as sulfur, nitrogen, and oxygen. This means high flexibility in the structure, coordination mode, and coordination number of the complexes produced [6].

In view of the stability of the filled d sublevel, the element shows few of the characteristics of transition metals despite its position in the d-block of the periodic table. It resembles other transition metals in the formation of stable complexes with O, N and S-donor ligands and with ions like cyanide, halide etc. The d^{10} configuration affords no crystal field stabilization, which implies that the stereochemistry of a Zn^{2+} complex depends on the size and polarizing power of this ion. Because of this versatility towards different kinds of ligands and its flexibility towards coordination number ranging from two to six, the

zinc(II) ion provides various types of chelate complexes. Among these complexes, some have attracted special attention as model compounds for the active sites of zinc-containing enzymes [7] and their functions strongly depend upon the coordination environment around the zinc ion. Therefore, for understanding or creating functional zinc complexes, it is important to consider the relationship of the coordination characteristics peculiar to the zinc ion. Biological activity of semicarbazones are found to increase on complexation with transition metals [9], higher activity being incorporated with substitution at N(4) position [10]. These observations were the impetus for us to build an N(4)-substituted semicarbazone moiety on 2-benzoylpyridine and 2-formylpyridine and synthesize zinc(II) complexes to study the coordinating behavior. In this chapter we describe the spectral studies of six new Zn(II) complexes of the ligands HL^1 and HL^3.

5.2. Experimental

5.2.1. Materials

Zinc(II) acetate dehydrate, zinc(II) bromide, sodium azide (Merck) were used as supplied. The solvents were purified by standard procedures before use.

5.2.2. Syntheses of complexes

5.2.2.1. Syntheses of [ZnL^1(OAc)]·3/2H$_2$O (15)

Hot methanolic solutions (15 ml) of zinc acetate dihydrate (0.219 g, 1 mmol) and the ligand HL^1 (0.240 g, 1 mmol) were mixed with constant stirring. The mixture was heated under reflux for 2 h. and cooled. The complex separated was filtered, washed thoroughly with water, methanol and then ether and dried *in vacuo* over P_4O_{10}.

5.2.2.2. Syntheses of [Zn(HL^1)(OAc)(SCN)]·1/2H$_2$O (16)

A hot methanolic solution (15 ml) of 0.240 g (1 mmol) the ligand, HL^1 and a methanolic solution of potassium thiocyanate, KSCN (0.097 g, 1 mmol) were mixed with constant stirring. A hot methanolic solution (10 ml) of 0.219 g (1 mmol) zinc acetate dihydrate was added to it with constant stirring. The mixture was refluxed for 4 h. On cooling the complex was separated out. It was filtered, washed thoroughly with water, methanol and then ether and dried *in vacuo* over P$_4$O$_{10}$.

5.2.2.3. Syntheses of [ZnL^{1}N$_3$] (17)

A hot methanolic solution (15 ml) of the ligand HL^1 (0.240 g, 1 mmol) and a methanolic solution of sodium azide (0.065 g, 1 mmol), were mixed with constant stirring. A hot methanolic solution of 0.219 g (1 mmol) of zinc acetate dihydrate was added to the above mixture with constant stirring. The mixture was heated under reflux for 3 h. and cooled. The complex separated was filtered, washed thoroughly with water, methanol and then ether and dried *in vacuo* over P$_4$O$_{10}$.

5.2.2.4. Syntheses of [ZnL^3(OAc)] (18)

This compound was prepared by refluxing a mixture of hot methanolic solutions of the ligand HL^3 (0.329 g, 1 mmol) and zinc acetate dihydrate (0.219 g, 1 mmol) for 4 h. and cooled. The complex separated was filtered, washed thoroughly with water, methanol and then ether and dried *in vacuo* over P$_4$O$_{10}$.

5.2.2.5. Syntheses of [Zn(HL^3)Br$_2$] (19)

A solution of semicarbazone, HL^3 (0.329 g, 1 mmol) in 15 ml of methanol was treated with a methanolic solution of zinc(II) bromide (0.225 g, 1 mmol). The solution was heated under reflux for 4 h. The resulting solution

was allowed to stand at room temperature and after slow evaporation yellow single crystals suitable for single crystal analysis were separated out.

5.2.2.6. Syntheses of [Zn$_2$(HL^3)$_2$(N$_3$)$_4$ (20)

Hot methanolic solutions of HL^3 (0.329 g, 1 mmol) (15 ml) and 0.065 g sodium azide (1 mmol) were mixed with constant stirring. A hot methanolic solution (20 ml) of (0.219 g, 1 mmol) zinc acetate dihydrate was added to it with constant stirring. The mixture was heated under reflux for 3 h. On cooling single crystals suitable for single crystal XRD analysis were separated out.

5.2.3. Physical measurements

Elemental analyses were carried out using an Elementar Vario EL III CHNS analyzer at SAIF, Kochi, India. Infrared spectra were recorded on a JASCO FT-IR-5300 Spectrometer in the range 4000-400 cm^{-1} using KBr pellets and electronic spectra were recorded on a UV-vis Double Beam UVD-3500 Spectrophotometer using solution in methanol at the Department of Applied Chemistry, Cochin University of Science and Technology, Kochi 22, India. The molar conductivities were measured in DMF (10^{-3} M) solutions at 298 K with a Systronic model 303 direct-reading conductivity bridge. TG-DTG analyses of the complexes were carried out under nitrogen at a heating rate of 10 $^{\circ}$C min^{-1} in the range 50-1000 $^{\circ}$C using a Perkin Elmer Pyris Diamond TG/DTA analyzer at the Department of Applied Chemistry, CUSAT, Kochi, India.

5.2.4. X-ray crystallography

Single crystals of compounds [Zn(HL^3)Br$_2$] (**19**) and [Zn$_2$(HL^3)$_2$(N$_3$)$_4$] (**20**) suitable for X-ray diffraction studies were grown from its methanolic solutions by slow evaporation at room temperature. Single crystal of

dimensions 0.30x0.25x0.2 and 0.30x0.25x0.25 mm^3 of the complexes **19** and **20** respectively were selected and mounted on a Bruker SMART APEX diffractometer, equipped with a graphite crystal, incident-beam monochromator, and a fine focus sealed tube with Mo Kα (λ = 0.71073 Å) as the X-ray source. The crystallographic data along with details of structure solution refinements are given in Table 5.1. The unit cell dimensions were measured and the data collections were performed at 296(2) K. Bruker SMART software was used for data acquisition and Bruker SAINT software for data integration [11]. Absorption corrections were carried out using SADABS based on Laue symmetry using equivalent reflections [12]. The structure was solved by direct methods and refined by full-matrix least-squares calculations with the SHELXL–97 software package [13]. The graphics tool used was DIAMOND version 3.2g [14]. All non-hydrogen atoms were refined anisotropically. All the H atoms on C and N4 nitrogen of the complex **19** were placed in calculated positions, guided by difference maps and refined isotropically, with C–H and N–H bond distances of 0.93 Å and 0.86 Å. The hydrogen at the N3 nitrogen was located from difference map and restrained using DFIX instruction. Although the H atoms on C atoms of the complex **20** were placed in calculated positions guided by difference maps, the N3–H3N and N4–H4N were located from difference map and freely refined with the bond distances of 0.807(15) and 0.804(16) Å respectively.

Table 5.1 Crystal refinement parameters of complexes **19** and **20**

Parameters	[Zn(HL^3)Br$_2$] (19)	[Zn$_2$(HL^3)$_2$(N$_3$)$_4$] (20)
Empirical formula	C$_{19}$H$_{16}$Br$_2$N$_4$O Zn	C$_{38}$H$_{32}$N$_{20}$O$_2$Zn$_2$
Formula weight	541.55	931.62
Color	yellow	yellow
Temperature (T) K	296(2)	296(2)
Wavelength (Mo Kα) (Å)	0.71073	0.71073
Crystal system	Monoclinic	Monoclinic
Space group	*P*2$_1$/*c*	*P*2$_1$/*n*
Cell parameters		
a	7.8156(3) Å	11.4681(7) Å
b	19.2329(6) Å	12.0221(6) Å
c	13.5941(5) Å	15.1548(8) Å
α	90°	90°
β	90.8720(10)°	97.011(2)°
γ	90°	90°
Volume V (Å^3)	2043.18(13)	2073.8(2)
Z	4	2
Calculated density (ρ) (Mg m^{-3})	1.760	1.492
Absorption coefficient, μ(mm^{-1})	5.129	1.218
F(000)	1064.0	952.0
Crystal size(mm^3)	0.30 x 0.25 x 0.25	0.40 x 0.35 x 0.35
θ range for data collection	2.59 to 25.00°	2.11 to 28.23°
Limiting indices	-8≤h≤9, -22≤k≤22, -16≤l≤16	-14≤h≤15, -12≤k≤15, -18≤l≤20
Reflections collected	14826	34884
Unique Reflections (R$_{int}$)	3593 [R(int) = 0.0476]	5111 [R(int) = 0.0650]
Completeness to θ	25.00 99.5 %	28.23° 99.8 %
Absorption correction	Semi-empirical from equivalents	Semi-empirical from equivalents
Maximum and minimum transmission	0.277 and 0.234	0.6773 and 0.6438
Refinement method	Full-matrix least-squares on F^2	Full-matrix least-squares on F^2
Data / restraints / parameters	3593 / 0 / 244	5111 / 0 / 280
Goodness-of-fit on F^2	1.077	1.144
Final R indices [I > 2σ (I)]	R$_1$ = 0.0312, wR$_2$ = 0.0742	R$_1$ = 0.0309, wR$_2$ = 0.0893
R indices (all data)	R$_1$ = 0.0475, wR$_2$ = 0.0861	R$_1$ = 0.0417, wR$_2$ = 0.1043
Largest difference peak and hole (e Å^{-3})	0.559 and -0.520	0.384 and -0.631

$R_1 = \Sigma||F_o| - |F_c|| / \Sigma|F_o|$ $wR_2 = [\Sigma w(F_o^2 - F_c^2)^2 / \Sigma w(F_o^2)^2]^{1/2}$

5.3. Results and discussion

5.3.1. Analytical measurements

The colors, molar conductivities and partial elemental analyses data of the complexes are listed in Table 5.2. Zn complexes were found to form readily in methanol medium under reflux. The elemental analyses showed that the compounds **15, 17** and **18** can be assigned the general formula [ZnLX] (X=OAc, N$_3$; L=L^1, L^3). However, the compound **15** contains one mole of lattice water in its crystal. The compounds **16, 19** and **20** were assigned the formula [Zn(HL^1)(OAc)(SCN)], [Zn(HL^3)Br$_2$], and [Zn$_2$(HL^3)$_2$(N$_3$)$_4$] respectively. All these complexes are moderately soluble in acetonitrile and readily soluble in DMF. The molar conductivity measurements showed that all of them are non-electrolytes in nature [15]. The complexes **15**, **17** and **18** have ligands in the anionic form, whereas in **16, 19** and **20** have ligands coordinated in the amido form as evidenced by the single crystal XRD data and IR spectra. All the complexes are found to be diamagnetic as expected for a d^{10} Zn(II) system.

Table 5.2 Preliminary analytical data of Zn(II) complexes of HL^1 and HL^3

Compound	Color	Found (Calculated) %				$\Lambda_M{}^a$
		C	H	N	S	
[ZnL^1(OAc)]·H$_2$O (**15**)	yellow	46.94(47.20)	4.29(4.22)	14.69(14.68)	-	1
[Zn(HL^1)(OAc)(SCN)] (**16**)	yellow	45.75(45.56)	3.61(3.35)	16.56(16.60)	7.30(7.60)	27
[ZnL^{1}N$_3$] (**17**)	yellow	44.78(45.04)	3.43(3.20)	28.21(28.28)	-	19
[ZnL^3(OAc)] (**18**)	yellow	57.44(57.35)	3.63(4.13)	12.86(12.74)	-	12
[Zn(HL^3)Br$_2$] (**19**)	yellow	42.32(42.14)	3.12(2.98)	10.44(10.35)	-	20
[Zn$_2$(HL^3)$_2$(N$_3$)$_4$] (**20**)	yellow	48.87(48.99)	3.54(3.46)	29.92(30.07)	-	6

[a]Molar conductivity (ohm^{-1}cm^{2}mol^{-1}), 10^{-3} M DMF at 298 K

5.3.2. Crystal structure of the complex [Zn(HL^3)Br$_2$] (19)

The molecular structure of the mononuclear Zn(II) complex with the atom numbering scheme is shown in Fig. 5.1. The compound crystallizes in the monoclinic space group $P2_1/c$ and the coordination around the Zn(II) ion can be best described as a distorted square pyramidal (τ=0.3431). Metal atom is coordinated by azomethine nitrogen, oxygen atom, one pyridyl nitrogen from semicarbazone and two bromine atoms. The oxygen atom of the semicarbazone ligand coordinates the metal atom in amido form, which is confirmed by the double bond nature of C13–O1 (1.227 Å) and N3–C13 (1.373 Å) bond lengths [16]. The C13–N3 and N2–N3 bond distances (Table 5.3) reveal that the extensive delocalization of the ligand over the coordination framework is restricted. The angle between the two aromatic rings of 2-benzoylpyridine part of the semicarbazone ligand is 58.9(2)° and the angle between the phenyl ring of the semicarbazide part and the pyridyl ring is 14.2(2)°.
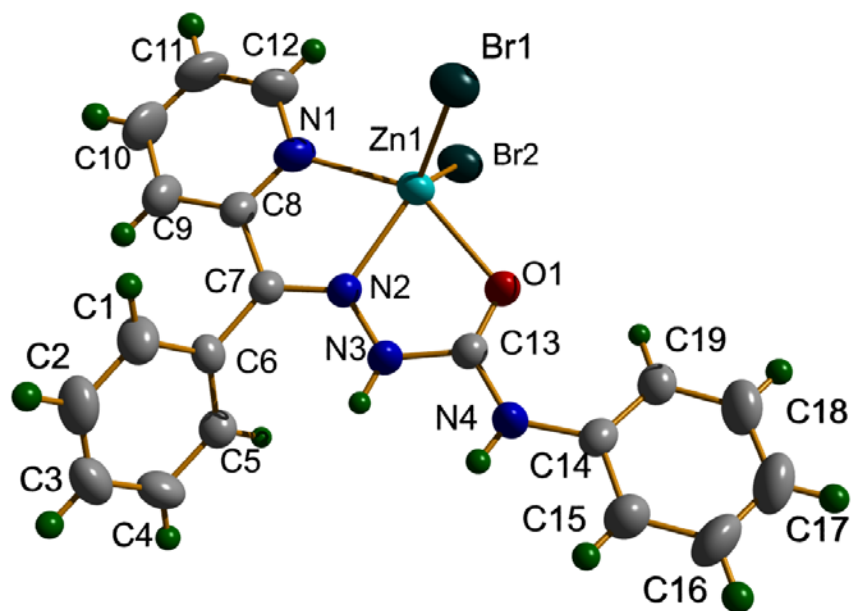
**Fig. 5.1** Structure and labeling diagram for compound [Zn(HL^3)Br$_2$] (**19**).

Table 5.3 Selected bond lengths (Å) and bond angles (°) of compound **19**

Bond lengths		Bond angles	
N(1)—Zn(1)	2.143(3)	C(7)—N(2)—N(3)	122.2(3)
C(13)—O(1)	1.227(4)	C(7)—N(2)—Zn(1)	121.1(2)
C(13)—N(4)	1.341(4)	N(3)—N(2)—Zn(1)	116.2(2)
C(13)—N(3)	1.373(5)	N(2)—N(3)—C(13)	115.3(3)
N(2)—N(3)	1.361(4)	C(13)—N(4)—C(14)	129.3(3)
N(2)—Zn(1)	2.126(3)	C(13)—O(1)—Zn(1)	113.9(2)
N(3)—H(3A)	0.8600	N(2)—Zn(1)—N(1)	73.68(11)
N(4)—H(4A)	0.8600	N(2)—Zn(1)—O(1)	72.72(10)
O(1)—Zn(1)	2.250(2)	N(1)—Zn(1)—O(1)	146.35(10)
Zn(1)—Br(2)	2.3700(6)	N(2)—Zn(1)—Br(2)	125.76(9)
Zn(1)—Br(1)	2.3862(6)	N(1)—Zn(1)—Br(2)	98.56(9)
		O(1)—Zn(1)—Br(2)	99.35(7)
		N(2)—Zn(1)—Br(1)	118.40(9)
		N(1)—Zn(1)—Br(1)	98.99(9)
		O(1)—Zn(1)—Br(1)	98.47(8)
		Br(2)—Zn(1)—Br(1)	115.84(2)

The bond distances to Zn are in the order $Zn–N_{(azo)} < Zn–N_{(py)} < Zn–O_{(ketoxy)} < Zn–Br2 < Zn–Br1$. The bond lengths ($Zn–N_{(azo)}$, $Zn–N_{(py)}$, $Zn–Br$) are very close to other reported Zn complexes of thiosemicarbazones [17,18]. The basal plane could involve either Br1 or Br2 with semicarbazone moiety, Zn–Br1 is marginally longer and it can be designated as the apical bond. The Zn atom is displaced with a distance of 0.6892 Å above the basal plane. The selected bond lengths and bond angles are given in Table 5.3. The *cis* angles N(2)–Zn(1)–Br(1) and Br(2)–Zn(1)–Br(1) are 118.40(9)° and 115.84(2)° and *trans* angles N(1)–Zn(1)–O(1) and N(2)–Zn(1)–Br(2) are 146.35(10)° and

125.76(9)° respectively indicating that the compound **19** has large distortion from square pyramidal geometry [19].

The unit cell packing diagram of the complex **19** viewed along *a* axis is given in Fig. 5.2. It can be observed that the molecules are packed so that the two consecutive molecules are centerosymmetrically arranged one over the other along a axis. The same arrangement was viewed only with the coordination frame work along c axis as shown in Fig. 5.3.
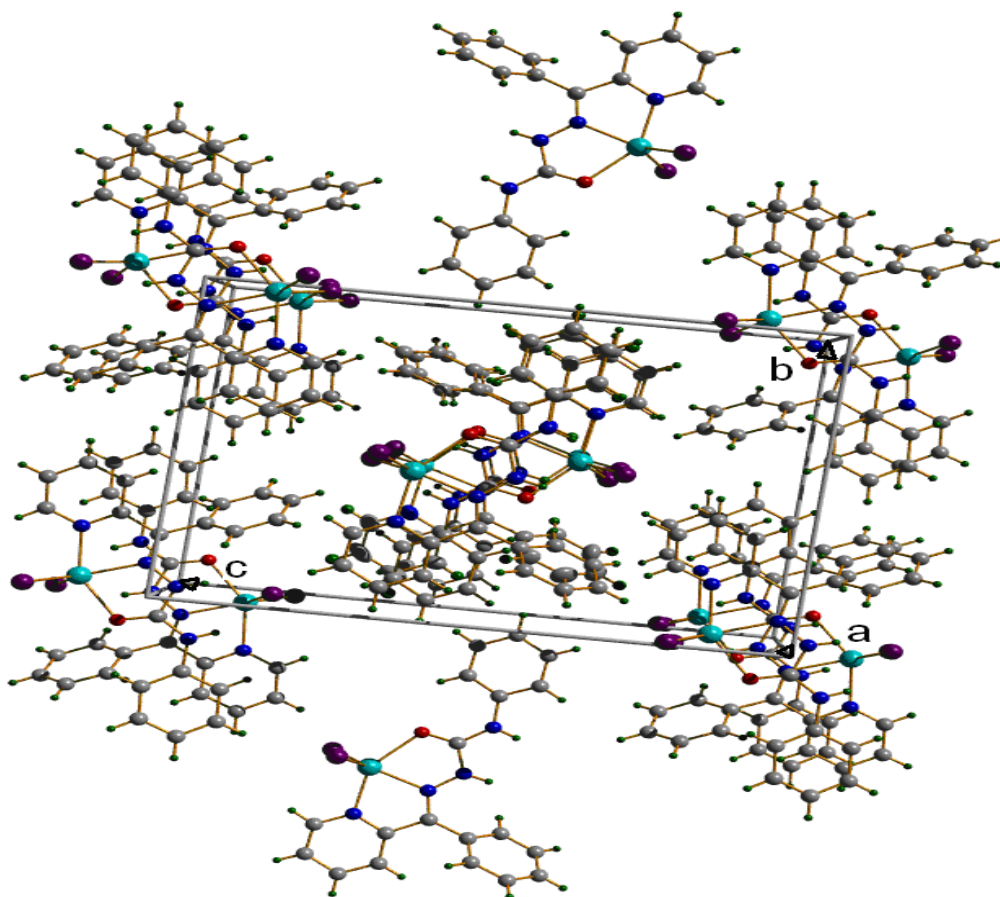
Fig. 5.2 Unit cell packing diagram of compound [Zn(HL^3)Br$_2$] (**19**) along a axis.
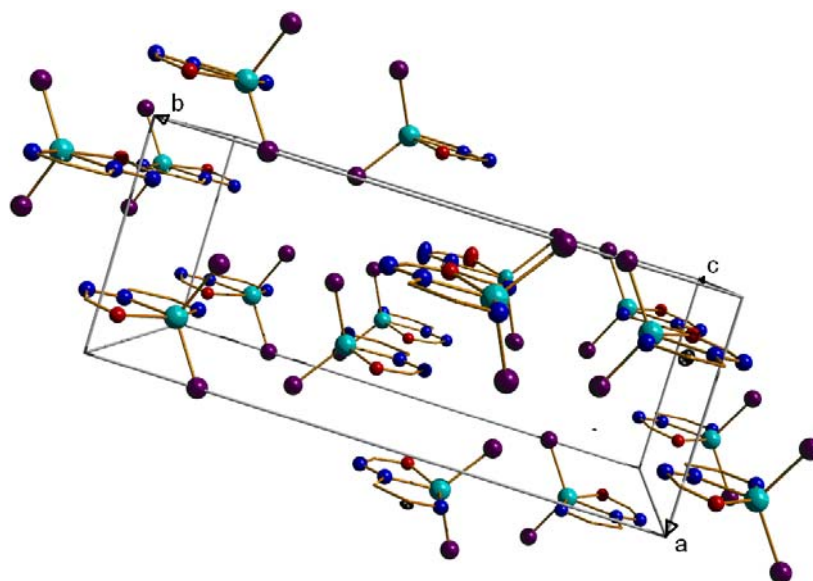
Fig. 5.3 Two different arrangements of the central ring of the compound [Zn(HL^3)Br$_2$] (**19**) in the unit cell.

The diverse $\pi\cdots\pi$ stacking present in the molecular arrangement is tabulated in Table 5.4. One $\pi\cdots\pi$ interaction has the distance between the two centroid of the rings of 3.8295(19) Å whereas the other has the Cg$\cdots$Cg distance of 3.938(3) Å (Fig. 5.4). In addition to these interactions there is a lone pair$\cdots\pi$ interaction between the Br1 atom and the phenyl ring of the 2-benzoylpyridine part of the ligand with a X$\cdots$Cg distance of 3.9859(17) Å as shown in Fig. 5.5.

Table 5.4 Interaction parameters of the compound [Zn(HL^3)Br$_2$] (**19**)

Hydrogen bonding interactions

D—H⋯A	D—H (Å)	H⋯A (Å)	D⋯A (Å)	∠D—H⋯A(°)
N(3)—H(3A)⋯Br(1)^a	0.86	2.71	3.377(3)	135
N(4)—H(4A)⋯Br(1)^a	0.86	2.89	3.584(3)	139
N(4)—H(4A)⋯Br(2)^b	0.86	2.87	3.482(3)	129
C(11)—H(11)⋯Br(1)^c	0.93	2.93	3.655(6)	136
C(19)—H(19)⋯O(1)	0.93	2.35	2.935(5)	121

$\pi\cdots\pi$ interactions

Cg(I)···Cg(J)	Cg—Cg(Å)	α (°)	β (°)	γ(°)
Cg(1)···Cg(1)[b]	3.8295(19)	0	18.48	18.48
Cg(5)···Cg(3)[b]	3.938(3)	14.2(2)	7.99	22.16

Y-X···Cg(π -ring) interactions

Y—X(I)···Cg(J)	X···Cg (Å)	γ (°)	Y—X···Cg
Zn(1)—Br(1)···Cg(4)[a]	3.9859(17)	11.87	117.81(3)

Cg (1) = Zn(1), O(1), C(13), N(3), N(2)
Cg (2) = Zn(1), N(1), C(8), C(7), N(2)
Cg (3) = N(1), C(8), C(9), C(10), N(11)
Cg (4) = C(1), C(2), C(3), C(4), C(5), C(6)
Cg (5) = C(14), C(15), C(16), C(17), C(18), C(19)
Equivalent position codes: a = 1-x,1-y,1-z; b = -x,1-y,1-z ; c = x,1/2-y,-1/2+z
D, donor; A, acceptor; Cg, centroid; α, dihedral angles between planes I and J; β, angle between Cg···Cg and Cg(J)_perp; γ, angle between Cg···Cg and Cg(I)_perp
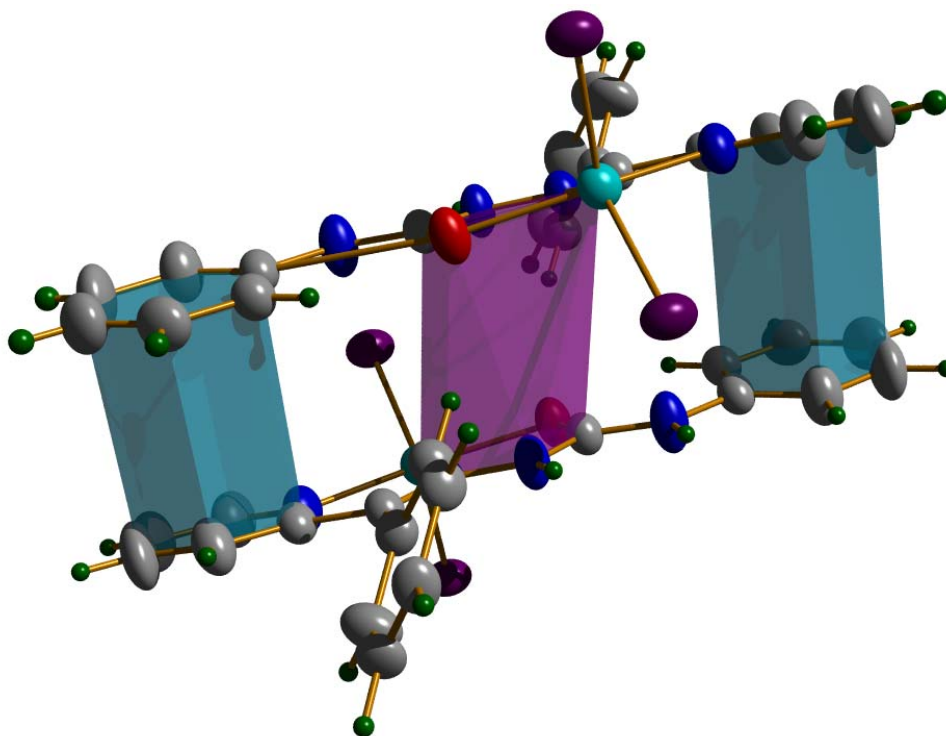

Fig. 5.4 $\pi\cdots\pi$ interactions between the molecules of the complex [Zn(HL³)Br₂] (**19**).
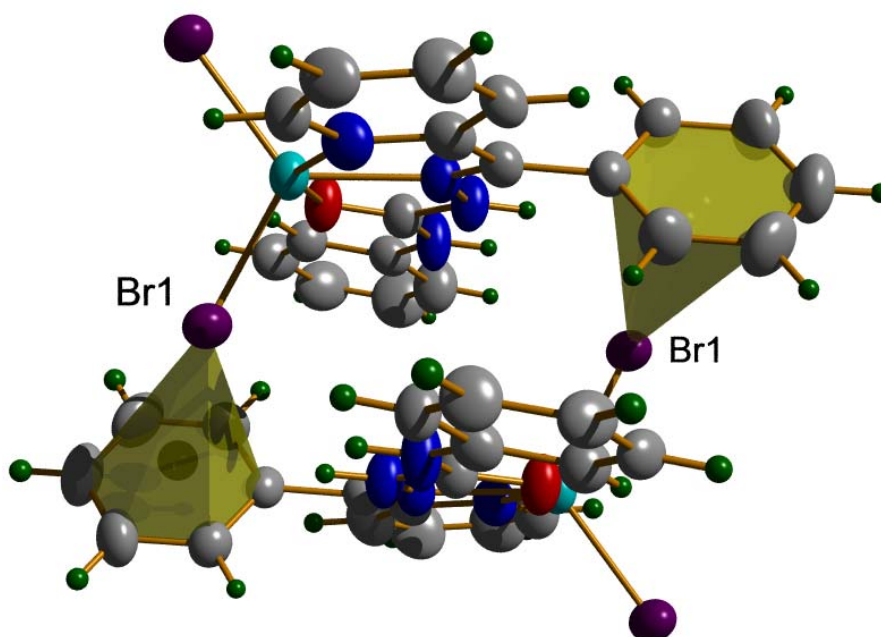
Fig. 5.5 Lone pair⋯π interactions of the compound [Zn(HL^3)Br$_2$] (**19**).

A bifurcated hydrogen bonding network is established between the hydrogen atom attached at N4 nitrogen and the two Br atoms of two adjacent molecules. Moreover, a non-conventional hydrogen bonding interaction is also observed between the H atom attached to pyridine ring and the Br atom of the adjacent molecule assembling a three dimensional network in the lattice as shown in Fig. 5.6. In addition to the conventional and non-conventional intermolecular hydrogen bonding interactions found in the molecular system, the presence of a non-conventional intramolecular interaction between hydrogen atom attached at the phenyl ring and the oxygen atom of the same molecule composes almost a coplanar arrangement of phenyl ring of the semicarbazide part with the semicarbazone skeleton of the ligand with very small twisting angle of 7.52º between the ring and the semicarbazone skeleton.
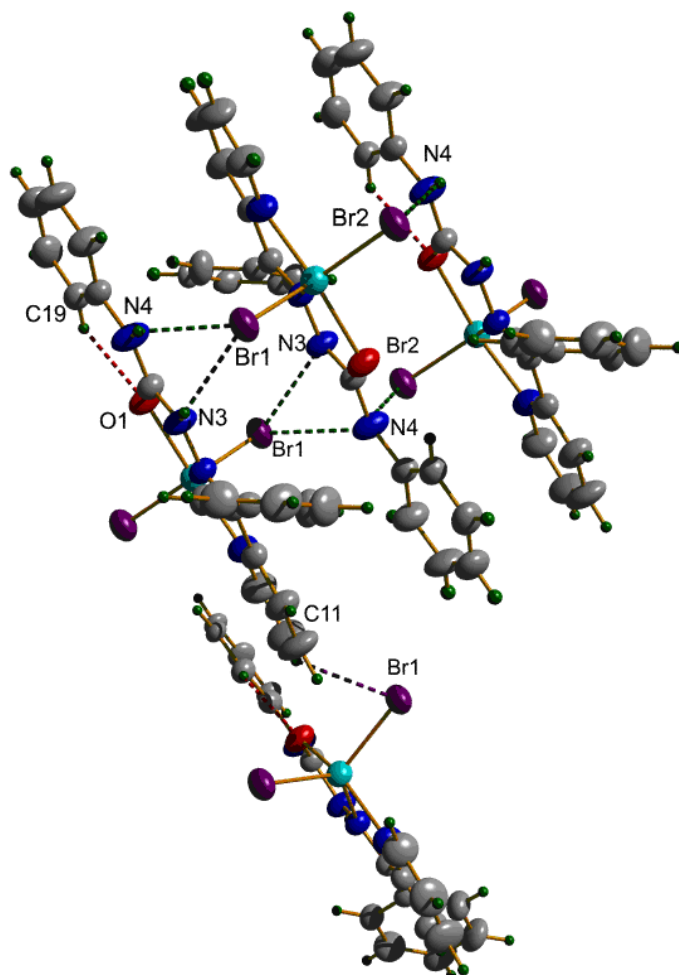
Fig. 5.6 Intermolecular hydrogen bonding network of the compound [Zn(HL^3)Br$_2$] (**19**).

5.3.3. Crystal structure of the complex [Zn$_2$(HL^3)$_2$(N$_3$)$_4$] (20)

The compound **20** crystallizes in the monoclinic space group $P2_1$/n. Fig. 5.6 shows the molecular structures of the dimeric complex with atom numbering scheme. Each Zn atom is hexacoordinated by azomethine nitrogen, oxygen atom from the ligand, one pyridyl nitrogen and three azide nitrogen atoms in which two atoms involve bridging of the two central metal atoms (Fig. 5.7). The oxygen atom from both ligands are coordinated in their amido forms

which is confirmed by the double bond nature of C13–O1 (1.233 Å) and C13–N3 (1.386 Å) bond lengths [20]. Zn(1)–N(5) bond distance is the shortest among all other coordinated bonds around the metal centre which shows that the azide nitrogen involved in bridging with other metal centre is strongly bonded with its parent metal atom than the bonding with free azide anion (Table 5.5). The angle between the two aromatic rings of 2-benzoylpyridine part of the semicarbazone ligand is 70.36(12)° and the angle between the phenyl ring of the semicarbazide part and the pyridyl ring is 27.27(14)°.
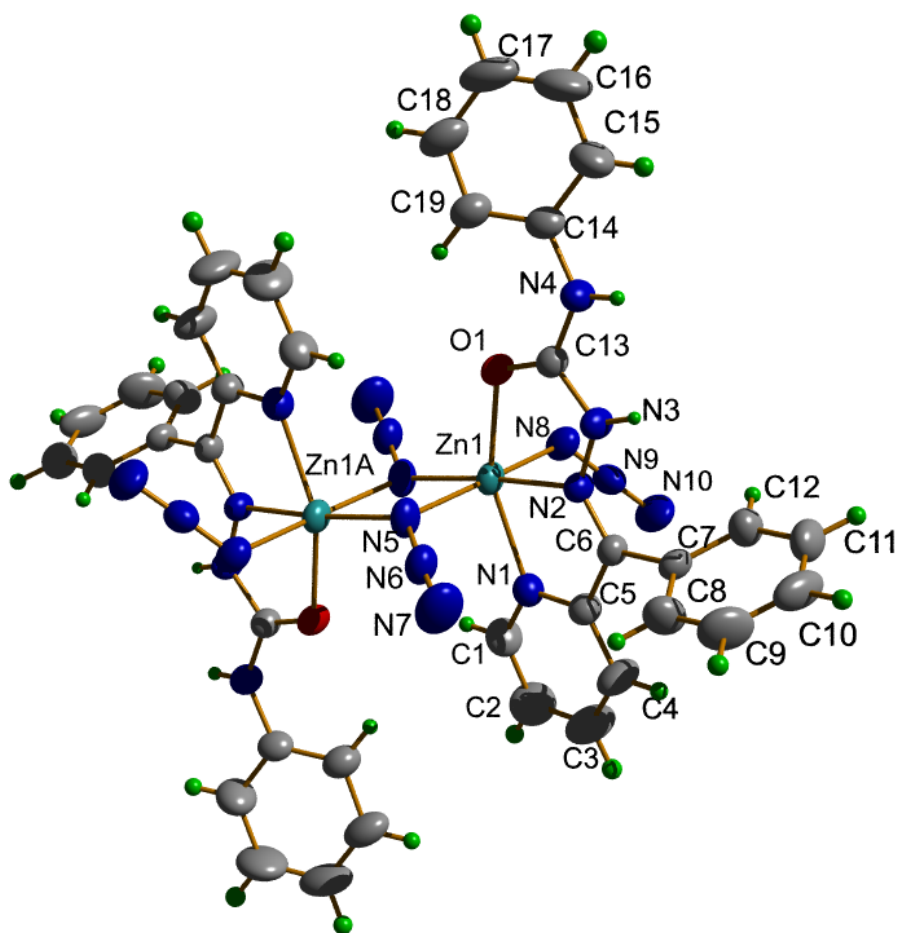
**Fig. 5.7** Structure and labeling diagram of compound [Zn$_2$(HL^3)$_2$(N$_3$)$_4$] (**20**).

Table 5.5 Selected bond lengths (Å) and bond angles (°) for the complex **20**

Bond lengths		Bond angles	
N(1)—Zn(1)	2.1843(17)	Zn(1A)—N(5)—Zn(1)	100.48(7)
N(2)—N(3)	1.3502(19)	N(7)—N(6)—N(5)	177.2(2)
N(2)—Zn(1)	2.1309(13)	N(9)—N(8)—Zn(1)	119.77(15)
N(5)—Zn(1)	2.0287(15)	N(10)—N(9)—N(8)	178.0(2)
N(5)—Zn(1A)	2.2422(17)	C(13)—O(1)—Zn(1)	113.78(11)
N(8)—Zn(1)	2.1086(17)	N(5A)—Zn(1)—N(8)	98.48(7)
O(1)—Zn(1)	2.2189(12)	N(5A)—Zn(1)—N(2)	171.43(6)
C(13)—N(4)	1.341(2)	N(8)—Zn(1)—N(2)	89.95(6)
C(13)—N(3)	1.386(2)	N(5A) —Zn(1)—N(1)	104.03(7)
C(13)—O(1)	1.233(2)	N(8)—Zn(1)—N(1)	93.34(6)
		N(2)—Zn(1)—N(1)	73.75(6)
		N(5A)—Zn(1)—O(1)	107.81(6)
		N(5)— Zn(1)—O(1)	90.63(6)
		N(8)—Zn(1)—O(1)	90.05(6)
		N(2)—Zn(1)—O(1)	73.53(5)
		N(1)—Zn(1)—O(1)	147.10(5)
		N(5A)—Zn(1)—N(5)	79.52(7)
		N(8)—Zn(1)—N(5)	178.00(6)
		N(2)—Zn(1)—N(5)	92.05(5)
		N(1)—Zn(1)—N(5)	87.11(6)

The *cis* angles N(5A) –Zn(1)–N(1), N(2)–Zn(1)–N(1), N(5A) –Zn(1)–O(1) and N(2)–Zn(1)–O(1) are 104.03(7)°, 73.75(6)°, 107.81(6)° and 73.53(5)° and *trans* angle N(1)–Zn(1)–O(1) is 147.10(5)° indicating that the compound **20** has large distortion from octahedral geometry [21]. The non bonded Zn1···Zn1A distance is 3.2861(3) Å.

Fig. 5.8 shows the packing arrangement of molecules along b axis. The perspective view of the coordination polyhedron of the molecular arrangement

along a axis illustrates that the molecules are packed so that the molecules are orthogonal to each other along b and c axes (Fig. 5.9). A supramolecular hydrogen bonding network is established between the molecules in zig-zag manner as shown in the Fig. 5.10. The presence of a non-conventional intramolecular interaction between hydrogen atom attached at the phenyl ring and the oxygen atom of the same molecule gives almost a coplanar arrangement of phenyl ring of the semicarbazide part with the semicarbazone skeleton of the ligand making the conformation stable.
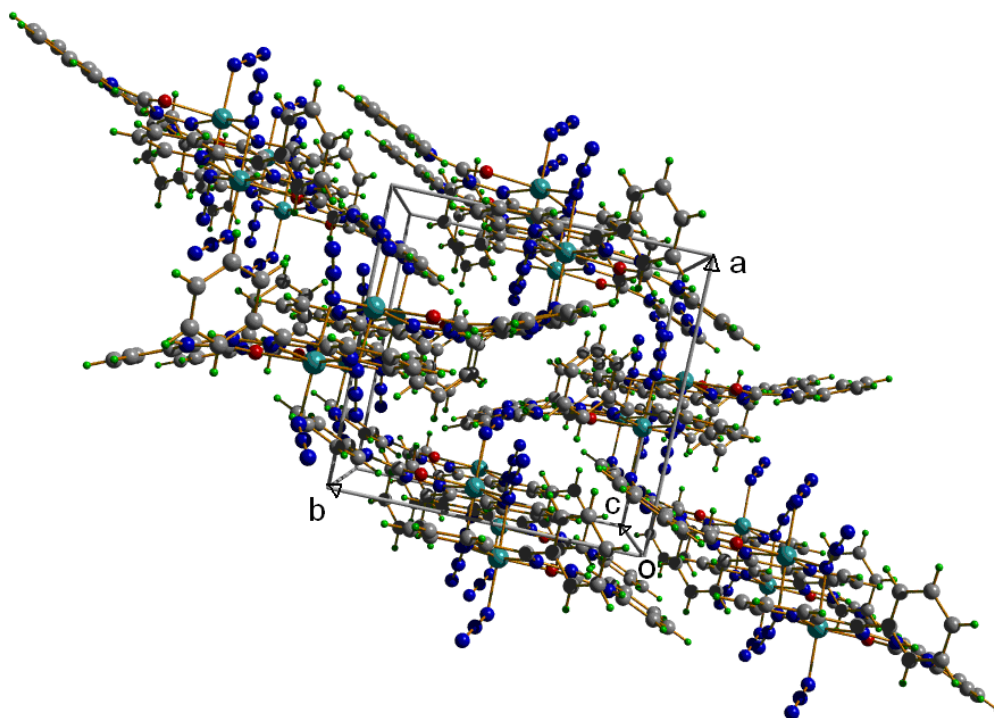
Fig. 5.8 Unit cell packing diagram of compound $[Zn_2(HL^3)_2(N_3)_4]$ (**20**) along b axis.
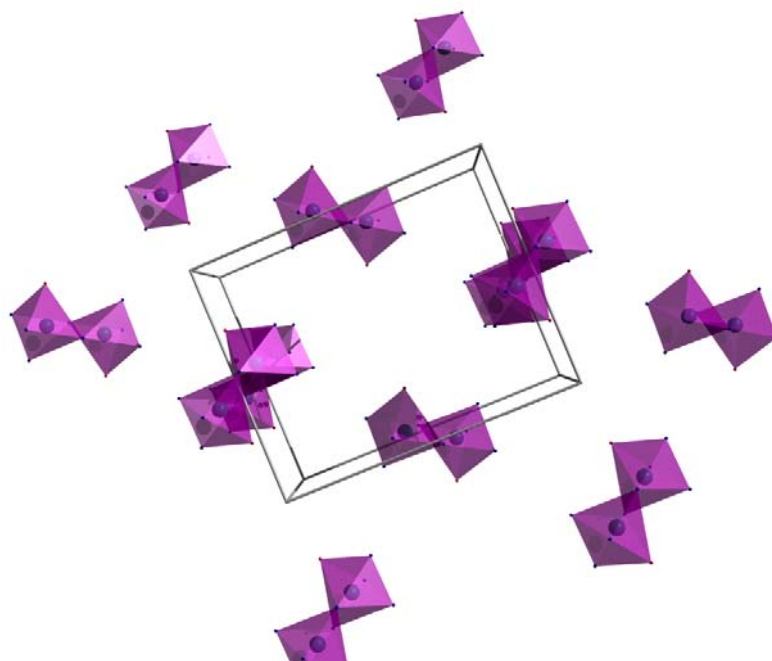
Fig. 5.9 Coordination polyhedron of the compound $[Zn_2(HL^3)_2(N_3)_4]$ (**20**) in a unit cell along a axis.
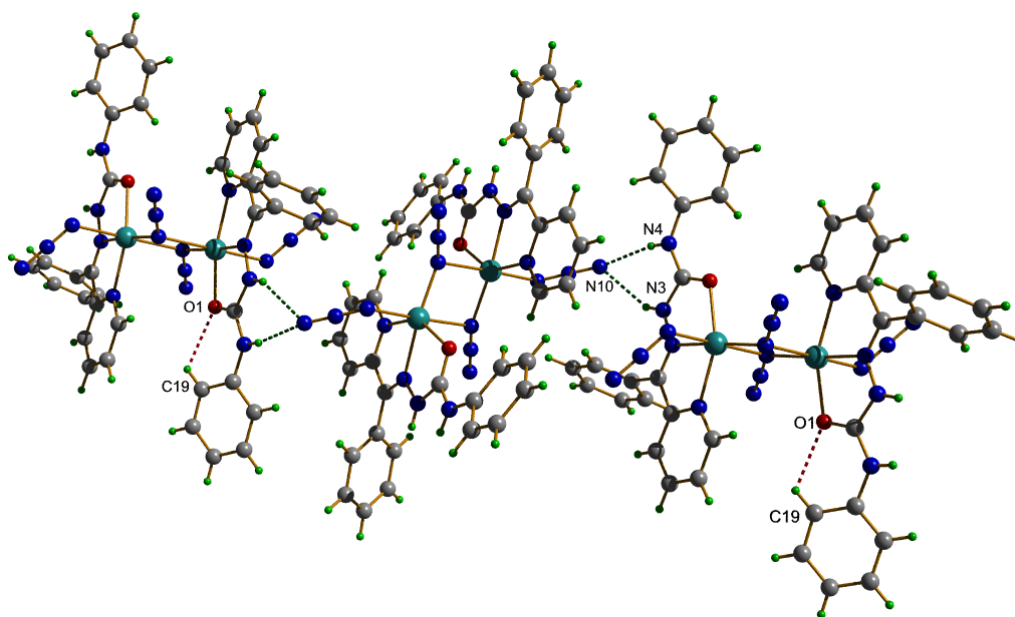
Fig. 5.10 Hydrogen bonding interactions of compound $[Zn_2(HL^3)_2(N_3)_4]$ (**20**).

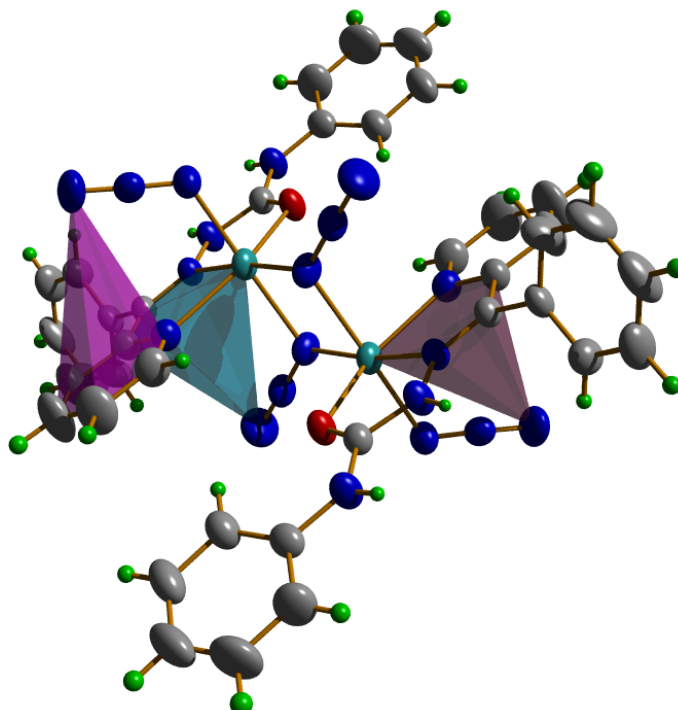In addition to this two types of three lone pair–π interactions (Table 5.6) are also observed between the terminal nitrogen of the free azide moiety and the metal chelate ring coordinating through pyridyl nitrogen and the azomethine nitrogen and pyridyl ring of the ligand with X···Cg distances of 3.366(2), 3.461(2) and 3.792(3).

Fig. 5.11 Lone pair–π interactions between the molecules of the compound $[Zn_2(HL^3)_2(N_3)_4]$ **(20)**.

Table 5.6 Interaction parameters of compounds $[Zn_2(HL^3)_2(N_3)_4]$ **(20)**

Hydrogen bonding interactions

D—H···A	D—H (Å)	H···A (Å)	D···A (Å)	∠D–H···A(º)
N(3)—H(3N)···N(10)ª	0.808(18)	2.326(17)	3.036(3)	147.1(17)
N(4)—H(4N)···N(10)ª	0.81(2)	2.14(2)	2.916(3)	161.6(19)
C(19)—H(19)···O(1)	0.93	2.40	2.954(3)	118

Y–X···Cg (π-ring) interactions

Y–X(I)···Cg(J)	X···Cg (Å)	γ (°)	Y–X···Cg
N(6)–N(7)···Cg(3)[b]	3.366(2)	4.08	58.45(14)
N(9)–N(10)···Cg(3)[b]	3.461(2)	11.43	54.23(13)
N(9)–N(10)···Cg(4)[b]	3.792(3)	25.28	81.91(14)

Cg (3) = Zn(1), N(1), C(5), C(6), N(2)
Cg (4) = N(1), C(8), C(9), C(10), N(11)
Equivalent position codes: a= 1/2-x,1/2+y,1/2-z ; b= x,y,z
D, donor; A, acceptor; Cg, centroid; α, dihedral angles between planes I and J; β, angle between Cg···Cg and Cg(J)_perp; γ, angle between Cg···Cg and Cg(I)_perp

5.3.4. Infrared spectral studies

The IR spectra of the free ligands when compared with those of complexes confirm the coordination of the semicarbazone to the metal. The significant bands observed in the IR spectra of ligands and its complexes with the tentative assignments are presented in the Table 5.7.

Table 5.7 Infrared spectral assignments (cm^{-1}) of ligands and their Zn(II) complexes

Compound	ν(N–H)	ν(C=N)	ν(^{2}N=C)	ν(N–N)	ν(Zn–N$_{azo}$)	ν(C=O)
HL^1	3372	1597	-	1143	-	1693
[ZnL^1(OAc)]·H$_2$O (**15**)	-	1605	1575	1141	518	-
[Zn(HL^1)(OAc)(SCN)] (**16**)	3314	1605	-	1145	510	1687
[ZnL^{1}N$_3$] (**17**)	-	1602	1552	1135	512	-
HL^3	3375	1600	-	1132	-	1698
[ZnL^3(OAc)] (**18**)	-	1603	1564	1135	506	-
[Zn(HL^3)Br$_2$] (**19**)	3303	1605	-	1140	506	1670
[Zn$_2$(HL^3)$_2$(N$_3$)$_4$] (**20**)	3312	1605	-	1128	508	1665

The IR spectra of the complexes except the complex [ZnL^1(OAc)]·H$_2$O (**15**) do not exhibit a broad absorption band at 3420 cm^{-1}, which may be due to the –OH stretching mode of water, indicating the absence of water molecule in the complexes. A broad band at 3450 cm^{-1} for the complex **15** indicates the

presence of lattice water molecule. Weak bands in the region 506-518 cm^{-1} assignable to ν(Zn–N$_{azo}$) indicate the coordination of azomethine nitrogen atom to the metal atom in all the complexes [22,23]. In the IR spectra of the ligands HL[1] and HL[3], the bands at 3372 and 3375 cm^{-1} respectively corresponding to the ν([2]N–H) indicate that the ligands remain as amido forms in the solid state [22]. The absence of these bands in the complexes **15**, [ZnL[1]N$_3$] (**17**) and [ZnL[3](OAc)] (**18**) (Fig. 5.12, 5.14 and 5.15) shows that the ligands in these complexes are in iminolate form. The bands corresponding to the newly formed C=N bond [ν(C=[2]N)] are due to the iminolization of the ligands and the ν(N–N) frequency shifts from 1028 to 1045 cm^{-1} bands confirm the iminolization and the subsequent deprotonation of the ligands during complexation. But the absence of these bands in the other complexes indicates that the ligand is in the amido form. This was confirmed by the single crystal XRD data of the compounds **19** and **20** (Fig. 5.16, 5.17). The ν(C=N) bands of semicarbazones are found to be shifted to lower frequencies by 3-8 cm^{-1} in all complexes indicating the coordination *via* the azomethine nitrogen. The ν(Zn–N$_{azo}$) bands further confirm the coordination of the metal through azomethine nitrogen [24].

Coordinated water should exhibit bands at 825, 575 and 500 cm^{-1}. The absence of bands in these regions in the spectrum of complex **15** shows that the water molecule is not coordinated but is present as lattice water [25].

In addition to all these bands the presence of a strong sharp stretching band at 2058 cm^{-1}, a strong band at 1331 cm^{-1} and a broad band at 695 cm^{-1} assignable to δ(N–N–N) for the compound **17** indicates the presence of coordinated azido group in the complex (Fig. 5.14). The spectrum of the complex [Zn(HL[1])(OAc)(SCN)] (**16**) exhibits a sharp band at 2069 cm^{-1} and a medium band at 689 cm^{-1} correspond to ν(CN) and ν(CS) of SCN group respectively. This shows monodentate S bonded thiocyanate group. The presence of asymmetric stretching bands at 1582 and 1441 cm^{-1} indicates

monodentate nature of the acetato group in the complex [22]. The similar observation is found for the complex [ZnL³(OAc)] (**18**). The presence of monodentate nature of the acetato group can be attributed by the presence of asymmetric stretching bands at 1558 and 1434 cm^{-1} in the spectrum of the complex (Fig. 5.15). A strong sharp stretching band at 2056 cm^{-1}, a strong band at 1343 cm^{-1} and a broad band at 687 cm^{-1} in the spectrum of the compound **20** (Fig. 5.17) indicates the presence of coordinated azido group in the complex. This was confirmed by the single crystal XRD data of the compound **20**.
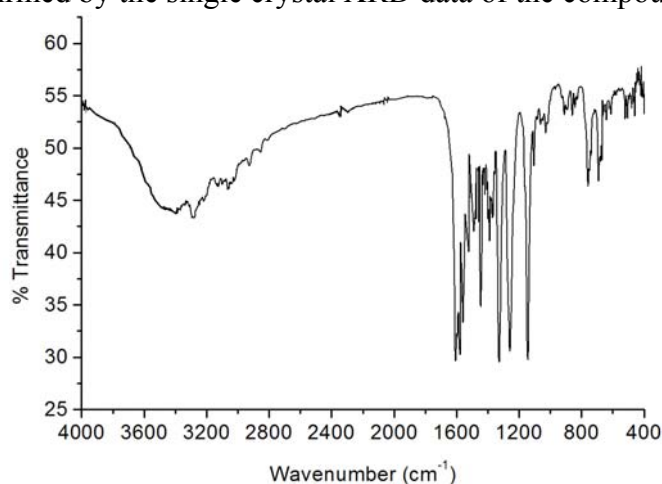
Fig. 5.12 IR spectrum of [ZnL¹(OAc)]·H$_2$O (**15**).
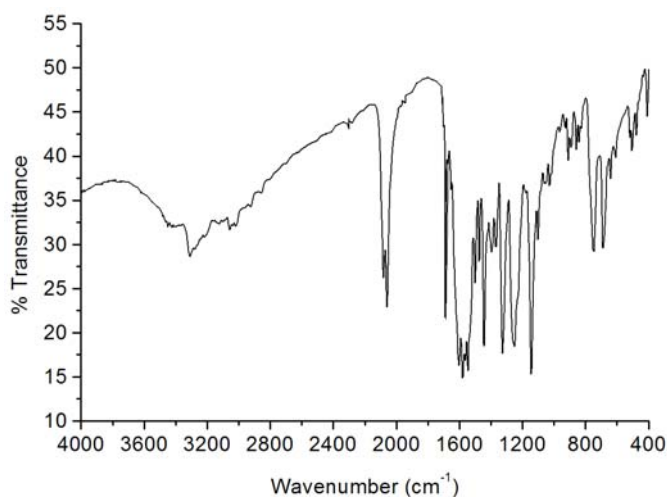
Fig. 5.13 IR spectrum of [Zn(HL¹)(OAc)(SCN)] (**16**).
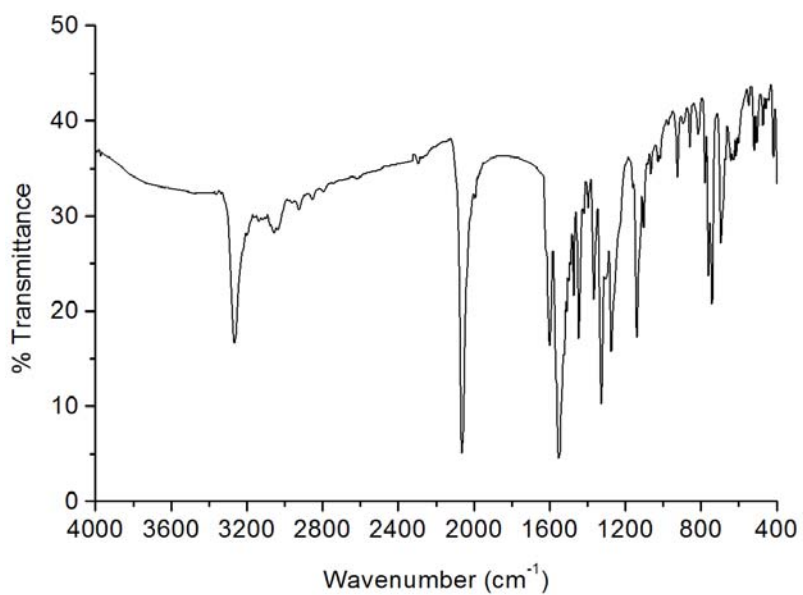
Fig. 5.14 IR spectrum of [ZnL^{1}N$_3$] (**17**).
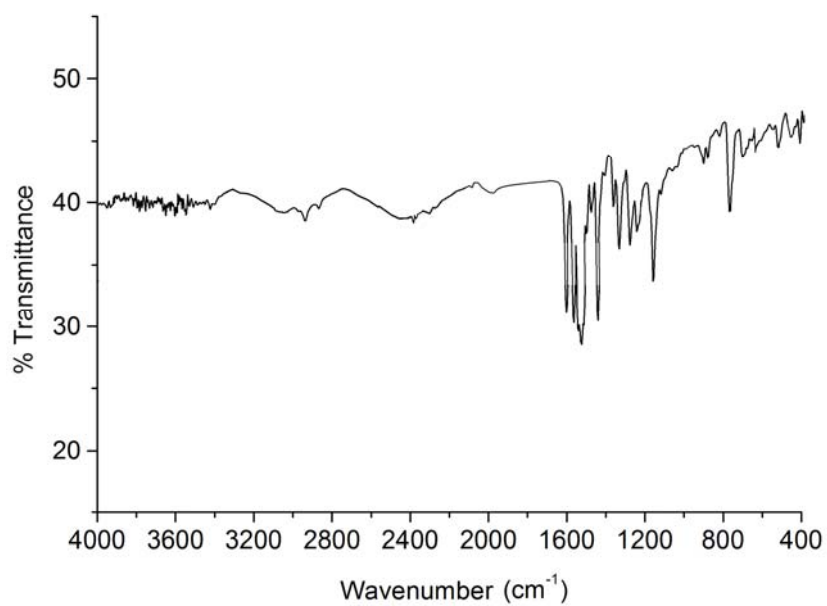
Fig. 5.15 IR spectrum of [ZnL^3(OAc)] (**18**).

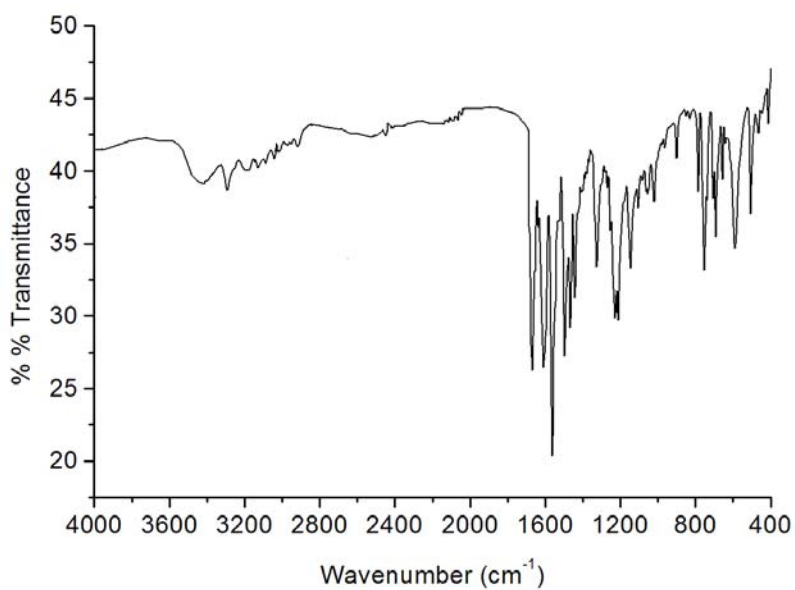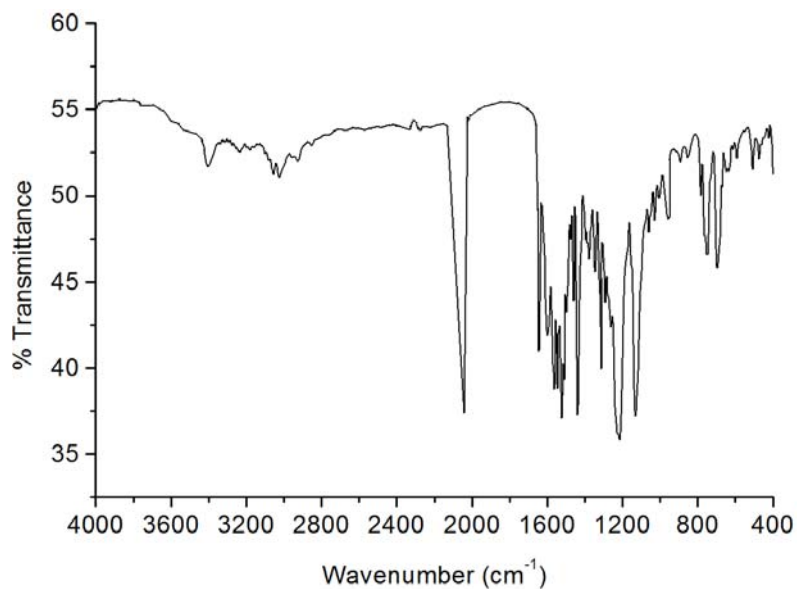**Fig. 5.16** IR spectrum of [Zn(HL^3)Br$_2$] (**19**).

Fig. 5.17 IR spectrum of [Zn$_2$(HL^3)$_2$(N$_3$)$_4$] (**20**).

5.3.5. Electronic spectral studies

The electronic spectra of the ligands and complexes were recorded in acetonitrile. The electronic spectral assignments of the two ligands and the complexes are given in Table 5.8. The electronic spectra of the ligands HL^1 and HL^3 showed slight shift in energy on complexation (Fig. 5.18-5.23). This indicates coordination *via* the pyridyl nitrogen, azomethine nitrogen. Because of the coordination *via* oxygen atom of C=O the C=O bond is weakened and conjugation system is enhanced after the formation of the complex [26].

In addition to these intra-ligand bands, a new band in the range 24800-25160 cm^{-1} is observed in the spectra of the all complexes. These bands can safely be assigned to metal to ligand charge-transfer transitions and this confirms the coordination of the ligands with the metal ion. No appreciable absorptions are observed below 20000 cm^{-1} in DMF solution which is in accordance with the d^{10} electronic configuration of Zn(II) ion.

Table 5.8 Electronic spectral assignments of Zn(II) complexes

Compound	MLCT	Intraligand transitions
HL^1	-	32000, 38100, 42500
$[ZnL^1(OAc)]\cdot H_2O$ (**15**)	24980	33830, 42650
$[Zn(HL^1)(OAc)(SCN)]$ (**16**)	24940	33750, 42250
$[ZnL^1N_3]$ (**17**)	24800	33650, 42050
HL^3	-	32660, 37797, 42793
$[ZnL^3(OAc)]$ (**18**)	25080	32940, 40200
$[Zn(HL^3)Br_2]$ (**19**)	25160	32900, 40160
$[Zn_2(HL^3)_2(N_3)_4]$ (**20**)	25100	33020, 40200
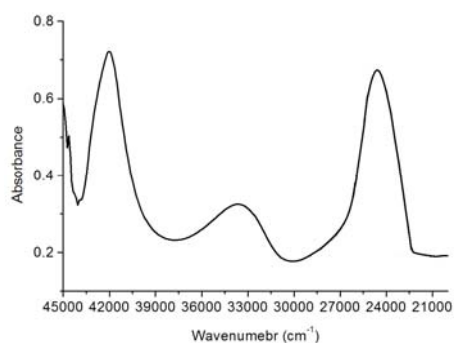
Fig. 5.18 Electronic spectrum of complex [ZnL^1(OAc)]·H$_2$O (**15**).
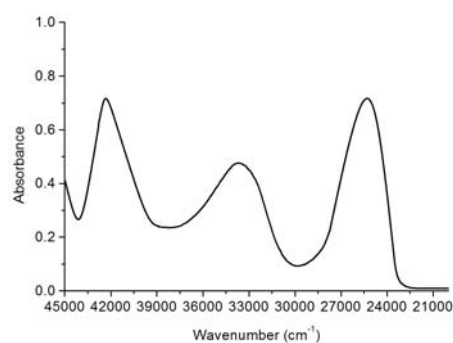
Fig. 5.19 Electronic spectrum of complex [Zn(HL^1)(OAc)(SCN)] (**16**).
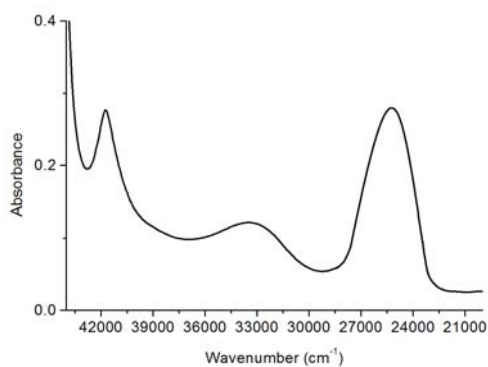
Fig. 5.20 Electronic spectrum of complex [ZnL^{1}N$_3$] (**17**).
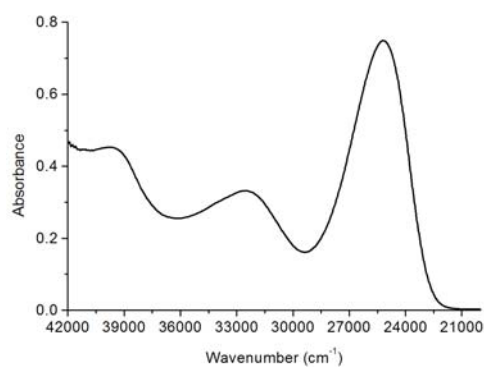
Fig. 5.21 Electronic spectrum of complex [ZnL^3(OAc)] (**18**).
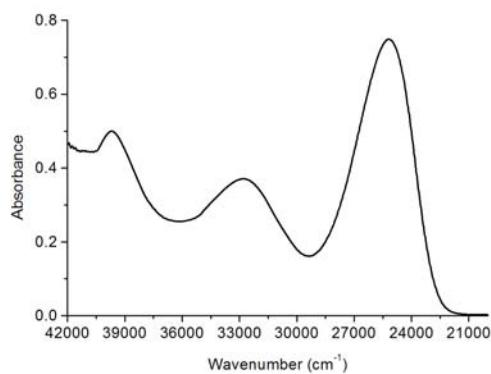
Fig.5.22 Electronic spectrum of complex[Zn(HL^3)Br$_2$] (**19**).
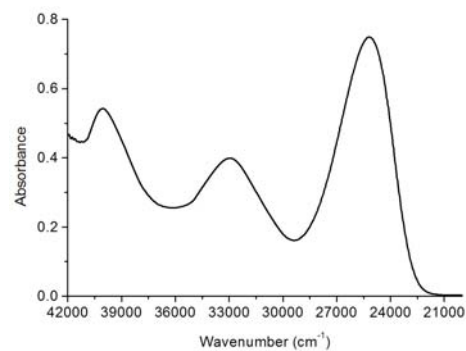
Fig.5.23 Electronic spectrum of complex [Zn$_2$(HL^3)$_2$(N$_3$)$_4$] (**20**).

5.3.6. Thermogravimetric studies

The thermogravimetric analysis of the complex $[ZnL^1(OAc)] \cdot H_2O$ (**15**) clearly shows a weight loss of 4.4% below 100 ^{o}C confirming the presence of one mole of lattice water molecule in it. The total weight loss of 78.5% in the temperature range 200-800 ^{o}C can be assigned to the weight loss during the dissociation of the ligand and acetato group present in the complex (Fig. 5.24).
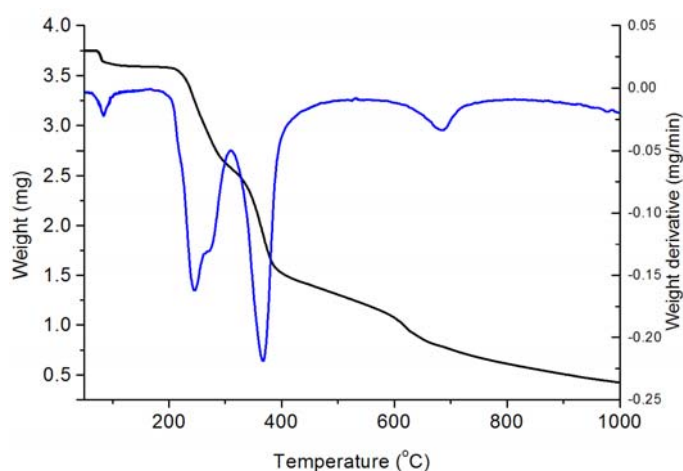
Fig. 5.24 Thermogram of the compound $[ZnL^1(OAc)] \cdot H_2O$ (**15**).

The compound $[Zn(HL^1)(OAc)(SCN)]$ (**16**) has no weight loss below 200 ^{o}C which confirms supporting with the IR data that it contains no lattice water molecules. The total weight loss (85.2%) of the four consecutive losses in the range from 200-600 ^{o}C is due to the removal of the ligand, acetato group and the thiocyanato group present in the complex (Fig. 5.25). The complex $[ZnL^3(OAc)]$ (**18**) contains no lattice water molecule since its thermogram does not show any weight loss below 200 ^{o}C (Fig. 5.26). The ligand and the acetato group are removed in the temperature range 200-800 ^{o}C with a weight loss of 85.6%.
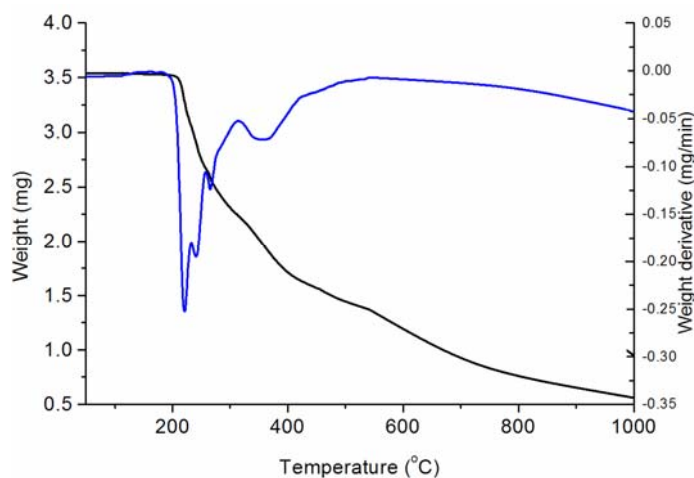
Fig. 5.25 Thermogram of the compound [Zn(HL^1)(OAc)(SCN)] (**16**).
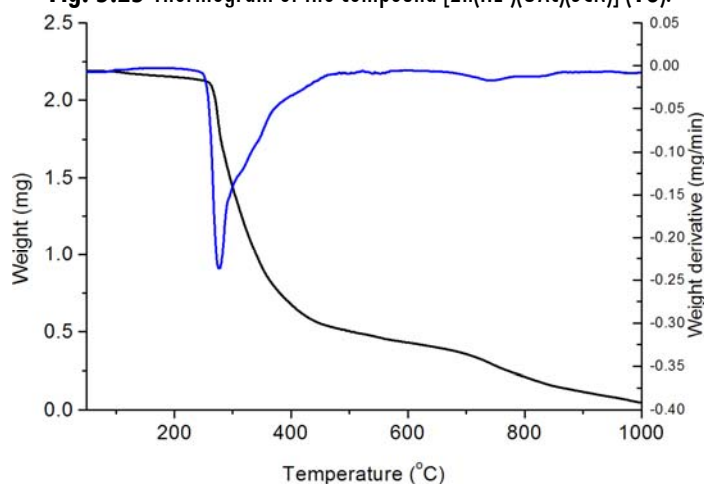
Fig. 5.26 Thermogram of the compound [ZnL^3(OAc)] (**18**).

The complex [Zn(HL^3)Br$_2$] (**19**) showed weight loss (29.0%) at around 300 ^{o}C suggests the dissociation of the two bromine atoms from this complex (Fig. 5.27). It is noted that the presence of the two bromine atoms is already confirmed by the XRD studies. The total weight loss of the ligand and the two bromine atoms (88.5%) confirms the molar ratio of the ligand and the metal in the complex.
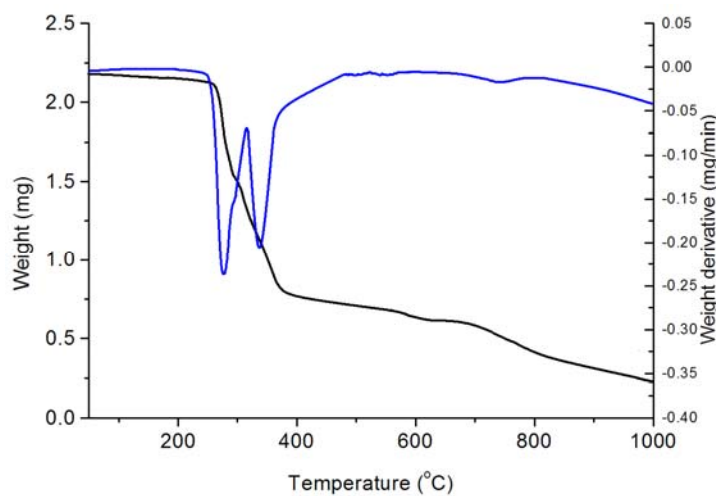
Fig. 5.27 Thermogram of the compound [Zn(HL^3)Br$_2$] (**19**).

References

[1]   H.H. Sandstead, J. Lab. Clin. Med. 124 (1994) 322.

[2]   N.W. Solomons, Nutr. Rev. 56 (1998) 27.

[3]   C.A. Heyneman, Ann. Pharmacother 30 (1996) 186.

[4]   A.S. Prasad, F.W. Beck, S.M. Grabowski, J. Kaplan, R.H. Mathog, Proc. Assoc. Am. Physicians 109 (1997) 68

[5]   K. Simmer, R.P. Thompson, Acta Paediatr. Scand. Suppl. (1985).

[6]   T. Matsukura, H. Tanaka, Biochemistry 65 (2000) 817.

[7]   G. Parkin, Chem. Commun. (1971) 2000.

[8]   P. Malatesta, G.P. Accinelli, G.P. Quaglia, Ann. Chim. Rome 49 (1959) 397.

[9]   D.L. Klayman, J.F. Bartosevich, T.S Griffin, C.J. Manson, J.P. Scovill, J. Med. Chem. 22 (1979) 885.

[10]   S.B. Padhye, G.B. Kauffman, Coord Chem. Rev. 63 (1985) 127.

[11]   SMART and SAINT, Area Detector Software Package and SAX Area Detector Integration Program, Bruker Analytical X-ray; Madison, WI, USA, 1997.

[12]   SADABS, Area Detector Absorption Correction Program; Bruker Analytical X-ray; Madison, WI, 1997.

[13]   G.M. Sheldrick, *SHELX-PLUS, Crystal Structure Analysis Package*; Bruker Analytical X-Ray, Madison, WI, USA, 1997.

[14]   K. Brandenburg, Diamond Version 3.2g, Crystal Impact GbR, Bonn, Germany, 2010.

[15]   W.J. Geary, Coord. Chem. Rev. 7 (1971) 81.

[16]   A. Sreekanth, U.L. Kala, C.R. Nayar, M.R.P. Kurup, Polyhedron 23 (2004) 41.

[17]   K.A. Ketcham, J.K. Swearingen, A. Castineiras, I. Garcia, E. Bermejo, D.X.West, Polyhedron 20 (2001) 3265.

[18]   E. Bermejo, A. Castineiras, I. Garcia-Santos, D.X. West, Z. Anorg. Allg. Chem. 630 (2004) 1097.

[19]   J. Schnödt, M. Sieger, B. Sarkar, J. Fiedler, J.S. Manzur, C-Y Su, W. Kaim, Z. Anorg. Allg. Chem. 637 (2011) 930.

[20]   I. Garcia, E. Bermejo, A.K. El Sawaf, A. Castineiras, D.X. West, Polyhedron 21 (2002) 729.

[21]   G. Murphy, C.O. Sullivan, B. Murphy, B. Hathaway, Inorg. Chem. 37 (1998) 240.

[22]   K. Nakamoto, Infrared and Raman Spectra of Inorganic and Coordination compounds, fifth ed., Wiley, New York, 1997.

[23] D.F. Xiang, C.Y. Duan, X.S. Tan, Q.W. Hang, W.X. Tang, J. Chem. Soc., Dalton Trans. 7 (1998) 1201.

[24] V. Stefov, V.M. Petrusevski, B. Soptrajanov, J. Mol. Stru. 293 (1993) 97.

[25] E. Bermejo, A. Castineiras, I.G- Santos , D.X. West, Z. Anorg, Allg. Chem. 630 (2004) 1097.

[26] L. Latheef, M.R.P. Kurup, Polyhedron 27 (2008) 35.

.........................&&&.........................

Synthesis, spectral studies and structures of cadmium(II) complexes of N⁴-phenylsemicarbazones

6.1. Introduction

Cadmium is found as an impurity in zinc carbonate. Cadmium containing ores are rare and are found to occur in small quantities. Gadreenockite (CdS), the only cadmium mineral of importance, is nearly associated with sphalerite (ZnS) [1,2]. The important commercial use of cadmium was as an electrodeposited coating on iron and steel for corrosion protection. Nickel-cadmium batteries are the second-largest application, with pigment and chemical uses third. Sizable amounts are used in low-melting-point alloys and in automatic fire sprinklers, and relatively smaller uses are in brazing alloys, solders, and bearings. Cadmium compounds are used as stabilizers in plastics and the production of cadmium phosphors. Because of its great neutron-absorbing capacity, especially the isotope 113, cadmium is used in control rods and shielding for nuclear reactors [3].

Cadmium is a catalytic inhibitor of DNA Topoisomerase II, a nuclear enzyme [4]. The mobilization and immobilization of cadmium in the environment in organisms, have been shown to depend on the complexation of chelating nitrogen donors [5]. Complexes of Cd(II) with different molecular architectures

with the same ligand showing strong fluorescence have been reported [6]. The most stable form of cadmium is Cd^{2+}. Cadmium(II) complexes have tetrahedral, square pyramidal, trigonal bipyramidal and octahedral geometries. There is substantial interest in the coordination chemistry of cadmium complexes because of the toxic environmental impact of cadmium.

Cadmium is well known to form complexes with acetates and carboxy-ligands to yield both charged and neutral compounds [7]. The possibility of forming structures with higher coordination numbers has resulted in the observation of unusual coordination geometries about the metal atom and the formation of polymeric species [8]. Cd^{2+} forms most stable complexes with soft donor atoms (S>>N>>O). Generally the stability of the complexes increases with the number of coordination groups contributed by the ligand. It has also been reported that some cadmium complexes of thiosemicarbazones can show quite large SHG efficiency [9].

6.2. Experimental

6.2.1. Materials

Cadmium(II) bromide tetrahydrate, cadmium(II) acetate dehydrate, cadmium(II) chloride, potassium thiocyanate and sodium azide (all are BDH, AR grade) were used without further purification. All solvents were purified by standard methods.

6.2.2. Synthesis of complexes

6.2.2.1. Synthesis of [Cd(HL¹)Br₂] (21)

Methanolic solutions of HL^1 (0.240 g, 1 mmol) and $CdBr_2 \cdot 4H_2O$ (0.344 g, 1 mmol) were mixed and heated under reflux for 4 h. The formed complex was filtered, washed with ether and dried over P_4O_{10} *in vacuo*.

6.2.2.2. Synthesis of [Cd(HL^1)(OAc)$_2$]·3H$_2$O (22)

A solution of the semicarbazone, HL^1 (0.240 g, 1 mmol) in methanol was mixed with methanolic solution of cadmium(II) acetate dihydrate (0.266 g, 1 mmol) and the mixture was heated under reflux for 4 h. and cooled. The complex separated was filtered, washed thoroughly with ether and dried over P$_4$O$_{10}$ *in vacuo.*

6.2.2.3. Synthesis of [Cd(HL^1)Cl$_2$] (23)

A solution of semicarbazone, HL^1 (0.240 g, 1 mmol) in methanol was treated with a methanolic solution of cadmium(II) chloride (0.183 g, 1 mmol). The solution was heated under reflux for 5 h. The resulting solution was allowed to stand at room temperature and after slow evaporation the crystals formed were separated out and washed with ether and dried over P$_4$O$_{10}$ *in vacuo.*

6.2.2.4. Synthesis of [CdL$_2^1$] (24)

A methanolic solution of HL^1 (0.240 g, 1 mmol) and potassium thiocyanate (0.097 g, 1 mmol) were mixed with a methanolic solution of cadmium(II) acetate dihydrate (0.266 g, 1 mmol) and heated under reflux for 5 h. On slow evaporation, single crystals suitable for single crystal XRD were separated from the mixture.

6.2.2.5. Synthesis of [CdL^{1}N$_3$] (25)

A methanolic solution of HL^1 (0.240 g, 1 mmol) and Cd(CH$_3$COO)$_2$·2H$_2$O (0.266 g, 1 mmol) were mixed and heated under reflux for 2 h. and then methanolic solution of NaN$_3$ (0.065 g, 1 mmol) was also added into the mixture. The resulting mixture was refluxed for 4 h. and cooled at

room temperature. The formed crystals were filtered, washed thoroughly with ether and dried over P_4O_{10} *in vacuo.*

6.2.2.6. Synthesis of [CdL³(OAc)] (26)

A solution of semicarbazone, HL^3 (0.316 g, 1 mmol) in methanol was treated with a methanolic solution of cadmium(II) acetate dihydrate (0.266 g, 1 mmol). The solution was heated under reflux for 4 h. The resulting solution was allowed to stand at room temperature and after slow evaporation the formed crystals were separated out and washed with ether and dried over P_4O_{10} *in vacuo.*

6.2.2.7. Synthesis of [Cd(HL³)Cl₂] (27)

A solution of semicarbazone, HL^3 (0.316 g, 1 mmol) in methanol was treated with a methanolic solution of cadmium(II) chloride (0.183 g, 1 mmol). The solution was heated under reflux for 5 h. The resulting solution was allowed to stand at room temperature and the crystals formed were separated out and washed with ether and dried over P_4O_{10} *in vacuo.*

6.2.2.1. Synthesis of [Cd₂L³₂Br₂] (28)

A methanolic solution of HL^3 (0.316 g, 1 mmol) and $CdBr_2 \cdot 4H_2O$ (0.344 g, 1 mmol) were mixed and heated under reflux for 4 h. The mixture was kept at room temperature. The single crystals suitable for single XRD analysis were separated.

6.2.3. Physical measurements

Elemental analyses were carried out using a Vario EL III CHNS analyzer at the SAIF, Kochi, India. Infrared spectra were recorded on a JASCO FT-IR-5300 Spectrometer in the range 4000-400 cm^{-1} using KBr pellets and Electronic spectra were recorded on a UV-vis Double Beam UVD-3500

Spectrophotometer using solution in methanol at the Department of Applied Chemistry, Cochin University of Science and Technology, Kochi 22, India. TG-DTG analyses of the complexes were carried out under nitrogen at a heating rate of 10 ^{o}C min^{-1} in the range 50-1000 ^{o}C using a Perkin Elmer Pyris Diamond TG/DTA analyzer at the Department of Applied Chemistry, CUSAT, Kochi, India.

6.2.4. X-ray crystallography

Single crystals of compound **24** and **28** suitable for X-ray analysis were obtained from its methanolic solutions and were found to be triclinic space group P^{-1} and monoclinic space group $P2_1/n$ respectively. X-ray diffraction measurements were carried out on CrysAlis CCD diffractometer with graphite-monochromated Mo Kα ($\lambda = 0.71073$ Å) radiation. The program CrysAlis RED was used for data reduction and cell refinement [10]. The structures were solved by direct methods using SHELXS [11] and refined by full-matrix least-squares refinement on F^2 using SHELXL [12]. The N–H hydrogen atoms were located from difference Fourier maps and refined isotropically. The remainder of the H-atoms were included in calculated positions and refined as riding atoms using default SHELXL parameters. The structures of the compounds **24** and **28** were plotted using the program DIAMOND version 3.2g [13]. The crystallographic data along with the structural refinements are given in Table 6.1.

Table 6.1 Crystal data and structure refinement parameters of **24** and **28**

Description	$[CdL^1{}_2]$ **(24)**	$[Cd_2L^3{}_2Br_2]$ **(28)**
Empirical formula	$C_{26} H_{22} Cd N_8 O_2$	$C_{38}H_{30}Br_4Cd_2N_8O_2$
Formula weight	590.93	1175.12
Temperature (K)	296(2)	293(2)
Wavelength Å	0.71073	0.71073
Crystal system	Triclinic	Monoclinic
Space group	P^{-1}	$P2_1/n$
Unit cell dimensions		
a (Å)	11.3844(9)	11.699(2)
b (Å)	15.4220(12)	12.628(3)
c (Å)	21.0100(17)	14.627(3)
α (°)	72.393(4)	90.00
β (°)	81.533(3)	105.98(3)
γ (°)	82.978(3)	90.00
Volume (Å^3)	3465.8(5)	2077.4(8)
Z	4	2
D_{calc} (g/cm^3)	1.133	1.879
Absorption coefficient	0.660 mm^{-1}	4.914 mm^{-1}
F(000)	1192.0	1132
Crystal size (mm^3)	0.35 x 0.30 x 0.25	0.35 x 0.2 x 0.1
θ range for data collection	1.02-28.47°	2.1- 33.26 °
Limiting indices	$-15 \leq h \leq 15, -20 \leq k \leq 20,$ $-28 \leq l \leq 28$	$-18 \leq h \leq 18, -19 \leq k \leq 191,$ $-22 \leq l \leq 22$
Reflections collected	62913	8001
Independent reflections	17370	3676
Refinement method	Full-matrix least-squares on F^2	Full-matrix least-squares on F^2
Data / restraints / parameters	9741 / 0 / 669	6233 / 0 / 248
Goodness-of-fit on F^2	1.065	0.997
Final R indices [I>2σ(I)]	$R_1 = 0.0873$, w$R_2 = 0.1589$	$R_1 = 0.0427$, w$R_2 = 0.0996$
R indices (all data)	$R_1 = 0.1145$, w$R_2 = 0.3065$	$R_1 = 0.1015$, w$R_2 = 0.1216$

$$R_1 = \Sigma||F_o| - |F_c|| / \Sigma|F_o| \qquad wR_2 = [\Sigma w(F_o{}^2 - F_c{}^2)^2 / \Sigma w(F_o{}^2)^2]^{1/2}$$

6.3. Results and discussion

6.3.1 Analytical measurements

The analytical data of all the complexes are given in Table 6.2. All the compounds except the complex **25** were prepared by direct reaction between the semicarbazones and the corresponding cadmium(II) salts, while the compound **25** was prepared by the replacement of the acetate in $Cd(CH_3COO)_2 \cdot 2H_2O$ by the azide ion. Elemental analyses data of all the complexes reveal that metal and ligand are in the ratio 1:1 in all the complexes except the complex **24**. The ligand/ligands interact with Cd(II) ion in neutral form in complexes **21**, **22**, **23** and **27** whereas in complexes **24**, **25**, **26** and **28** they react in anionic form.

Table 6.2 Preliminary analytical data of Cd(II) complexes of HL^1 and HL^3

Compound	Color	$\lambda_m{}^a$	Found (Calcd) %		
			C	H	N
$[Cd(HL^1)Br_2]$ (**21**)	yellow	40	30.43(30.47)	1.93(2.36)	10.93(10.93)
$[Cd(HL^1)(OAc)]_2 \cdot 3H_2O$ (**22**)	yellow	07	38.66(38.91)	4.02(4.61)	10.65(10.68)
$[Cd(HL^1)Cl_2]$ (**23**)	yellow	27	36.44(36.86)	2.77(2.86)	12.91(13.23)
$[CdL^1{}_2]$ (**24**)	yellow	31	53.46(53.61)	4.16(4.00)	18.24(18.52)
$[CdL^1N_3]$ (**25**)	yellow	07	39.53(39.66)	2.43(2.82)	24.32(24.90)
$[CdL^3(OAc)]$ (**26**)	yellow	04	51.57 (51.81)	3.77 (3.73)	11.46 (11.51)
$[Cd(HL^3)Cl_2]$ (**27**)	yellow	17	45.41 (45.76)	3.37 (3.03)	11.25 (11.24)
$[Cd_2L^3{}_2Br_2]$ (**28**)	yellow	26	39.08(38.77)	2.74(2.74)	9.63(9.52)

^{a}Molar conductivity (ohm^{-1}cm^{2}mol^{-1}), 10^{-3} M DMF at 298 K

6.3.2. Crystal structure of the complex [CdL$^1_2$] (24)

The compound **24** crystallizes in the triclinic space group P^{-1}. Fig. 6.1 shows the molecular structures of two asymmetric units A and B of this complex with atom numbering scheme. Cd atoms in these compounds are coordinated by azomethine nitrogens (N3 and N7), pyridyl nitrogens (N4 and N8) and iminolate oxygens (O1 and O2). The structure and labeling diagram of the molecule **A** is shown in Fig. 6.2. In both compounds **A** and **B**, the Cd atom is hexacoordinated in which both ligands are coordinated in their iminol forms. The bond distances between coordinated atoms and Cd of the two asymmetric units are in the order Cd–N$_{(azo)}$< Cd–N$_{(pyridyl)}$< Cd–O$_{(iminol)}$ though all distances vary in **A** and **B** slightly. The bond length Cd–N$_{(azo)}$ of the unit **B** is less than that of in **A**, which shows that the azomethyl nitrogen of **B** is strongly bonded with Cd atom than **A** and slightly shorter than the reported Cd–N$_{(azo)}$ bond distances [14] and which supports the significant out-of-plane π-bonding [15]. The Cd–O$_{(iminol)}$ bond lengths of the unit **B** is again shorter than that of **A** whereas the bond distances of Cd–N$_{(pyridyl)}$ are slightly larger for **B** than in **A**. The phenyl rings of one of the ligands in **A** and **B** are slightly twisted away by angles of 25.6^o and 28° respectively from the plane of the semicarbazone skeleton of the corresponding ligands. Table 6.3 shows selected bond lengths and bond angles of the compound **24**.
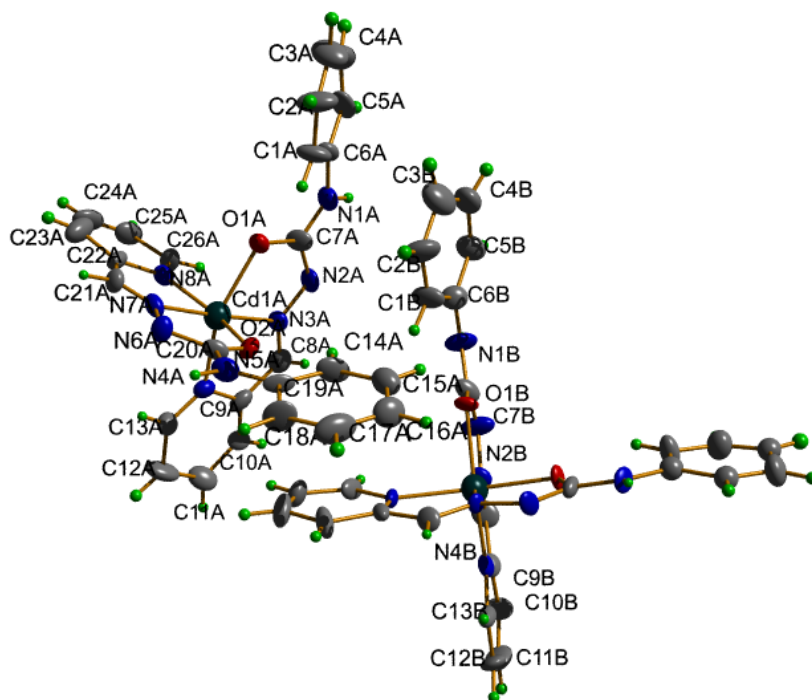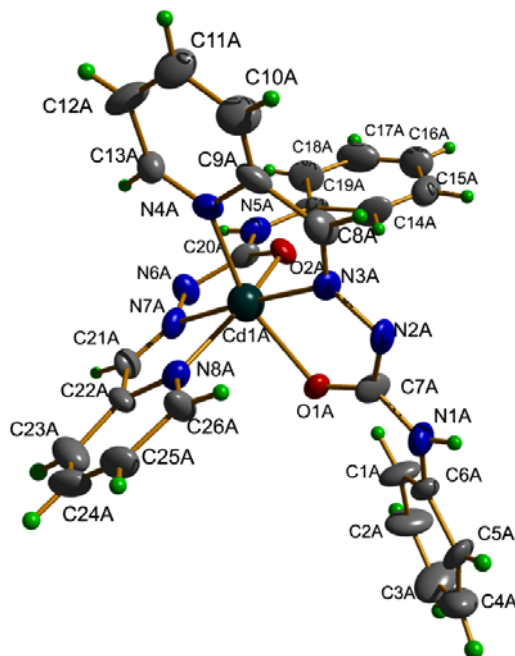
Fig. 6.1 Asymmetric unit of compound [CdL$^1_2$] (**24**).

**Fig. 6.2** Structure and labeling diagram of **A** of the compound [CdL$^1_2$] (**24**).

Table 6.3 Selected bond lengths (Å) and bond angles (°) for the two asymmetric units A and B

| Bond lengths			Bond angles		
	A	**B**		**A**	**B**
Cd1–O1	2.112(11)	2.107(11)	O1–Cd1–O2	89.3(4)	88.6(4)
Cd1–O2	2.128(12)	2.085(10)	O1–Cd1–N3	77.5(5)	78.2(5)
Cd1–N3	1.992(12)	1.972(12)	O1–Cd1–N8	156.9(5)	154.9(5)
Cd1–N4	2.065(14)	2.070(14)	O2–Cd1–N7	99.3(5)	103.7(5)
Cd1–N7	2.003(13)	1.963(10)	N3–Cd1–N7	89.9(5)	91.8(5)
Cd1–N8	2.069(14)	2.084(12)	N4–Cd1–N8	102.9(5)	97.0(5)
C7–O1	1.278(19)	1.266(19)	O1–Cd1–N4	94.0(5)	94.2(5)
C20–O2	1.264(18)	1.262(19)	Cd1–O2–C20	77.2(5)	77.6(4)
C6–N1	1.45(2)	1.37(3)	Cd1–N3–N2	154.3(5)	154.3(5)
C7–N1	1.29(2)	1.30(2)	Cd1–N4–C9	79.4(5)	76.7(6)
C7–N2	1.34(2)	1.38(2)	O1–Cd1–N7	176.8(6)	174.2(5)
N2–N3	1.39(2)	1.38(2)	O2–Cd1–N3	102.0(5)	108.2(5)
C20–N5	1.32(2)	1.347(19)	O2–Cd1–N4	103.8(6)	101.3(5)
N6–N7	1.362(19)	1.380(16)	O2–Cd1–N8	96.8(5)	96.1(5)
			N3–Cd1–N4	77.6(5)	77.4(5)
			N3–Cd1–N8	111.5(10)	112.0(11)
			N4–Cd1–N7	113.0(10)	112.8(9)
			N7–Cd1–N8	125.7(15)	127.1(17)
			Cd1–O1–C7	112.6(13)	113.6(14)
			C6–N1–C7	117.3(10)	115.5(10)
			N3–N2–C7	118.1(12)	120.6(12)
			Cd1–N3–C8	124.3(14)	123.8(14)
			N2–N3–C8	112.8(11)	113.7(12)
			Cd1–N4–C13	129.1(12)	128.1(12)

The coordination of the semicarbazone to the Cd atom through iminol oxygen in anionic form is confirmed by the bond length of C7–O1 [(1.278(19), 1.266(19) Å for **A** and **B** respectively] and C20–O2 [(1.264(18), 1.262(19) Å for **A** and **B** respectively] which is very close to the reported values of

semicarbazone complexes. Moreover, the bond lengths of C7–N2 [1.39(2) Å and 1.38(2) for **A** and **B** respectively] and C20–N5 [1.32(2) Å and 1.347(19) for **A** and **B** respectively] are comparable to the value reported for other semicarbazone complexes [16], which reveal extensive delocalization over entire coordination framework. The extensive delocalization over the semicarbazone moiety is evidenced by the bond length of N2–N3 (1.34 and 1.38 Å for **A** and **B**) and N6–N7 (1.362 and 1.380 Å for **A** and **B**), which is in between the single and double bond distance values. Both structures have distorted octahedral coordination around the metal atom. The angular structural parameter (τ) is calculated by $\tau = (\beta - \alpha)/60$, where β is the greatest trans angle and α is the second greatest trans angle; τ is 0 for rectangular octahedron [17]. The value of the τ for the two structures **A** and **B** are 0.3316 even though their bond angles vary. Therefore the amount of distortion in both structures is same.

The unit cell contains four molecules (Fig. 6.3). Though there is no such intermolecular classic hydrogen bonding interactions, there are two types of intramolecular hydrogen bonds O1···H–C1 and O2···H–C14 (Fig. 6.4) which make the molecule more stable in that configuration (Table 6.4). In addition to this, a π–π interaction (Table 6.4) is also observed between the pyridyl ring and the phenyl ring of the B type adjacent molecules with a Cg···Cg distance of 3.892(12) Å (Fig. 6.5). Three types of C–H···π interactions (Fig. 6.6) are also observed between phenyl and pyridyl hydrogens of the molecule B and phenyl and pyridyl rings of the adjacent A molecules in the crystal (Table 6.4).
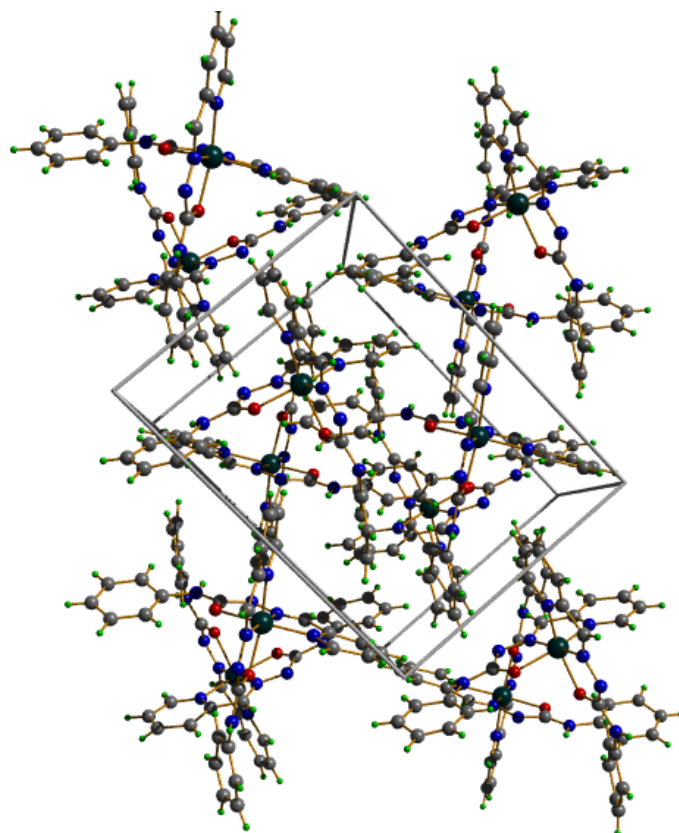
Fig. 6.3 Unit cell packing diagram of compound [CdL$^1_2$] (**24**).
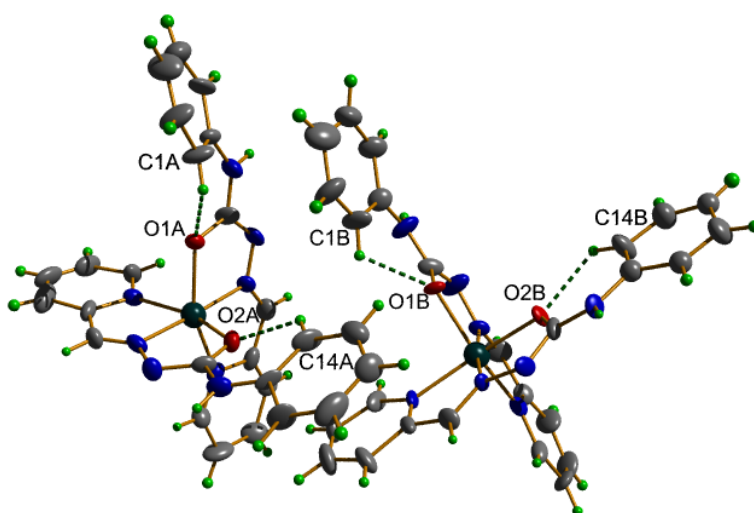
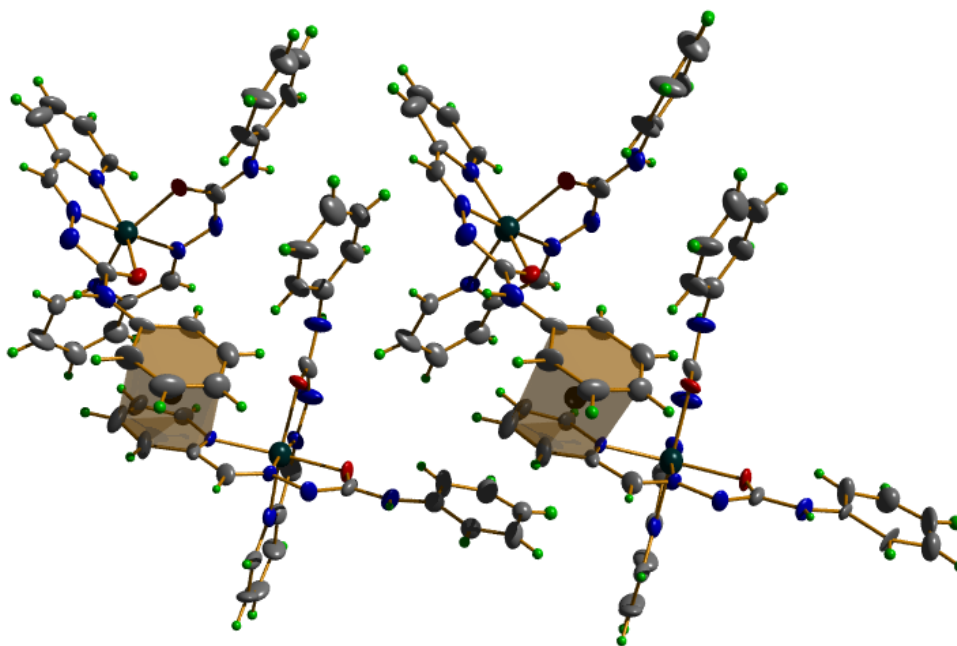**Fig.6.4** Intramolecular hydrogen bonding interactions of compound [CdL$^1_2$] (**24**).

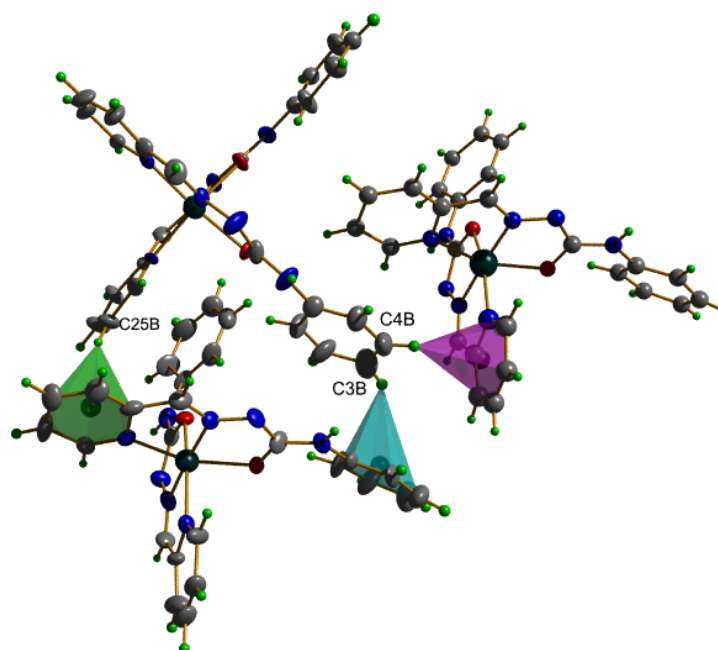Fig. 6.5 π···π interactions between the molecules of the compound [CdL$^1_2$] (**24**).

Fig. 6.6 C–H···π interactions between the molecules of the compound [CdL$^1_2$] (**24**).

Table 6.4 Interaction parameters of compounds [CdL$^1_2$] (**24**)

Hydrogen bonding interactions

D—H···A	D—H (Å)	H···A (Å)	D···A (Å)	∠D—H···A(°)
C1A—H···O1A	0.93	2.35	2.84(2)	113
C1B—H···O1B	0.93	2.32	2.81(2)	113
C14A—H···O2A	0.93	2.28	2.85(2)	119
C14B—H···O2B	0.93	2.24	2.81(2)	119

π···π interactions

Cg(I)···Cg(J)	Cg—Cg(Å)	α (°)	β (°)	γ(°)
Cg(14)···Cg(16)^a	3.892(12)	2.2(10)	29.53	27.86

C–H···π interactions

X—H(I)···Cg(J)	H···Cg (Å)	X···Cg (Å)	∠X–H···Cg (°)
C3B—H···Cg(7)^c	2.99	3.58(3)	123
C4B—H···Cg(6)^b	2.69	3.50(3)	147
C25B—H···Cg(5)^c	2.86	3.76(2)	165

Cg(5) = N4A, C9A, C10A, C11A, C12A, C13A
Cg(6) = N8A, C22A, C23A, C24A, C25A, C26A
Cg(7)= C1A, C2A, C3A, C4A, C5A, C6A
Cg(14) = N8B, C22B, C23B, C24B, C25B, C26B
Cg(16) = C14B, C15B, C16B, C17B, C18B, C19B
Equivalent position codes: a=-1+x,y,z ; b=1+x,y,z ; c= x,y,z
D, donor; A, acceptor; Cg, centroid; α, dihedral angles between planes I and J; β, angle between Cg···Cg and Cg(J)_perp; γ, angle between Cg···Cg and Cg(I)_perp

6.3.3. Crystal structure of the complex [Cd$_2$L$^3_2$Br$_2$] (28)

Fig. 6.6 shows the molecular structure of the binuclear centrosymmetric Cd(II) complex with the atom numbering scheme. Both Cd centres being hexacoordinated and the coordination around the Cd(II) ion can be best described as a distorted octahedron with a CdO$_1$N$_2$Br$_3$ chromophore. Each Cd atom is coordinated by azomethine nitrogen, oxygen atom from the ligand, one

pyridyl nitrogen and three bromine atoms. The bromine atoms (Br2) bridges the two cadmium atoms leaving the other bromine atom (Br1) free. The coordination of oxygen from the semicarbazone ligand occurs in amido form, confirmed by the double bond nature of C7–O1 (1.231) Å and N2–C7 (1.385) Å bond lengths [18]. The C8–N3 and N2–N3 bond distances are 1.277(5) Å and 1.359(3) Å respectively, which reveal that extensive delocalization over the entire binuclear coordination framework is restricted. The dihedral angle between the two aromatic rings of benzoylpyridine part of the semicarbazone ligand is 87.9(3)° and the dihedral angle between the phenyl ring of the semicarbazide part and the pyridyl ring is 20.6(3)°. Table 6.5 shows the selected bond lengths and bond angles of the compound **28**.
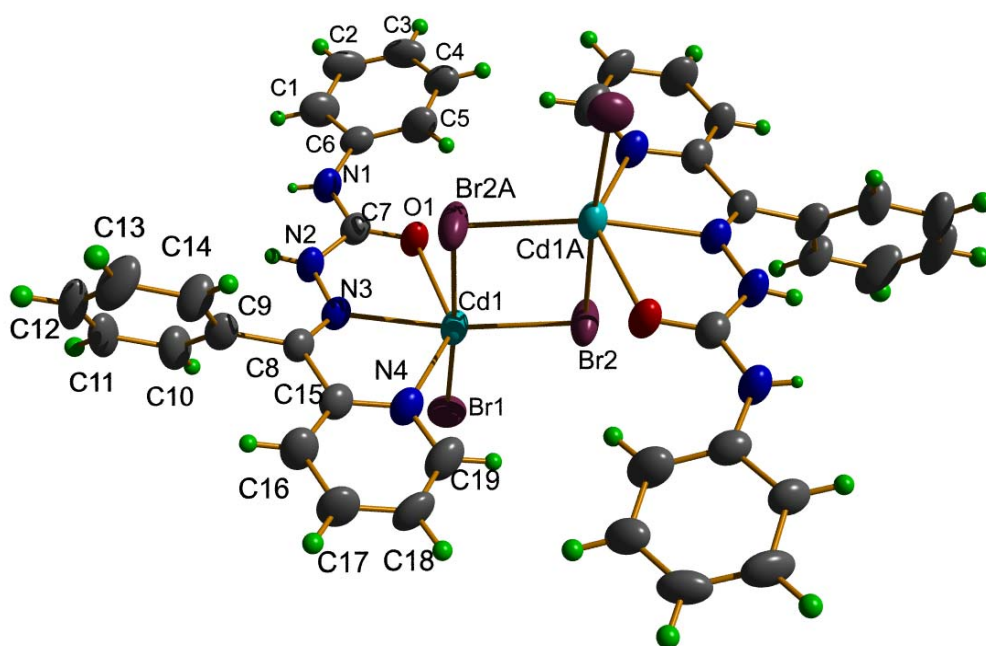

Fig. 6.6 Structure and labeling diagram for compound [Cd$_2$L$^3_2$Br$_2$] (**28**).

Table 6.5 Selected bond lengths (Å) and bond angles (°) of compound [Cd$_2$L$^3_2$Br$_2$] (**28**)

Bond lengths		Bond angles	
Cd(1)—Br(1)	2.6496(9)	Br(1)—Cd(1)—Br(2)	98.46(4)
Cd(1)—O(1)	2.376(3)	Br(1)—Cd(1)—O(1)	94.25(9)
Cd(1)—N(3)	2.354(3)	Br(1)—Cd(1)—N(3)	95.33(9)
Cd(1)—Br(2)	2.5892(9)	Br(1)—Cd(1)—N(4)	94.31(10)
Cd(1)—N(4)	2.362(4)	Br(1)—Cd(1)—Br(2)A	175.70(4)
Cd(1)—Br(2)A	2.9505(10)	Br(2)—Cd(1)—O(1)	111.29(7)
O(1)—C(7)	1.229(5)	Br(2)—Cd(1)—N(3)	166.22(9)
N(1)—C(6)	1.409(6)	Br(2)—Cd(1)—N(4)	110.21(8)
N(1)—C(7)	1.338(5)	Br(2)—Cd(1)—Br(2)A	85.33(4)
N(2)—N(3)	1.360(5)	O(1)—Cd(1)—N(3)	67.66(10)
N(2)—C(7)	1.378(6)	O(1)—Cd(1)—N(4)	135.74(11)
N(3)—C(8)	1.276(5)	O(1)—Cd(1)—Br(2)A	86.22(9)
N(4)—C(15)	1.342(6)	N(3)—Cd(1)—N(4)	68.35(10)
N(4)—C(19)	1.337(5)	N(3)—Cd(1)—Br(2)A	80.89(9)
Cd1···Cd1A	4.0809(14)	N(4)—Cd(1)—Br(2)A	82.42(10)
		Cd(1)—Br(2)—Cd(1)A	94.67(4)
		Cd(1)—O(1)—C(7)	117.7(3)
		C(6)—N(1)—C(7)	128.2(4)
		N(3)—N(2)—C(7)	116.2(3)
		Cd(1)—N(3)—N(2)	116.5(2)
		Cd(1)—N(3)—C(8)	121.0(2)

In the case of this Cd-semicarbazone complex, Cd–O bond distance is Cd1–O1, 2.376(3) Å, and Cd–N bond distances of Cd1–N3 and Cd1–N4 are 2.354(3) Å 2.362(4) Å respectively. The Cd1–O1 bond distance is less than the other Cd–O bond distances (2.405 – 2.475 Å) reported for other octahedral Cd(II) complexes showing more stronger coordination through oxygen in amido form towards the metal atom than the reported complexes [14] whereas the Cd1–N3 and Cd1–N4 bond distances are larger than the other Cd–N bond distances (2.239 Å), which supports the lack of significant out-of-plane π-bonding. The *cis* angles Br(2)–Cd(1)–O(1) and O(1)–Cd(1)–N(3) are 111.29(7)° and 67.66(10)° and *trans* angle O(1)–Cd(1)–N(4) is 135.74(11)° indicating that the compound **28** has large distortion from octahedral geometry [19]. The Cd1···Cd1A distance is 4.0809(14) Å.

The unit cell packing diagram of the complex **28** viewed along *a* axis is given in Fig. 6.7. It can be observed that the molecules are packed in a zig-zag manner in two directions as shown in Fig. 6.8. Ring puckering analysis shows that the rings containing metal atom have no significant puckering. The diverse π···π stacking is present in the molecular arrangement (Fig. 6.9) with Cg···Cg distances of 3.4213 and 3.3600 Å (Table 6.6).
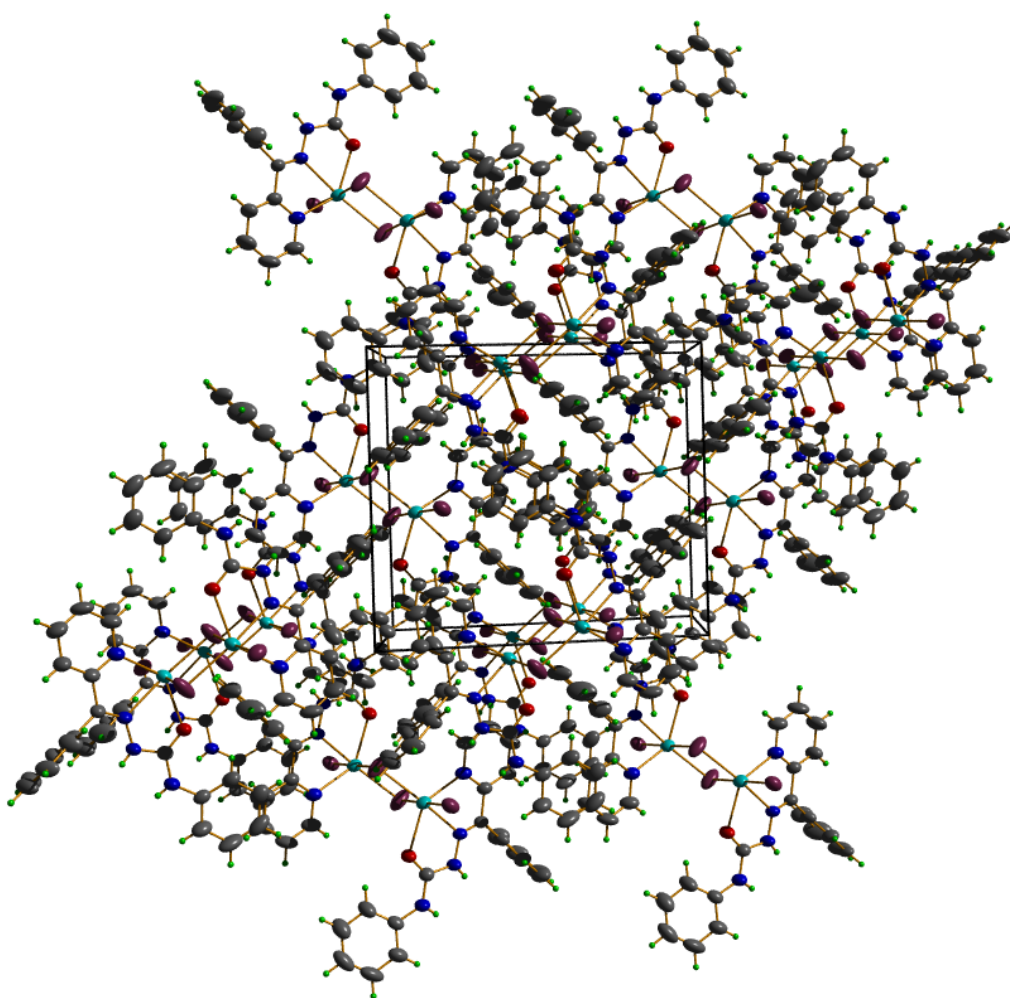
**Fig. 6.7** Unit cell packing diagram of compound $[Cd_2L^3_2Br_2]$ (**28**) along a axis.
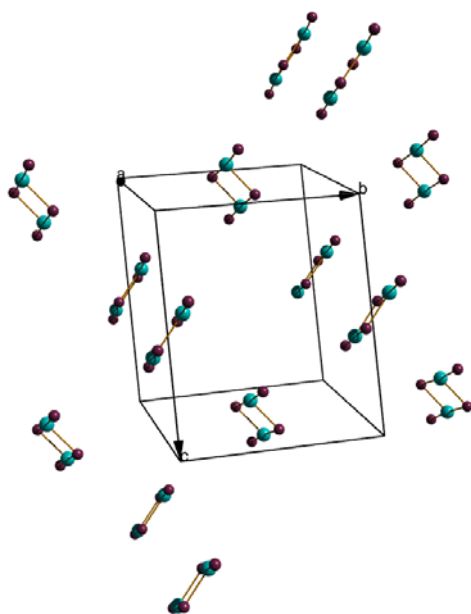
Fig. 6.8. Two different arrangements of the central ring of the compound [Cd$_2$L$_2^3$Br$_2$] (**28**) in the unit cell.

3.4247(15)

3.3597(18)
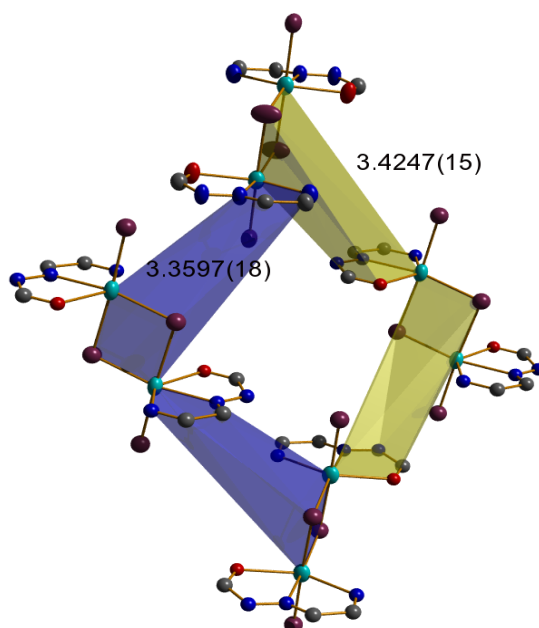
Fig. 6.9 $\pi \cdots \pi$ interactions between the molecules of the complex [Cd$_2$L$_2^3$Br$_2$] (**28**) with centroid-centroid distances.

A supramolecular hydrogen bonding network is established between the molecules in the unit cell in two different directions trough Br atom and hydrogens attached in N1 and N2 atoms as shown in Fig. 6.10.
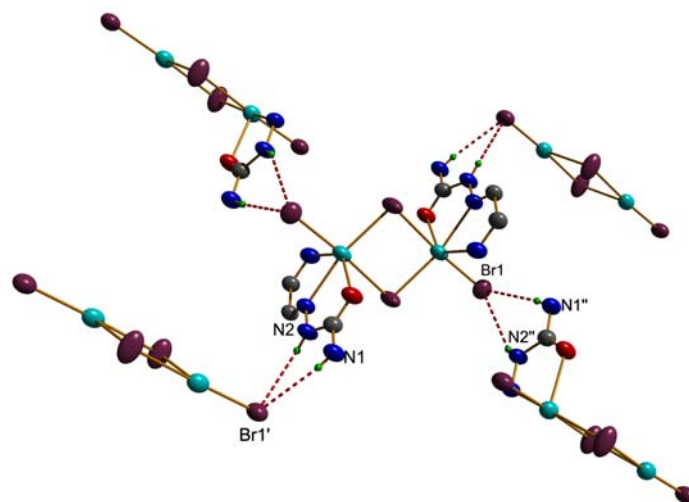
Fig. 6.10 Intermolecular hydrogen bonding network of the compound $[Cd_2L^3_2Br_2]$ **(28)**.

Table 6.6 Interaction parameters of the compound $[Cd_2L^3_2Br_2]$ **(28)**

Hydrogen bonding interactions

D—H···A	D—H (Å)	H···A (Å)	D···A (Å)	∠D—H···A(°)
N(2)—H···Br(1)[a]	0.77(5)	2.90(5)	3.565(4)	146(5)
N(1)—H···Br(1)[a]	0.73(4)	2.64(4)	3.367(4)	172(4)
C(5)—H(5)···O(1)	0.93	2.30	2.885(6)	120
C(18)—H(18)···Br(1)	0.93	2.90	3.731(5)	150

$\pi \cdots \pi$ interactions

Cg(I)···Cg(J)	Cg···Cg(Å)	α (°)	β (°)	γ(°)
Cg(2)···Cg(1)[b]	3.4213(16)	89.96(11)	59.52	70.29
Cg(3)···Cg(1)[b]	3.3600(18)	84.96(12)	57.21	70.75

Cg (1) = Cd(1), Br(1), Cd(1)A, Br(2)A,
Cg (2) = Cd(1), O(1), C(7), N(2), N(3)
Cg (3) = Cd(1), N(3), C(8), C(15), N(4)
Equivalent position codes: a = 3/2 –x,1/2+y,1/2-z; b = x,y,z
D, donor; A, acceptor; Cg, centroid; α, dihedral angles between planes I and J; β, angle between Cg···Cg and Cg(J)_perp; γ, angle between Cg···Cg and Cg(I)_perp

6.3.4. Infrared spectral studies

The IR spectral bands most useful for the determination of the mode of coordination are given in Table 6.7. Bands at 1693 and 1698 cm^{-1} respectively in the semicarbazones HL^1 and HL^3 have significant contribution from C=O stretching vibration and absence of such bands in the complexes **24, 25** and **26** confirming the coordination through iminolate oxygen. The presence of bands at 1677, 1668, 1678, 1671 and 1660 cm^{-1} for the complexes **21, 22, 23, 27** and **28** respectively support the amido form of the two semicarbazones in these complexes.

On coordination of the azomethine nitrogen of the ligand HL^1, the IR stretching frequency ν(C=N) at 1597 cm^{-1} shifts to 1592, 1588, 1593, 1590 and 1593 cm^{-1} for the complexes **21, 22, 23, 24** and **25** respectively and for the ligand HL^3, the frequency ν(C=N) at 1600 cm^{-1} shifts to 1596, 1594 and 1594 cm^{-1} for the complexes **26, 27** and **28** respectively [20-22]. The spectra of the complexes exhibit a systematic positive shift in the position of ν(N–N) bands by 5-23 cm^{-1} for the ligand HL^1 and by 7-13 cm^{-1} confirm the coordination of the azomethine nitrogen in both ligands. This shift to higher region is due to the increase in the double bond character off-setting the loss of electron density *via* donation to the metal. The bands appearing in the region 485-502 cm^{-1} correspond to ν(Cd–N$_{azo}$) for complexes **21-28** again confirm the coordination of the azomethine nitrogen [23]. Coordination of pyridyl nitrogen of the ligand HL^1 causes the out-of-plane bending vibrational band to shift from 600 cm^{-1} to higher frequencies 630, 632, 628, 623 and 636 cm^{-1} for complexes **21-25** respectively and for HL^3 the shift from 602 cm^{-1} to higher frequencies 620, 633 and 635 cm^{-1} for the complexes **26, 27** and **28** respectively [24]. Presence of bands at 1584 and 1541 cm^{-1} for the complexes [CdL$^1_2$] (**24**). and [CdL^{1}N$_3$] (**25**) of the ligand HL^1 and the bands at 1582 cm^{-1} for the complex [CdL^3(OAc)]

(**26**) of the ligand HL^3 are assigned to the newly formed v(C=N) band after enolization [25]. The asymmetric and symmetric stretching vibrations of the acetate group appear at 1562 and 1434 cm^{-1} respectively for the complex **26** having the separation value Δv=128 cm^{-1} suggests the presence of chelating acetate group linked with the metal center [26,27]. Meanwhile the asymmetric and symmetric stretching vibrations of the acetate group appear at 1561 and 1365 cm^{-1} respectively for the complex [Cd(HL^1)(OAc)$_2$]·3H$_2$O (**22**) having the separation value Δv = 196 cm^{-1} suggests the presence of unidentate type of acetate group linked with the metal center [28]. The azido complex [CdL^{1}N$_3$] (**25**) exhibits a strong band at 2041 cm^{-1} corresponding to v_a(N–N–N) stretching vibration of the coordinating azido group.

**Table 6.7** IR spectral assignments for semicarbazones and their cadmium(II) complexes

Compound	v(^{2}NH)	v(C=N)	v(C=O)	v(C=N)^a	v(N–N)	v(Cd–N$_{azo}$)
HL^1	3372	1597	1693	-	1143	-
[Cd(HL^1)Br$_2$] (**21**)	3416	1592	1677	-	1166	485
[Cd(HL^1)(OAc)$_2$]·3H$_2$O (**22**)	3380	1588	1668	-	1150	489
[Cd(HL^1)Cl$_2$] (**23**)	3254	1593	1678	-	1153	500
[CdL$^1_2$] (**24**)	3290	1590	-	1584	1148	490
HL^3	3375	1600	1698	-	1132	-
[CdL^{1}N$_3$] (**25**)	3318	1593	-	1541	1139	598
[CdL^3(OAc)] (**26**)	3427	1596	-	1582	1139	502
[Cd(HL^3)Cl$_2$] (**27**)	3437	1594	1671	-	1145	500
[Cd$_2$L$^3_2$Br$_2$] (**28**)	3414	1594	1660	-	1140	490

^{a} Newly formed C=N
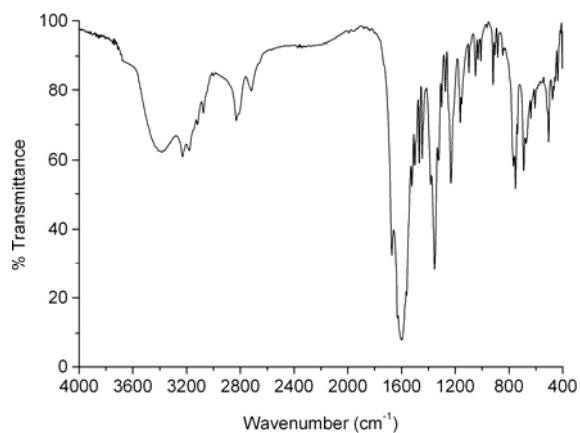
Fig. 6.11 IR spectrum of the compound [Cd(HL^1)Br$_2$] (**21**).
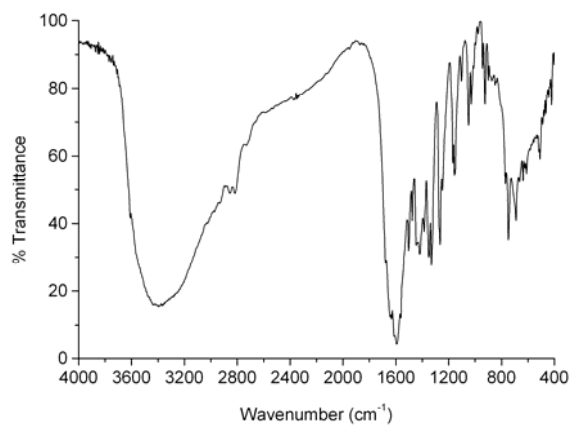
Fig.6.12 IR spectrum of the compound [Cd(HL^1)(OAc)$_2$]·3H$_2$O (**22**).
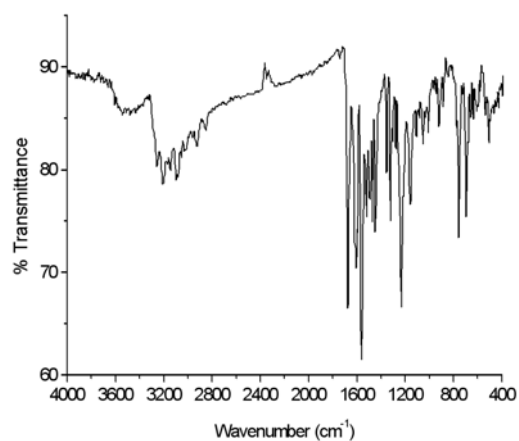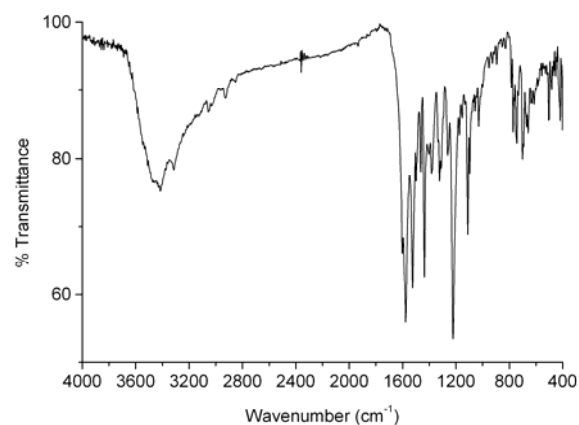

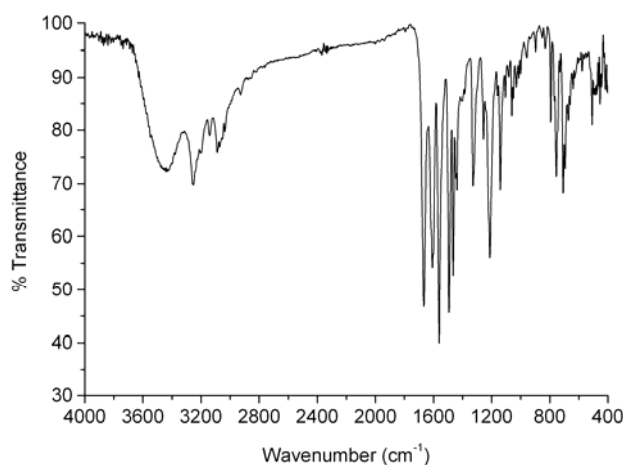**Fig. 6.13** IR spectrum of the compound [Cd(HL^1)Cl$_2$] (**23**).
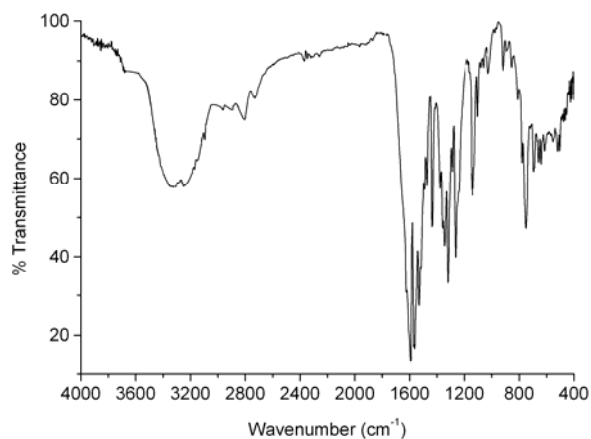
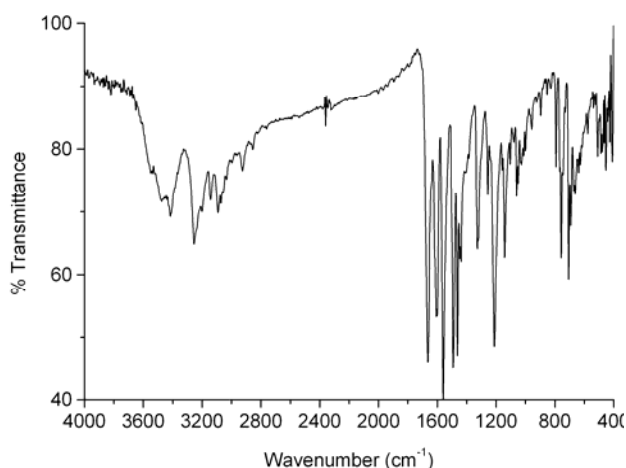**Fig. 6.14** IR spectrum of the compound [CdL$^1_2$] (**24**).
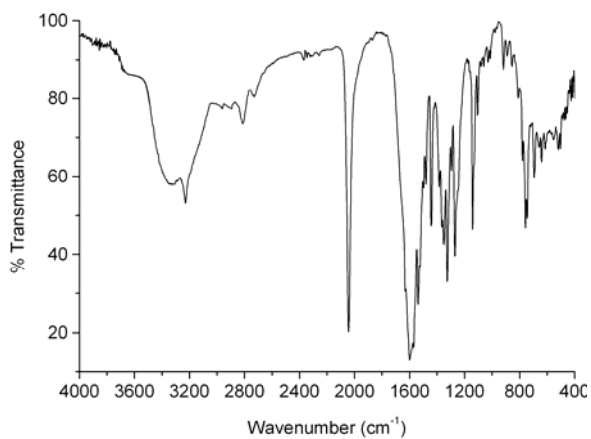
Fig.6.15 IR spectrum of the compound [CdL^{1}N$_3$] (**25**).

Fig.6.16 IR spectrum of the compound [CdL^3(OAc)] (**26**).

Fig. 6.17 IR spectrum of the compound [Cd(HL^3)Cl$_2$] (**27**).

Fig.6.18 IR spectrum of the compound [Cd$_2$L$^3_2$Br$_2$] (**28**).

6.3.5. Electronic spectral studies

The electronic absorption bands of the Cd(II) complexes, recorded in methanol solution, are given in Table 6.8. The energy of intraligand bands are slightly changed upon complexation. This is due to the involvement of C=O bond and azomethine nitrogen atom in coordination [26]. The intraligand transitions are observed in the region 32220-42500 cm^{-1} for the compounds **21-25** whereas for the complexes **26-28** intraligand transitions are in the range

32670-43260 cm^{-1}. The new bands observed for the complexes **21-25** in the region 25150-26025 cm^{-1} and for the complexes **26-28** in the region 27350-27645 cm^{-1} are assigned to Cd(II) →O transitions. No appreciable absorptions occurred below 20000 cm^{-1} in methanol solution indicating the absence of *d-d* bands which is in accordance with d^{10} configuration of Cd(II) ion. Electronic spectra of complexes are presented in Figs. 6.19-6.26.

Table 6.8 Electronic spectral assignments for the semicarbazones and its cadmium(II) complexes

Compound	MLCT	n →π*/π→π*
HL^1	-	32000, 38100, 42500
[Cd(HL^1)Br$_2$] (**21**)	25730	32500, 38820, 42050
[Cd(HL^1)(OAc)]$_2$·3H$_2$O (**22**)	25725	32350, 39075, 41350
[Cd(HL^1)Cl$_2$] (**23**)	26025	32560, 38700, 42500
[CdL$^1_2$] (**24**)	25860	32220, 38860, 42300
[CdL^{1}N$_3$] (**25**)	25150	32280, 38860, 42030
HL^3	-	32660, 37797, 42793
[CdL^3(OAc)] (**26**)	27645	32670, 38900, 43020
[Cd(HL^3)Cl$_2$] (**27**)	27575	32720, 39950, 43260
[Cd$_2$L$^3_2$Br$_2$] (**28**)	27350	32750, 40060, 42800
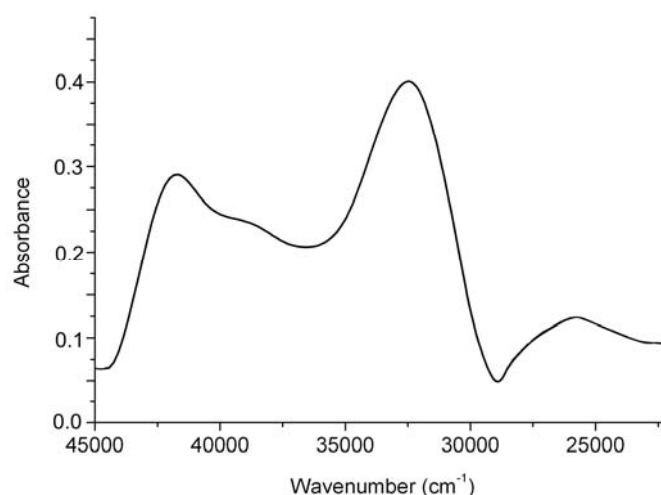
Fig. 6.19 Electronic spectrum of the compound [Cd(HL^1)Br$_2$] (**21**).
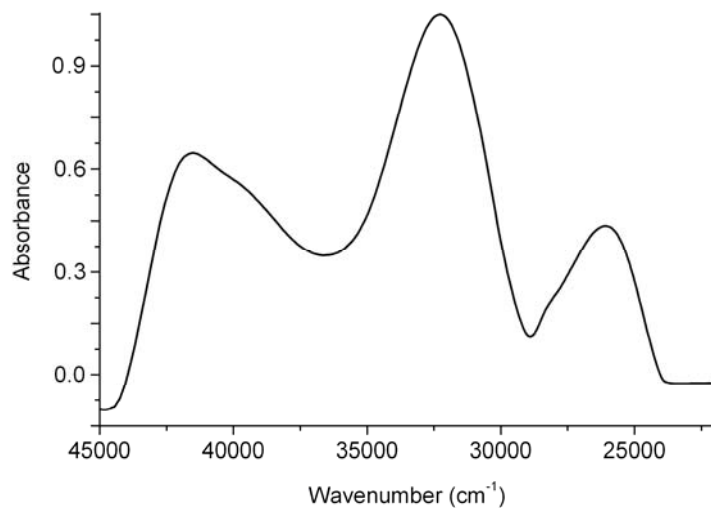
Fig. 6.20 Electronic spectrum of the compound [Cd(HL¹)(OAc)₂]·3H₂O (**22**).
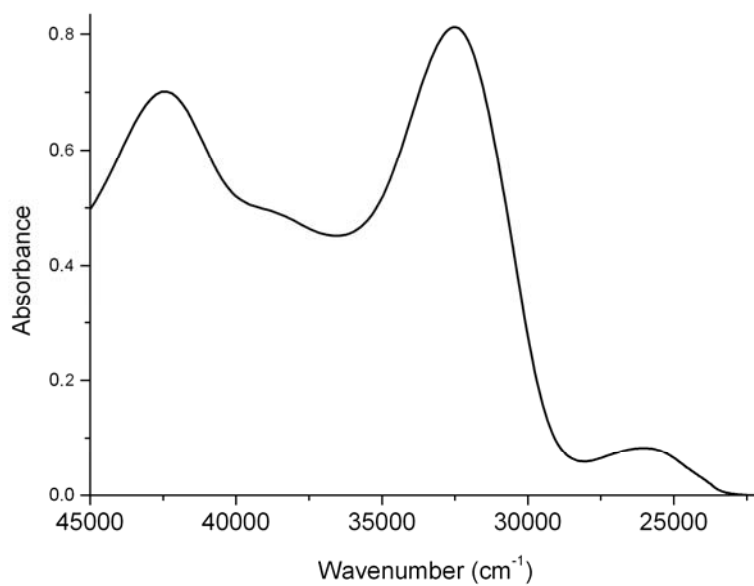
Fig. 6.21 Electronic spectrum of the compound [Cd(HL¹)Cl₂] (**23**).

Fig. 6.22 Electronic spectrum of the compound $[CdL^1_2]$ (**24**).
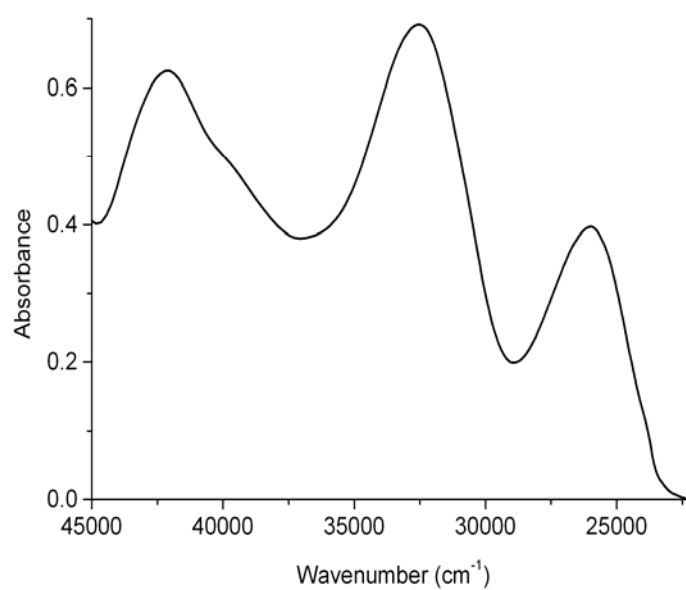
Fig. 6.23 Electronic spectrum of the compound $[CdL^1N_3]$ (**25**).
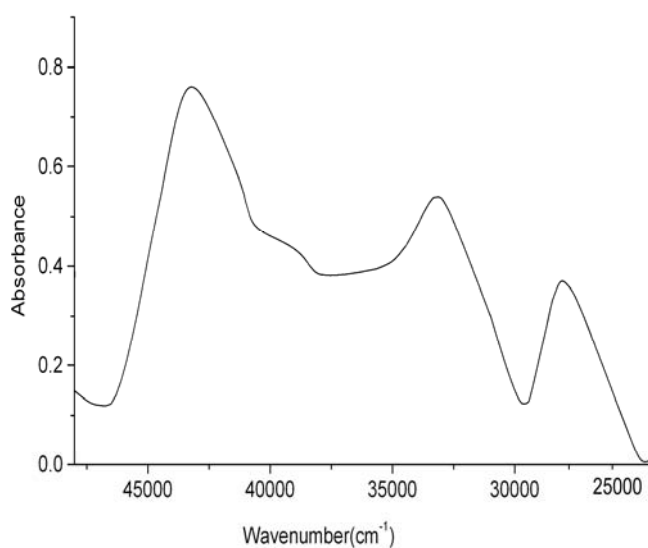
Fig.6.24 Electronic spectrum of the compound [CdL³(OAc)] (**26**).
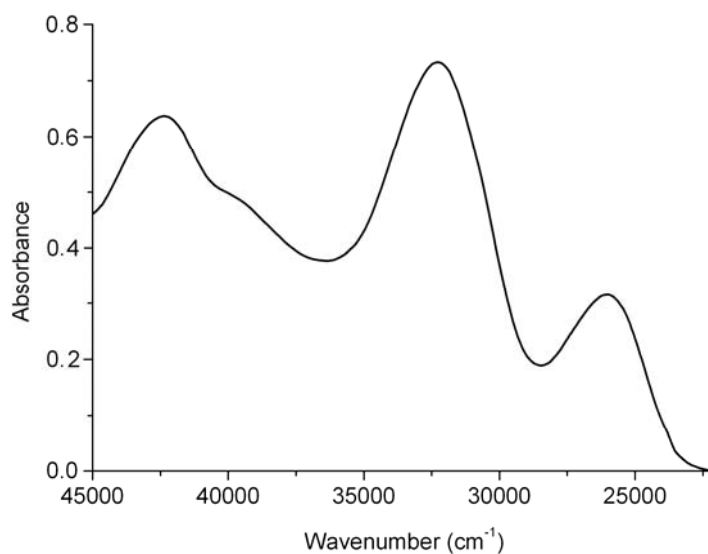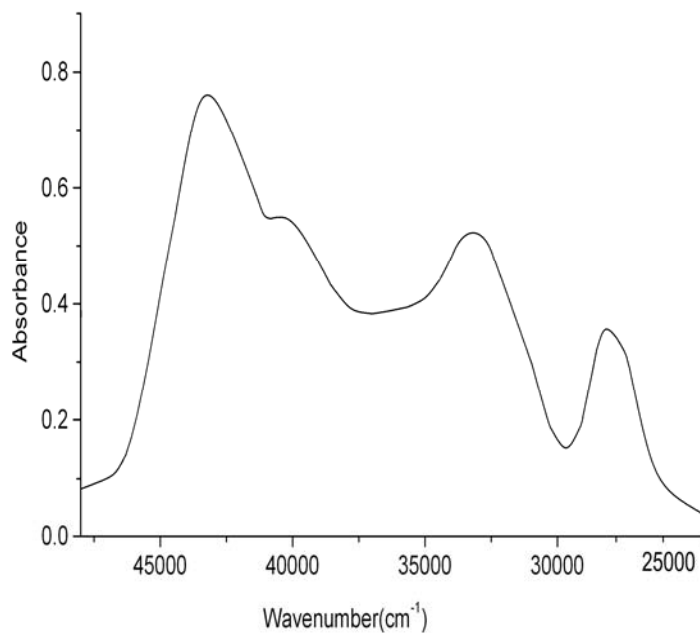

Fig.6.25 Electronic spectrum of the compound [Cd(HL³)Cl₂] (**27**).
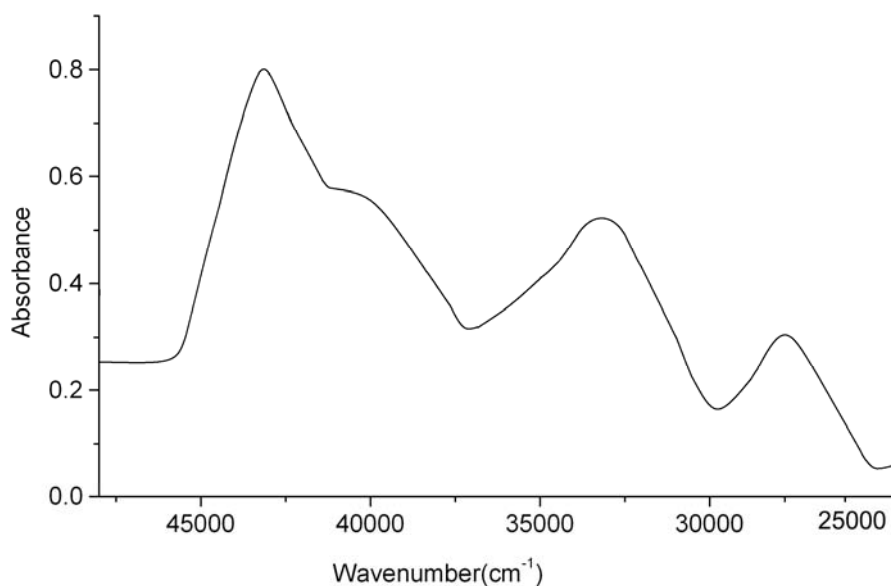
Fig. 6.26 Electronic spectrum of the compound [Cd$_2$L$^3_2$Br$_2$] **(28)**.

6.3.6. Thermogravimetric studies

As we discussed in the previous chapters, thermal analyses helps us valuable information regarding the thermal stability and nature of water molecules in complexes. It also helps us to distinguish the lattice water molecules and coordinated water molecules present in the compound and in some cases it helps to find out the composition of the compounds. Reports show that the weight losses for lattice water are below 200 ºC [29] and weight losses due to coordinated water molecules are in the range of 200–350 ºC [30]. There are two weight losses in the complex **21**. The first weight loss (31.6%) at around 300 ºC may be because of the removal of the two bromine atoms and the second weight loss (46.8%) in the range 450-570 ºC shows the removal of the ligand from the complex (Fig.6.27).
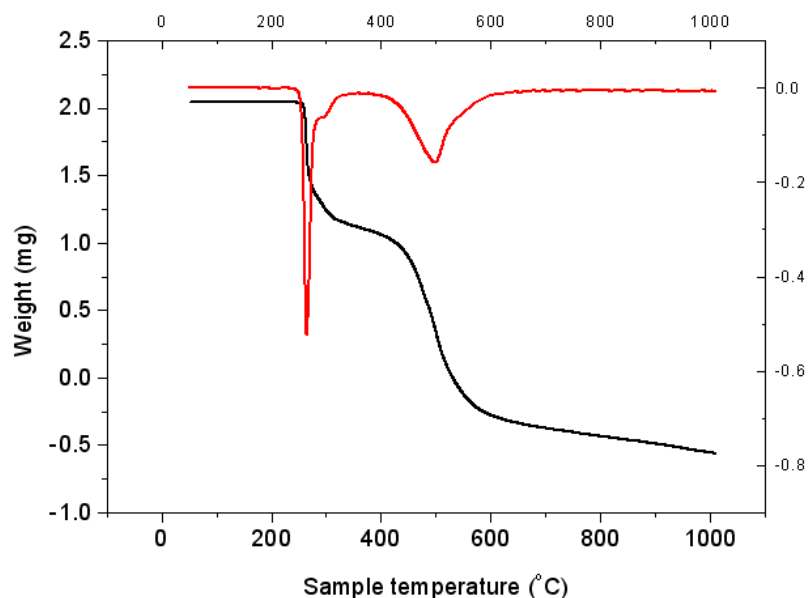
Fig. 6.27 Thermogram of the compound [Cd(HL^1)Br$_2$] (**21**).

The similar behavior was observed in the compound **23** as it contains chlorine atoms instead of bromine. Hence the initial removal took place in the range 270-325 ^{o}C with a percentage weight loss of 17% and its second weight loss is due to the HL ligand decomposition which was terminated at around 600 ^{o}C (Fig. 6.28). Similar explanation can be attributed to the complex **27** (Fig. 6.29) as it has the same composition but with the ligand HL^3 instead of HL^1. The thermogram observed for in the complex **28** also resembles the thermal behavior of the complex **21** of which the structure is confirmed by single crystal XRD studies. The two bromine atoms are removed first at around 300 ºC, which is confirmed by doing the TG analysis for the complex **28** for which we got the single crystal and the two ligands attached in the complex is removed in the range 450-600 ^{o}C (Fig. 6.30). Both ligands (HL^1 and HL^3) in the complexes are decomposing approximately in the same temperature range (450-600 ^{o}C).
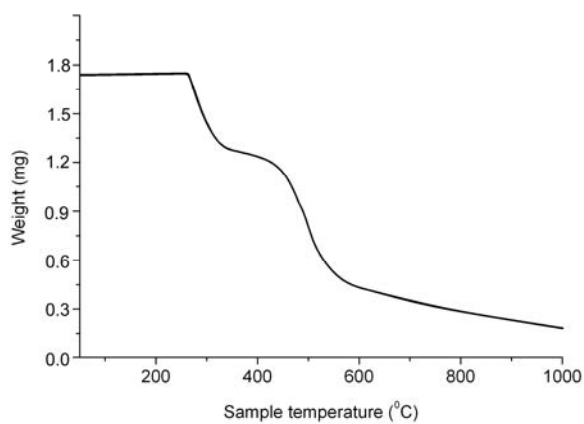
Fig. 6.28 Thermogram of the compound [Cd(HL^1)Cl$_2$] (**23**).
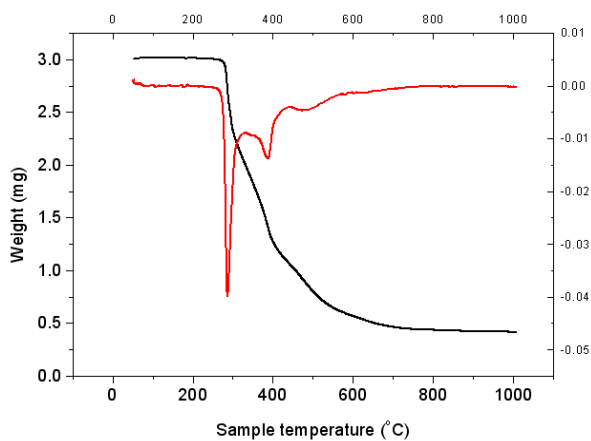
Fig. 6.29 Thermogram of the compound [Cd(HL^3)Cl$_2$] (**27**).
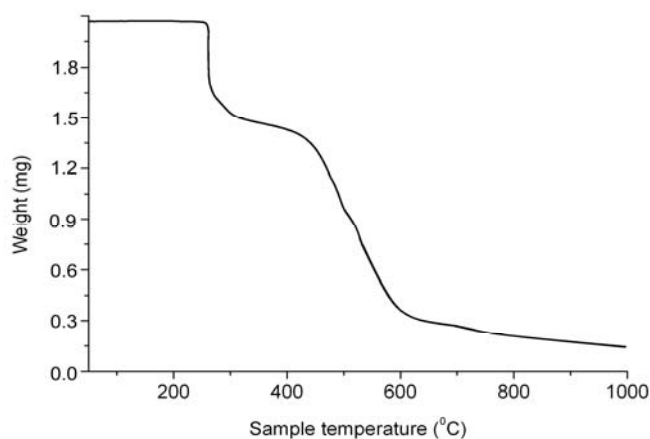
Fig. 6.30 Thermogram of the compound [Cd$_2$L$^3_2$Br$_2$] (**28**).

There is a weight loss only the complex **22** in the region 150–190 ºC indicates the presence of lattice water molecules whereas all the other complexes do not have such peaks in that range showing the absence of lattice water molecules in their structures. Moreover, its percentage weight loss of the complex **22** (10.5%) confirms that it has three lattice water molecules (Fig. 6.26). The percentage weight loss of ligands (HL^1 and OAc) and water (78.6%) of this complex again confirms the composition (Fig. 6.25). Similar decomposition was obtained for the complex **26** (with HL^3 ligand) where there are no such water molecules attached. Except the weight loss of water molecule here also the decomposition started at around 300 ºC with a weight loss of 12.3% due to the removal of one acetato moiety and the decomposition of ligand (HL^3) continued till 600 ºC (Fig. 6.27).
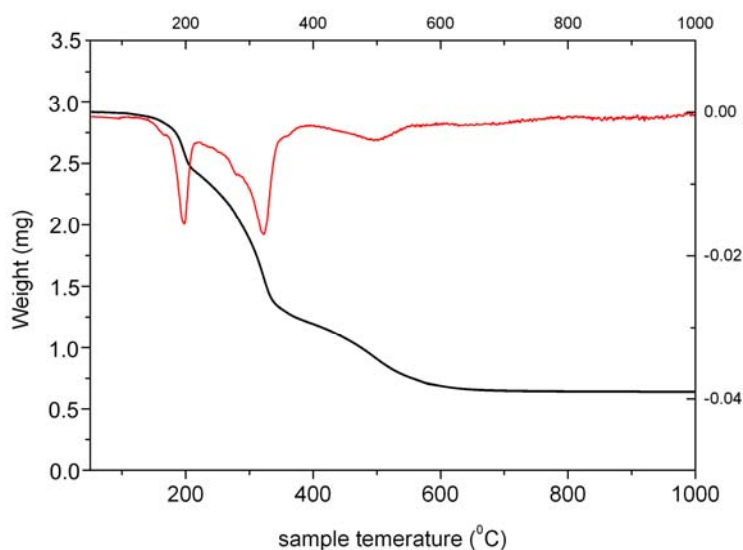
Fig. 6.26 Thermogram of the compound [Cd(HL^1)(OAc)$_2$]·3H$_2$O (**22**).
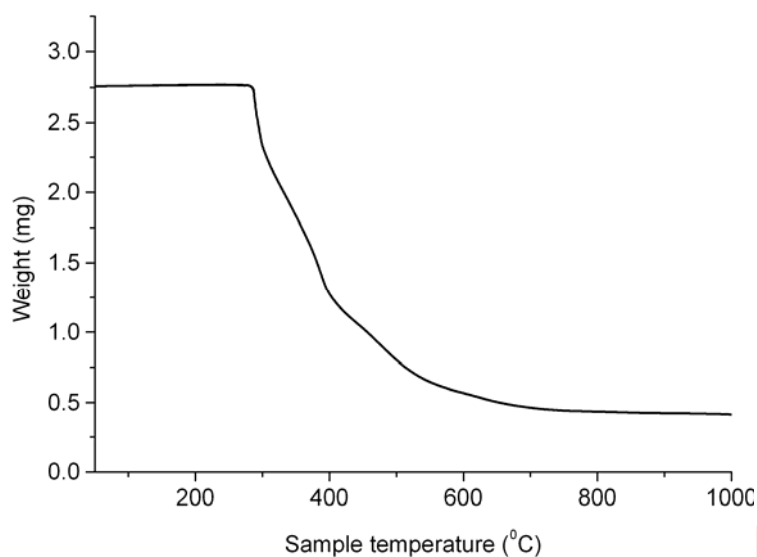
Fig.6.27 Thermogram of the compound [CdL³(OAc)] (**26**).

Since the complex **24** has only two ligands (HL^3), the decomposition began at around 325 $^{\rm o}$C as the other complexes having HL^3 ligand decomposed and ended at 600 $^{\rm o}$C giving a total percentage weight loss of 84.9% confirming the composition (Fig. 6.28).
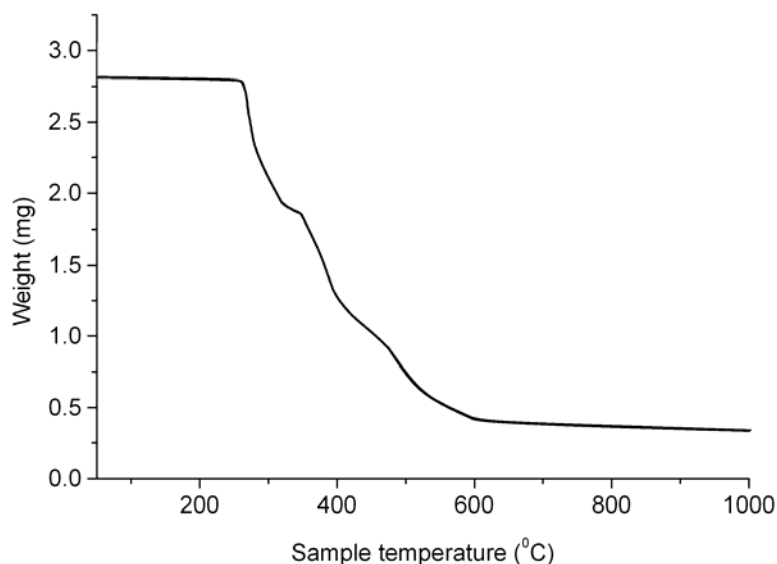
Fig. 6.28 Thermogram of the compound [CdL$^1_2$] (**24**).

References

[1]   F. Michael, "New Mineral Names" American Mineralogist 65 (1980) 1065.

[2]   L. Pag, J.N. Lindner, G. Davies, D.E. Seitz, B.L Karger, *Anal. Chem.* 51 (1979) 433.

[3]   M.N. Hughes, The Inorganic Chemistry of biological Processes, Wiley, NewYork, 1981.

[4]   X. Wu, J.C. Yalowich, B.B. Hassinoff, J. Inorg. Biochem. 105 (2011) 833.

[5]   A. Majumder, G.M. Rosair, A. Mallick, N. Chattopadhyay, S. Mitra, Polyhedron 25 (2006) 1753.

[6]   J-C. Dai, X-T. Wu, Z-Y. Fu, C-P. Cui, S-M. Hu, W-X. Du, L-M. Wu, H-H. Zhang, R-Q. Sun, Inorg. Chem. 41 (2002) 1391.

[7]   M.L. Post, J. Trotter, J. Chem. Soc., Dalton Trans. 7 (1974) 674.

[8]   P.A. Prasad, S. Neeraj, S. Natarajan, C.N.R. Rao, J. Chem. Commun. 14 (2000) 1251.

[9]   C.Y. Duan, Y.P. Tian, C.Y. Zhao, X.Z. You, T.C.W. Mak, Polyhedron 16 (1997) 2857.

[10] CrysAlis CCD and CrysAlis RED Versions 1.171.29.2 (CrysAlis171. NET), Oxford Diffraction Ltd., Abingdon, Oxfordshire, England, 2006.

[11] G.M. Sheldrick, Acta Cryst. A46 (1990) 467.

[12] G.M Sheldrick, SHELXS-97, Program for X-ray Crystal Structure Refinement, University of Göttingen, Germany, 1997.

[13] K. Brandenburg, H.Putz GbR Diamond Version 3.2g, Crystal Impact GbR, Bonn, Germany, 2011.

[14] A.F. Cameron, R.H. Nuttall, D.W. Taylor, J. Chem. Soc., Chem. Commun. 3 (1971) 129.

[15] L. Latheef, M.R.P. Kurup, Spectrochim. Acta A 70 (2008) 86.

[16] T.A. Reena, E.B. Seena, M.R.P. Kurup, Polyhedron 27 (2008) 3461.

[17] G. Murphy, C.O. Sullivan, B. Murphy, B. Hathaway, Inorg. Chem. 37 (1998).

[18] U.L. Kala, S. Suma, M.R.P. Kurup, S. Krishnan, R.P. John, Polyhedron 26 (2007) 1427.

[19] A.F. Cameron, R.H. Nuttall, D.W. Taylor, J. Chem. Soc., Dalton Trans. 15 (1972) 1608.

[20] A. Sreekanth, H.-K. Fun, M.R.P. Kurup, Inorg. Chem. Commun. 7 (2004) 324.

[21] V. Philip, V. Suni, M.R.P. Kurup, M. Nethaji, Polyhedron 25 (2006) 1931.

[22] V. Philip, V. Suni, M.R.P. Kurup, M. Nethaji, Polyhedron 24 (2005) 1133.

[23] A. Majumder, G. M. Rosair, A. Mallick, N. Chattopadhyay, S. Mitra, Polyhedron 25 (2006) 1753.

[24] V. Philip, V. Suni, M.R.P. Kurup, M. Nethaji, Spectrochim. Acta A 64 (2006) 171.

[25] K. Nakamoto, Infrared and Raman spectra of Inorganic and Coordination compounds, fifth edition, Wiley, NY, 1997.

[26] A. Sreekanth, U.L. Kala, C.R. Nayar, M.R.P. Kurup, Polyhedron 23 (2004) 41.

[27] R. Kruszynski, A. Turek, J. Coord. Chem. 57 (2004) 1089.

[28] F.P. Pruchnik, U. Dawid, A. Kochel, Polyhedron 25 (2006) 3647-3652.

[29] S. Kavlak, H. Kaplan Can, Z.M.O. Rzaev, A. Guner, J Appl Polym Sci, 100 (2006) 3926.

[30] G.A. Nazri., C. Julien, Solid State Ionics 80 (1995) 271.

........................৵৵৵........................

Summary and conclusions

The metal complexes of semicarbazones play an essential role in agriculture, pharmaceutical and industrial chemistry and they are used as catalysts, in various biological systems, polymers and dyes, besides some uses antifertility and enzymatic agents. The biological properties of semicarbazones are often related to metal ion coordination. Firstly, lipophilicity, which controls the rate of entry in to the cell, is modified by coordination. Also, the metal complex can be more active than the free ligand. The mechanism of action can involve binding to a metal *in vivo* or the metal complex may be a vehicle for activation of the ligand as the cytotoxic agent. Recently it has been shown that semicarbazones of aromatic and unsaturated carbonyl compounds have anticonvulsants properties. Moreover, coordination may lead to significant reduction of drug-resistance. They are also used as spectrophotometric agents as well for the analysis of metal ions and are frequently used in the qualitative organic analysis of carbonyl compounds.

Recently, thiosemicarbazones have been synthesized and screened against the three parasitic cysteine proteases cruzain, falcipain-2, and rhodesain and against their respective parasite sources. The results obtained suggested that thiosemicarbazones represent validated leads that kill several species of protozoan parasites through the inhibition of cysteine proteases as well as through action against other targets. Furthermore, semicarbazones, which can also be regarded as urea derivatives, have gained considerable importance in recent years in the design of enzyme inhibitors, as replacement for the amide (–CO–NH–) bond in peptidomimetics and as sources of self-complementary

bidirectional hydrogen bonding motif in supramolecular chemistry. Since peptides have poor metabolic stability and limited oral absorption, they are rarely useful drug candidates.

The thesis deals with the syntheses and characterization of some transition metal complexes of three N^4-phenylsemicarbazone ligands, 2-pyridine carboxaldehyde-N^4-phenylsemicarbazone, 3-ethoxysalicylaldehyde-N^4-phenylsemicarbazone and 2-benzoylpyridine-N^4-phenylsemicarbazone. Thesis is divided into six chapters.

Chapter 1

This chapter gives an introduction to semicarbazones, their mode of bonding in complexes and applications in different areas. The objectives of the present work, the details of different analytical and spectroscopic techniques used for the characterization of metal complexes are also presented in this chapter.

Chapter 2

Chapter 2 deals with the syntheses of two new semicarbazones and a reported semicarbazone and their characterization by elemental analyses, FTIR, ^{1}H NMR, UV–Vis spectra and single crystal XRD studies.

The thiosemicarbazones synthesized were;

1. 2-formylpyridine-N^4-phenylsemicarbazone

2. 3-ethoxysalicylaldehyde-N^4-phenylsemicarbazone

3. 2-benzoylpyridine-N^4-phenylsemicarbazone

The single crystal studies of the ligand 3-ethoxysalicylaldehyde-N^4-phenylsemicarbazone reveals that it is a planar molecule which has

intermolecular and intramolecular bifurcated hydrogen bond in its molecular crystal.

Chapter 3

Chapter 5 describes the syntheses and characterization of five Ni(II) complexes. All the compounds were characterized by various spectral studies. Magnetic susceptibility measurements reveal that all the nickel complexes are paramagnetic except two compounds which suggest square planar geometry around their metal centres. The semicarbazones are found to coordinate in the neutral form in two complexes and in anionic form in the other complexes as evidenced by the IR spectral data. The single crystal studies show that a complex has two asymmetric molecules in its unit cell with four ClO_4^- counter ions and seven lattice water molecules outside the coordination sphere. Each Ni atom has a distorted octahedron environment with a number of intermolecular hydrogen bonding interactions with the perchlorate ions and water molecules.

Chapter 4

This chapter describes the syntheses and characterization of two copper complexes of the semicarbazone ligands. Both the complexes are characterized by various techniques such as elemental analyses, FTIR, EPR, electronic spectral studies, thermogravimetric analyses, conductance, magnetic susceptibility measurements and single crystal XRD studies. Magnetic susceptibility measurements clearly indicate that all compounds are paramagnetic in nature. The molar conductivity measurements in 10^{-3} M DMF solution reveal that all the complexes are non-electrolytic in nature. The semicarbazones are found to coordinate in the neutral form in two complexes and in anionic form in the other complexes. EPR spectra of the compounds in

DMF at 77 K displayed axial features with five superhyperfine splitting and in all complexes the $g_{\parallel} > g_{\perp} > 2.0023$ but one complex has $g_{\perp} > g_{\parallel}$ relationship.

These complexes have square planar, square pyramidal, trigonal bipyramidal geometries. The single crystal studies reveal that two complexes are dimeric bridged compounds with distorted square pyramidal coordination around the metal centre. The thermal studies show that the five complexes have lattice water while two complexes have coordinated water in their complexes.

Chapter 5

This chapter describes the syntheses and characterization of six Zn(II) complexes. The characterization techniques include elemental analyses, FTIR, electronic spectral studies, thermogravimetric analyses, magnetic susceptibility measurements, conductance measurements and single crystal XRD studies. All the complexes are non-electrolytic as well as diamagnetic compounds. The IR spectral studies show that the semicarbazone ligands are coordinated in neutral form in three complexes and in anionic form in the other three complexes. The single crystal XRD studies of two complexes show that one of the complexes is a monomeric with a distorted square pyramidal arrangement around the zinc(II) metal atom and the other is a dimeric with a distorted square pyramidal arrangement around the zinc(II) metal atom with one dimensional supramolecular hydrogen bonding network among these molecules in zig-zag manner.

Chapter 6

This chapter deals with the syntheses and characterization of eight cadmium(II) complexes. The complexes were characterized by elemental analyses, IR, UV-Vis, thermogravimetric analyses, conductance and single crystal XRD studies. The molar conductivity measurements in DMF (10^{-3} M)

solutions indicate that all the complexes are non-electrolytes. The thermal analyses show that one of the compounds has three moles of lattice water in its complex.

Single crystal data were collected for two complexes and one of the complexes reveal that it contains two asymmetric units in the unit cell. An extensive delocalization over entire coordination framework is established with a distorted octahedron arrangement around the cadmium(II) centre. Even in the absence of intermolecular hydrogen bond, CH ⋯ π and π⋯π interactions helps to construct the crystal system. The other complex shows that it is a binuclear centrosymmetric structure with distorted octahedron arrangement around the cadmium(II) centre with Cd⋯Cd distance of 4.0809(14) Å. The packing of the molecules are arranged in zig-zag manner with a two-dimensional supramolecular hydrogen bonding network in the crystal system.

........................ॐॐॐ........................

Curriculum Vitae

PERSONAL PROFILE

Date of Birth	30th December 1971
Permanent address	No. 6C,
	Old Waidya Road,
	Dehiwala
	Sri Lanka
E_mail	eesans@yahoo.com
Present employment	Senior Lecturer in Chemistry
	Eastern University, Sri Lanka
	Chenkaldy, Sri Lanka

EDUCATION

1993-1997	B. Sc. Special degree in Chemistry
	University of Jaffna, Sri Lanka
	(Second class upper division)
1999-2001	M. Phil. in Chemistry (sponsored by NSF)
	University of Peradeniya, Sri Lanka

Papers published during this period:

1. Spectral, thermal, structural, dielectric and microhardness studies of gel grown diaquasuccinatocadmium(II) hemihydrate, V.S. Dhanya, M.R. Sudarsanakumar, S. Suma, M.R.P. Kurup, **M. Sithambaresan**, S.M. Roy, Spectrochimica Acta Part A 93 (2012) 295– 299.

2. Bis{-2-[bis(pyridin-2-yl)methylidene]hydrazinecarbothioamidato} bis[bromidocopper(II)] methanol disolvate, R. J. Kunnath, **M. Sithambaresan**, M. R. P. Kurup, A. Natarajan, A. A. Aravindakshan, *Acta Cryst.* E68 (2012) m346-m347.

3. 2-(3-Ethoxy-2-hydroxybenzylidene)-N-phenylhydrazinecarboxamide, **M. Sithambaresan,** M. R. P. Kurup, Acta Cryst. E67 (2011) o2972.

4. Dimethyl-2-[phenyl(pyridin-2-yl)methylidene]hydrazinecarbothioamide, K. Jayakumar, **M. Sithambaresan**, M. R. P. Kurup, Acta Cryst. E67 (2011) o3195.

5. Spectral studies of copper(II) complexes of tridentate hydrazone ligands with heterocyclic compounds as coligands: X ray crystal structure of one acyl hydrazone copper(II) complex, Nancy Mathew, **M. Sithambaresan**, M.R.P. Kurup, Spectrochim. Acta A 79 (2011) 1154-1161.

6. N'-[(E)-Furan-2-ylmethylidene]pyridine-3-carbohydrazide, Jessy Emmanuel, **M. Sithambaresan**, M. R. P. Kurup, Acta Cryst. E67 (2011) o3267.

7. Synthesis, spectral characterization and crystal structure of copper(II) complexes of 2-benzoylpyridine-*N*(4)-phenylsemicarbazone, M.R.P. Kurup, Binu Varghese, **M. Sithambaresan**, Suja Krishnan, S.R. Sheeja, E. Suresh, Polyhedron 30 (2011) 70-78.

8. (E)-2-(4-Benzyloxy-2-hydroxybenzylidene)-N-phenylhydrazinecarbothioamide, K. Nisha, **M. Sithambaresan**, M. R. P. Kurup, Acta Cryst. E67 (2011) o3420.

9. Syntheses and EPR spectral studies and crystal structures of manganese(II) complexes of neutral NN donor bidentate Schiff bases and azide/thiocyanate as coligand, Sreesha Sasi, **M. Sithambaresan**, M.R.P. Kurup, H.-K. Fun, Polyhedron 29 (2010) 2643-2650.

10. *N'*-{(*E*)-[4-(Benzyloxy)-2-hydroxyphenyl]methylidene}-4-nitrobenzohydrazide hydrate, B. Joseph, **M. Sithambaresan**, M. R. P. Kurup, Acta Cryst. E (in press).

11. (2*E*)-2-[(2-Hydroxy-4-methoxyphenyl)(phenyl)methylidene]-*N*-phenylhydrazinecarboxamide dimethyl formamide monosolvate, Annie C.F., J.M. Jacob, **M. Sithambaresan**, M. R. P. Kurup, Acta Cryst. E (in press).